Air flow through large openings in buildings

Subtask-2   Technical Report

edited by J. van der Maas

International Energy Agency

Energy Conservation in Buildings and
Community Systems Programme

Annex 20 : Air Flow Patterns within Buildings

Subtask 2 : Air Flows between Zones

AIR FLOW THROUGH LARGE OPENINGS IN BUILDINGS

edited by **J. van der Maas**
LESO-PB, EPFL, CH 1015 Lausanne, Switzerland

An Annex 20 Technical Report of participants in subtask 2.1:

Francis Allard, INSA - CNRS, Lyon, France
Dominique Bienfait, CSTB, Marne-la-Vallée, France
Fariborz Haghighat, Concordia University, Montreal, Canada
Georges Liébecq, University of Liège, Belgium
Koos van der Maas, EPFL, Lausanne, Switzerland
Roger Pelletret, CSTB, Sophia Antipolis, France
Luk Vandaele, BBRI, Limelette, Belgium
Richard Walker, BRE, Garston,Watford, United Kingdom

JUNE 1992

Preface

International Energy Agency

The International Energy Agency (IEA) was established in 1974 within the framework of the Organisation for Economic Co-operation and Development (OECD) to implement an International Energy Programme. A basic aim of the IEA is to foster co-operation among the twenty-one IEA Participating Countries to increase energy security through energy conservation, development of alternative energy sources and energy research development and demonstration (RD&D). This is achieved in part through a programme of collaborative RD&D consisting of forty-two Implementing Agreements, containing a total of over eighty separate energy RD&D projects. This publication forms one element of this programme.

Energy Conservation in Buildings and Community Systems

The IEA sponsors research and development in a number of areas related to energy. In one of these areas, energy conservation in buildings, the IEA is sponsoring various exercises to predict more accurately the energy use of buildings, including comparison of existing computer programs. building monitoring, comparison of calculation methods, as well as air quality and studies of occupancy. Seventeen countries have elected to participate in this area and have designated contracting parties to the Implementing Agreement covering collaborative research in this area. The designation by governments of a number of private organisations, as well as universities and government laboratories, as contracting parties, has provided a broader range of expertise to tackle the projects in the different technology areas than would have been the case if participation was restricted to governments. The importance of associating industry with government sponsored energy research and development is recognized in the IEA, and every effort is made to encourage this trend.

The Executive Committee

Overall control of the programme is maintained by an Executive Committee, which not only monitors existing projects but identifies new areas where collaborative effort may be beneficial. The Executive Committee ensures that all projects fit into a pre-determined strategy, without unnecessary overlap or duplication but with effective liaison and communication. The Executive Committee has initiated the following projects to date (completed projects are identified by *).

Annex 1:	Load energy determination of buildings (*)
Annex 2:	Ekistics & advanced community energy systems (*)
Annex 3:	Energy conservation in residential buildings (*)
Annex 4:	Glasgow commercial building monitoring (*)
Annex 5:	Air infiltration and ventilation centre
Annex 6:	Energy systems and design of communities (*)
Annex 7:	Local government energy planning (*)
Annex 8:	Inhabitants behaviour with regard to ventilation (*)
Annex 9:	Minimum ventilation rates (*)
Annex 10:	Building HVAC system simulation (*)
Annex 11:	Energy auditing (*)
Annex 12:	Windows and fenestration (*)
Annex 13:	Energy management in hospitals (*)
Annex 14:	Condensation and energy (*)
Annex 15:	Energy efficiency of schools (*)
Annex 16:	BEMS 1 - User interfaces and system integration
Annex 17:	BEMS 2 - Evaluation and emulation techniques
Annex 18:	Demand controlled ventilating systems
Annex 19:	Low slope roofs systems
Annex 20:	Air flow patterns within buildings
Annex 21:	Calculation of energy & environmental performance of buildings
Annex 22:	Energy efficient communities
Annex 23:	Multizone air flow modelling
Annex 24:	Heat, air & moisture transport in new and retrofitted insulated envelope parts
Annex 25:	Real time simulation of HVAC systems and fault detection

I

Annex 20: Air Flow Patterns within Buildings

A task-sharing Annex to the International Energy Agency's Implementing Agreement for a Program of Research and Development on Energy Conservation in Buildings and Community Systems.

Objectives: To evaluate the performance of single- and multi-zone air and contaminant flow simulation techniques and to establish their viability as design tools.

Start: May 1, 1988

Duration: 3 1/2 years

Completion: November 1, 1991

Subtasks: The work is organized in two parallel subtasks
1. Room air and contaminant flow
2. Multi-zone air and contaminant flow and measurement techniques

Participating Countries: Belgium, Canada, Denmark, Finland, France, Germany, Italy, The Netherlands, Norway, Sweden, Switzerland, United Kingdom, and the United States of America.

Operating Agent: The Swiss Federal Office of Energy (BEW). Contractor The Energy Systems Laboratory of the Swiss Federal Institute of Technology (ETH), Zurich, Switzerland. Executive OA: Dr. Alfred Moser.

Subtask leader 1 (single room): Ir. Tony Lemaire, TNO Building and Construction Research, P.O. Box 29, NL-2600 AA Delft, The Netherlands.

Subtask leader (multi-zone): Dr. Claude-Alain Roulet, LESO-PB, EPFL - Ecublens, CH-1015 Lausanne, Switzerland.

Specific Objectives of Subtask 1

. To evaluate the performance of 3-dimensional complex and simplified air flow models in predicting flow patterns, energy transport, and indoor air quality

. to show how to improve air flow models

. to evaluate applicability as design tools

. to produce guidelines for selection and use of models

. to acquire experimental data for evaluation of models.

Specific Objectives of Subtask 2

. to develop new algorithms for specific problems, as flow through large openings, inhabitant behaviour, air-flow-driven contaminants, or multi-room ventilation efficiency

. to develop new, or improve existing measurement techniques

. to collect and test input data sets of experimental data (reference cases for code validation)

Cover: Atelier P.G. Ulmer, CH-8200 Schaffhausen

Acknowledgements

SYNOPSIS

This technical report of subtask 2 of the IEA/ECB-Annex 20 (Air Flow Patterns Within Buildings) concerns a research project called "Air Flows Through Large Openings In Buildings". The work performed in this project was based on a literature review (chapter 2) showing the needed experimental work to improve the modeling of both airflow through doors and windows. New studies of interzonal airflow and single sided ventilation at seven laboratories in Europe and Canada, have then been carried out in this project's framework and have led to improved models.

The interzonal air flow research (chapter 3) was based on three test rooms (respectively at the University of Liège, at INSA Lyon and at CSTB Sophia Antipolis) and mainly focused on natural convection; the aim was to improve the knowledge and the numerical prediction of heat and mass transfer through doorways. This goal was achieved through a joint research effort which was based on the comparison of experimental results. Moreover, these experimental results have been used to validate a C.F.D (Computational Fluid Dynamics) model developed at Concordia University.

The test cell results include validated models to compute the mass flows in large openings assuming either isothermal air volumes or linear temperature profiles in both rooms; the discharge coefficients that have been found from the steady state experiments is about 0.43, in agreement with reference experiments used by ASHRAE but measured under very different circumstances. Local discharge coefficients have also been determined. Moreover interzone (thermal resistance) models are discussed, describing the transition between bulk driven flow and boundary layer driven flow and offering the opportunity to include time-dependent boundary conditions. Such a model would allow a better evaluation of the energy consequences of inhabitant behavior without the need to use complete building thermal models. Finally, C.F.D models, as those developed at Concordia University, seem well adapted to fulfill the task of validating simplified models.

The single sided ventilation studies (chapter 4) were designed to determine the effect of wind on the ventilation and/or heat loss rates through openings in one external wall only. Collaboration between four european laboratories led to the following contributions :

- CSTB test house at Bouin, France, with horizontal slit, to measure internal pressures and the effect of air compressibility

- BBRI attic test room at Gent, Belgium, with open window, to monitor long term ventilation rates and assess possible correlations with measured parameters including wind, temperature and surface pressures

- BRE office at Garston, England, with open window, to assess the time dependence of ventilation rates following the opening of the window, due to the combined effect of the wind and the thermal properties of the room.

- EPFL offices at Lausanne, Switzerland, with open window, to study the energy consequences of user behaviour by measuring the time dependence of cooling induced by natural ventilation for rooms of different thermal mass.

The main concern was to relate air exchange rate with parameters measured locally at the opening. The more general problem of relating this rate, or these local parameters, to reference measurements significantly distant from the building, is briefly discussed.

Table of Contents

Nomenclature

Note: in formulas and figures reproduced from the literature this nomenclature could not always be respected. In case of doubt, one should always consult the reference of the source.

ACH:	Air changes per hour	(1/h)
ACR :	Air change rate	(m^3/s)
A :	Opening area	(m^2)
A_{eff} :	Effective area	(m^2)
b :	Wall thermal effusivity	$b = \sqrt{(\lambda \rho c)}$
b :	Air density gradient	(kg/m^4)
b_t :	Turbulent pressure gradient	(Pa/m)
C_1 :	Wind coefficient	(−)
C_2 :	Stack coefficient	(−)
C_3 :	Turbulent coefficient	(−)
C_c :	Contraction coefficient	(−)
C_d :	Discharge coefficient	(−)
C_p :	Heat capacity of air	(J/kg K))
C_s :	Area fraction for heat transfer	(−)
E:	Euler number	(−)
E:	Exchange ratio	(−)
f :	Frequency	(Hz)
F :	Non-dimensional ventilation	(−)
g :	Acceleration of gravity	(9.81 m/s^2)
Gr :	Grashof number	(−)
h_c :	Convective heat transfer coefficient	(W/Km^2)
h_T :	Heat transfer coefficient	(W/Km^2)
H :	Height of the opening	(m)
Hr :	Height of a room	(m)
K :	Orifice coefficient	(−)
m'_{ij} :	Air mass flow rate from zone i to zone j	(kg/s)
m'_S :	Mass flow rate of supplied air	(kg/s)
Nu :	Nusselt number	(−)
P:	Pressure	(Pa)
Pt:	Turbulent pressure	(Pa)
Pr:	Prandtl number	(−)
q:	Heat flux density	(W/m^{2}K)
Q:	Volume flow rate	(m^3/s)
R:	Gas constant for air	287 (J/kgK)
Ra:	Rayleigh number	(−)
S_i :	Internal surface area	(m^2)
T_{in} :	Inside air temperature	(°C)
T_{out} :	Outside air temperature	(°C)

T :	Air temperature	(K)
u :	Air velocity	(m/s)
V:	Volume	(m^3)
XH:	Air specific humidity	(kg water/kg dry air)
z:	Vertical position	(m)
Zn:	Vertical position of a neutral plane	(m)
W:	Width of the opening	(m)
Wr:	Width of a room	(m)
β:	Perfect gas expansion coefficient	(K^{-1})
δp:	Pressure variation	(Pa)
ΔT:	Air temperature difference	(K)
ρ:	Air density	(kg/m^3)
θ:	Area reduction coefficient	(–)
Φ:	Heat flow rate	(W)

sub /upperscripts

t :	top
b :	bottom
r :	room
h :	hot
c :	cold
n :	neutral
i :	inside
o :	outside
w:	wall
W :	wind

1. INTRODUCTION: STATE OF THE ART AND GOALS

There exist quite a few algorithms which are used in computer models to describe air flow through large internal and external openings. However, the algorithms are based on simplifying assumptions and the practical range of validity of these models is not well known. For example, real situations can be imagined where these simplifications are clearly not justified, and there is a need to know the error one makes in using them and for these cases new, more accurate algorithms should be developed.

It is essential that one can clearly indicate which situations can be described with confidence by the investigated models. The scope of the subtask 'Large Openings' was to test the range of validity of available algorithms, and where possible, to develop new ones. In the following section, we present (i) the international status of 'Large Opening' research at the beginning of Annex XX, as well as the specification of new research topics from literature surveys, (ii) the research potential of Annex XX participants and (iii) the research goals that have been set. Finally (iv) an overview over the report and the achievements of this task of the Annex XX is provided.

1.1. Status of air flow through large openings in buildings, research needs

Literature reviews, including a synthesis of present research and possible future topics on air flow through large openings, have been presented as early Annex XX working documents, and formed a basis for the planning of the subtask *[Warren, 1988; Sandberg, 1989; Vandaele and Wouters, 1989; Van der Maas, 1989b]*. These documents can be summarized as follows:

1.1.1. Air flow through large internal openings. The subject of air flow through large openings connecting two spaces at different temperatures, concerns principally what in heat- and mass-transfer literature is called "Natural convection in enclosures".

In building physics one is interested in situations which are more complicated than the idealized cases treated generally in specialized literature. A real room contains heating equipment or is connected to a HVAC, contains furniture, and its walls do not have uniform thermal properties. However, the models used in multizone ventilation models are not able to deal with these cases.

A literature survey has shown *[Sandberg, 1989, Vandaele and Wouters, 1989]* that almost exclusive attention has been directed to *vertical* openings such as doorways. The algorithm which is most often implemented assumes that the flow is one-dimensional and that the interconnected rooms are at constant temperature, the only free parameter being the discharge coefficient. The three-dimensional nature of the flow and the presence of a vertical temperature gradient are then neglected and the discharge coefficient appears to vary from experiment to experiment. From these literature surveys follow a number of potential future research items:

The *discharge coefficient* reported in the literature varies between 0.3 and 0.8, and it is not understood what causes the differences.

The transition between *gravity driven* flow and *boundary layer driven* flow should be clarified. In particular how do *wall temperatures* and *heat transfer* influence boundary layer driven flow?

How to treat flow through *horizontal* openings and staircases is virtually unknown, in particular for the interesting case when colder (denser) air is placed above a reservoir with warmer air.

The uncertainties connected to the use of the *Bernoulli model for linear or arbitrary temperature profiles* are also largely unknown. In particular, what is the role of *turbulence* effects when the steady flow is low, and how does natural convection combine with forced ventilation (*mixed convection*)?

1.1.2. Air flow through large external openings. The description of air flow through large external openings is basically the same as for internal openings as long as there is no wind. Therefore, the research on large external openings was mainly concentrated on wind effects *[Warren 1988]*.

Flows induced by *fluctuating wind pressures* and *eddy circulation* have been observed in single-sided ventilation. However, it is difficult to characterize fluctuating pressures at the position of the window when the wind characteristics are only known far from the building. A different challenge is how to relate these fluctuating wind pressures to the total air exchange through the single large opening, and how to deal with cases where internal doors are open. The ventilation through a single opening is the combined effect of wind and buoyancy, but the available data show a large spread in values. Crossventilation is of considerable importance in warm climates but very few data are available.

All these wind related topics, in particular *single-sided ventilation*, need further measurement and modeling efforts to provide better understanding.

1.2. Research facilities in Annex 20 participating countries

In Belgium, the University of Liège has a facility for the measurement of heat and mass transport through a door in a climatic room *[Baranowski et al, 1989; Tang and Robberechts, 1989]*, while the Belgium Building Research Institute (BBRI) in Limmelen has started a ventilation study in an 'attic with openable window' *[Vandaele and Wouters, 1989]*.

At the Ecole Polytechnique Fédérale in Lausanne, Switzerland, a model is under development for the description of time-dependent ventilation and cooling after the opening of a window or door *[van der Maas et al, 1989a]*.

At Concordia University in Montreal, Canada, a numerical code has been developed for the calculations of inter-zone air flow through a door *[Haghighat et al., 1989]*, and a model is under development for the case of single-sided-ventilation due to turbulent flow.

France joined Annex 20 with three research groups active in the field. The CSTB research group in Marne-la-Vallée is studying the influence of turbulent wind on ventilation *[Mounajed, 1989; Riberon et al., 1989]*. Both the CSTB group in Sophia Antipolis *[Pelletret 1988a]* and the INSA group in Lyon *[Allard et al., 1987]* have climatic test rooms to study heat and mass transfer through a door.

In Delft, Holland, a field tested, single-sided ventilation model was developed *[De Gids and Phaff, 1982]* and single-sided ventilation by eddy penetration was measured in a windtunnel *[Crommelin and Vrins, 1988]*.

In the UK there has been considerable interest in air flow through staircases *[Riffat 1989; Mokhtarzadeh et al., 1989; Zohrabian et al, 1989]*. At the Building Research Establishment (BRE) extensive studies have been made on single-sided ventilation *[Warren, 1986, 1988]*, but funding was difficult to obtain.

In Fort Collins, United States, a Bernoulli model taking temperature stratification and forced convection into account has been developed *[Hill et al., 1986]*, and the transition between boundary layer flow and gravity driven flow is under study *[Boardman et al., 1989; Neymark et al., 1989; Scott et al.,* 1988].

Unfortunately the US could not contribute to the Annex 20 task on large openings due to lack of funding. The contribution of Holland to subtask 2 shifted fully to other multizone problems as ventilation efficiency and pollutant transport. The UK finally, contributed with an experiment in collaboration with the EPFL.

1.3. Research goals, planning and report overview.

In the early stage of Annex 20, literature surveys were completed and a literature review is presented in chapter 2. At the Fourth expert meeting (November 1989) research planning was initiated. The scope of the work was to test the range of validity of available algorithms, and to develop new ones, wherever possible.

Air flow through large *internal* openings. Similar measurements in three existing laboratory setups were planned:

-       the University of Liège (section 3.2),

-       the INSA in Lyon (section 3.3)

-       the CSTB in Sophia Antipolis (section 3.4)

The main differences between the inter zone mass and heat transfer experiments would be in the ways heating and cooling were produced in the two zones.

To facilitate comparison, the velocities in each opening and the associated zone temperature profiles needed to be compared with the Bernoulli model, both with the hypothesis of isothermal zones and assuming linear temperature stratification. The validity of a constant discharge coefficient could then be tested directly. Only after completing this dimensional analysis, would one proceed to discuss correlations for interzonal heat transfer using non-dimensional numbers.

Canada would contribute (section 3.5) by making numerical simulations of interzone mass transfer with the Concordia numerical code. To validate the code, comparisons would be made with calculations performed with another numerical code (PHOENIX code) and with experimental data.

In a synthesis (section 3.6) the results of the test cell experiments are intercompared, and compared with the literature. Some new model developments are also presented (section 3.7).

Air flow through large *external* openings. New measurements of single-sided ventilation in the presence of wind and/or stack effect, were planned by four laboratories. Recently proposed ventilation models were tested and as a new aspect of the research, not only ventilation rates but also the dynamic heat loss rate induced by ventilation would be measured, thereby stressing the energy aspect of ventilation. In section 4 of this report, four new full scale experiments on single-sided ventilation are presented

-       CSTB in Marne la vallée (F) has measured the air flow rate due to fluctuating wind pressures using a rotatable test house(section 4.2).

-       BBRI in Limmelen (B), measured the single-sided ventilation through a roof window for various wind conditions(section 4.3).

-       BRE at Garston, Watford (UK) tested a model coupling ventilation and heat transfer under windy conditions (section 4.4).

-       LESO-EPFL in Lausanne (CH) studied energy consequences of user behavior and measured ventilative heat loss rates (section 4.5).

A summary, conclusions and research recommendations are concluding the report (chapter 5).

Contents of chapter 2

2 LITERATURE REVIEW

Air may flow differently at the top of a doorway than at the bottom. This bi-directional flow, characteristic of large opening behavior, has a variety of causes which can be classified broadly in two categories, those which induce steady flow by virtue of their mean value, and those whose effect is due to their fluctuating nature.

The first category includes the effects of mean wind velocity, the gravitational flows due to density gradients, the effects of boundary layer flows developed in a cavity, and the coupling effects induced by ventilation or heating systems.

The second category represents the fluctuating air flows due to fluctuating pressures. These fluctuating pressures may be caused by the turbulent characteristics of approaching wind or by turbulence induced by the building itself. In some cases, especially when the average value of the pressure drop through the opening is small compared to the fluctuating pressure, these fluctuating flows can significantly increase the air exchanges.

Due to the high number of parameters involved and the complexity of the physical phenomena driving air through a large opening, it becomes virtually impossible to arrive at a general solution of this problem. It is then natural to elaborate simplified models using a small number of parameters to quantify the order of magnitude of the phenomena, in particular when they are too difficult to predict by a deterministic approach..

The general topic of air flows in buildings has received a great deal of interest as is shown by the many previous experimental investigations in this field and various elementary models have already been proposed.

In this chapter we present the basic physics and review the literature that is relevant to the investigations conducted in the framework of the Annex 20 subtask 'Air flow through large openings in buildings'; investigations described in subsequent chapters 3 and 4.

2.1. Bulk Density Flow

The classical simplified approach of the so-called gravitational flow, is the application of the continuity equation and Bernoulli's theorem on both sides of the large opening. This is equivalent to assume the interzone air flow to be a steady flow (no variation with time) of an incompressible, non-viscous fluid of constant density, that is only driven by pressure gradients on both sides of the opening.

In the following it is shown how the Bernoulli equation is derived from the Navier-Stokes equation and then how empirical coefficients like the discharge coefficient and non-dimensional numbers like the Froude number, link real world observations to the idealized model. As is demonstrated with examples from the literature, many practical situations are reasonably well characterized by this kind of semi-empirical model, but some other situations are poorly described and need further investigation.

2.1.1 The equations of motion, and various approximations

The dynamics of general fluid dynamics is based on the conservation of mass principle (expressed in the continuity equation) and the conservation of momentum principle (expressed in the Navier-Stokes equation). The derivation of these equations can be found in textbooks on fluid dynamics, but the following paagraphes are provided to show the origin of various assumptions leading to the Bernoulli theorem and serve as references for the literature review and discussions in later chapters.

The only external force that will be considered is that of gravity, which exerts a body force $\rho \mathbf{g}$ per unit volume on each element of fluid (where ρ is the local density and $\mathbf{g}$ is the acceleration due to gravity). ρ may vary due to differences in temperature or to concentration but the fluid will be regarded as incompressible. The compressibility of gases becomes only significant e.g. in deep layers as in atmospheric physics or at high velocities as in jets.

When ρ varies with height, the pressure variation in the fluid is given by the hydrostatic equation:

$$p = p_0 - g \int_0^z \rho \ dz \tag{2.1}$$

This shows that the fluid is in equilibrium only when the density, as well as the pressure, is constant in every horizontal plane.

The continuity equation applied to a given volume expresses the fact that the difference between the inflowing mass and the outflowing mass equals the time rate of change of the mass in the volume. For incompressible flows the continuity equation in vector notation is:

$$\nabla . \mathbf{u} = 0 \tag{2.2}$$

Three forces can be distinguished when considering the acceleration dv/dt of a fluid element (i) a force field $\mathbf{F} = -\rho \mathbf{g}$, (ii) a gradient in the pressure field P and (iii) friction forces $\mathbf{F}(\mu)$ related to the viscosity μ. Applying Newton's second law of motion one obtains the Navier-Stokes differential equation for viscous flow:

$$\rho \frac{Du}{Dt} = - \nabla p + \rho\, g + F\,(\mu) \qquad (2.3)$$

The acceleration vector Du/Dt, concerning an observer moving at the velocity of the liquid (Euler coordinates), can be decomposed as follows

$$\frac{Du}{Dt} = \frac{\partial u}{\partial t} + (u.\nabla)\, u = \frac{\partial u}{\partial t} + \frac{1}{2}\,\nabla\, u^2 + (\nabla\wedge u)\wedge u \qquad (2.4)$$

where for steady-state situations the partial derivative with respect to time is zero. This steady-state description can be used as a good approximation over time intervals where the change of the velocity field is negligeably small.

The modeling of dissipating friction forces in the last term $F(\mu)$ is just what makes fluid dynamics a difficult subject (the interested reader is referred to the textbooks). For perfect fluids (non-viscous flows), the last term in Eq. 2.3 is neglected and one obtains the Euler equations of motion.

It can be shown that only differences of density ρ' from some standard value ρ_0 are relevant in determining the effect of gravity. The Euler equations can be written in terms of the deviations p' and ρ' (one sets $p=p_0+p'$ and $\rho=\rho_0+\rho'$) from a reference state of hydrostatic equilibrium:

$$\rho \frac{Du}{Dt} = - \nabla p' + \rho'\, g, \quad \text{where} \quad \nabla p_0 = \rho_0 g \qquad (2.5)$$

In a two-layer system, for example, the layer with the standard density ρ_0 may be regarded as weightless, and that with density $\rho=\rho_0+\rho'$ as if it were acted on by a reduced gravitational acceleration $g'=g\rho'/\rho_0$ *[Turner 1973]*.

After divison of this equation by the reference density ρ_0

$$\left(1+\frac{\rho'}{\rho_0}\right)\frac{Du}{Dt} = -\frac{1}{\rho_0}\nabla p' + \frac{\rho'}{\rho_0}\, g \approx \frac{Du}{Dt} \qquad (2.6)$$

it is seen that the density ratio ρ'/ρ_0 appears twice, in the first (inertia) term and in the buoyancy term. When ρ'/ρ_0 is small, it produces only a small correction to the inertia compared to a fluid of density ρ_0, but it is of primary importance in the buoyancy term. The *Boussinesq approximation* (Eq. 2.6) consists essentially of neglecting variations in so far as they affect inertia, but retaining them in the buoyancy terms, where they occur in the combination $g'=g\rho'/\rho_0$. Eqs. 2.3 and 2.4 combine for non-viscous flow into the Euler equations:

$$\rho \left(\frac{\partial u}{\partial t} + \frac{1}{2}\,\nabla\, u^2 + (\nabla\wedge u)\wedge u\right) = - \nabla p + \rho\, g \qquad (2.7)$$

For a steady flow, Eq. 2.7 can be integrated along a streamline and for any two points on this trajectory the equation can be written as:

$$p_1 + \rho g z_1 + \rho \, \frac{\mathbf{u}_1{}^2}{2} = p_2 + \rho g z_2 + \rho \, \frac{\mathbf{u}_2{}^2}{2} = cst \tag{2.8}$$

This is the Bernoulli theorem for inviscid rotational flow expressing the total conservation of mechanical energy along a trajectory with three terms representing pressure energy, potential energy and kinetic energy. The constant is in principle varying from streamline to streamline.

Irrotational flow: When integrating Eq.2.3 with the additional requirement of irrotational flow $\nabla_\wedge u = 0$, the flow is a *potential* flow, and the Bernoulli equation is obtained without being restricted to a streamline, the constant being the same for all the streamlines in the flow.

When viscous forces can not be neglected as for the case of flow through a pipe or duct, the loss in mechanical energy caused by fluid internal friction results in a loss of pressure, and the Bernoulli equation can then be *generalized* by adding a pressure drop term Δp_f to Eq.2.8:

$$p_2 - p_1 + \rho \, \frac{1}{2}\left(\mathbf{u}_2{}^2 - \mathbf{u}_1{}^2\right) + \rho g (z_2 - z_1) + \Delta p_f = 0 \tag{2.9}$$

2.1.2 Orifice flow coefficients (Cc, Cd, Eu, Fr, Re)

A fluid flowing through an orifice forms a jet which is usually illustrated in the textbooks by the discharge of a liquid into the atmosphere, but the basic considerations apply as well to the flow of liquids into liquids or of gases into gases. Indeed the flow of a layer of heavy fluid under lighter fluid has many features in common with the hydraulics of a stream with a free surface. In nature most flows of this kind are turbulent but they can for many purposes be accurately described using perfect fluid theory, with possibly the addition of terms to take into account friction on the bottom and at the interface, and the overall energy losses.

It turns out that for cases where the motion is confined and completely defined by solid boundaries, the effect of gravitational attraction is only an increase of the pressure in direct proportion to the elevation, and no change of the flow pattern will result.

Therefore, and for reference, fluid flow without the presence of the gravitational field will be considered first. For irrotational flow, the velocity and pressure field can then be found for any boundary geometry through the use of the continuity and Bernoulli equations. The jet profile in such potential flow is also completely determined.
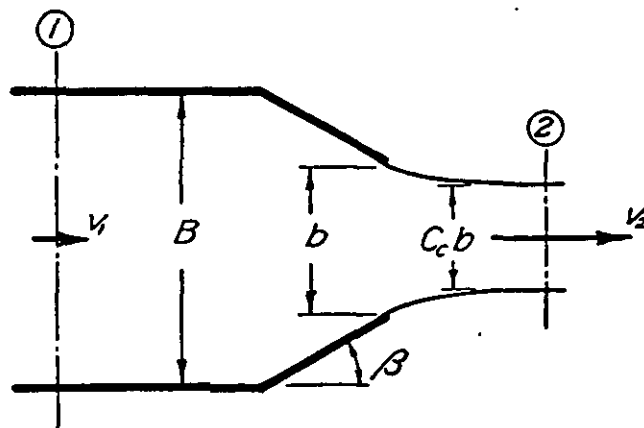

Figure 2.1 Boundary parameters for a two-dimensional outflow illustrating the definition of the coefficient of contraction C_C

Contraction coefficient. The ratio between the final cross-sectional area of a jet and that of the opening is called the coefficient of contraction, C_c. If only normal stresses act, the magnitude of this coefficient will depend entirely upon the boundary geometry. This is illustrated in Figure 2.1 for a two-dimensional boundary, where an orifice (angle β, diameter b) is placed at the end of a conduit (diameter B). More than a century ago it was shown by Kirchhoff that the contraction coefficient for irrotational flow from a plane orifice ($\beta=90°$) in a large container would have the magnitude $\pi/(\pi+2) = 0.611$.

b/B	$\beta=45°$	$\beta=90°$	$\beta=135°$	$\beta=180°$
0.0	0.746	0.611	0.537	0.500
0.5	0.752	0.644	0.599	0.586
0.7	0.768	0.687	0.652	0.646
0.9	0.829	0.781	0.761	0.760
1	1	1	1	1

Table 2.1 Values for the contraction coefficient C_c for boundary characteristics indicated schematically in Figure 2.1 (Rouse 1946).

Typical C_c values for the boundary characteristics indicated schematically in Figure 2.1, are given in Table 2.1 *[Rouse 1946]*. These values for C_c illustrate the influence of the opening position of doors on the air flow between a corridor and a large room.

Discharge coefficient. To compute the rate of discharge through the orifice, we write the continuity Eq.2.1 and the Bernoulli Eq.2.7 between sections 1 and 2 of Figure 2.1:

$$p_1 - p_2 = \Delta p = \frac{\rho}{2}\left(u_2{}^2 - u_1{}^2\right)$$

(2.10)

The free surface of the jet is determined by the condition that the velocity is constant because the pressure is required to be at the atmospheric pressure.

The rate of flow $Q = u_1 B = u_2 C_c b$ yields the outflow velocity u_2 in terms of density, the pressure change and the geometrical characteristics of the boundary. The coefficient of discharge is now defined by:

$$C_d = \frac{Q/b}{\sqrt{\dfrac{2\Delta p}{\rho}}} = \frac{C_c}{\sqrt{1 - C_c{}^2 (b/B)^2}}$$

(2.11)

Experiments indicate that the values of C_c listed in Table 2.1 apply with good approximation to the three-dimensional case as well, if the ratio b/B is replaced by a ratio of areas. Note that the coefficient of contraction is also defined as a ratio of the jet and orifice *areas* .

10

The Euler number. The special case of steady, irrotational flow, in which the only accelerative force is provided by a gradient in the fluid pressure provides a convenient basis for evaluating the effect of other forces like the gravitational force. The solution for the distribution of velocity and pressure around any given form of boundary is unique, and a particular value of the dimensionless ratio $\Delta p/(\rho u^2/2)$ characterizes the flow at each point in the flow pattern. The quantity $\Delta p/(\rho u^2/2)$ may be considered to represent the ratio of a typical unit accelerative force $(\Delta p/L)$ to a typical unit inertial reaction $(\rho u^2/2L)$; its constancy is seen to result from the fact that no other force than fluid pressure is assumed to act.

If other forces like gravity or viscosity are playing a significant role, the ratio $\Delta p/(\rho u^2/2)$ does not remain constant. The non-dimensional Euler number is then defined as the parameter:

$$Eu = \frac{u}{\sqrt{2\Delta p/\rho}} \tag{2.12}$$

Comparison with Eq. 2.11 shows that the Euler parameter is identical with the discharge coefficient. The Euler number provides a quantitative measure of the importance of other forces than the pressure gradient (e.g. gravity, viscosity) in the flow pattern.

Gravity and the Froude number. The integration of the Euler Eq. 2.7, yields the Bernoulli theorem, a relationship between any two points on a streamline for rotational inviscid steady flow:

$$p + \rho \frac{1}{2} u^2 + \rho g z = cst \tag{2.13}$$

For irrotational flow, Eq. 2.7 may also be integrated along lines normal to the streamlines and the constant in Eq. 2.12, has the same magnitude throughout the moving fluid (Boussinesq approximation). With the continuity equation, the velocity and pressure distribution are determined by the boundary geometry.
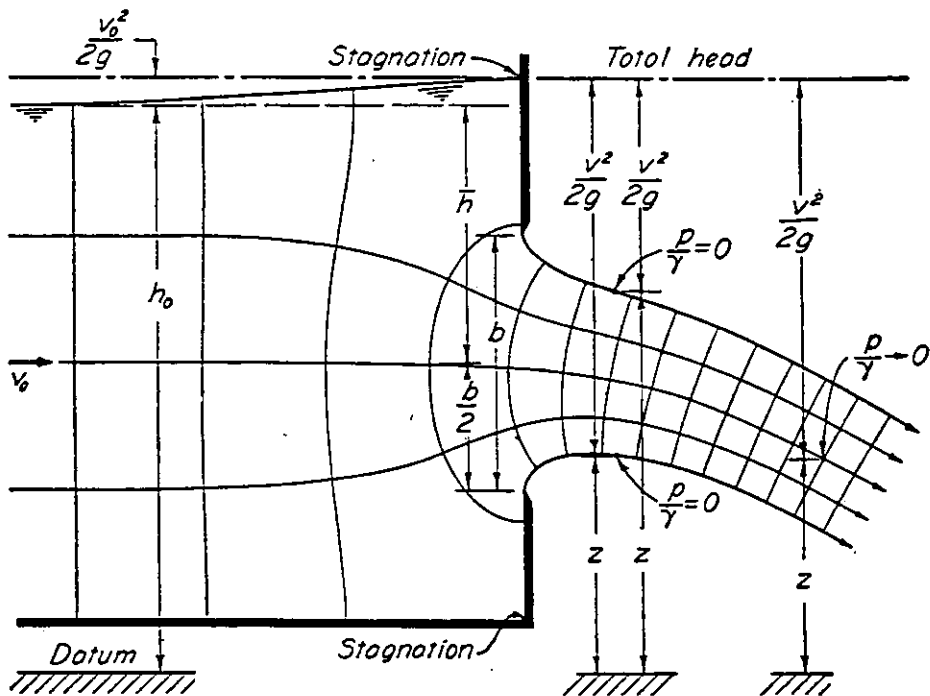

Fig. 2.2. Perfect fluid flowing out of a container forming a jet (Rouse, 1946).

A typical case where gravity is partly responsible for the fluid acceleration is where fluid flows out of a container in the form of a horizontal jet (Figure 2.2). We recall that for a perfect fluid (irrotational flow) this picture, the discharge of a fluid into the atmosphere, is similar to the case of two fluids of different densities, one penetrating into the other; the density in the Euler equation being replaced by the density difference (Eq. 2.5). For our requirements, the description of outflowing air through a window is completely analogous where h is the neutral level i.e., the level where inside and outside air pressures are equal.

The hydrostatic pressure inside the container is given by Eq. 2.1, the surface of the liquid being at atmospheric pressure, p_{atm}. So long as the distance h, between the fluid level in the container and the center of the slot is large with respect to the opening height b, the average pressure difference $\Delta p = \rho g h$ is well defined. From Eq. 2.12, the mean velocity of the contracted jet is $\sqrt{(2gh)}$, and the volume flow rate is calculated with the help of Eq. 2.10. The free surface of the jet is required to be at p_{atm}, and according to Eq. 2.12, for every point of the jet profile $\rho g z + \rho u^2/2 = p_{atm}$. Note that the form of the jet is similar to the ballistic path of a projectile.

The velocity at any point in the contracted jet will have the magnitude:

$$u = \sqrt{u_0^2 - \frac{2g}{\rho}(h-z)} \qquad (2.14)$$

where u_0 is the velocity of the approaching uniform flow, and where z varies between $\pm b/2$. For $h \gg b$, the velocity is nearly constant and the volume flow rate Q is easily found from the contraction coefficient Eq. 2.10. When the height of b can not be neglected compared with h, Q is obtained by integrating the product of velocity and local contraction factor over the opening. Because u_0 depends on the integral, the computation of Q requires iteration. Simplifications are possible when u_0 is approximately zero or when the local contraction coefficient can be replaced by a mean value.
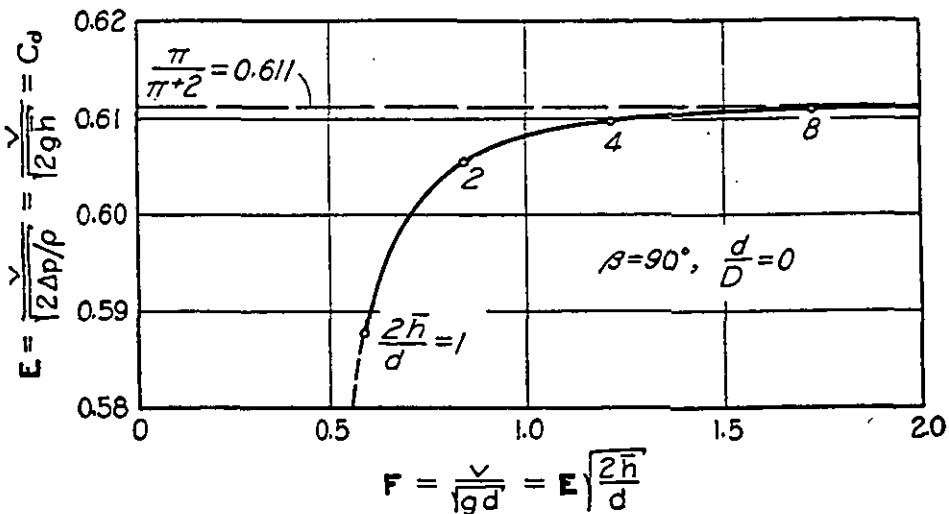


Fig. 2.3. Variation of the Euler number with the Froude number for a circular orifice.

For perfect fluids, the situation where $h < b/2$ (Figure 2.2), and called in hydraulics 'flow over a weir' [Rouse 1946], is completely analogous to the case of outstreaming air through a window, where the neutral level h, the height where inside and outside pressures are equal, is situated in the opening.

The Froude number. This number is used in hydraulics to compare the inertial and buoyancy terms in Eq. 2.7. For u, a typical velocity and L, a typical length scale characterizing buoyancy the Froude number Fr is defined by $Fr^2=u^2/gL$ and the larger the ratio the smaller will be the relative effect of gravity. When differences in density are significant, g is replaced by $g'=g\rho'/\rho_0$ (see Eq. 2.6) and the densimetric Froude number is defined as:

$$Fr = \frac{u}{\sqrt{g'L}} \qquad (2.15)$$

The inverse square of the Froude number $1/Fr^2$, is called *Richardson* number in the field of heat transfer, or *Archimedes* number, Ar, in ventilation engineering. Ar is used in the latter field to characterize non-isothermal jet behavior. Note, that for a perfect gas the relative density difference, ρ'/ρ_0, equals the relative absolute temperature difference, $\Delta T/T$, and so $g'=g\,\Delta T/T$.
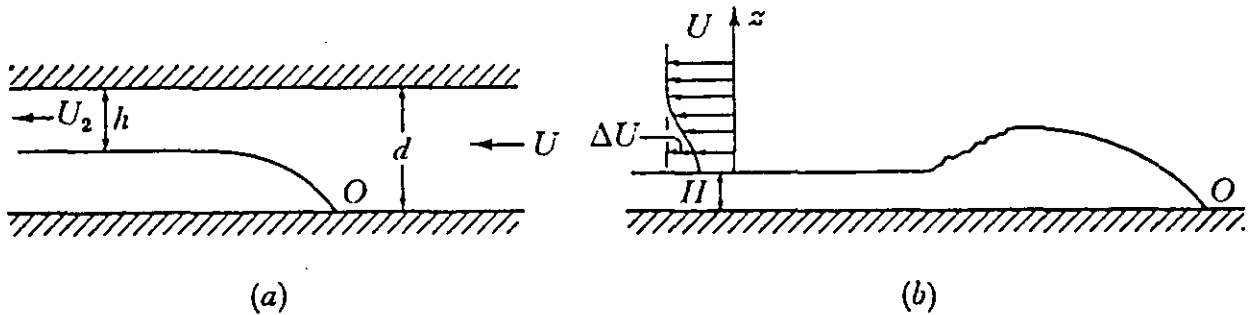

Figure 2.4. Two-dimensional flow of a heavy layer. (a) Frictionless flow in a channel, (b) a real flow under a deep lighter layer *(Turner, 1973)*.

Gravity current. The phenomena of cold air entering a hallway after the opening of a door is treated in the literature as a gravity current. This approach is illustrated in Figure 2.4 with the 'lock exchange' problem, for two-dimensional frictionless flow entering a channel of depth d, at a velocity u. Because the channel is closed, continuity requires the lighter fluid to flow out through the top of the entrance forming an interface at the neutral level near midheight. Application of the continuity and Bernoulli equations near the interface *[Turner, 1973]*, shows that the Froude number based on the channnel height d, $Fr=u/(g'd)^{0.5})$ equals 0.5. Calculating also the Euler number (2.12) using for Δp the maximum hydrostatic pressure difference $\rho g'd/2$, it is found that the Euler and Froude number become identical. This allows interpretation of Fr=Eu=0.5 as a discharge coefficient. Interestingly, now taking d equal to the opening height and increasing the channel height, Fr increases to about 0.6 which is the value of the contraction coefficient .

The Reynolds number. This non-dimensional number compares the relative importance of inertial forces and viscous forces, and depends on the flow velocity u, the typical length L (e.g. the opening diameter) and the kinematic viscosity ν :

$$Re = \frac{uL}{\nu} \qquad (2.16)$$

The energy dissipation and therefore the pressure loss in a duct increase with Reynolds number and duct length. For large openings in buildings, the 'duct length' is generally small and for natural convection the Reynolds number is generally less than 10^5. An evaluation of the Reynolds number dependence of the discharge coefficient can be made *[Lamrani 1987]*. A discussion of the fundamentals of airflow in ducts can be found in handbooks on air-

conditioning engineering *[e.g. ASHRAE 1989; Jones 1985]*. When viscous pressure losses are included, flow coefficients can be defined as a function of the Reynolds number, or otherwise when pressure loss terms are included in the Bernoulli equation it is called the generalized Bernoulli equation. In practice however, the effects due to flow contraction and to viscous effects are difficult to separate. In particular when there is two-way flow in an opening, the velocity and the Reynolds number increase with the distance from the neutral level. Therefore the use of a phenomenological 'discharge coefficient' is widespread, and various interpretations of its measured value are possible.

2.1.3 Application of the Bernoulli equation

The classical approach of the so-called gravitational flow assumes air flows through large openings to be driven by density fields on both sides of the opening. Each room is considered as a semi-infinite reservoir, all walls are assumed to be in thermal equilibrium with the air enclosed in each cavity, i.e. no boundary layer flows, and each streamline is assumed to be horizontal.

The usual way to solve this general problem is to apply Bernoulli's equation in the plane and on both sides of the opening, which is limited to non-viscous, incompressible flow and valid for a stationary flow regime.

Assuming hydrostatic pressures (Eq.2.1) on both sides (labels o and i) of the opening, then the velocity in the opening $u(z)$ is obtained from Eq. 2.8. First assuming $z_0 = z_i$ (i.e. a horizontal streamline), the pressure difference P_0-P_i is known by taking taking two points far from the opening where the velocities are about equal. Then using $u^2 >> u_o^2 - u_i^2$, the velocity in the opening is :

$$u(z) = \left[\frac{2}{\rho}\left((Pi_0 - Po_0) - gz\,(\rho_i - \rho_o)\right)\right]^{1/2} \tag{2.17}$$

where ρ is the density of the flowing medium. This velocity is the maximum theoretical velocity in a non-viscous fluid. This reasoning can be generalized for ideal fluids (to curved streamlines in the flow through a 'window' as in Figure 2.2), by considering the horizontal velocity component rather then the velocity along a streamline.

The mass flow below the neutral plane at $z=z_n$ is obtained directly by integration of Eq. 2.17 :

$$\dot{m}_{0,Zn} = Cd\,W\int_0^{Zn} \rho_0(z)\,u(z)\,dz \tag{2.18}$$

In Eq. 2.18, Cd is called the discharge coefficient which for real fluids is a phenomenological coefficient. It includes both viscous effects and local contraction of the flow due to the presence of an opening. Similar to Eq. 2.18, the mass flow above the neutral level is obtained by integration between $z=Zn$ and H. The position of a single neutral plane Zn is defined for general (not crossing) density profiles by writing the mass conservation through the opening. In a computer programme, Zn can then be obtained numerically by an iteration procedure. Multiple neutral levels (Figure 2.7) are to be expected when the two zone-temperature profiles are crossing, one additional neutral level for each crossing *[Otis and Jones, 1988]* .

The approximations used in practice, can be distinguished according to the degree of detail that is taken into account for the density function. While Eq. 2.17 is general and valid for all density profiles $\rho=\rho(z)$, approximate solutions with only a few input parameters are preferred for example for use in multi-zone models. *Simplifications that are frequently used are (i) the density of the air in each zone is constant, (ii) the temperature of the air varies linearly with height and, (iii) the density of the air varies linearly with height.* In the following sections it will be shown how these cases are worked out.

2.1.3.1 Constant air density/temperature approximation. Many authors have dealt with the approach of constant air density (or temperature) for each zone *[Emswiler 1926, Brown and Solvason 1962, Graf 1964, Shaw and Whyte 1974, Shaw 1976, Lidwell 1977]* and provided elementary solutions of purely natural convection or mixed convection (Figure 2.5).
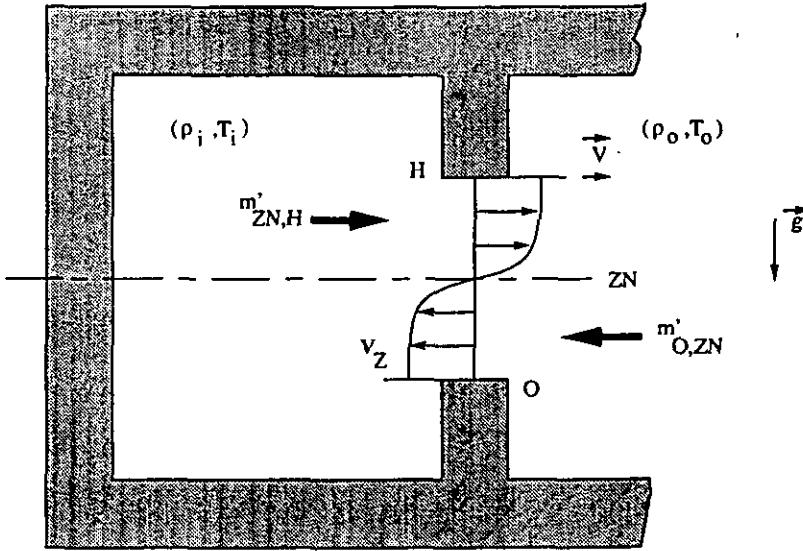

Figure 2.5: The basic problem of gravitational flow through a vertical opening.

Without net flow, the classical approach assumes a neutral level at H/2, but we can precisely calculate the position of the neutral plane Zn. The latter is defined by writing the mass conservation through the opening which leads to ($\rho_0 > \rho_i$):

$$\frac{Zn}{H - Zn} = \left(\frac{\rho_i}{\rho_0}\right)^{1/3} \approx 1 - \frac{\rho_0 - \rho_i}{3\rho_0} \tag{2.19}$$

When the zone density depends only on temperature, the Gay-Lussac law for gas expansion is used to relate densities and temperatures:

$$\rho = \rho_0 \left(1 - \beta \left(T - T_0\right)\right) \quad \Rightarrow \quad \frac{\rho_0 - \rho}{\rho_0} = \frac{T - T_0}{T} \tag{2.20}$$

where temperatures are in Kelvin and β is the expansion coefficient for perfect gases ($\beta = 1/T$). From Eq. 2.19 it is seen that the neutral plane in this isothermal zone model stays rather close to the middle of the opening: for example a density decrease of 3% causes a shift in Zn of about 1%, this means for dry air at room temperature (T $\approx$ 300K) a 10K temperature increase, or about 3% absolute humidity (moisture content) increase.

At the end, a direct integration of the velocity from the bottom of the opening to Z_n, delivers the value of the mass flow:

$$\dot{m}_{0,Zn} = Cd \frac{W}{3} \left(8 g H^3 \rho_i \Delta \rho\right)^{0.5} \approx Cd \frac{W}{3} \left(g H^3 \rho_i \left[\Delta \rho + \frac{\Delta \rho^2}{2\rho_0}\right]\right)^{0.5} \tag{2.21}$$

where the term ρ_i' is given by:

$$\rho_i = \frac{\rho_i}{\left(1 + \left(\frac{\rho_i}{\rho_0}\right)^{1/3}\right)^3} \approx \frac{\rho_i}{8}\left[1 + \frac{\rho_0 - \rho_i}{2\rho_0}\right] \qquad (2.22)$$

and the expansion to first order in $\Delta\rho = \rho_0 - \rho_i$, is for later comparison with the literature.

Supply air. In the case of a supply of air in one zone, the solution of the gravitational flow through the opening can be obtained in a similar way as the basic solution by writing a new mass balance equation through the opening *[Shaw and Whyte 1974, Shaw 1976]*: .

$$m_S' - m_{12}' + m_{21}' = 0 \qquad (2.23)$$

Figure 2.6 describes this new configuration where a flow m_S' is provided to zone 1, m_{12}' represents the mass flow going from zone 1 to zone 2, and m_{21}' the flow from zone 2 to 1.
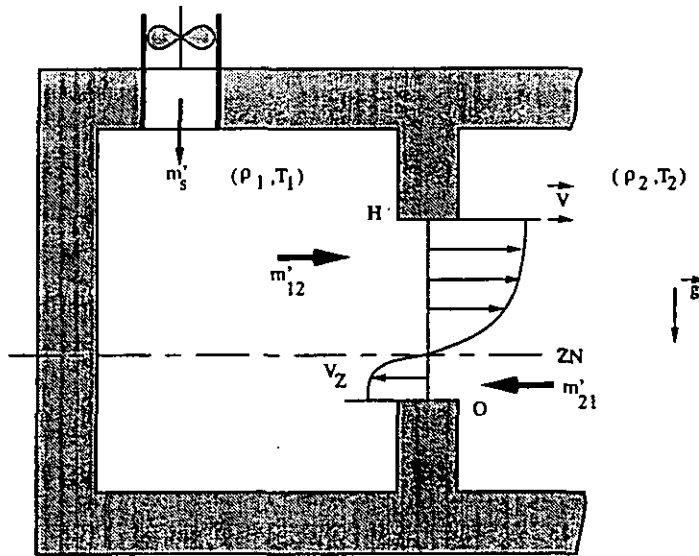
Figure 2.6 : Supply of air in one zone.

Finally the position of the neutral plane Zn is given by an *implicit equation*:

$$m_N' \left[\left(\frac{Zn}{H}\right)^{3/2} - \left(\frac{\rho_i}{\rho_0}\right)^{1/2}\left(1 - \frac{Zn}{H}\right)^{3/2}\right] + m_S' = 0 \qquad (2.24)$$

With

$$m_N' = \frac{2}{3} Cd\, \rho_0 W \left[2g\frac{\Delta\rho}{\rho_0}\right]^{1/2} H^{3/2} \qquad (2.25)$$

For large absolute values of m_S' or small values of $\Delta\rho$, Zn is not situated in the opening, and Eq. 2.24 can not be used.

The *simplest case of zero-supply, constant temperature difference and the neutral level at half door height* leads to a practical estimate for the massflow [in kg/s]:

$$m' \approx \frac{1}{3} Cd \, \bar{\rho} \, WH^{3/2} \, \Delta T^{1/2} \sqrt{\frac{g}{T}} \approx 0.04 \, WH^{3/2} \, \Delta T^{1/2} \qquad (2.25a)$$

2.1.3.2 Linear pressure or temperature gradients. In the preceding problem the air density in both zones is presumed to be uniform. Uniform air density is a good approximation when the vertical temperature variation over the opening height in each zone is much smaller than the horizontal temperature difference. In fact, because of thermal stratification, or gradients of concentration of any species (humidity, pollutants), this assumption is restrictive and does not allow for the general behavior of a large vertical opening.

A density ρ depending only on temperature can be written in terms of reference temperature T_0 and corresponding density ρ_0 (Eq. 2.20), $\rho = \rho_0 T_0/T$. A linear temperature variation $T = T_0 (a+bz)$ then corresponds also to a nearly linear density variation. In fact this is true to first order in the ratio b/a,

$$\rho = \frac{\rho_0}{a+bz} \approx \frac{\rho_0}{a} \left(1 - \frac{b}{a} z\right) \qquad (2.26)$$

the error in the approximation being of order $O((b/a)^2)$. Putting in some numbers, this means that for temperature gradients as large as 10K/m, the error is only 0.1%. This is insignificant compared to the uncertainty in the linearization of an experimental temperature profile which easily amounts to an error of few percent. Therefore, while for the comparison of numerical codes 0.1% is considered significant, in the practice of the modeling of air flow in buildings the difference between a linear temperature profile and a linear pressure profile, can be neglected.

It is interesting to note that with the same vertical pressure gradient in each room, the calculated velocity profiles are not modified because the interzone pressure difference is independent of height. However, zone temperature gradients always modify the inter-zone heat transfer (see section 2.2.1).

These effects of temperature gradients have been pointed out by several authors dealing with air flow circulation in passive solar buildings. In fact, in various experimental studies *[Balcomb et al.,1983; Weber, 1980; Hill et al., 1986; Pelletret, 1989]*, it appears that most of the configurations can be represented quite well by uniform temperature gradients, without considering density differences caused by humidity or pollutants.

The main consequences of the interzonal horizontal temperature difference approaching the total vertical temperature variation are, a shift in neutral level and an asymmetric velocity profile. When the interzonal temperature difference is further reduced various neutral levels may appear in the height of the opening. Since the vertical density gradient is generated by the complete flow pattern existing in the room being considered, it is impossible to give an exhaustive description of the problem and many neutral planes may theoretically exist. *Otis and Jones [1988]* discuss this point and show that every crossing of the two temperature profiles in the zones, corresponds to an additional neutral level; a simple geometric method can then be used for locating the multiple neutral planes knowing one of them. The assumption of linear temperature profiles therefore limits the number of neutral levels to two, i.e. only one crossing of the profiles is possible. With a complementary assumption of constant density gradients, a complete set of equations giving the position of the two possible neutral planes and the values of the flow both ways can be developed.

Hill [1985] studied the case of density gradients due to a linear thermal stratification in a two zone configuration and then extended the method to more complex configurations. The neutral planes occur at the heights at which the zone pressures are the same and the horizontal velocity in the aperture is equal to zero (Figure 2.7).

17
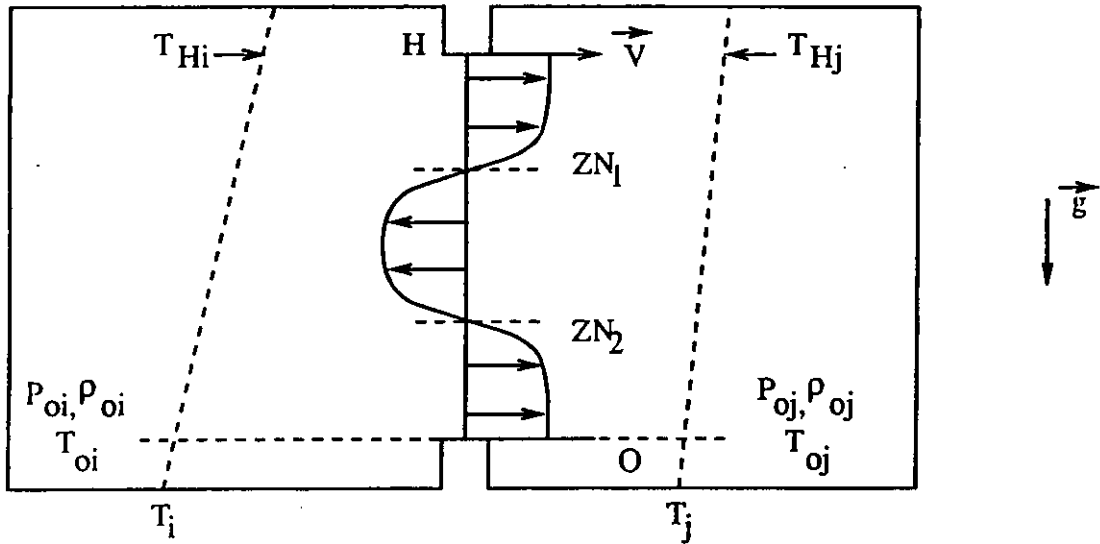
Figure 2.7: Illustration of a linear temperature stratification configuration.

With uniform temperature gradients in the zones, $T_i(z)=T_{0i} + b_i\, z$ and $T_j(z)=T_{0j} + b_j\, z$), the horizontal velocity in the aperture is still given by Bernoulli 's equation under a new formulation. Using Eqs. 2.17, 2.20 and 2.26,

$$u(z) = \left[\frac{2}{\rho}(P_{0i} - P_{0j}) + 2\beta g\left((T_{oi} - T_{oj})z + (b_i - b_j)\frac{z^2}{2}\right)\right]^{1/2} \tag{2.27}$$

The mass transfer is then determined by the continuity equation applied at the opening. Eq. 2.28 gives the general form of the continuity equation in the case of two neutral planes in the opening:

$$W\, Cd\left[\int_0^{Z_{n2}} \rho\, u\, dz + \int_{Z_{n2}}^{Z_{n1}} \rho\, u\, dz + \int_{Z_{n1}}^H \rho\, u\, dz\right] = 0 \tag{2.28}$$

where ρ represents the density of flowing air. Since the unknown reference pressures are contained in both neutral height definitions and the integrals, a numerical method has to be used to find these pressures and finally solve the problem. *Pelletret and Khodr-Mneimne [1988]* describe such a method valid for any kind of temperature profile as long as there are two or less neutral planes.

2.1.4. Comparison of experimental values for the discharge coefficient

In all the preceding equations, the discharge coefficient Cd depends both on the contraction coefficient Cc, characteristic for the opening shape (§2.1.2), and on the character of the flow. The value of the contraction coefficient for sharp-edged orifices is 0.6 and for inviscid irrotational flow, Cd≈Cc for the flow out of a large container (Figure 2.1 and Table 2.1). Pressure losses on the other hand are expected to decrease the value of Cd, as a function of the Reynolds number. A brief review indicates that these values can be as low as 0.25 and up to 0.75 for large openings.

18

Mahajan and Hill [1986], in an experimental study of interzonal natural convection for various aperture configurations, mentioned Cd values of 0.33; in another study *[Mahajan 1986]* Cd≈0.45 for a wide range of interzone temperature differences 0.5<ΔT<15. The zones were strongly stratified but an isothermal.zone temperature model was used for the analysis.

In a detailed study of the time-dependence of the flow, *Wilson and Kiel [1990]* report on short duration (up to 120 s) gravity driven flow through an open exterior door in a sealed room. The discharge coefficient Cd, is found to depend on the interzonal temperature difference (Figure 2.8) and increases from 0.4 to 0.6. They propose the correlation *[see also ASHRAE, 1989]*.

$$Cd \equiv K = (0.4 + 0.0045\Delta T), \quad 0.5<\Delta T<40 \qquad (2.28a)$$
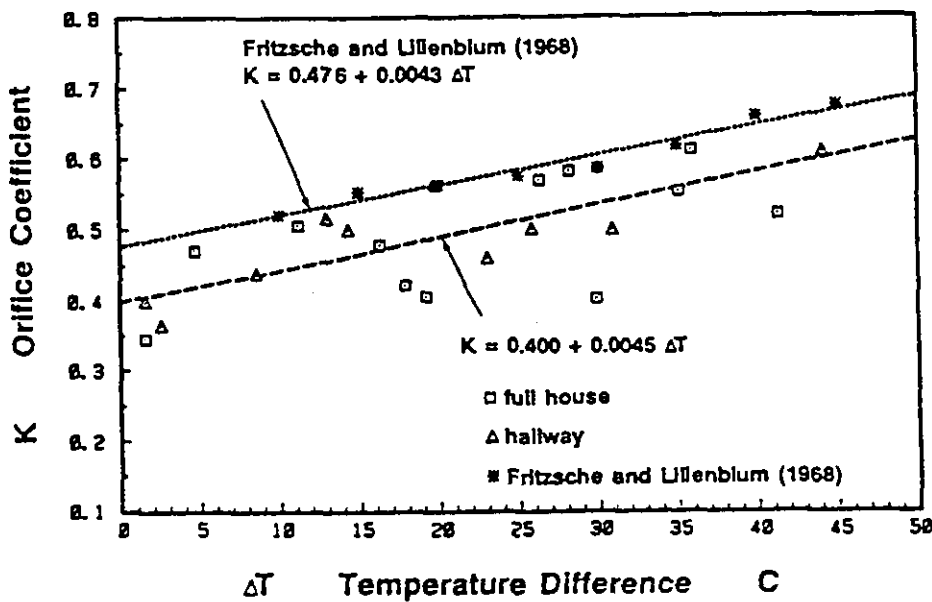

Figure 2.8 Measured discharge coefficient as a function of inside-outside temperature difference; K≡Cd *(Wilson and Kiel 1990)*.

Nevertheless, they obtained values around 0.60 for a scale model using fresh water and salt solution. The values of Cd are interpreted as the combined effect of streamline contraction (Cd=0.6) and mixing of the hot and cold airstream at the neutral level (Figure 2.9a). They explained the low values of Cd found in the real scale experiment by pointing out an important interfacial mixing at low temperature differences. This mixing between the inflow and outflow results in a modified velocity profile near the interfacial layer (Figure 2.9b).

The higher values given by the model are due to a lower Reynolds number. This leads to a more stable flow and decreases the interfacial mixing effect. About 15% higher K values were found *[Fritzsche and Lilienblum, 1968]* measuring orifice coefficients on the door of a cold room. This difference is attributed to differences in ambient turbulence levels.

These conclusions contradict Riffat's results. *Riffat [1989]*, in a very different setup where the air flow between the upper and lower level of a house were studied, found the discharge coefficient to decrease with interzonal temperature differences. Cd varying from 0.6 for a temperature difference of 1K, to 0.25 for 10K.

19
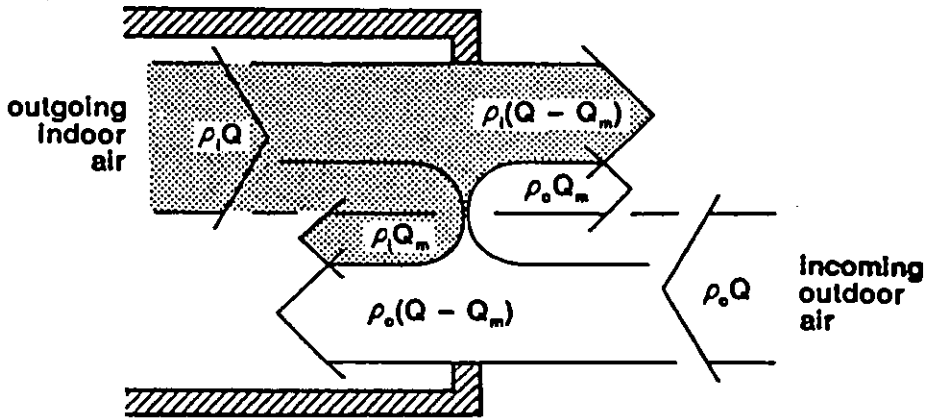
Figure 2.9a Reentrainment by cross-stream interfacial mixing between counterflowing streams (Wilson and Kiel 1990).
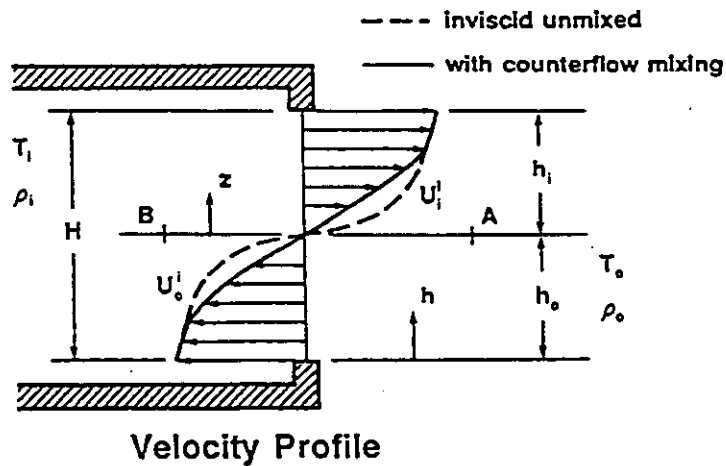
Velocity Profile
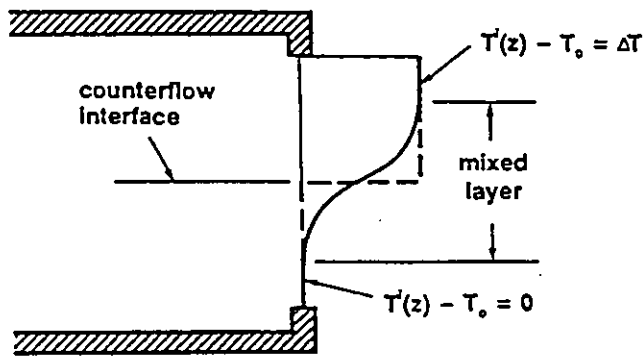
**Temperature Difference Profile**

Figure 2.9b Inviscid and actual velocity and temperature profiles in the doorway of a sealed room. (Wilson and Kiel 1990).

Pelletret [1990] and Allard and Utsumi [1992], in studies of the variation of the discharge coefficient with Reynolds number over the opening height, find values of up to Cd≈0.8. They tested the assumption of the Bernoulli model, said to be one-dimensional, that the *horizontal* air velocity *component* (which determines the flowrate) can be calculated at every height from the hydrostatic pressure difference between the zones; this means that the influence of the vertical force of gravity on the horizontal flow rate is neglected, that friction has a negligeable effect, that the flow is irrotational (no mixing), and that the air in each zone is at rest.

Also recently, *Van der Maas et al. [1989]*, reproduced the *Lane-Serff et al. [1987]* experiments in a water model leading consistently to the theoretically expected value for the Froude number, which means that only flow contraction is significant. They also reproduced results in air of *Hill et al. [1986]* who, using a Bernoulli model including stratification, found Cd≈0.75 from velocity measurements in the central vertical plane of the opening. They concluded that because the velocity profile in the opening can become very asymmetric due to stratification, one should not analyse such a situation as if the velocity profile was parabolic (i.e. zones of uniform temperature). Using the wrong model would than necessarily lead to Cd values that are too low.

Finally, noting that all authors claim close correlation between their data and the model chosen, it becomes clear that more precision is needed in the definition of the discharge coefficient, and in the experimental conditions used for its determination.

2.1.5 Boundary layer flows

Since the experimental work of *Janikowsky et al. [1978]*, many quantitative studies have been done of pure natural convection flows between two zones. Two-dimensional partitions have been considered *[Bejan and Rossie, 1981; Nansteel and Greif, 1981]*.
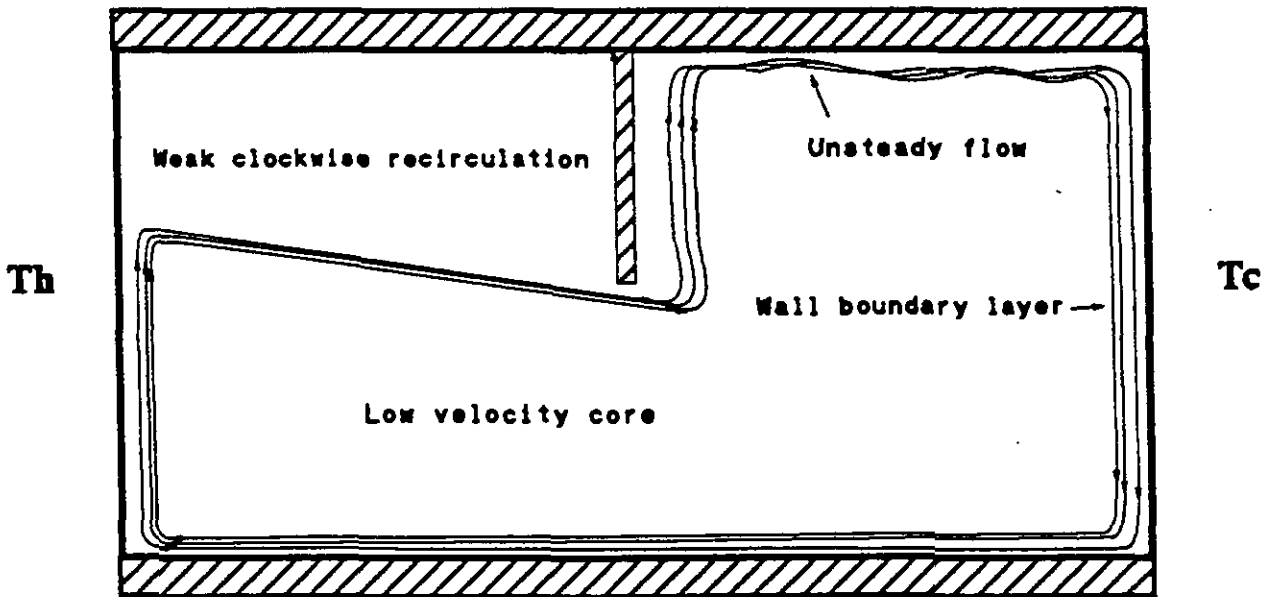

Figure 2.10 Schematic diagram of two-zone enclosure and typical boundary layer flow pattern as observed by Nansteel and Greif for $10^{10} \leq Ra_L \leq 10^{11}$

In this last case the flow visualization revealed the existence of three relatively distinct regions at Rayleigh numbers of approximatively 10^{11}. As shown in Figure 2.10, the flow pattern consists of an inactive core with very low velocities in the central part of the opening, a region of very weak circulation in the upper part of the warmer cavity (or in the lower part of the colder space) and a peripheral boundary layer flow dominating the process.

These results were confirmed by *Bajorek and Lloyd [1982]* at lower Rayleigh numbers, by *Lin and Bejan [1983]* and by additional experiments of *Nansteel and Greif [1984]* on three-dimensional partitions.

Numerical simulations in laminar regime developed by *Kelkar and Patankar [1987]* and *Goux [1987]* are in good agreement with these experiments. More recently, simulations at high Rayleigh numbers by *Haghigat et al. [1990]* showed agreement for three-dimensional cases.

An interesting result of these studies is that a partition tends to damp out the flow in subregions that are subjected to stable boundary conditions. This effect reduces the effective wall area exposed to the primary flow, as can be seen in the flow patterns shown on Figure 2.10. This reduction in actively participating surface area produces a proportional reduction in heat transfer when compared to an enclosure without intervening partitions. The reduction results from the formation of a relatively hot, stagnant layer of air near the ceiling of the hot zone. It is worth noting, that this can only occur for boundary conditions where the heat flow is downward : when the ceiling in the hot zone is relatively cold and heatflow is upward, the flow will tend to go up and along the ceiling.

2.1.6 Horizontal openings

To complete the overview of the literature concerning bulk air flow through large openings, horizontal openings should be discussed.
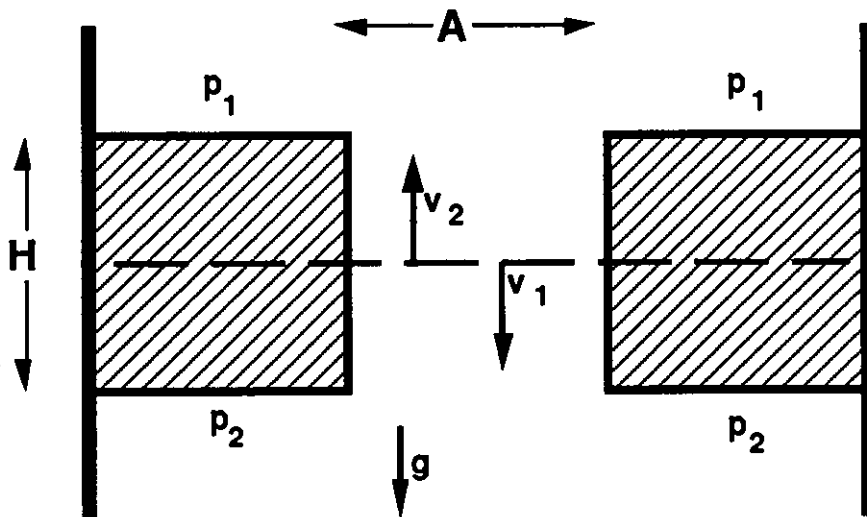

Figure 2.11. Schematic representation of natural convection through an opening in horizontal position

One-way flow. The simplest way to represent a horizontal opening in multizone modeling is by providing a discharge coefficient and treating the relation between pressure difference and flow as for crack-flow This description of one-way flow however, does not include the

threshold-effect. This means that when the air density above a partition of thickness H, is lower by $\Delta\rho$, there will be no flow as long as the pressure difference has not exceeded the value $\Delta\rho gH$. If on the other hand the dense fluid is above and two-way flow would naturally occur, the pressure difference needed to suppres the counter current is expected to be near the value $\Delta\rho gH$. For practical cases the numerical value of this pressure is a fraction of a pascal and probably not significant. However, we do not know of any study of this particular effect.

Two-way flow. For the modeling of the spreading of contaminants, it is important to know when two-way flow exists and how it behaves. The most interesting aspect of horizontal openings is that in which the fluid above the opening has a greater density than the fluid below. In this case an unstable condition is reached and an exchange occurs between the lighter fluid *flowing upward and the heavier flowing downward.*This problem was first studied in air by *Brown [1962]*, but few authors have made a consistent contribution towards solving it. Also the situation can become special when the opening is part of a natural convective loop (as can be found for example in staircases heated from below).

In a recent paper *Epstein [1988]* discusses the buoyancy exchange flow through small openings in horizontal partitions. He presents an experimental study using brine above the partition and fresh water below the partition and identifies four different regimes as the aspect ratio L/D (partition thickness, L, to diameter of the opening, D) is increased. Figure 2.11 describes this configuration.
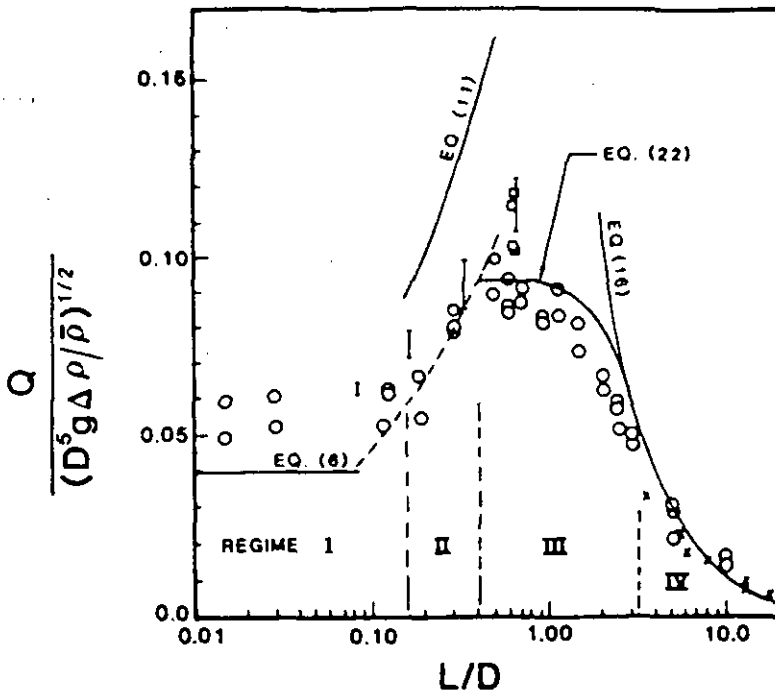
Figure 2.12 Experimental results for counter-current exchange flow through a single horizontal opening.

The measured volume exchange rate Q, is transformed into a dimensionless Froude number and plotted in Figure 2.12 as a function of the aspect ratio L/D. The four flow Regimes are marked I to IV. One can note that Q/D^2 represents an average flow velocity, $(Lg\Delta\rho/\rho)^{0.5}$ represents the maximum Bernoulli velocity based on the partition height L, and the dimensionless Froude number $(Q/D^2) / (L\, g\Delta\rho/\rho)^{0.5}$ would be a constant for Bernoulli flow. This number multiplied by $(L/D)^{0.5}$ is an increasing function of L/D for Bernoulli flow (regime II in Figure 2.12).

Regime I: L/D is smaller than 0.1. Taylor instability leads to the intrusion of each liquid into one another and an oscillatory exchange is observed. Applied to a building and for example

using a partition thickness of 0.2m, Regime I would apply to openings larger than 2m in diameter.

Regime II: L/D in the range 0.1 to 0.4. The flow rate is obtained by applying Bernoulli's equation and assuming that the pressure losses are due entirely to entrance and exit losses. The exchange flow data with air *[Brown, 1962]* are shown to be consistent with the newer data obtained with fresh and salt water.

Regime III: For intermediate values of L/D (range 0.4 to 3), there is combined turbulent diffusion (see discussion of regime IV) and Bernoulli flow.

Regime IV: The progress of each liquid into the other was observed to be much slower in vertical tubes with large L/D (>3) than in the other three regimes investigated by Epstein. The countercurrent flow appeared to comprise packets of low and high density liquid, the motion of the packets was chaotic and random in appearance and the process was viewed as one of turbulent diffusion. The measured rates are correlated by the Froude number and are in approximate agreement with a $(L/D)^{-1.5}$ dependence of Q, as predicted by the proposed turbulent diffusion model.

This paper of *Epstein [1988]* gives a good description of the flow processes but it remains limited to purely natural convection effects, but the results seem difficult to extend to more general configurations.

Much more work is needed to describe accurately the behavior of horizontal openings in natural or mixed convection configurations. The few papers found in the literature do not allow us to include such configurations in a multizone infiltration code.
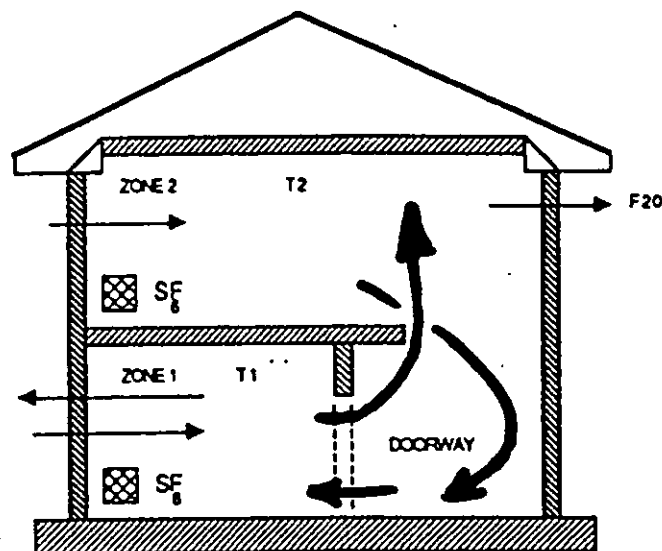
Figure 2.13 Interzone air flows in a house via a doorway *(Riffat, 1989)*.

Two more situations where air flow through horizontal partitions plays a role are illustrated in Figures 2.13 and 2.14. First there is the example of interzone air flows in a house via a doorway which have been studied by *Riffat, [1989]*. The room at the ground floor is heated with convective heaters. The hot air flows via the top of the doorway to the staircase to the top of the first floor, while the cold air flows from the bottom of the first floor via the staircase to the bottom of the ground floor, causing counterflow to exist in the staircase (Figure 2.13). The flow is interpreted in terms of a single discharge coefficient as a function of the temperature difference between the centres of the upper and lower floor. It is observed that the discharge coefficient decreases strongly with temperature difference. This represents the combined effect

of the counterflow in the staircase and the air flow through a door in the presence of (probably) strong stratification. It is difficult to interpret the flow through the staircase in terms of the parameter L/D for a horizontal partition, also because the air flow is not evenly distributed over the cross-section.
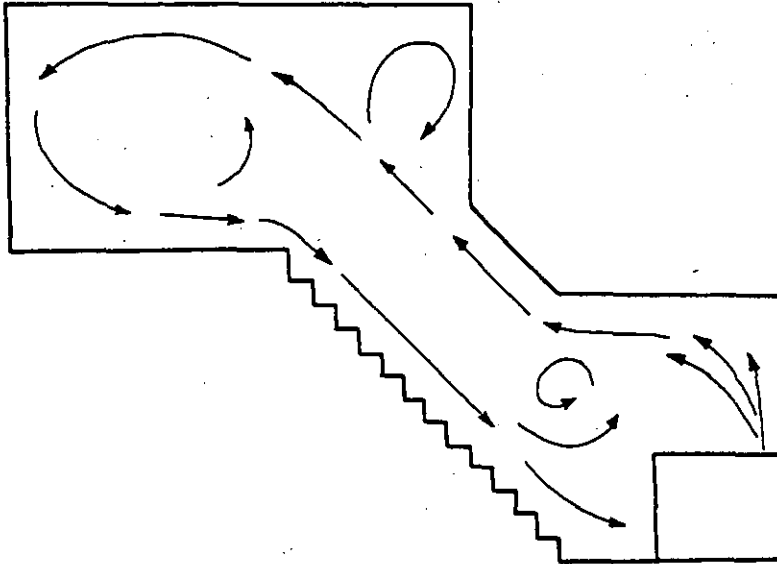
Figure 2.14 A two-dimensional view of the flow pattern in a stairwell; sloping ceiling (Zohrabian et al. 1989)

As a second example (Figure 2.14), we have 'buoyancy driven flow in a stairwell' model studied by [Zohrabian et al. 1989]. Two-way boundary-layer flow dominates and a horizontal partition is difficult to identify. The interpretation of the results in terms of a multizone ventilation model does not seem to be straight forward.

2.2   Heat Transfer Through Large Openings

Since one of the main consequences of large opening behavior, pointed out in recent decades, was their influence on the thermal behavior of buildings, many authors have looked for empirical correlations giving the total heat transfer rate through the opening as a function of its geometry and of the thermal state of each zone.

Brown and Solvason [1962] were the first to conduct heat transfer measurements in an air-filled enclosure that was divided into hot and cold regions by a single partition with a centrally located rectangular opening. The analysis in their publication has become the reference for later studies of interzonal natural convection heat transfer. However, we will first show the general procedure to calculate heat flows as an application of the Bernoulli equation.

2.2.1   Heat transfer calculation with the Bernoulli equation

Once the mass flows are calculated by integrating the velocity profiles (Eq. 2.17 and 2.18) and the neutral level found from the requirement of mass conservation (Eq. 2.28), the heat flow (enthalpy flow) through a large opening can also be calculated. The simplest picture is obtained when the zone temperatures can be considered constant, and the heat flow in each direction equals the product of massflow, temperature and heat capacity at constant pressure C_p. The net heatflow (in Watt) is then written as (Figure 2.6),

$$\Phi = \Phi_{12}\text{-}\Phi_{21} = Cp\,(m_{12}'\,T_1 - m_{21}'\,T_2)\tag{2.29}$$

For a general temperature profile an integration over height, below and above the neutral level, has to be performed, for example

$$\Phi_{0,Zn} = C_p\,Cd\,W\int_0^{Zn} \rho_0(z)\,u(z)\,T_0(z)\,dz\tag{2.30}$$

and the net heat flow equals $\Phi = \Phi_{0,Zn} - \Phi_{Zn,H}$.

Because when each zone has the same vertical temperature gradient, the zone temperature difference is independent of height and the massflows are not modified (section 2.2.1), an approximate analytical expression can be found for the case of linear temperature profiles and no net massflow.

The heat flow is then expressed in terms of an average zone temperature difference, ΔT, and the temperature gradients b_h and b_c for the hot and cold zones respectively *[Balcomb et al. 1983, 1984; Boardman et al. 1989].:*

$$\Phi = m'\,C_p\,[\Delta T + 0.3H(b_h + b_c)]\tag{2.31}$$

This approximation should be valid when there is no net massflow and for temperature gradients that are not too different.

2.2.2 Heat transfer correlations

Inter-zone convective heat transfer in buildings is reviewed in detail by *Barakat [1985]*. With the basic assumptions of inviscid flow and isothermal fluid reservoirs *Brown and Solvason [1962]* derived the Bernoulli expression for mass flow m' (see Eq. 2.21, with $\rho_i' \approx (\rho_i - \rho_0)/2 = \bar{\rho}$) and the heat transfer through the partition by air flow between the hot and the cold zone: $\Phi = C_p \, m' \, \Delta T$. Defining the heat transfer coefficient

$$h_T = \Phi/(W \, H \, \Delta T) \tag{2.32a}$$

a Nusselt number $Nu_T = h_T H/k$ can be calculated where k is the thermal conductivity of the air. They demonstrated that the Bernoulli expression is equivalent to a correlation between non-dimensional scaling parameters:

$$Nu_T = \frac{h_T H}{k} = \frac{C}{3} \sqrt{\frac{g'H^3}{\nu^2} \frac{C_p \mu}{k}} = \frac{C}{3} \sqrt{Gr} \, Pr = \frac{C}{3} \sqrt{Ra \, Pr} \tag{2.32}$$

which is a relationship between Nusselt, and Grashof (or Rayleigh Ra=Gr Pr) numbers, based on the interzone air temperature difference, ΔT and the aperture height, H. In recent literature, Rayleigh numbers in the heat transfer correlations are preferred and not Grashof numbers (see discussion in *[Bejan 1984]* Chapter 4). For air this difference is a nearly constant factor Pr~0.7.

In order to show the dependence of the heat transfer on the dimensions of the aperture configuration, the enclosure height or length is chosen as the length scale and is used to define Nu and Ra numbers.

Using the room height, H_r, as a reference, Eq. 2.32 becomes :

$$Nu = \frac{C}{3} \left(\frac{W}{Wr}\right)^a \left(\frac{H}{Hr}\right)^b (Ra_H \, Pr)^c \qquad \text{with a=1, b=1.5 and c=0.5} \tag{2.33}$$

where H/Hr and W/Wr , are the ratios of doorway height to total room height and doorway width to total room width, respectively. The temperature difference used in the definition of Nusselt and Rayleigh numbers, ΔT, is the temperature difference between the fluid in the hot and cold zones.

For the understanding of experimental plots, it is useful to know the order of magnitude of the non-dimensional numbers i.e.

air : $\quad Ra \approx 10^8 \, \Delta T \, H^3 \qquad$ (Pr=0.7)

water : $\quad Ra \approx 10^{11} \, \Delta T \, H^3 \qquad$ (Pr=7) .

Wall temperature correlations. In many experiments the hot zone is heated by a vertical hot wall and the cold zone cooled by a cold wall. Nusselt and Rayleigh numbers are then based on the *difference in wall temperatures*, ΔT_w, allowing the interzone heat transfer to be correlated with the internal *surface temperatures* of the enclosure. The general form of the empirical correlation is still written as Eq. 2.33, but the exponents a, b, and c are smaller. Experiments on scale models were performed with water *[Nansteel and Greif 1984]* to study the influence of the opening width and height and the thermal conductance of the partition on the heat transfer between the hot and cold wall.

Nansteel and Greif [1981] observed a flow pattern as in Figure 2.10, exhibiting a low velocity core and fluid flow concentrated in boundary layers. The following correlations are reported ($A_p = H/H_r$):

$$Nu_L = 0.748 \, A_p^{0.256} \, Ra_L^{0.226} \tag{2.33b}$$

for a 2D water filled enclosure with conducting partition, and

$$Nu_L = 0.762 \, A_p^{0.473} \, Ra_L^{0.226} \tag{2.33c}$$

for a non-conducting partition. Note the particular choice of L as a characteristic length.

The flow pattern in a three dimensional enclosure was found to be very different from that in the 2-D case. Nevertheless similar correlations were found:

$$Nu_L = 1.19 \, A_p^{0.401} \, Ra_L^{0.207} \tag{2.33d}$$

Baumann et al [1983] presented results in terms of a heat transfer coefficient h and reformatted previous results taking H as a characteristic length :

$$h = 1.03 \, A_p^{0.47} \left(\frac{\Delta T}{H}\right)^{0.22} \tag{2.33e}$$

for the 2-D case, and

$$h = 1.95 \, A_p^{0.25} \left(\frac{\Delta T}{H}\right)^{0.22} \tag{2.33f}$$

for the 3-D case. In both cases ΔT was calculated as half the difference between the surface temperatures.

Correlations of interzone heat transfer results are derived from experimental data using a logarithmic plot of Nusselt versus Rayleigh numbers (e.g. Figure 2.16b), but a problem in the use of these correlations is that they are not universal but depend on the particular experimental configuration.

Barakat [1985] in his review of existing correlations notes that heat transfer through a large opening of height H can be estimated by a general correlation in the form of

$$\frac{Nu_H}{Pr} = C \, Gr_H^b \tag{2.34}$$

Where b is approximately 0.5, and C lies between 0.22 and 0.33 depending on the reference temperature difference. The temperature difference used to calculate the Grashof number can be the difference between the average room temperatures or the difference between the inflowing and outflowing air.

More recently, *Khodr-Mneimne [1990]*, using a full scale experiment where the heating source is made of electrical heaters proposed a general correlation of $Nu/Pr = C \, Gr^{1/2}$ for various sizes of large openings (from 0.46 to 1.85 m^2). For a standard large opening of 0.9 by 2m, C=0.29 was proposed. The objective of the work was mainly to give a general way to include the heat transfer due to the air flow crossing a large opening in more general thermal codes. Various reference temperature differences have been tested, and the author finally selected the difference in mean air temperature of each zone which is the usual parameter given by multizone thermal models.

2.3. Transition Between Bulk Density and Boundary Layer Flow

Anderson [1986] concluded that the natural convection flow regime that governs the flow through the aperture (density driven or boundary-layer driven flow) strongly affects the geometric dependence of the heat transfer. In the density driven flow, the heat transfer depends strongly on both the aperture height and the aperture width ratio. On the contrary, in the boundary-layer driven flow regime, the heat transfer depends weakly upon the aperture height ratio, and is independent of the aperture width ratio. Starting from these remarks, it should be possible to predict when the flow through an opening is due to bulk density effect or to boundary-layer flow. When reducing the width of an opening in boundary layer flow regime the flow will eventually be blocked. This blockage will result in the formation of large temperature differences across the doorway, and cause a transition from boundary layer flow to bulk-density driven flow. Anderson proposed a simple flow blockage criteria based on geometrical ratios:

$$\frac{W}{Wr} \frac{H}{Hr} \div \frac{N}{Ra_H^{*1/5}} \qquad (2.35)$$

where N is the number of active heat transfer surfaces in the room and Ra_H^* is the flux modified Rayleigh number.

Scott et al. [1988] recognized that there are two types of flow regime. In the density driven flow regime, the fluid temperature in each zone is close to the wall temperature (Figure 2.15a), and the *isothermality factor* , the ratio $\Delta T/\Delta T_w = (T_H-T_C)/(T_H'-T_C')$ is near to unity, and the velocity profile in the opening is nearly parabolic. Heat transfer is described by the correlation Eq. 2.33, with exponents b and c close to 1.5 and 0.5 respectively.

On the other hand, the boundary layer driven flow regime (Figure 2.15b) is characterized by a large temperature drop at the walls (the isothermality factor $\Delta T/\Delta T_w$ is nearly zero) and the flow is concentrated at the top and bottom of the aperture. Heat transfer is described by the correlation Eq. 2.33, with exponents b and c close to 0.4 and 0.2 respectively. This result is essentially the same as the 'wall temperature correlation' described in section 2.2.2 .
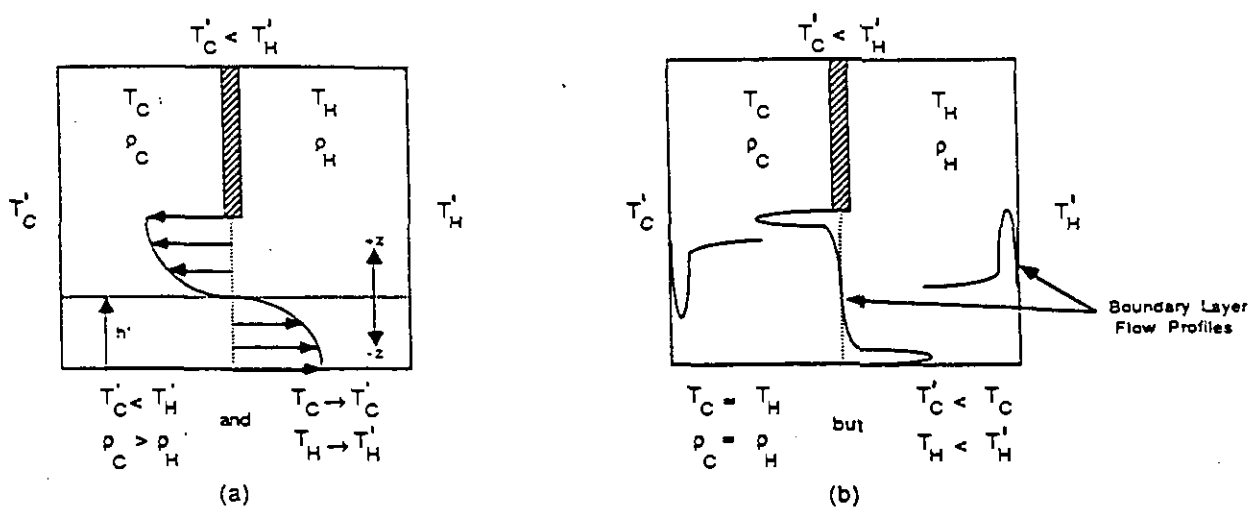

Figure 2.15 Typical heat transfer regimes (a) bulk density flow (b) boundary layer driven flow; $\Delta T=T_H-T_C$, $\Delta T_w=T_H'-T_C'$ (Scott et al. 1988)
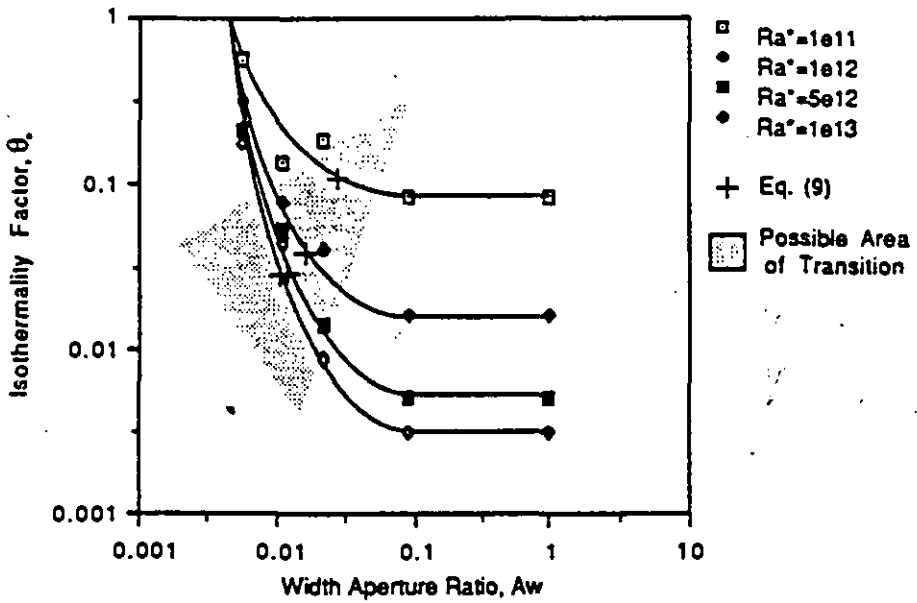
Figure 2.16a The influence of the aperture width ratio, $A_w = W/W_r$, on the factor $\theta = \Delta T/\Delta T_w$ (waterfilled scale model, *Scott et al. 1988*).
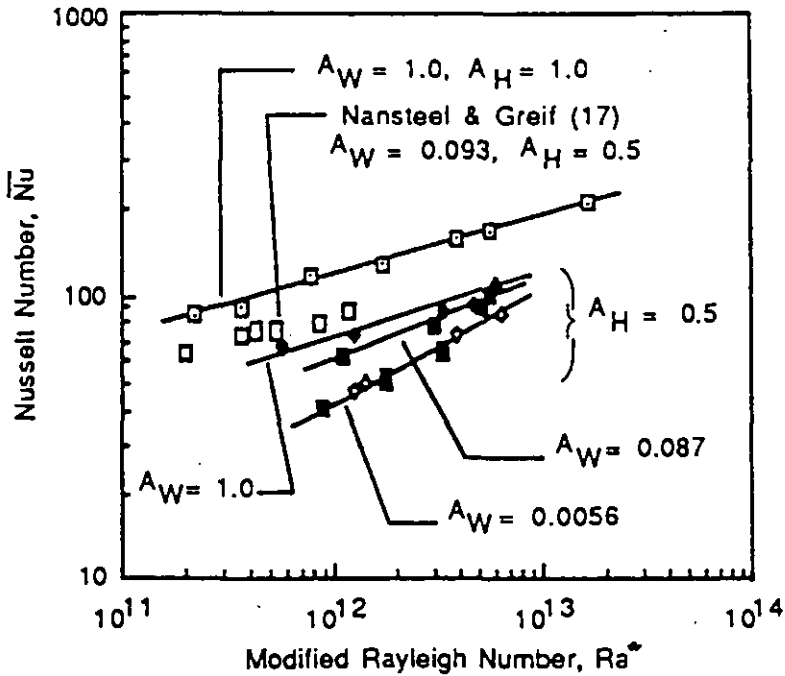
Figure 2.16b By increasing the aperture width ratio, $A_w = W/W_r$, the exponent c of the Nusselt Rayleigh correlation Eq. 2.33, decreases from 0.5 to 0.2 . *(Scott et al. 1988)*.

To observe the transition from the boundary layer driven flow to the density driven flow regime, *Scott et al. [1988]* had to make the width of the opening smaller than $A_w = 0.1$, to 'block' the boundary layer flow and to drive the two zones to different temperatures (Figure 2.16a and 2.16b). Their boundary layer flow blockage model used a continuity argument, to compare the flow in the vertical boundary layers (cross section $W\delta$) with the area of the aperture.

Neymark et al. [1989] and *Boardman et al. [1989]* developed Nusselt-Rayleigh correlation equations using a resistance model (Figure 2.17). The thermal resistances considered were the boundary layer resistances at the hot and cold walls, and the aperture resistance. The correlations were used to fit data on a waterfilled scale model and an airfilled full scale test cell. The thermal boundary conditions were chosen to be representative of conditions in a passive solar building interior, a constant heat flux hot wall, and a constant temperature cold wall.

The model. The wall boundary layer resistance R_w is handled as for vertical plate heat transfer. For turbulent flow this means $Nu_{Hr} = ARa^n = (R_w kW)^{-1}$, with $n=1/3$ and $A=0.1$. Since the boundary layer separates from the hot wall at about the aperture height (Figure 2.10), H is taken as the characteristic height for the hot wall, and Hr for the cold wall. This means that the wall heat transfer coefficient, depending directly on the wall air temperature difference, $h_w \approx (T_w - T_a)^{1/3}$, varied between 1 and 3 [W/m-K].

For the aperture resistance a parabolic velocity profile is assumed and the aperture mass flow rate corresponding to ΔT is m' (Eq. 2.21 with $\rho_i \approx \rho_0$, i.e. $\rho_i' = \rho_i/8$).

The temperature stratification in each zone is taken linear with gradients b_h and b_c for the hot and cold zone respectively. The aperture heat flow is then obtained for $\Delta T = T_H - T_C$, using Eq. 2.31 and a resistance model (Figure 2.17)

$$(T_h - T_c)/R_{ap} = \Phi = m' C_p [\Delta T + 0.3H(b_h + b_c)] \qquad (2.36)$$
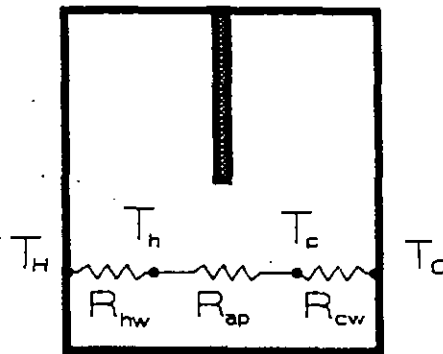
Figure 2.17 Schematic of resistance model (*Scott et al. 1988*)

Assuming that stratification scales linearly with the overall length scales and temperature differences, the temperature gradients are written as follows

$$(b_h + b_c) = F \Delta T_w (1/H + 1/H_r) \qquad (2.37a)$$

where F is a free coefficient. Equating the aperture and cold-wall heat transfer, a nonlinear expression in terms of the ratio $\Delta T/\Delta T_w$ is obtained. Finally the Nusselt number describing the heat transfer across the enclosure is written as $Nu = [kW(R_w + R_{ap})]^{-1}$.

Results. It was observed that the vertical temperature stratification in the hot and cold zone was almost linear for air, but not in water where the temperature changed strongly around the neutral level. Measured doorway velocites in air were generally smaller than the calculated parabolic profile using a discharge coefficient of 0.6 (Figure 2.18). Height and width of the opening were varied systematically. The measured Nusselt numbers

$$Nu_{meas} = [k \, W \, (C \, R_w + D \, R_{ap})]^{-1} \tag{2.37b}$$

and temperature ratios

$$(\Delta T / \Delta T_w)_{meas} = B \, (\Delta T / \Delta T_w)_{model} \tag{2.37c}$$

were compared with the model resulting in the fitting parameters: B=0.91, C=0.83, D=0.69 and F=0.27. The parameters B C and D are close to unity which is the right order of magnitude, and the fit could be made better by choosing a smaller wall resistance R_w.

We note from Eq. 2.37a, that the fitted value for F is about one third the theoretically maximum value of the temperature gradient in the door, $\Delta T_w / H$:

$$(b_h + b_c) / (\Delta T_w / H) = F \, (1 + H/H_r) \approx (0.35 \pm 0.1) \tag{2.38}$$

Unfortunately the stratification parameter F has not been determined independently. In principle the values of the parameters B, C, D and F are only valid for the thermal boundary conditions considered, but the model can probably be extended to other configurations .
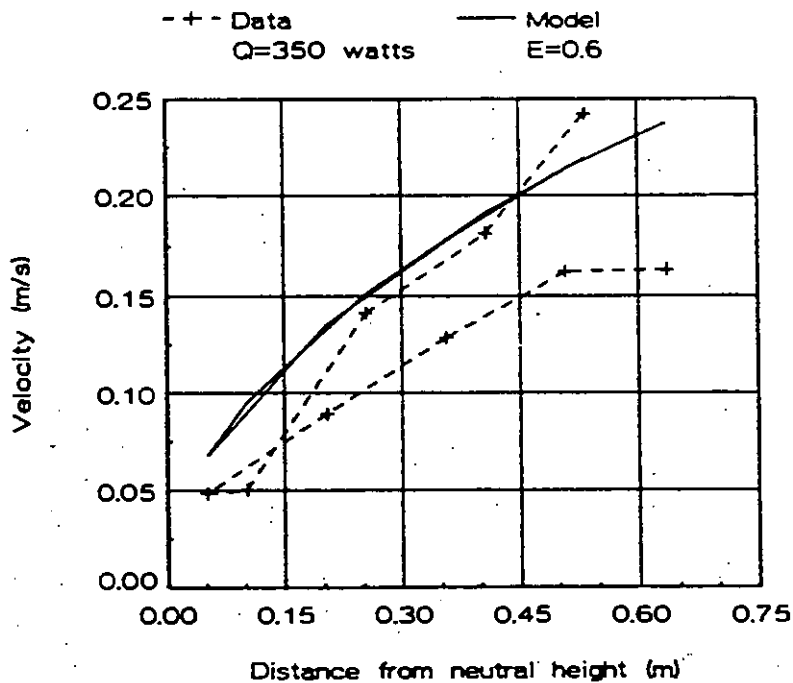
Figure 2.18. Doorway velocity profile for a heatflow of 350W. The bulk density velocity profile is shown as a solid line and the experimental data as a dashed line. The upper (lower) dashed line in both plots represents the flow in the upper (lower) portion of the doorway.

The survey of studies of inter-zone convective heat transfer through large vertical openings presented in sections 2.2 and 2.3, shows that very few boundary conditions have been studied, that most of the experiments were performed in scale models using fluids other than air, and that very few studies (if at all) examined inter-zone heat transfer under combined natural and forced convection.

2.4. Transient Flows and Turbulence Effects Through Vertical Openings

The class of problems where time variation plays a significant role, actually comprises two very different kinds of configurations :

● The transient behavior of flows due to a slow evolution in time of boundary conditions.

● The effect of turbulence or fluctuating pressure fields.

2.4.1 Transient flows

The distinguishment between transient and steady-state phenomena in a discussion of air flow in buildings is a matter of time-scale. After opening a door or window, outside air replaces inside air on a time scale of minutes, depending on parameters like the room dimensions, the window size, the wind velocity and the inside-outside temperature difference.

The inside air flow pattern changes on a timescale of hours due to a slow evolution of the boundary conditions including wall temperatures, wind velocity and direction and outside temperature. For the present discussion we will not bother about the longer timescales as the diurnal and seasonal variations.
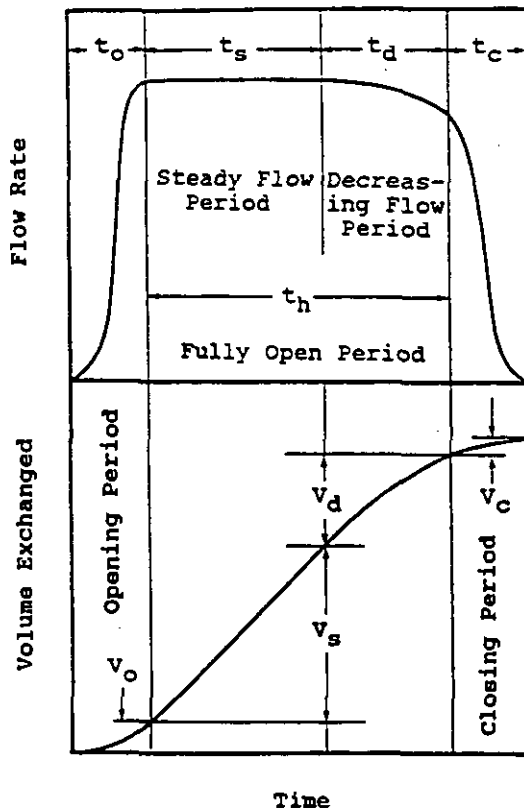

Figure 2.19. Idealized flow rate and volume exchange for a typical door cycle
(Kiel and Wilson, 1986).

The more common way to solve the time dependent problem is to combine the steady-state air flow model with models dealing with thermal simulation or any other phenomena driving the

air flow, and to give a complete description of the coupled process. However, in some cases it is better to use a simpler approach and to give an estimate of the evolution in time of the flow through an opening caused by a single perturbation.

2.4.1.1 Opening and closing of a door. *Wilson and Kiel [1990]* studied the unsteady buoyancy flow that occurs during the door opening and closing period. *Kiel and Wilson [1986]* investigated the time dependence of the flow rate that results from the effect of limited interior volume. Initially a gravity wave of cold outside air enters the space, bounces back at the rear wall and then, during the filling phase, the air flow rate reduces quasi exponentially to zero.

They used full scale experiments and a water scale model to show that the transient flow due to the opening or closing of doors can be predicted using quasi steady-state equations and gravity current theory as defined by *Benjamin [1968]*.

Later they also considered the pumping effect caused by a moving door *[Kiel and Wilson 1989]* and found that the air flow during the opening and closing cycle can be neglected for opening periods longer than about one minute (Figure 2.19). Moreover, the pumping action of the door becomes more significant when the inside-outside temperature difference is small.

During the gravity driven flow period (i.e. before the gravity wave reflects at the rear wall) the air change rate was measured and compared with the Bernoulli model. *Wilson [1990]* then concluded that interfacial mixing of the counterflows near the neutral level is important, the exchange of momentum between the counterflows resulting in reduced flow at low interzonal temperature difference ΔT (Figure 2.8).

2.4.1.2 Transient ventilation heat loss rates. The ventilation and heat transfer following the opening of a door or window is a dynamic process. Both the air temperatures and the wall temperatures vary with time. The general problem is complicated because it involves simultaneously heat and mass transfer in spaces of various geometries with non-homogeneous surroundings and therefore the coupling with a complex thermal simulation of the whole building

However when one is interested in the energy consequences of inhabitant behaviour with regard to the opening of doors and windows, a simplified model with a few measurable parameters would be suitable.

Van der Maas et al. [1989, 1990, 1991] proposed such a simplified description of the cooling problem. As illustrated in Figure 2.20, it comprises a ventilation model, a model for heat transfer (main parameter: effective surface area for heat transfer) and a model for the wall surface temperature (main parameter: average thermal effusivity).
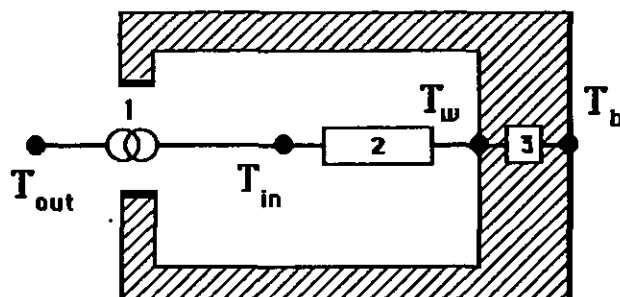

Figure 2.20. The equivalent circuit for the modelling of ventilation heat loss rate. The ventilation heat loss rate (1), the heat transfer resistance (2) the dynamic wall resistance (3). T_{in} is the inside air temperature and T_w is the wall surface temperature.

The heat loss rate Φ, resulting from a ventilation rate Q, is proportional to the temperature difference between the in and out flowing air, and the calculation of the heat loss rate reduces to the problem of calculating the outflowing air temperature.

As a first approximation the inside air temperature, T_{in}, is taken uniform (single zone thermal model). The heat loss rate is then written as:

$$\Phi = Q \rho C_p (T_{in} - T_{out}) \tag{2.39}$$

Due to the heat transfer resistance between the air and the walls, T_{in} is situated in between the inside wall surface temperature and the outside air temperature. This is illustrated in Figure 2.20 where the heat source 1, represents the ventilation heat loss rate given by Eq. 2.39.

The wall surface temperature T_w is changing slowly and is approximated by solving the heat equation for a half-infinite homogeneous wall exposed to a heat flux density q [Van der Maas et al. 1989]:

$$T_w (t) - T_w (0) = \frac{1}{b\sqrt{\pi}} \int_0^t q (t-\tau) \, \tau^{-1/2} d\tau \tag{2.40}$$

where $b = \sqrt{\rho c \lambda}$ (the square root of the product of thermal conductivity, density, and specific heat) is the thermal effusivity of the wall material (ISO 1987). It is seen that T_w is an integral over the time history of q. The integral has a simple solution when q is constant or can be approximated by a series of step functions.

The difference between the wall surface temperature and the temperature of the nearby air, $T_w - T_{in}$, is given by:

$$T_w - T_{in} = \frac{\Phi}{C_s h_c S_i} = \frac{Q \rho C_p (T_{in} - T_{out})}{C_s h_c S_i}$$

$$\tag{2.41}$$

The new parameters in Eq. 2.41, are the total inside surface area S_i, the convective heat transfer coefficient h_c and the coefficient C_s, the fraction of S_i active in convective heat transfer. It was found that a constant value of $h_c = 6 W/m^2 K$ is consistent with the data (the value is typical for low velocity forced convection). The concept of C_s is illustrated in Figure 2.21.
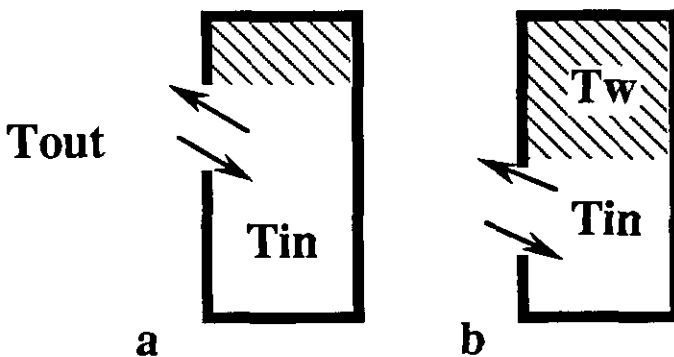

Figure 2.21. Above the upper level of the window, the trapped warm air (dashed) is at the same temperature as the wall:p the ceiling and wall surface above the top of the window do not cool by convection. The coefficient C_s is about 0.8 in (a) and 0.4 in (b).
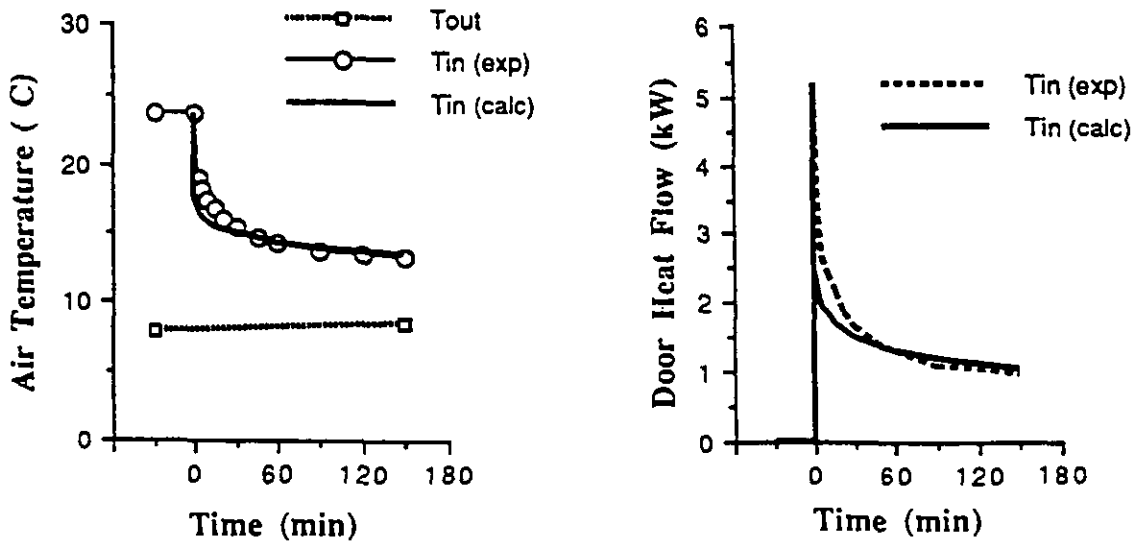
Figure 2.22: Changing room temperature and heat loss rate after opening a door
(see: Van der Maas et al. 1990).

It was shown in full scale experiments that the model predictions compared rather well with the measured decrease in inside air temperatures over a one night period (Figure 2.22). Note that for a drop in inside-outside temperature of, e.g. 10%, the ventilation rate decreases by 5% and the heat loss rate decreases by 15%.

Numerical. The transient flows are usually solved in numerical modeling with a quasi-steady-state description of the dynamical process for each time step. Bernoulli's flow theory or any other correlation is used to calculate the steady-state flow corresponding to the boundary conditions of each time step. The main assumption is that the flow will be fully developed instantaneously and will follow the imposition of new boundary conditions at each time step.

The variation of the boundary conditions can be given by hourly variation of average wind speed and direction, by a schedule of occupancy or of the working of mechanical ventilation systems, or by the evolution in time of the thermal state of the building itself.

2.4.2 Turbulence effects and fluctuating pressures

None of the general laws previously described enables us to quantify the effect of an unsteady wind or of a large scale turbulence on the air exchange rate through an opening.

Experimental results from *Bienfait et al. [1990]* have shown that these effects can be particularly significant in the case of single-sided ventilation or when the wind direction is parallel to openings in two opposite facades. Figure 2.23 presents these two configurations where a steady-state calculation gives no air exchange.

Wouters [1987] indicates that in a special case where wind effect and stack effect are neutralizing each other, the role of fluctuating flows on the real air exchange becomes significant. Figure 2.24 indicates this gap between steady-state calculations and the expected effects of turbulence. Nevertheless, as pointed out by *Vandaele and Wouters [1989]* in their review paper, very few correlations have been proposed and most of them concern very particular configurations.

These fluctuating flows are created by the effects of turbulence due to local wind characteristics. They depend on the turbulence characteristics of the incoming wind and on the turbulence induced by the building itself.

36

These mechanisms have been studied on scale models or full scale cells, and wind tunnel visualizations have been used to describe the main phenomena. Fluctuating pressures due to turbulence in the air flowing through an opening cause simultaneous positive and negative pressure fluctuations of the inside air.
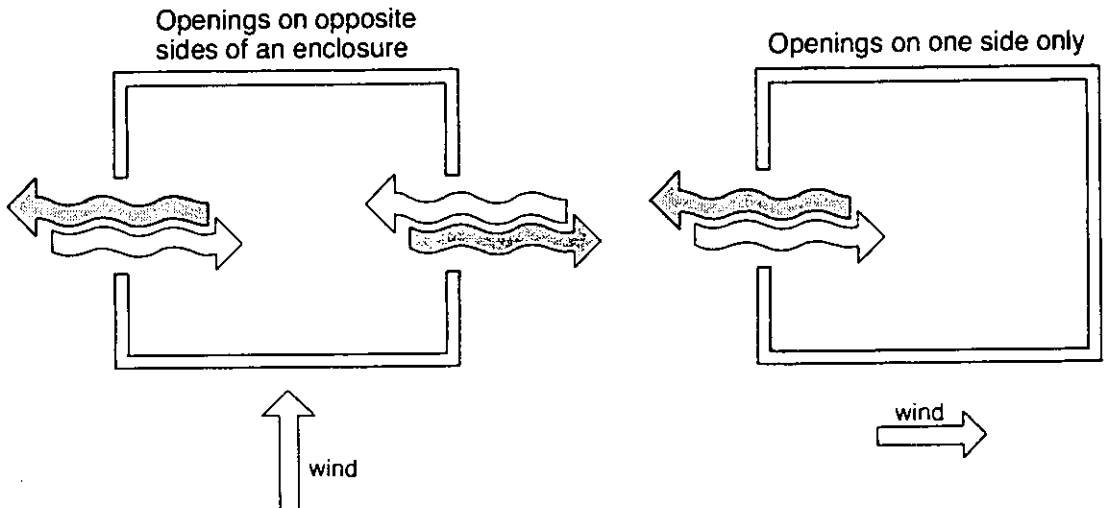
Figure 2.23: Two cases of non steady-state ventilation (Liddament, 1986).
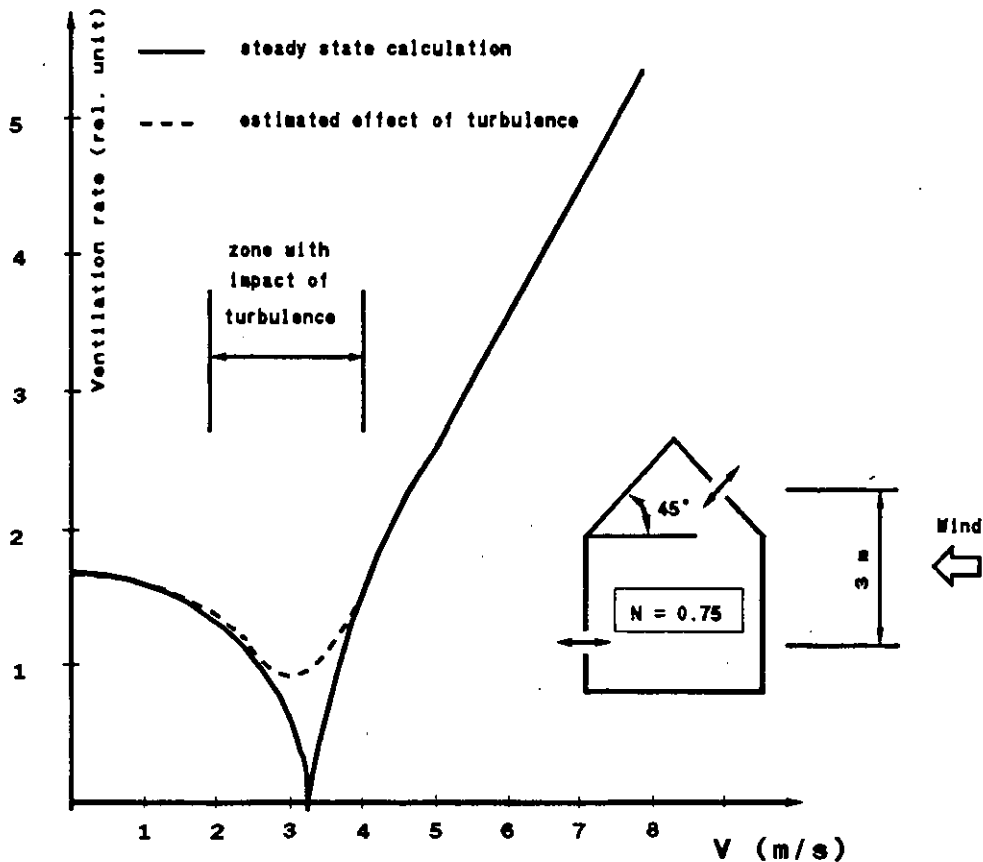
Figure 2.24: Effect of turbulence on ventilation rate.

Cockroft and Robertson [1976], and *Warren [1977]* described this phenomenon as an adiabatic compression and expansion of the inside air. The result is simultaneous incoming and outgoing flows through the opening. Figure 2.25, from *Crommelin and Vrins [1988]*, illustrates this behaviour.
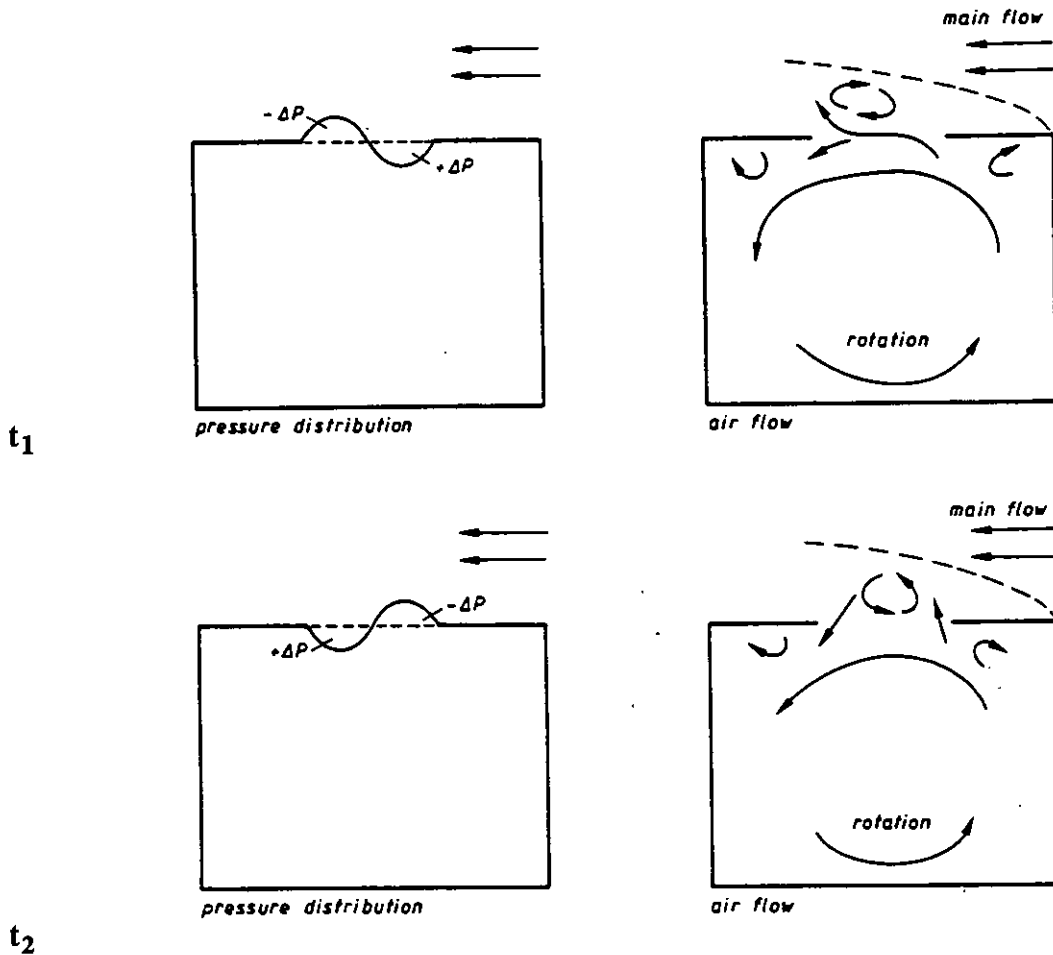

Figure 2.25: Air flow through the window opening at time t_1 and t_2
(Crommelin and Vrins, 1988).

Haghighat et al. [1991] proposed a model to calculate the pulsation flow in multizone buildings due to fluctuations in wind-induced pressures. The air flow through a building opening is influenced both by building characteristics: the resistance of openings to flow, the inertia of air masses in openings and the compressibility of the room air, and by frequency characteristics of wind pressures: their power spectra and the correlation among them. The root-mean-square values of the fluctuating air flow are calculated by a spectral analysis method in the frequency domain. The total air flows are obtained by combining both steady-state and pulsating flows.

These experimental investigations show the influence of the magnitude of the eddies. Eddies with dimensions of approximatively the same size as the opening give the maximum fluctuating effect on inflow and outflow. They create a rotational effect on the inside air. The fluctuating pressure field in the opening plane, due to the turbulence characteristics of wind, leads to a consistent exchange between the outside air and the inside air.

Because of the complexity of the problem and the high number of parameters influencing the development of the eddies along the facade of a building very few correlations have been proposed and implemented in multizone air flow models.

Etheridge [1984] assumed that the turbulent pressure distribution with respect to time has a Gaussian distribution and that the resultant flow can be expressed by Eq. 2.42:

$$\overline{m_t'} = F \; \frac{0.4 \sqrt{2}}{\pi} \; \frac{\Delta Pi_{rms}}{\overline{\Delta Pi}} \; \overline{m'}$$

(2.42)

where F is a linear function accounting for large mean pressure differences, Pi_{rms} is the root mean square pressure difference across the opening, and m' represents the steady-state flow rate.

Cockroft and Robertson [1976] showed that assuming an isotropic turbulence and using Gaussian probability distributions for wind velocity and flow rate gives a good agreement with experimental results obtained in a simulated wind.

In order to integrate this turbulence effect in a more general air flow model *[Phaff et al. 1980; De Gids and Phaff, 1982]* proposed an empirical correlation deduced from experimental work and gave a general expression for the ventilation rate, Q, through an open window as a function of temperature difference, wind velocity and fluctuating terms. An effective velocity, Ueff, was defined for single sided ventilation, and refers to the flow through half a window opening:

$$U_{eff} = \frac{Q}{A/2} = \sqrt{C_1 u_{met}^2 + C_2 \, H \, \Delta T + C_3}$$

(2.43)

where u_{met} is the meteorological wind velocity, C_1 is a dimensionless coefficient depending on the wind, C_2 is a buoyancy constant and C_3 is a turbulence constant. From the air change rate obtained with tracer gas measurements, an equivalent velocity through an area A/2, Ueq, was derived and fitted to Eq.2.44. The result of the fit is shown in Figure 2.26.
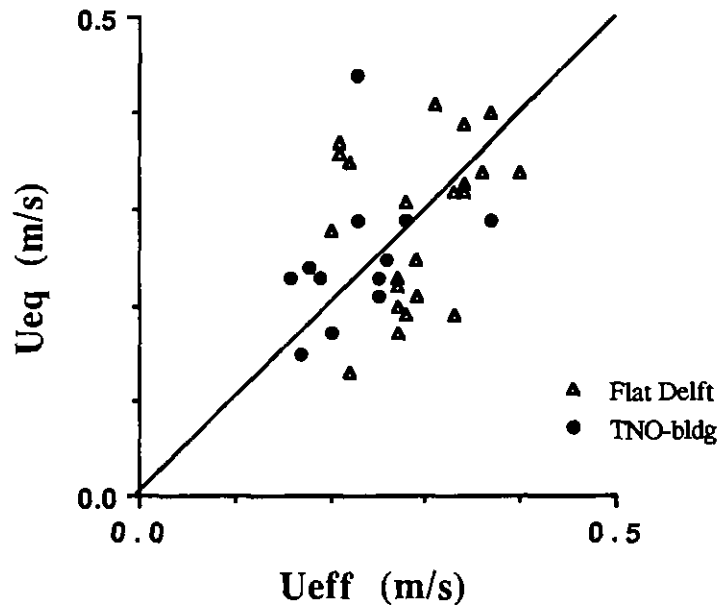

Figure 2.26 : The equivalent air velocity derived from tracer gas decay, Ueq, as a function of the effective velocity, Ueff, calculated from a fit to Eq. 2.43 *(De Gids and Phaff, 1982)*. The straight line corresponds to ideal agreement. The data refer to two buildings and are replotted from the source *(Phaff et al. 1980, Table 12)*.

A reasonable correspondance between measured and calculated values was obtained for the fitting parameters $C_1 = 0.001$, $C_2 = 0.0035$ and $C_3 = 0.01$.

The turbulent term C_3 is equivalent to an effective turbulence pressure that provides ventilation in the absence of stack effect or steady wind. More generally the effective velocity can be written as:

$$U_{eff} = \frac{Q}{A/2} = \sqrt{2/g \left(\Delta p_{wind} + \Delta p_{stack} + \Delta p_{turb} \right)}$$

(2.44)

To account for the observed air exchange through a doorway at very weak temperature differences, *Liddwell [1977]* proposed adding a turbulence pressure term, operative in opposite directions above and below the neutral level. This model is used to calculate concentration histories in dwellings by *Siren [1988]*.

More recently, *Allard and Utsumi [1992]* stating that the effect of the fluctuating term of pressure in a turbulent flow results in an increase of air change rate through a vertical opening proposed to represent this fluctuating driving phenomenon more generally by an equivalent fictitious pressure gradient giving the same air change rate:

$$\Delta P_t = P_{t\,o} + b_t\,z$$

(2.45)

These types of models, combining the effects of wind velocity, temperature difference and turbulence, should be able to predict the effect of fluctuating wind on the air flow exchange through an external opening in a multizone pressure network.

Ventilation parameter F. A practical way to describe wind induced ventilation is to define a dimensionless ventilation parameter F *[Warren, 1986; Crommelin and Vrins, 1988]* . The definition of F refers to the case of a rectangular opening of area A, where the air flowing in through one half of the opening must flow out through the other half at least when mass conservation is assumed (no compressibility) :

$$F = \frac{Q}{A\,u_w} < 0.5$$

(2.46)

based on the observation that ventilation increases nearly proportionally to the wind velocity, u_w, and the opening area, A. Note that the maximum value of F is 0.5 (Eq. 2.44).

From windtunnel experiments studying single-sided ventilation induced by turbulent wind, pressure fluctuations in the plane of the window are found to have a dominant influence. In particular eddies as large as the size of the window are important because they can completely penetrate into the space. *Crommelin and Vrins [1988]*, report that for air flow parallel to the façade of the scale model, F can be considered constant with a value of about 0.03, which is close to the windtunnel result found by *Warren [1986]*. For other inflow directions *Crommelin and Vrins [1988]*, have found decreased ventilation, with a minimum value for an opening at the lee side.

While the ventilation rate depends clearly on the wind velocity and its direction, the data in the literature show much scatter and the model correlation is hardly improved by taking wind direction into account. Many parameters are probably influencing the structure of the local wind at the the opening, parameters that are not yet clearly identified.

2.5. Numerical Modelling

2.5.1. Integrating large openings in multizone air flow models

Multizone air flow models are usually based on a pressure network definition describing at each time step the pressure field in a building. Assuming known air temperatures, the state variable defining each zone is its reference pressure at thermodynamical equilibrium, the control volume of this variable is called a zone which can be a room or a group of rooms having the same behavior, and they are linked together by nonlinear flow equations expressed in terms of pressure difference. Finally, mass conservation of air in each zone leads to a nonlinear system of pressure equations.

There are two ways of predicting air flow rates through large openings:

The A method consists in describing the air flow rate through the large opening using a nonlinear equation of the pressure drop, and including it directly in the pressure network.

The B method, at the contrary leads to solve independantly the problem and include the result as an unbalanced flow in the mass conservation equation of the described zone.

Using the B method, we can either take an explicit definition of the air flow given by a Bernoulli flow regime, or use directly any kind of correlation. In both cases the large opening is disconnected from the general pressure network, it is solved separately, and then represented by an unbalanced flow in the mass conservation equation of each zone. Since the flow is strongly dependent on the pressure field around and inside the building this solution leads to a high number of iterations and a direct approach appears more attractive. This method was used to avoid convergence problems in the resolution of the nonlinear system of pressure equations representing the mass conservation in each zone.

Using the A method, it is necessary to define large opening behaviors in terms of nonlinear equations of the pressure drop. The first possibility used in general codes such as TARP or CSTBbât was to describe the large opening as a conjunction of parallel small openings, properly located, and with only a one way flow allowed for each one. Each small opening is then described by a crack flow equation taking into account the local pressure drop. The whole system of nonlinear equations can be introduced directly into the pressure network. This solution was first proposed by *Walton [1984]* and *Roldan [1985]* and has been used later in various multizone models developed since *[Feustel et al. 1990]*. It leads to the definition of various flow elements in simulating one large opening.

An other way to solve this problem is to interpret the flow equations of large openings in terms of non linear pressure equations. *Walton [1989]* proposed this solution in the case of a vertical opening between two isothermal zones for steady-state flow. Following the approximation of the Bernoulli's flow, it is assumed that the velocity of the air flow at different heights is given by Eq. 2.17.

In the case of a neutral plane being located in the opening and taking this point as origin for altitude, since $P_i(Zn) = P_j(Zn)$, the mass flow through the doorway above and below the neutral level Zn are given by

$$m'_{Zn,H} = Cd \int_{z=0}^{z=H-Zn} \rho \ u_{ij}(z) \ W \ dz$$

(2.47)

$$m'_{0,Zn} = Cd \int_{z=-Zn}^{z=0} \rho \ u_{ij}(z) \ W \ dz$$

(2.48)

Walton [1989] reports that this model of doorways tends to be faster than the multiple opening approach. Details of the formulation in the ESP code and the COMIS code are given in the following.

2.5.1.1. ESP. The large opening routine in ESP *[Clarke 1985]* is a constant zone temperature routine adapted to a pressure network where the height of the reference nodes is known. The algorithm was proposed by *Cockroft [1979]* and the notation is explained in Figure 2.27. The air flow through the opening is expressed in terms of the node pressures p_1 and p_2, and the absolute zone temperatures:

$$Q = \frac{2}{3} C_d W h \sqrt{\frac{2}{\rho}} \frac{1}{C_t} \left(C_a^{1.5} - C_b^{1.5} \right)$$

(2.49)

where

$$C_a = (p_1 - p_2) + (1 - r_p) C_t$$
$$C_b = (p_1 - p_2) - r_p C_t$$
$$C_t = \frac{p\, g\, h\, M}{R} \left(\frac{1}{T_2} - \frac{1}{T_1} \right)$$

(2.50)

Here $r_p = h_p/h$, with h_p the height of the reference nodes on either side of the opening, M is the molar mass of air, and R is the perfect gas constant. For air : R/M=287[J/(kgK)]. p is the atmospheric pressure.
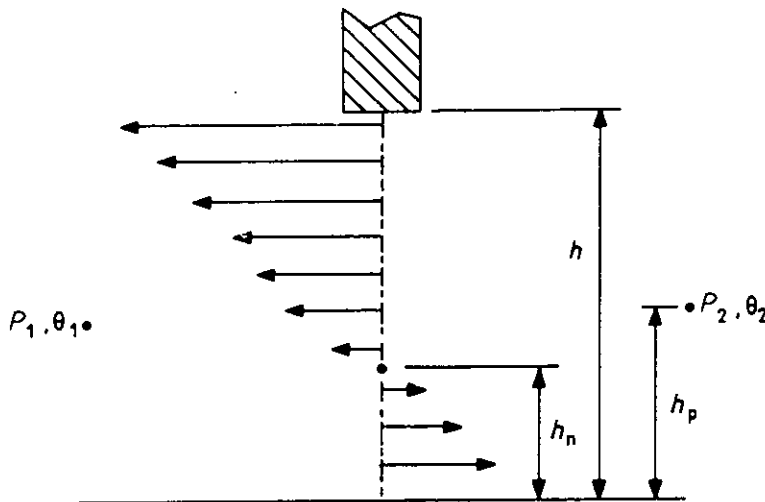

Figure 2.27 : Bidirectional flow across a doorway as implemented in the multizone building simulation programme ESP.

On evaluation, Eq. 2.49 yields a sum of real and imaginary parts. Real parts indicate a flow in

the positive direction and imaginary parts indicate a flow in the reverse direction. The equation has a singularity at infinity for Ct=0. In this case no buoyancy effects exist, and so an equation for crackflow can be used.

The neutral height h_n is found from $h_n = h(r_p - (p_1 - p_2)/C_t)$.

2.5.1.2. COMIS
The main objective in proposing a solution for large openings is to fit it easily into the network definition and to go as far as possible in the modeling of the various phenomena influencing the behavior of large openings. This point has been one of the first aims of COMIS (Feustel et al., 1990).

The main assumptions of this model described by Figure 2.28 are:

- Steady flow, inviscid and incompressible fluid

- Linear density stratification on both sides of the opening

- Turbulence effects represented by an equivalent pressure difference profile

- Effects of reduction of the effective area of the aperture represented by a single coefficient.
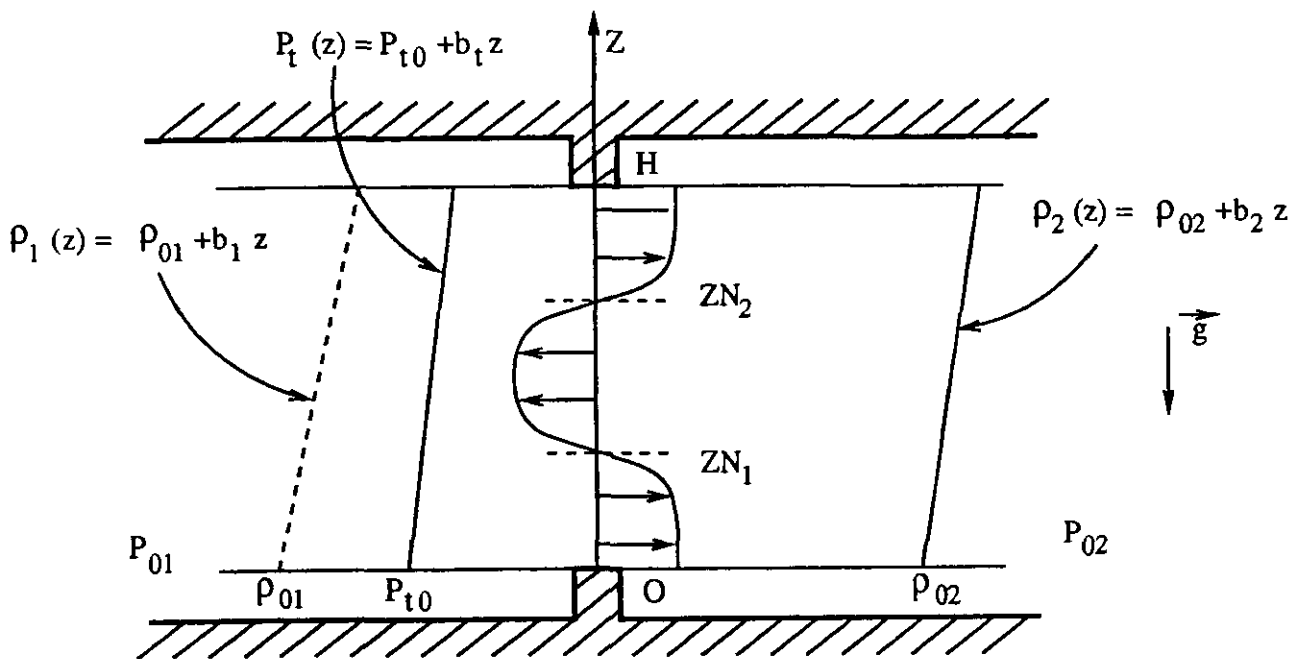
Figure 2.28: Multizone air flow simulation program, COMIS, for large openings.

The reference pressures on each side are given at the bottom of the opening. Assuming Bernoulli hypothesis on both sides of the opening, then the pressure difference at any level z is defined by :

$$P_1(z) - P_2(z) = (P_{01} - P_{02}) - g\left[\left(\rho_{01}z + b_1\frac{z^2}{2}\right) - \left(\rho_{02}z + b_2\frac{z^2}{2}\right)\right] + (P_{t0} + b_t z)$$

$$(2.51)$$

The locations of the two possible neutral planes are given by an equilibrium in pressure which leads to a zero velocity point. In order to find the air flows flowing in both ways through the opening, the following step is to integrate the velocity equation within the intervals defined by the physical limits of the opening and the position of the existing neutral planes. The general solution is:

$$\dot{m}_{0,z1} = Cd \; \theta \int_{z=0}^{z=z_1} \rho \, u\,(z)\, W \, dz$$

(2.52)

$$\dot{m}_{z1,z2} = Cd \; \theta \int_{z=z1}^{z=z2} \rho \, u\,(z)\, W \, dz$$

(2.53)

$$\dot{m}_{0,z2} = Cd \; \theta \int_{z=z2}^{z=h} \rho \, u\,(z)\, W \, dz$$

(2.54)

In these equations, Cd is assumed to be a characteristic of the whole opening and it has a constant value. θ is called the area reduction factor and it enables one to define the effective area of opening through which the air is flowing.

In the more general case, these integrals have no analytical solutions and they have to be computed by numerical means. This numerical solution is general, but it is also time consuming and as far as no density gradients exist, an analytical solution can be used to save computational time.

2.5.2 Air flow modelling using computational fluid dynamics (CFD)

Numerical simulation is being used to study the convective heat and mass transfer within and between zones. A majority of cases are dealing with single enclosures, but we are concerned here with the few concerning flow through large openings i.e. partitioned or two-zone enclosures. A short review of the use of CFD for natural convection flow in single zones can be found in *Haghighat et al.[1989, 1990, 1991]* .

Chang et al. [1982] undertook a finite-difference study of natural convection in a two-dimensional square enclosure with a partition mounted either on the ceiling or on the floor. One wall parallel to the partition was kept at cold while the opposite was kept hot; the ceiling and the floor were well insulated. The two-dimensional laminar flow cases for the Grashof number region from 10^3 to 10^8 were computed with different combinations of the partition geometry and location. It was found that when the partition was set close to the cold wall, the total heat transfer rate was reduced. The maximum heat transfer rate occurred when the partition was set slightly off the centre of the enclosure, towards the hot wall. The average Nusselt number, Nu, was plotted against the height ratio, the thickness ratio and the location of the partition. This model was not validated.

Kelkar and Patankar [1987] predicted natural convection in partitioned enclosures by numerical simulation. The partitions in their studies were two-dimensional. The opening on the partition ran through the whole width of the room; the flow conditions were laminar.

Haghighat et al.[1989, 1990a, 1990b] developed a numerical model to study heat and mass transfer phenomena in three-dimensional two-zone enclosures with turbulent flow. The model was applied to investigate the influence of door height and location on inter-zone natural convective heat transfer rate; the ventilation effectiveness and thermal comfort parameters in a

two-zone enclosure for different arrangement of door opening, ventilation supply and exhaust locations. The effect of infiltration on ventilation air movement in a partitioned enclosure was studied as well *[Wang et al. 1990]*. They found that the flow pattern and contaminant distribution in downstream zone were quite sensitive to the change of door location (Figure.2.29).
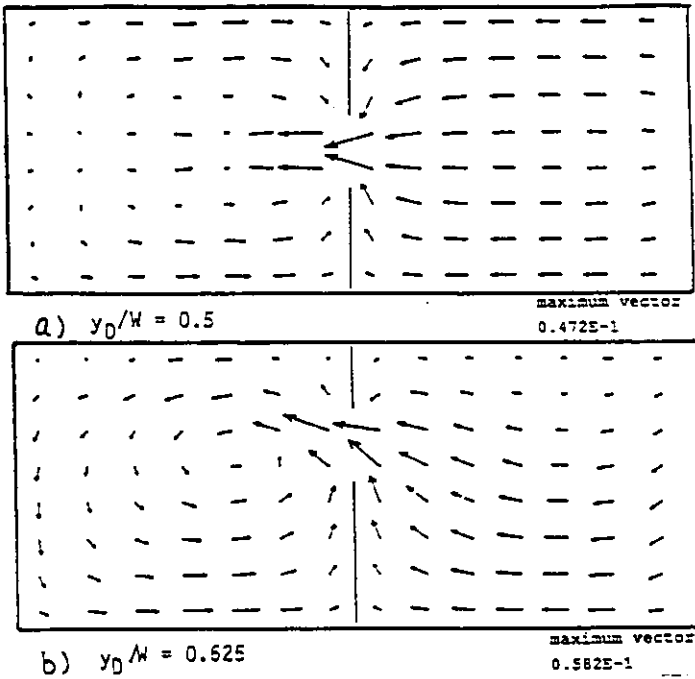

Figure 2.29 : The natural convection flow pattern in a horizontal plane with the door at y/W=0.5 and 0.875 (Haghighat et al 1991).

RE=400
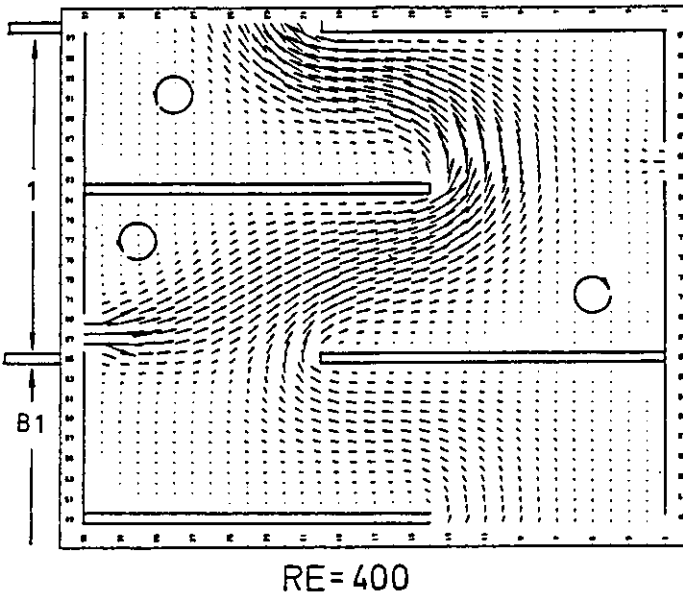
Figure 2.30 : A two-dimensional isothermal simulation of air flow between basement 1 and the secondfloor in a hospital stairwell. Infiltration through cracks at the door *(Münch, 1986)*.

In some cases, CFD can be used to visualize the flow field when the boundary conditions are provided by experiment, and the air flow is *isothermal*. As an example, 2D isothermal transport equations were used to calculate the flow of microorganisms in a hospital stair shaft *[Münch, 1986]*, the boundary conditions were the measured pressure differences over cracks near doors. The application of the numerical method was found to be of help to reduce the experimental work and to investigate the complex exchange mechanisms of microorganisms (Figure 2.30). Differences between the measured and calculated germ concentrations were in the range of 10%. However, the authors note that the transport of microorganisms depends strongly upon the difference in air temperature of the stairwell and its surroundings which determines the stack-effect and therefore the boundary conditions.

The effect of the absorption of radiated heat by the convecting fluid, can only be important when there is infra-red absorption by smoke or gases like CO_2, H_2O. An example is given in Figure 2.31.

A = 1.3	
B = 1.6	
C = 1.9	
D = 2.2	
E = 2.5	
F = 2.8	
G = 3.1	
H = 3.4	
I = 3.7	
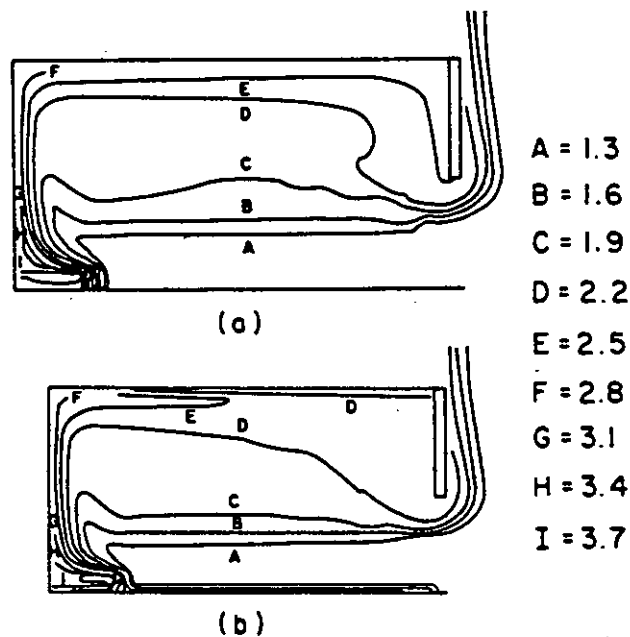
Figure 2.31 : Radiation effects on the temperature field in a vented enclosure (a) no radiation, (b) surface and gas radiation *(Lloyd , 1979)*.

Various commercial CFD packages are available today. Most of them have no problem in simulating forced convection airflow situations of complex geometries. On the other hand, natural and mixed convection situations are still subject of research. However in view of the increasing power /cost ratio in computer hardware, one can expect a further strongly growing interest in the use of CFD to predict airflow patterns in buildings.

2.6 Conclusions: Research Items for Annex 20, Subtask 2.1

For building simulation programs there is a need for algorithms to calculate the transport by air, of contaminants and heat. The relative importance and the value of parameters determining mass and heat transport through large openings is not very well known. With the help of this literature survey, the following new research needs can be identified:

Large *internal* openings research is needed on :

Discharge coefficients. There is a variety of definitions and values for discharge coefficients in the literature. One can refer to flow contraction (section 2.1.2) or interfacial mixing (section 2.1.4), and its value can pertain to velocity, massflow or heat flow. But it is not clear e.g., what the influence is of various heating and cooling boundary conditions in the interconnected zones. The origin of the large spread in literature values is not understood. Also for a given temperature stratification, the possible error due to the use of a linear temperature stratification approximation is difficult to estimate.

Boundary layer flow. The conditions for the transition between boundary layer driven flow and gravity driven layer flow and its importance for heat and mass flow is unclear.

Flow through horizontal openings. There is little information on the air flow through horizontal openings, in particular for contaminant dispersal, models are needed describing the transition between two-way flow and one way flow.

Numerical calculations. Experimental data that can be used for comparison with numerical calculations on interzone-flow are hardly available. Validated CFD codes can be of great help in reducing the number of steady-state experiments.

Dynamical modeling. Air flow and the transport of contaminants and heat is a dynamic process in an inhabited building but most efforts are on steady state studies. The limits of the use of steady state modeling when inhabitants are opening doors and windows are unknown.

Given the operational stage of experimental testcells, two in France and one in Belgium, it was possible to have a detailed look at the discharge coefficient and to perform three experiments differing mainly in the heating and cooling systems (see sections 3.2, 3.3 and 3.4). Canada contributed by showing that various features of the experiments can be reproduced by numerical calculation (section 3.5).

Finally some new directions in the modeling of mass and heat flow through large openings are described but not yet exploited (a contribution from Switzerland, section 3.7).

Large *external* openings research to improve the understanding of wind effects on single-sided ventilation in particular on :

Fluctuating wind. Air flow resulting from fluctuating wind and turbulence

Energy consequences of user behaviour. Transient ventilation and heat loss, by measuring and modeling the time dependence of the ventilation and heat loss during window opening.

Meteo data transfer. Characterization of the wind at the facade and near the opening from weather station data.

New measurements of single-sided ventilation in the presence of wind and/or stack effect, were performed by four laboratories in France (section 3.2), Belgium (section 3.3), United Kingdom (section 3.4) and Switzerland (section 3.5). Locally measured meteo data were used in order that the data could be interpreted without the complexities and uncertainties due to the meteo data transfer. As an illustration of the complexity of meteo data tranfer, a literature data set has been analysed in the introductory section 3.1.

Contents of chapter 3

3. NEW STUDIES OF AIR FLOW THROUGH LARGE INTERNAL OPENINGS

3.1 Discussion of Research Goals

3.1.1 The scope of the subtask

A validated and operational computer programme for the simulation of air flows in multi-zone buildings can help the design of energy efficient buildings. However whether the programme is valid for a given task depends on the structure of the computer code and the range of validity of the algorithms used to model the physical phenomena. It is therfore the scope of subtask 2.1 to test and extend the range of validity of existing algorithms on interzone heat and mass flow and, where possible, to develop new algorithms.

Barakat [1985], recommended that future research in inter-zone convective heat transfer should aim at the extention of the validity of existing correlations and cover:

    (i)   a wide variety of two-zone configurations and boundary conditions
    (ii)   combined natural and forced convection (coupling to air distribution system)
    (iii) the effect of partition thickness and conductance (e.g. sunspace)
    (iv) implementation of correlations in energy analysis programmes
    (v)   the ability of the improved correlations to predict energy consumption and indoor temperatures in multi-zone buildings

and future research should be directed towards the development of reliable convection correlations and design guidelines, in order to enable the building designer and energy analyst to take large openings as 'a heat transfer component' into account.

It was decided however that the work in subtask 2.1 would not aim in the first place at *empirical correlations* but rather *stress the understanding of the basic physical phenomena* behind the correlations. The various modeling approaches for heat and mass transfer are illustrated in Figure 3.1.

Indeed, in the heat transfer and fluid mechanics literature there is the tradition of handling complex situations by expressing heat transfer results in terms of empirical correlations between non-dimensional numbers (section 2.2). These correlations link directly the known boundary conditions (air temperatures or wall temperatures) to heat flow (Figure 3.1: models 5a and 5b). In physics on the other hand, the goal is understanding heat and mass flow in terms of simplified models relating dimensional physical quantities as velocity, temperature, energy and time.

The work in the subtask then stresses the measurement of velocities and temperatures (Figure 3.1: models 1 and 2), and interzone mass and heat flow (Figure 3.1: models 3 and 4), while considering empirical heat transfer correlations (Figure 3.1: model 5) as a secondary result.

Unless the zones are tightly temperature controlled, the air temperatures of zones that are communicating by open doors and staircases are not the same when the door is open or closed. This makes an estimate of heat flows uncertain, in particular when one considers occupied buildings, with users opening doors and leaving them open for some time. The resulting heat flow interacts with the thermal boundary conditions, introducing a time dependence in the model (Figure 3.1: model 6). In such a case, linking the air flow model with a building thermal model may become a necessity.

Model types for interzone heat and mass transfer
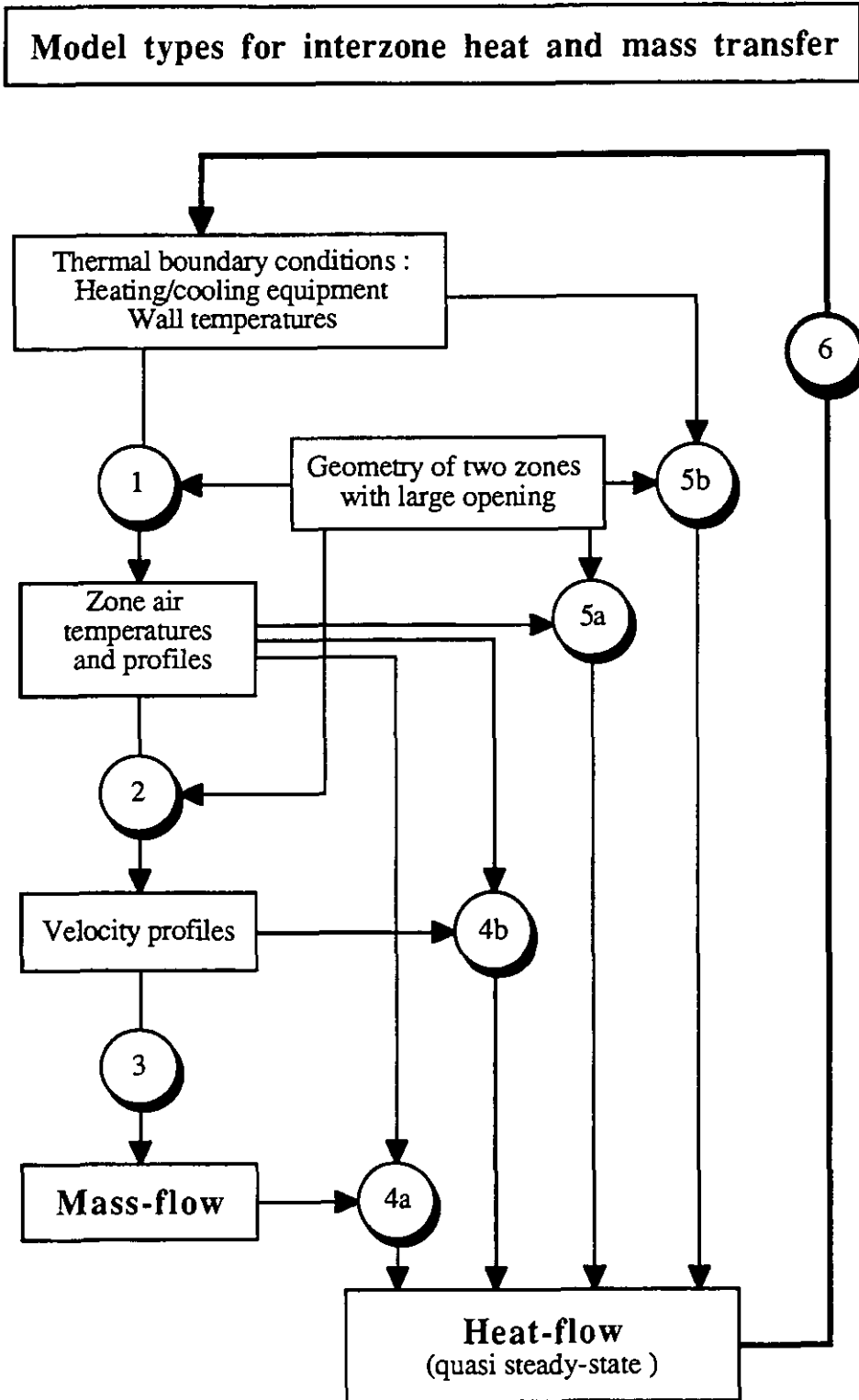
Figure 3.1 Relationships between the various types of modeling for interzone heat and mass transfer. Models 1, 2 and 3 represent the physical (dimensional) models to calculate mass-flow. Model 4 forms a link between mass and heat flow. Non-dimensional correlations (Models 5a, b) form a direct link between heat flow and boundary conditions. Changing boundary conditions (Model 6) cause time dependence (a succession of steady-state conditions).
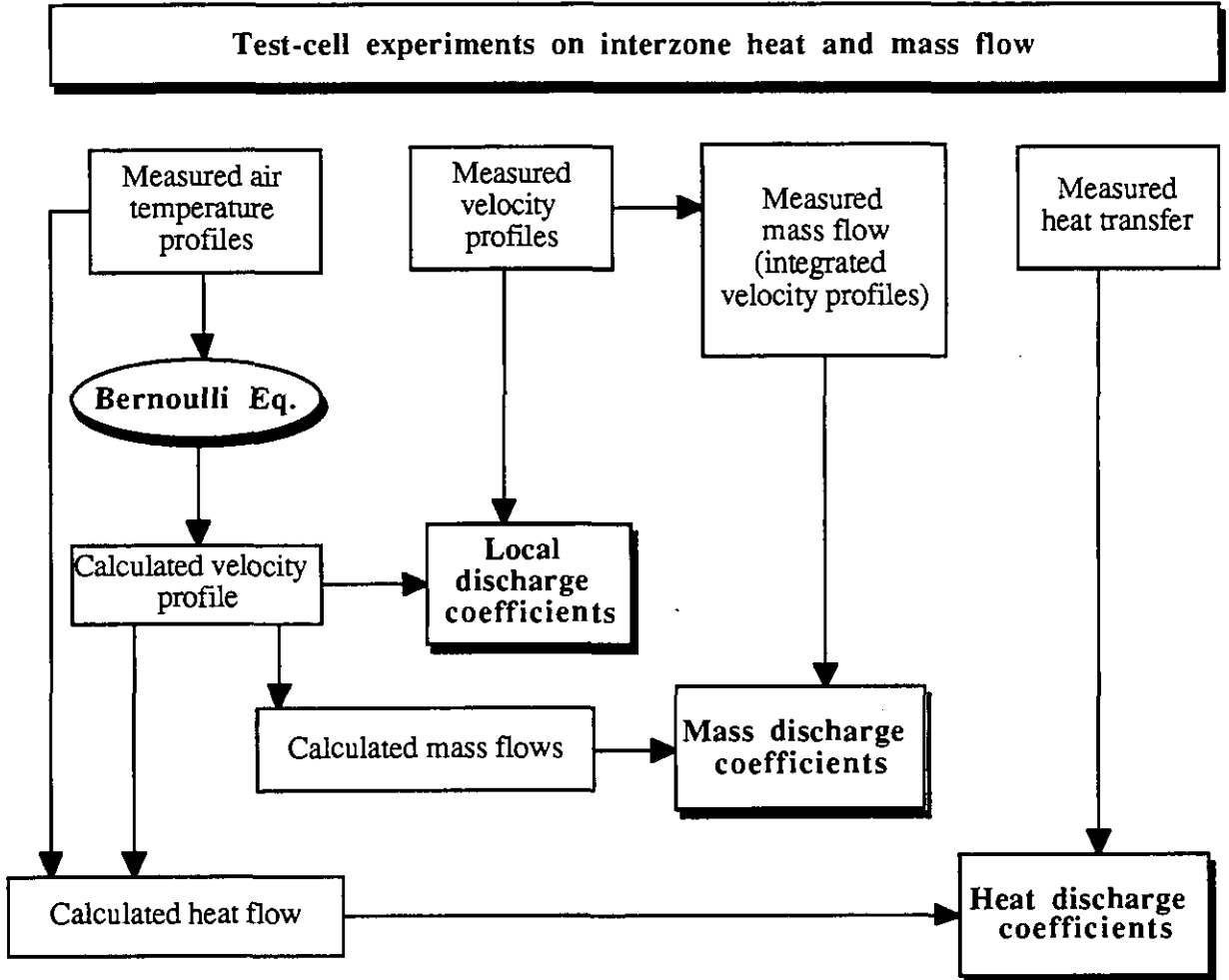
Figure 3.2 Relationships between local- mass- and heat- discharge coefficients determined in test cell experiments.

3.1.2 Working hypothesis for test cell experiments

From the literature review presented in chapter 2, it appears that there is a variety of definitions for discharge coefficients in the literature (it can be related to velocity, mass flow or heat flow), and experimental values vary over the range 0.3 to 0.8. The origin of the spread in values is not well understood.

Given the operational stage of experimental test cells, two in France and one in Belgium, it was possible to have a detailed look at the discharge coefficient and to perform three experiments differing mainly in the heating and cooling systems

To help the investigation of various aspects of the discharge coefficient the following *working hypothesis* was proposed

A.   The particular shape of the vertical temperature stratification depends on the details of the boundary conditions (Figure 3.1: model 1).

B.   The air velocities in the large opening can be calculated with the Bernoulli model from knowledge of the vertical temperature stratification in each zone (Figure 3.1: model 2).

C   The time dependent behaviour can be approximated by a succession of steady-state situations (Figure 3.1: model 6).

To predict the air temperature distribution from knowledge of the heating or cooling system and the wall temperatures in a closed room is already a large task (Moser 1991); the interaction with the two-way flow through the large opening adds to the complexity and makes the prediction of the zone air temperature stratification uncertain. Hypothesis A has not been verified in detail in subtask 2.1, and the main contribution was to verify hypothesis B through steady state mass flow studies in test cells (Figure 3.2).

It is good to recall here that the *energy aspect is always implicit* in inter-zone mass flow studies, because the heat transported by a given air flow depends both on the mass flows and the zone temperatures (Eq. 2.29).

In the following sections are presented the three test cell results obtained at the Université de Liège (section 3.2), the INSA de Lyon (section 3.3) and the CSTB de Sophia Antipolis (section 3.4). Next, the experimental results are compared with the computational fluid dynamics (CFD) code of the Concordia University, Montréal (section 3.5) and a discussion of the test cell results is presented for synthesis (section 3.6).

Further in section 3.7, are shown model developments at the EPFL de Lausanne and conclusions are drawn in section 3.8.

3.2   Liège University's Experimental Programme

3.2.1   Introduction

The experimental study carried out at University of Liège, started with a set of experiments in a calorimetric chamber *[Lebrun and Liebecq 1987]*. Then, a new set of experiments has been performed where the influence of the width of the door is studied for a number of heating and cooling loads *[Baranowsky et al. 1989]*. These first results have shown a relatively high dispersion in the correlations obtained.

After these preliminary results, a new series of tests was planned *[Fissore et al., 1990]*. In this new series, we try to approximate the experimental conditions to the hypothesis used for the mathematical model; mainly we try to eliminate the effect of air movement in the room due to the heating system. Therefore, the conditions of this group are close to the conditions of the mathematical model. This means that the present results can be used to validate the simplified mathematical model and also as a reference case to compare with other results of experiments performed in conditions close to a specific real condition.

3.2.2   Experimental facility and test procedure
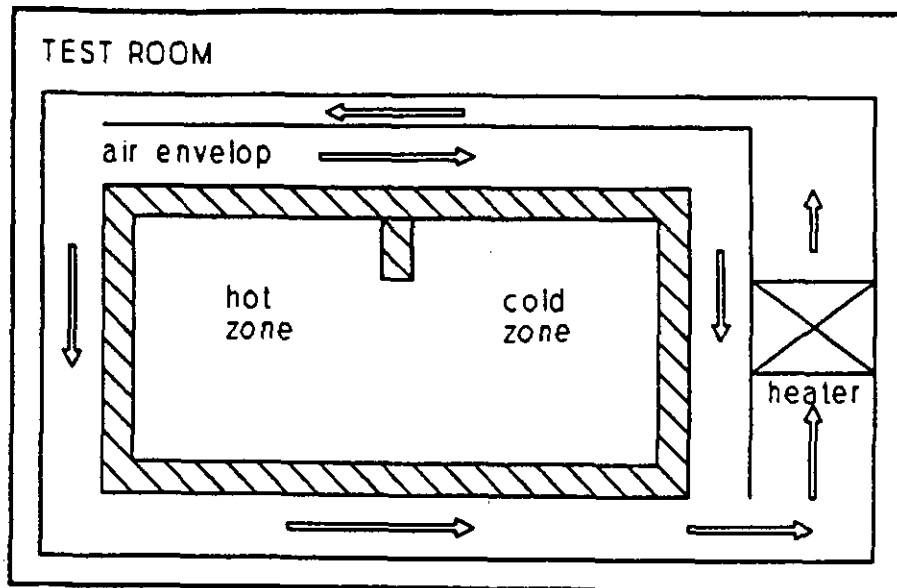
Figure 3.3: General principle of the calorimetric chamber.

Figure 3.3 shows a sketch of the test room used in this set of experiments, and Figure 3.4 shows a plane view and a cross section of this chamber. The calorimetric chamber is made of 100 mm polystyrene foam coated by 1 mm aluminum sheets on both sides. The two zones of the chamber are connected by an opening of 2.18 m height and 1 m width. The calorimetric chamber is bounded by a double envelope through which the air temperature is controlled. In the hot zone one vertical wall was covered with an electrical film heater and in the cold zone four vertical water-cooled radiators were placed.

Copper-constantan thermocouples are used for temperature measurements. The air temperature inside the chamber is measured in 8 columns with 11 points of measurement per column.

The location of each point is shown in Figure 3.5a, and the position of each column in the room is shown in Figure 3.5b. Furthermore, sixty nine points for surface temperature measurement are located along the walls of the chamber.

PLANE VIEW OF THE TEST ROOM

CROSS SECTION OF THE TEST ROOM
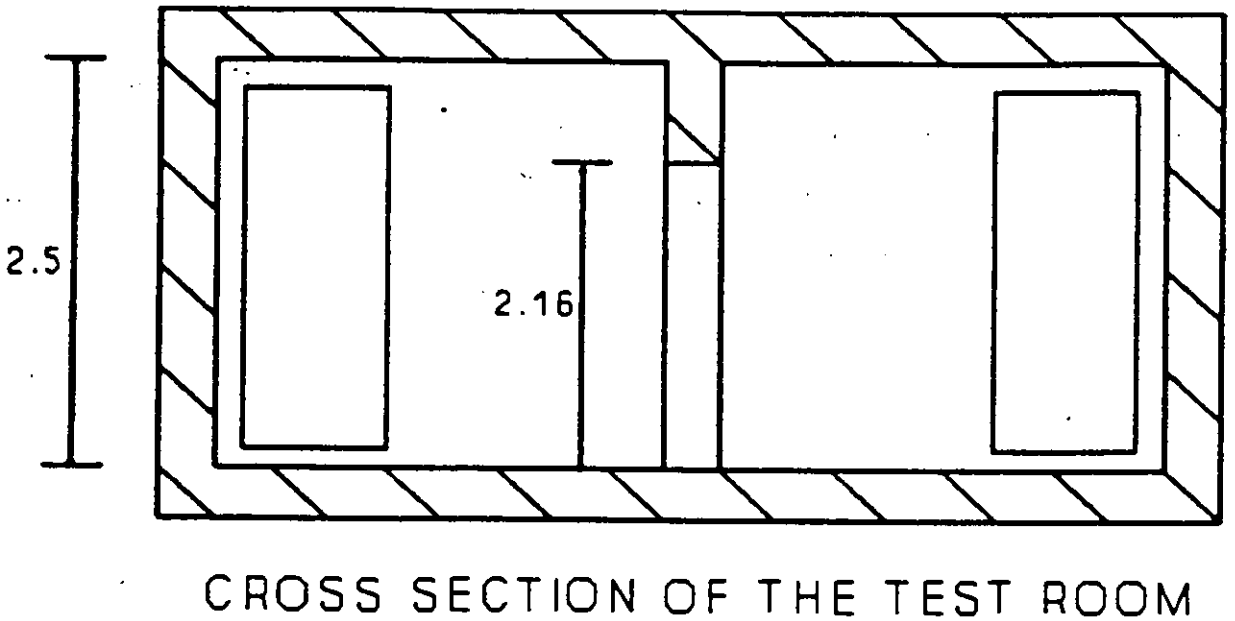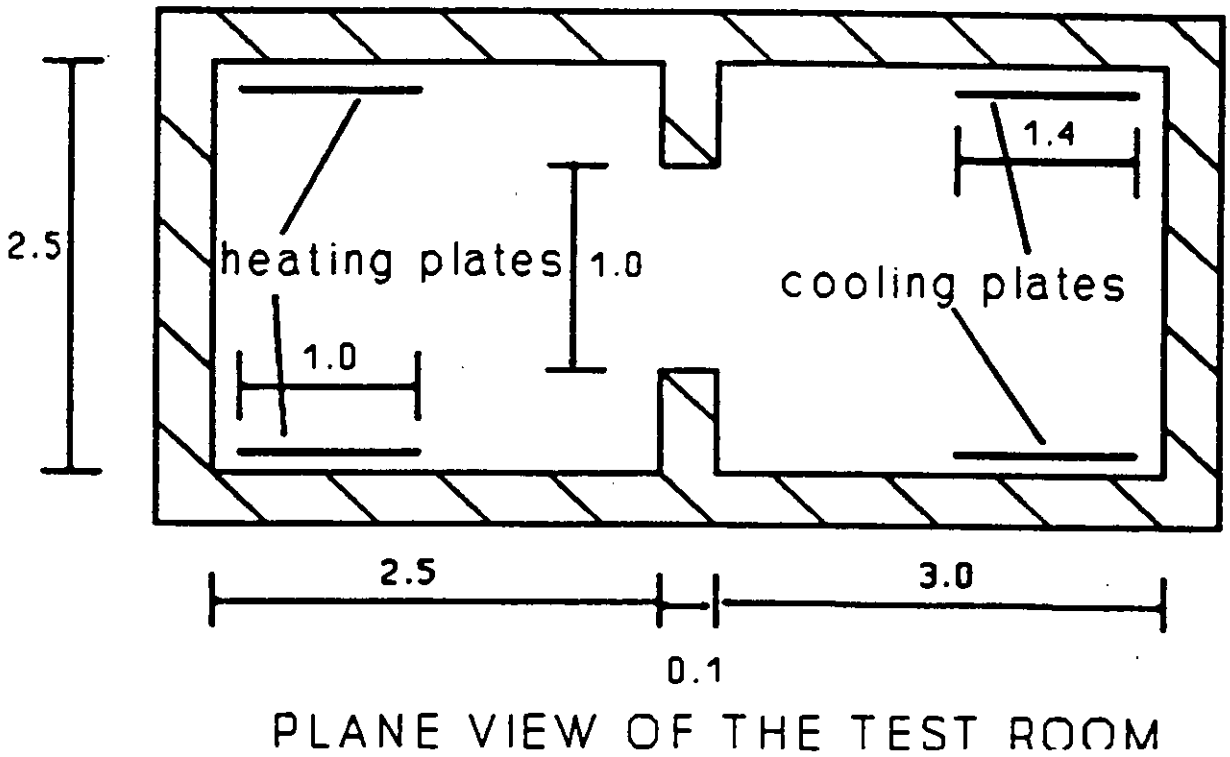
Figure 3.4: Sections of the test rooms

In the vertical plane of the opening, air temperature and velocity are measured respectively by thermocouples and by a hot wire anemometer (DISA 55D8, low velocity anemometer). A remote controlled trolley is used to move both sensors to any place in the opening. Figure 3.6 shows the location of each point of measurement in the plane of the opening.
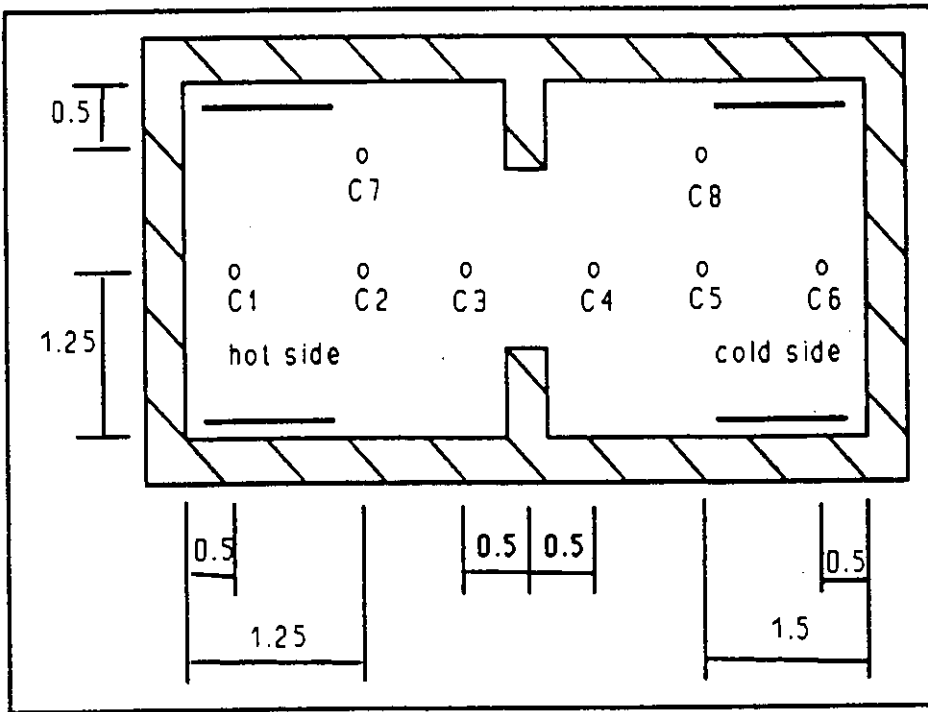
(a) column location
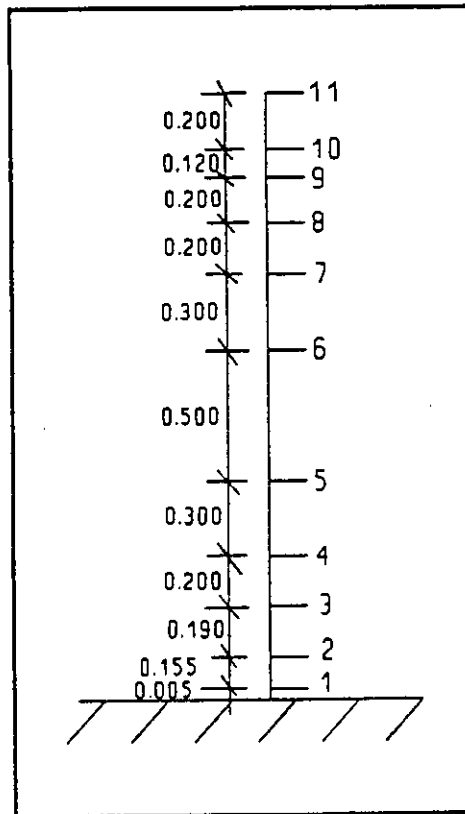
(b) vertical position

Figure 3.5: Measurement point location in the chamber
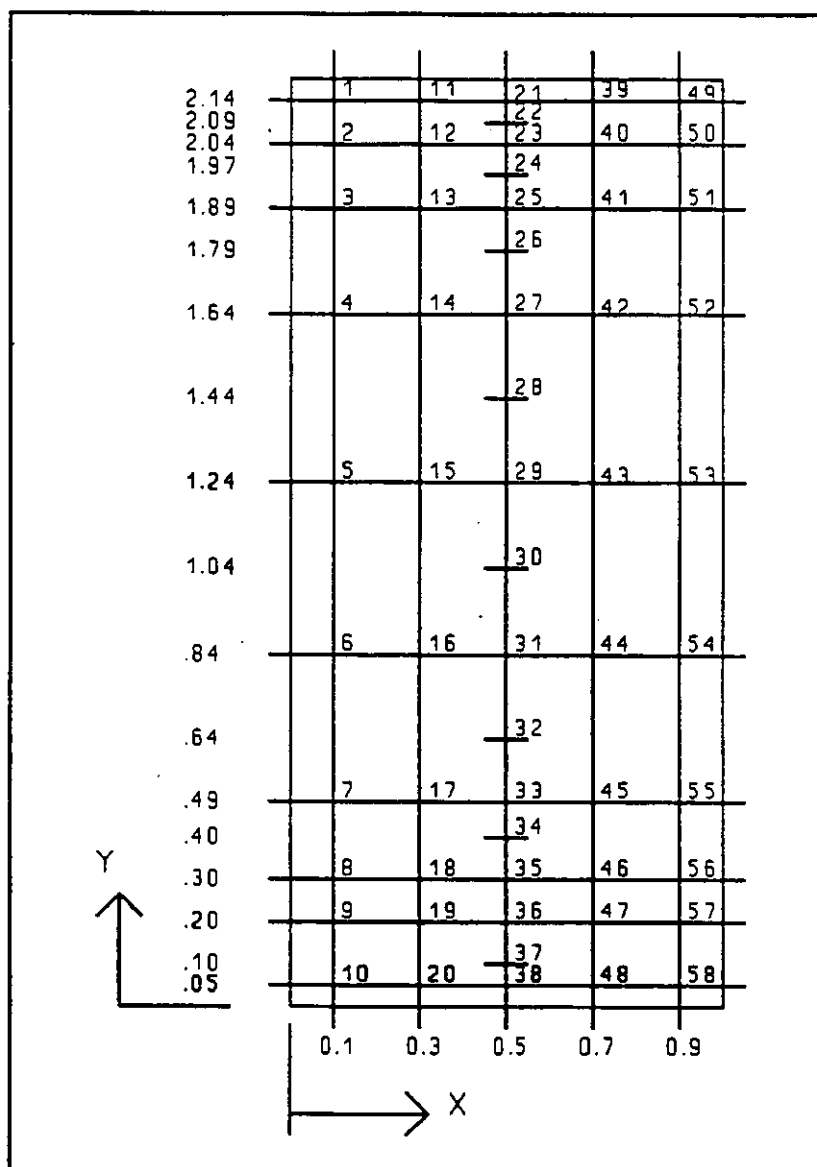
Figure 3.6: Measurement location in the opening.

The electric power provided to the active part of the hot wall, the flow rate and temperatures of the cooling water are measured continuously. A data logger ORION 3530 is used for data acquisition and also for the control of the temperature of the air in the envelope of the double walled calorimetric chamber.

Test procedure. The steady-state condition is reached after about 15 hours. All the temperatures and heating and cooling powers are then measured every 10 minutes and during 4 to 5 hours. During this period, measurements of air temperature and velocity are performed in each of the 58 points of measurement in the plane of the opening. The measurement time in each point is 2 minutes. At the end of each test a flow visualisation using smoke is also made.

A total of 5 tests with the same configuration and different heating and cooling powers were performed. Table 3.1 shows the main parameters of these experiments.

Test	Heating power (W)	Cooling power (W)
1	847	–786
2	245	–435
3	442	–602
4	854	–932
5	320	–493

Table 3.1: Main characteristics of the experiments

3.2.3 Results

Calculation of convective heat flows by heat balance of the chamber. Using direct measurements of the thermal field, we calculate the heating and cooling power supplied to both rooms, the conduction flux lost through the walls, and the radiative flux exchanged through the opening. Then, solving heat balances in each room, we can find the convective flux lost by each room through the opening (Φccon and Φhcon). These two flux should be symmetric, in reality differences due to errors in measurements, or another physical phenomenae not considered in the heat balance do exist. In the following part of the work we assume that the actual convective heat flow passing through the opening (Φcon) is equal to the mean value of Φccon and Φhcon. Table 3.2 gives a synthesis of the results obtained.

Test	Φ_{con} (W)	Φ_{hcon} (W)	Φ_{ccon} (W)
1	691	694	687
2	267	214	320
3	432	383	480
4	756	736	775
5	325	312	338

Table 3.2: Synthesis of the results

Thermal fields in both rooms. Figure 3.7 shows the vertical gradient of temperature for the test 1. Figure 3.7a shows the temperature in the hot room for the columns 1, 2 and 3. Figure 3.7b shows the temperature in columns 4, 5 and 6 for the cold room. We found an important gradient of temperature in the vertical plane. This is a typical situation for this configuration of heating and we will see in the next pages that it is very important to consider this stratification for the calculation of Φcon. In contrast, the temperature in the horizontal plane changes only near the opening.

3.2.4 Calculation of air flows through the opening

Before starting with the study of the air flow and velocity field, it is necessary to consider some results of the visualisation tests.
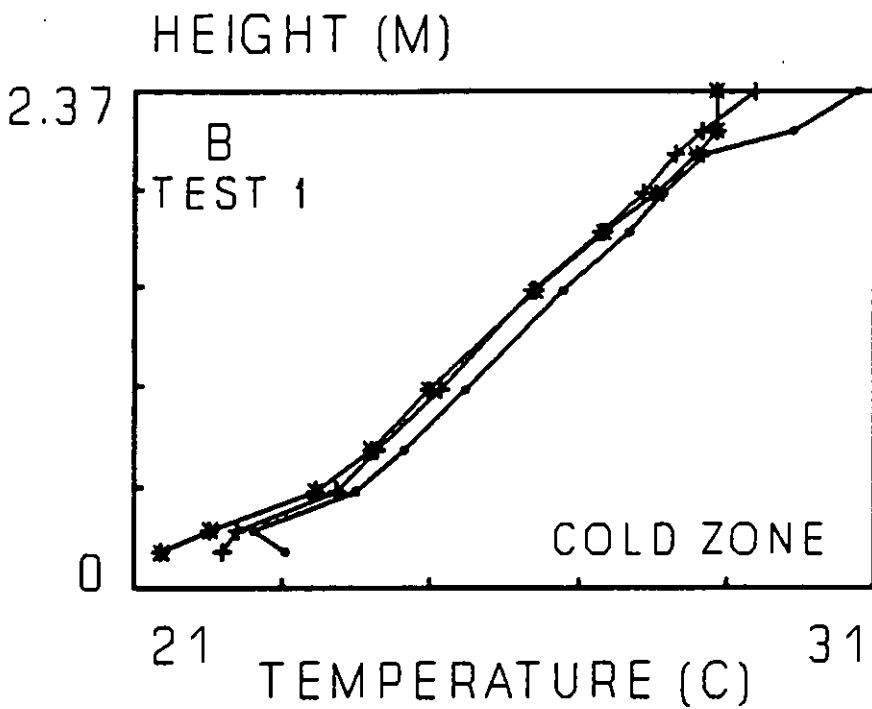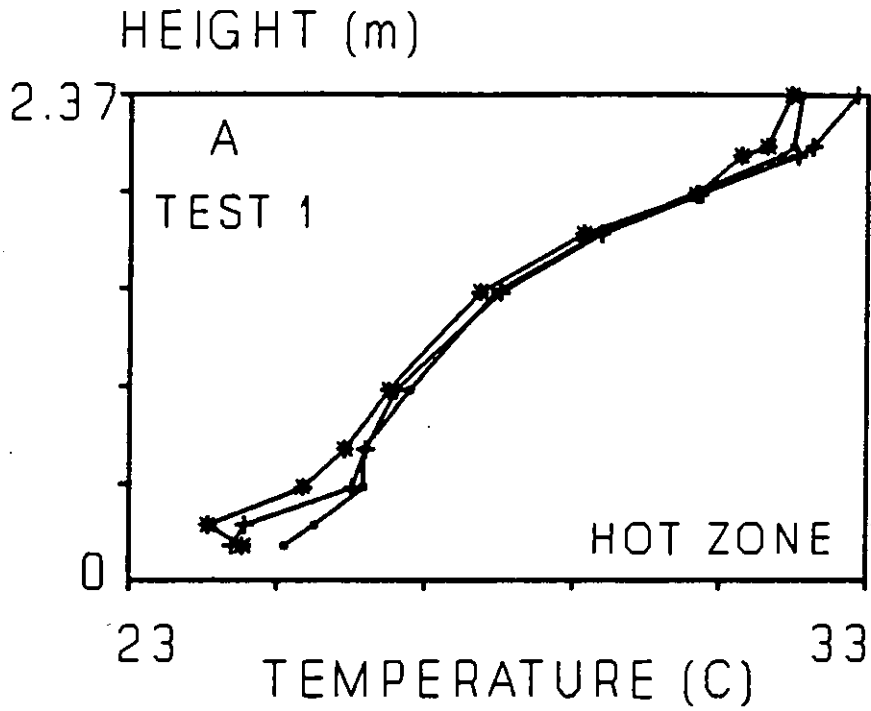
Figure 3.7 : Vertical temperature profiles in the chamber (Test 1)

CROSS SECTION

HOT SIDE

COLD SIDE

HEATING PLATES

HOT SIDE

COOLING PLATES

COLD SIDE
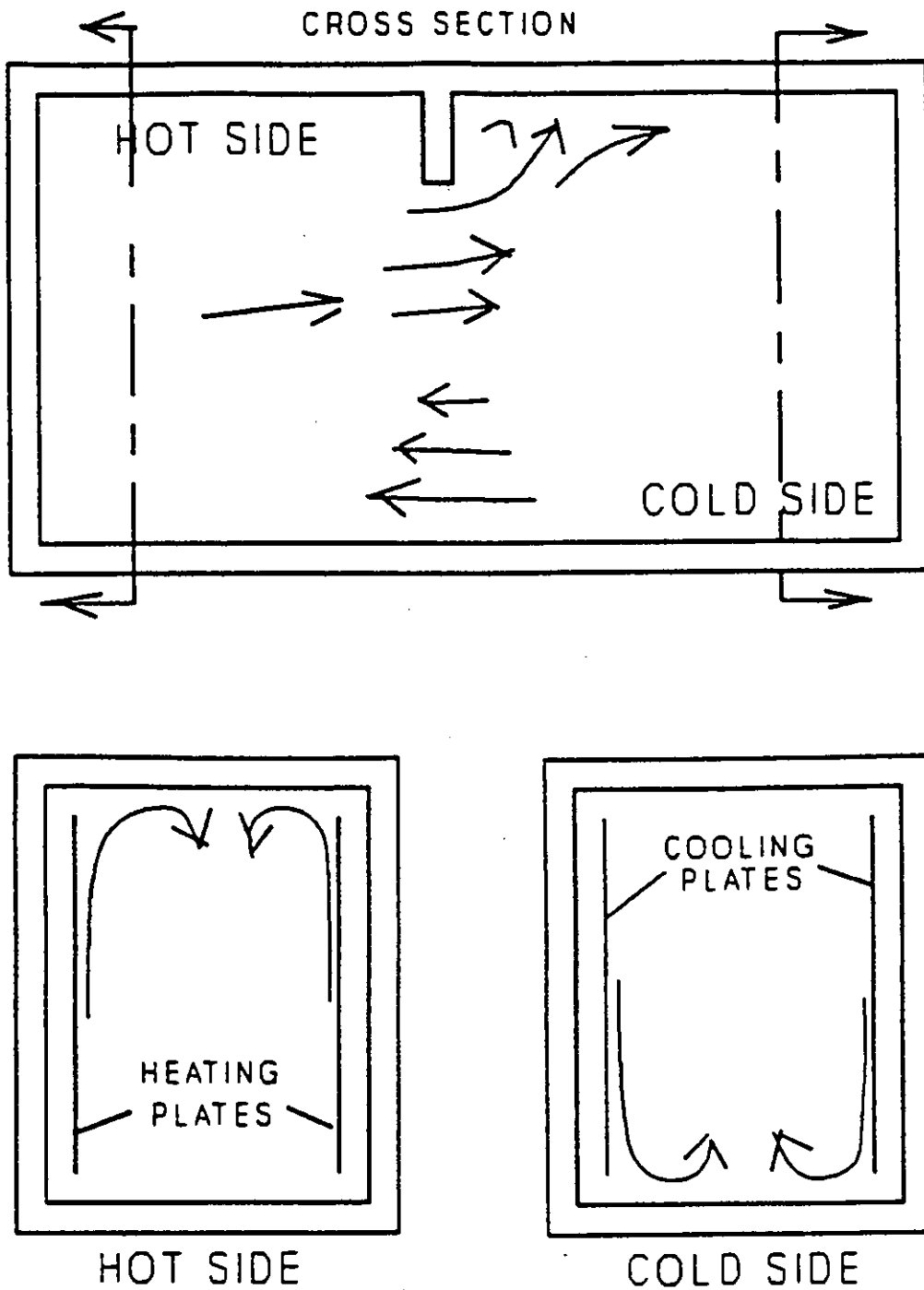
Figure 3.8 : Typical flow patterns in the chamber

Figure 3.8 shows a typical case of air movement. In the upper part of the cross section, we can see that the air flow is diverted to the ceiling and velocities are not strictly in the horizontal direction.

Both cooling and heating plates produce a convective plume, to the ceiling for the heating zone and to the floor for the cooling zone. But in both cases, this perturbation exists only close to the plates. When this flow reaches the end of the plate, it changes in direction and the air velocity becomes very small and does not affect the bulk-density-driven flow through the opening.

Figure 3.9 shows the vertical velocity profile in the opening for test 1. We can see that these different velocity profiles are very close.
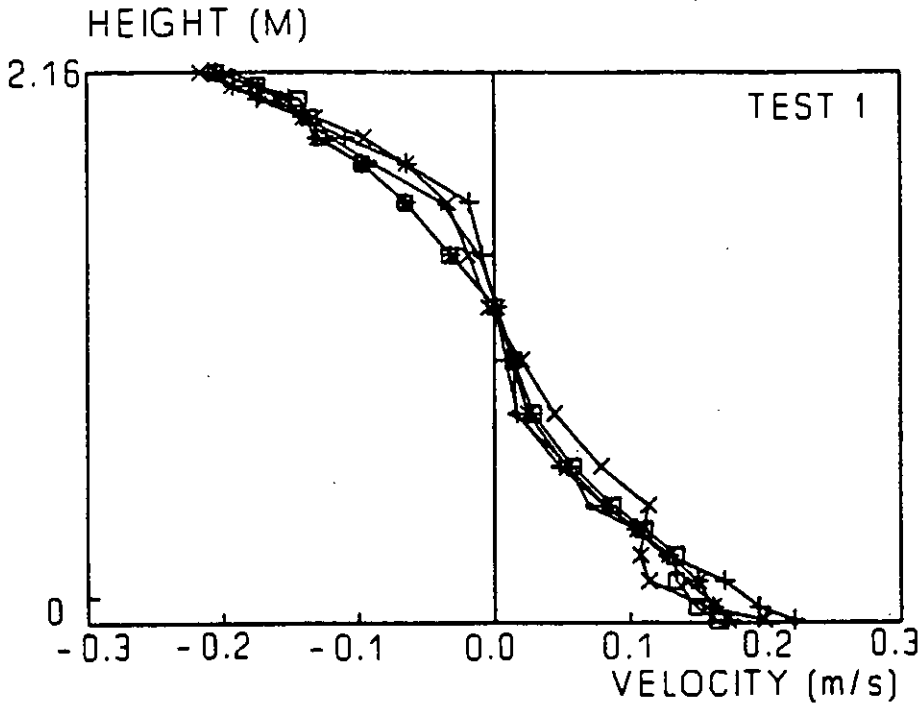
Figure 3.9 : Vertical velocity profiles through the opening (Test 1)

	All Data			Only Central Line			
Test	m+	m−	mv	m+	m−	mv	mv/mc
1	.110	.097	.103	.094	.094	.097	1.06
2	.095	.074	.085	.095	.076	.086	.99
3	.106	.089	.098	.099	.086	.093	1.05
						Mean	1.03

Table 3.3 : Calculated air flows

m+ : air flow calculated with velocities of the lower zone of the opening
m− : air flow calculated with velocities in the upper zone.
mv : (m+ + m−)/2 , flow calculated with all data.
mc : (m+ + m−)/2 , flow calculated considering only velocities in the central plane.

Figure 3.10 shows some variation in velocity profiles observed in an horizontal direction in the plane of the opening. To check the influence of non homogeneous velocity fields we calculate the air flow considering all the velocities measured in each test (58 point by test), and the air flow considering only velocities taken in the central plane of the opening (point 21 to 38). These values are shown in Table 3.3.
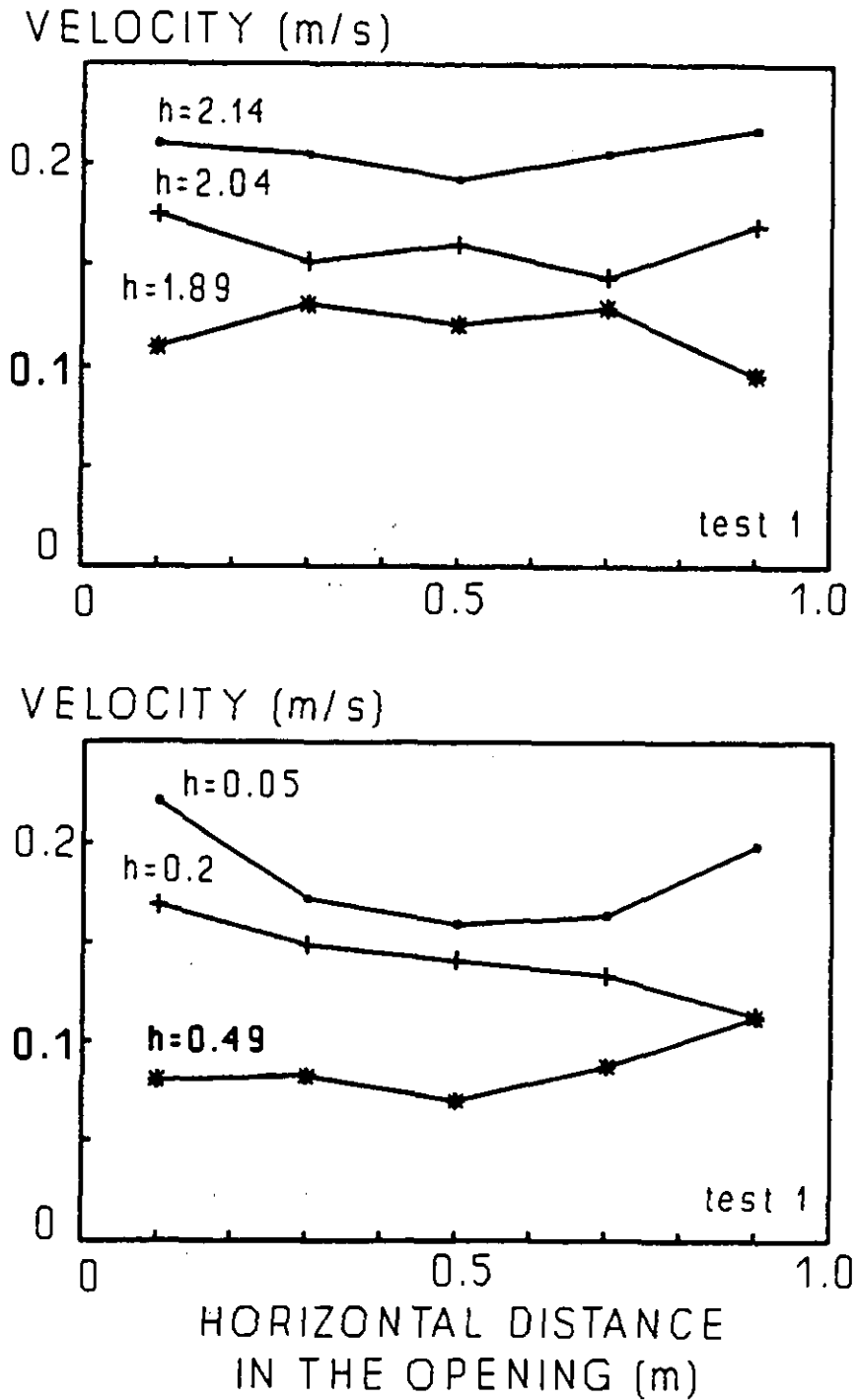
Figure 3.10 : Horizontal velocity profiles in the opening

The factor mv/mc (Table 3.3) shows that the air flow in the whole opening can be well represented by the air flow calculated only with data corresponding to the central line.

As we find some differences between the air flow calculated with measurements made in the upper zone and in the lower zone of the opening, in the calculations we will use the mean value of the two results.

In the following analysis we will calculate the velocity profiles in the centre line of the opening using Bernoulli's equation, with three different formulations for the temperature profile in each zone.

* Case A: the temperatures are used directly as measured
* Case B: a linear temperature gradient is fitted
* Case C: a mean temperature is calculated

A dimensionless stratification parameter is built using the temperature difference between the two rooms to characterise the thermal stratification in each zone. Table 3.4 shows b_1 (for hot zone), b_2 (for cold zone) and mean temperature for each side of the opening, Table 3.5 shows the results of calculation obtained with data of columns 1 and 6, and considering the cases A, B and C.

Test	b_1	b_2	Tm_1	Tm_2
1	2.98	3.05	27.89	25.59
2	2.47	3.25	22.97	21.55
3	2.69	3.19	24.00	22.39
4	2.91	3.21	27.22	24.82
5	2.33	2.77	23.02	21.53
Mean	2.68	3.09		

Table 3.4: Thermal stratification in both zones.

Test	m_A	m_B	m_C	m_A/m_B	Cd_A	Cd_B
1	.315	.346	.345	.91	.33	.31
2	.237	.256	.256	.93	.36	.33
3	.270	.292	.293	.93	.36	.33
4	.323	.353	.353	.92	.34	.33
5	.259	.284	.285	.93	.35	.33
			Mean	.93	.35	.33

Table 3.5: Calculated air flows and Cd coefficients.
$Cd_A = m_A/mv$ and $Cd_B = m_B/mv$.

We can see that differences of m_B and m_C are not significant, however m_B is about 7% higher than m_A. This difference is produced because in reality, the actual temperature profile is not linear. Furthermore, Cd coefficients are in good agreement with those found by *Mahajan [1987]* and *Wilson and Kiel [1990]*.

3.2.5 Calculation of convective heat flux

The knowledge of the velocity profile and temperature in the plane of the opening permit to calculate the heat flow by direct integration. In practice, we don't have the real profile of temperature in the opening, but we can estimate the mean value and the gradient of temperature in each zone. We propose to take an estimate of the heat flow through the opening using vertical temperature profiles of both zones, then the heat flow can be calculated using these temperature profiles as reference.

$$\Phi = C_p \, k_1 \left(\left| \int_0^{Z_n} m(z) \, T_2(z) \, dz \right| + \int_{Z_n}^{H} \left| m(z) \, T_1(z) \, dz \right| \right)$$

(3.1)

where

$T_1(z)$ is the vertical temperature profile in the hot zone

$T_2(z)$ is the vertical temperature profiles in the cold zone

k_1 is an empirical constant

$m(z)$ is the calculated mass flow.

We define:

$$Te_1 = \frac{\displaystyle\int_0^{Z_n} m(z) \, T_1(z) \, dz}{\displaystyle\int_0^{Z_n} m(z) \, dz}$$

(3.2)

and

$$Te_2 = \frac{\displaystyle\int_{Z_n}^{H} m(z) \, T_2(z) \, dz}{\displaystyle\int_0^{Z_n} m(z) \, dz}$$

(3.3)

as

$$m = \int_0^{Z_n} m(z) \, dz$$

(3.4)

Then,

$$\Phi = m \, k_1 \, C_p \, (Te_1 - Te_2)$$

(3.5)

The empirical constant k_1 takes into account all the simplifications in the formulations of these equations mainly the fact that the temperature profiles used are estimated in the rooms and not obtained in the opening. Table 3.6 shows the calculated heat fluxes and k_1 coefficients.

Test	Φ_{the} (W)	Φ_{con} (W)	k_1
1	738	691	.94
2	282	267	.95
3	431	432	1.00
4	798	756	.96
5	356	.325	.91
		Mean	.95

Table 3.6: k_1 coefficients

Considering that velocity measurements are the first source of uncertainty when calculating the mass flows, we propose to use direct evaluation of heat transfers calculated from heat balances of each room as a starting point to estimate the air flow from a standard temperature difference DT_e between the two rooms. Finally we define a new discharge coefficient as the ratio of this new expression of the mass flow mv' and the theoretical reference one m_B. Table 3.7 gives the results obtained using this method.

Test	m_v' (kg/s)	m_B (kg/s)	Cd'
1	.133	.346	.38
2	.121	.256	.47
3	.134	.292	.46
4	.142	.353	.40
5	.112	.284	.39
		Mean	.42

Table 3.7: Cd coefficients

3.2.6 Remarks and conclusion

The flow visualisation shows that air flow patterns in the rooms are influenced by the air temperature difference between rooms and not by the mixed convection produced by heating and cooling systems.

Finally, we can say that our experimental conditions are very close to the conditions required by Bernoulli's theory. Nevertheless, the inviscid flow condition is not checked and we have to define an empirical coefficient Cd to fit it with our experiments.

Present results show a mean value of Cd of:

Cd = 0.33 Calculated considering the measurements of velocity in the opening.

Cd = 0.42 calculated considering the heat balance of the calorimeter.

On the one hand, temperature measurements are more accurate than velocity measurements, but on the other hand the writing of heat balances of each zone needs the evaluation of radiative and conductive fluxes related to more hypothesis, and takes into account thermophysical properties of the wall of the chamber which introduce more uncertainty in the evaluation of the resulting mass transfer.

This comparison shows the difficulty in determining phenomenological discharge coefficients, their determination remains a very important task in this field for next years.

3.3 The Minibat Laboratory Facility, CETHIL, Centre de Thermique de l'INSA de Lyon, France

3.3.1 The experimental facility

The basis of INSA's experimental facility is the MINIBAT test cell *[Allard et al. 1988]* built in a controlled environment. Figure 3.11 presents a longitudinal section of this experimental test cell made of two single volumes of 3.1 by 3.1 by 2.5 m bounded on five sides by air volumes regulated at a constant air temperature, and connected together by a doorway.

The sixth side called the facade is removable, but we usually use a 10 mm thick single glazing. This facade is submitted to regulated climatic conditions created inside a climatic housing where we can vary the air temperature from $-10°C$ to $+40°C$ with a very good stability ($\sim 0.1°C$) in time.

A solar simulator and electrical heating films located along the surfaces of the internal surfaces of the walls of the two cells complete the set up and enable us to generate a wide range of boundary conditions.
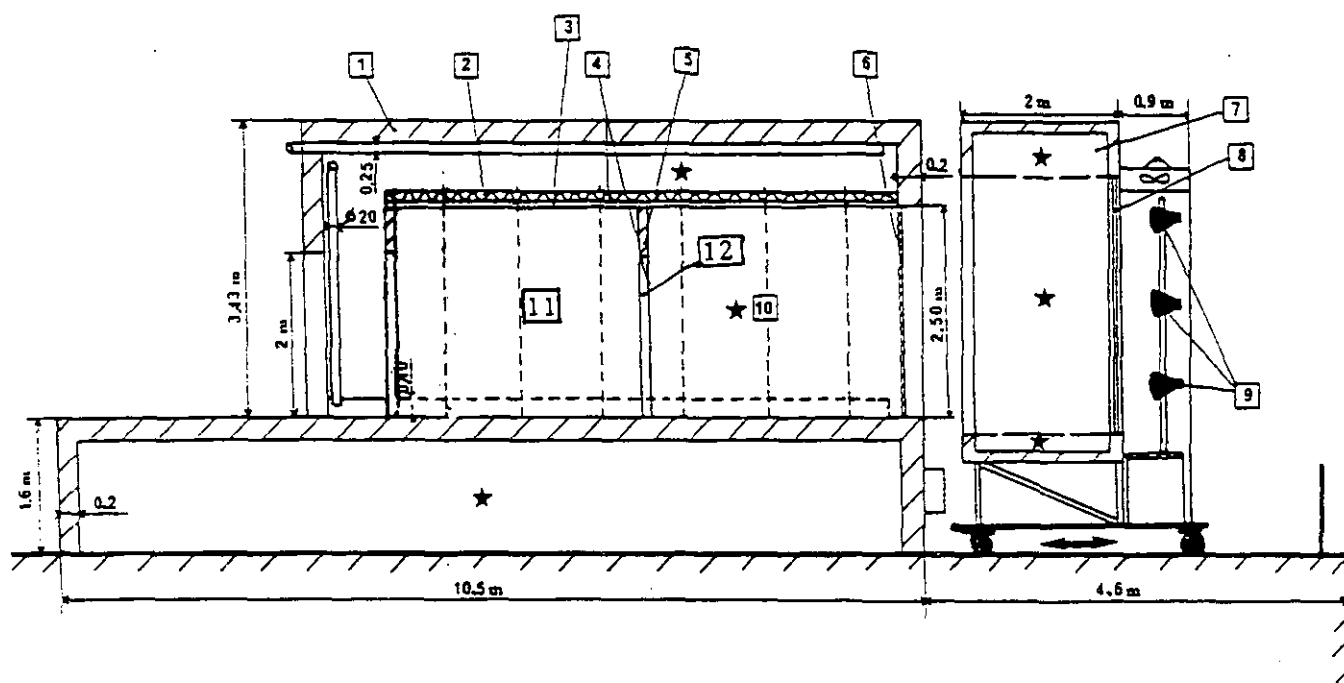
Nomenclature :

1 : external envelope (cellular concrete e=20 cm)
2 : fibreglass (e=5cm)
3 : plywood (e=2,5cm)
4 : gypsum board (e=1cm)
5 : fibreboard (e=5cm)
6 : glazing (e=1cm)
7 : mobile climatic housing

8 : double glazing (10-8-10 mm)
9 : solar simulator (12 lamps CSI 1000 W)
10 : test cell 1
11 : test cell 2
12 : doorway

Figure 3.11: Longitudinal section of MINIBAT

Measurement device. The measurement facilities consist of 300 probes, mainly 0.2 mm thermocouples which give us the temperature fields along the internal and external surfaces of the walls of both rooms.

RTD 100 Ω probes are used to control all climatic conditions in the various volumes surrounding the test cell. Each sensor has been calibrated in our laboratory in order to guarantee 0.05°C accuracy for RTD probes and 0.15°C for thermocouples.

Through the doorway air velocity is measured by a hot film probe and air temperature measurement are made by a 0.08 mm thermocouple. An autonomous displacement system enables us to move these two probes in the vertical plane of the doorway. Figure 3.12 shows a typical location of measurements within this plane.
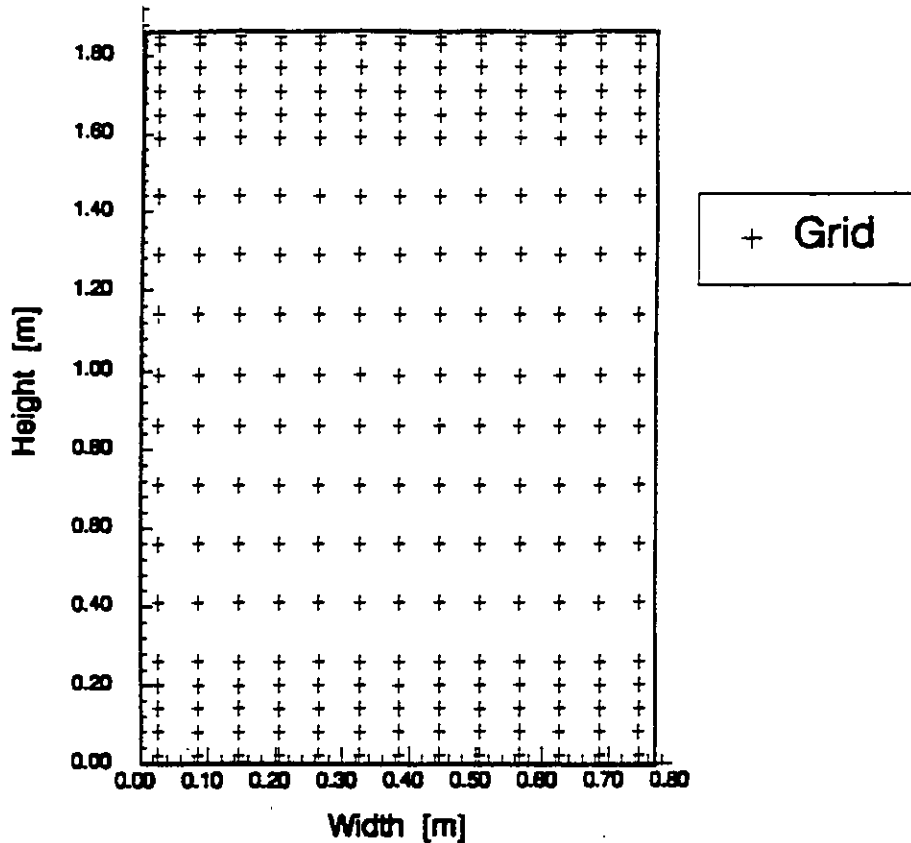
Figure 3.12: Measurement grid in the aperture

3.3.2 Aim of our study

The first goal of our study is to provide a better knowledge of heat and mass transfers through doorways. The literature review presented in chapter 2 has shown the important discrepancies existing between various authors concerning the definition of discharge coefficients.

Furthermore, an ambiguity remains on the physical model to be applied in order to predict the air flow rates through a large vertical opening since the transition between bulk density driven flows and boundary layer driven flows is not clearly defined.

In order to contribute to an improvement of physical knowledge and numerical prediction of heat and mass transfer through doorways, we focus mainly on small temperature differences between the two rooms and we use two different kinds of boundary conditions. Either a single active (hot or cold) vertical wall is imposed or two opposite vertical walls are active, one hot, the other cold. At first, only natural convection configurations are studied, avoiding any thermal or dynamic perturbation due to thermal plumes of heating systems, or of air jets from ventilation or air conditioning systems.

3.3.3 Main results

a) Definition of the different tests performed. The two first experiments correspond to a cold vertical face opposed to a hot vertical face. For the three last experiments, only one vertical face is active, the façade which is regulated at a different temperature than the others. In Table 3.8, ΔT_{21} represents the difference between the two central air temperatures measured in each room.

EXP:	$T_{s1}°C$	$T_{s2}°C$	$\Delta T°C$	$\Delta T_{21}°C$
1	7.5	38	30.5	2.7
2	12.5	38	25.5	2.9
3	3	16	13	1.28
4	11.7	17.9	6.2	.69
5	28	22.5	−5.5	−.64

Table 3.8: The different tests performed

b) Analysis of thermal gradients in both zones. We can notice on Figures 3.32 and 3.33 a regular vertical stratification of air temperature in each zone for all the five tests. In tests 1 and 2, an increase of the thermal gradient close to the ceiling appears in Figure 3.13. It can be explained by an increase of horizontal velocities in this region. A symmetric behavior can be seen in Figure 3.14 close to the ceiling.
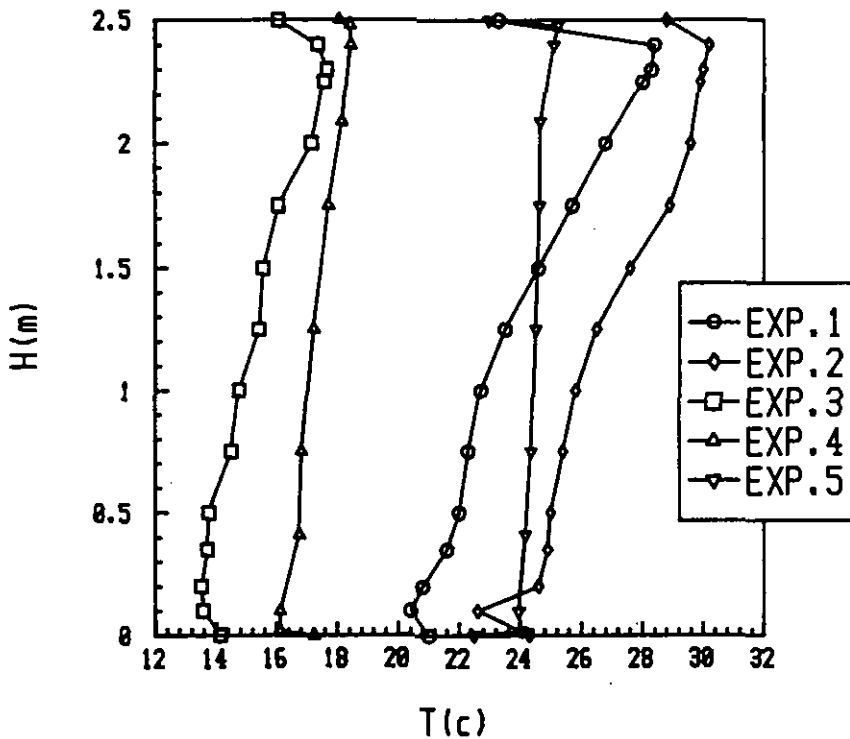
Figure 3.13 : Vertical profiles, hot ceiling
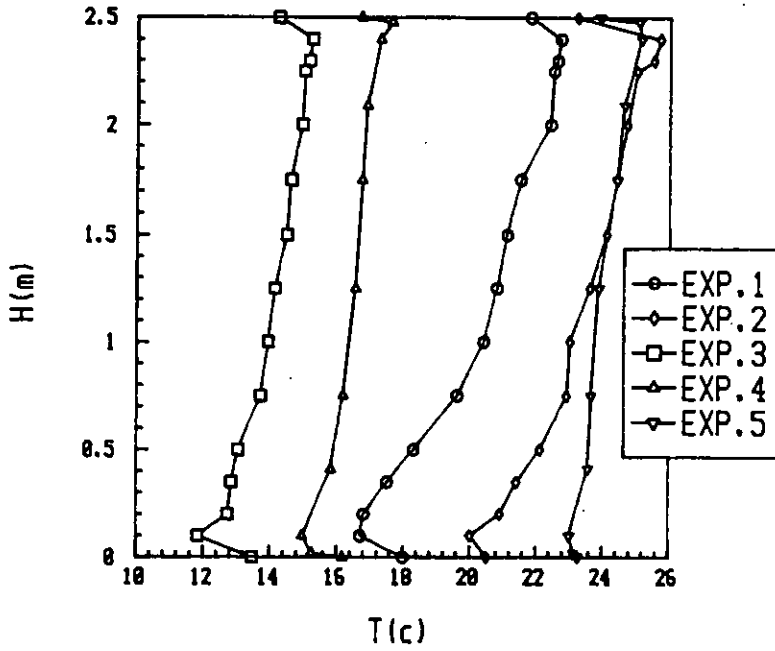
Figure 3.14 : Vertical profiles, cold ceiling

c) Velocity and temperature profiles through the opening. Figure 3.15 and 3.35 present respectively the temperature and velocity profiles measured along the vertical symmetry axis of the opening. These figures show that for experiments 1 and 2, the neutral level is located at the mid-height of the opening which fits very well with the symmetric (cold/hot vertical surface) boundary conditions.
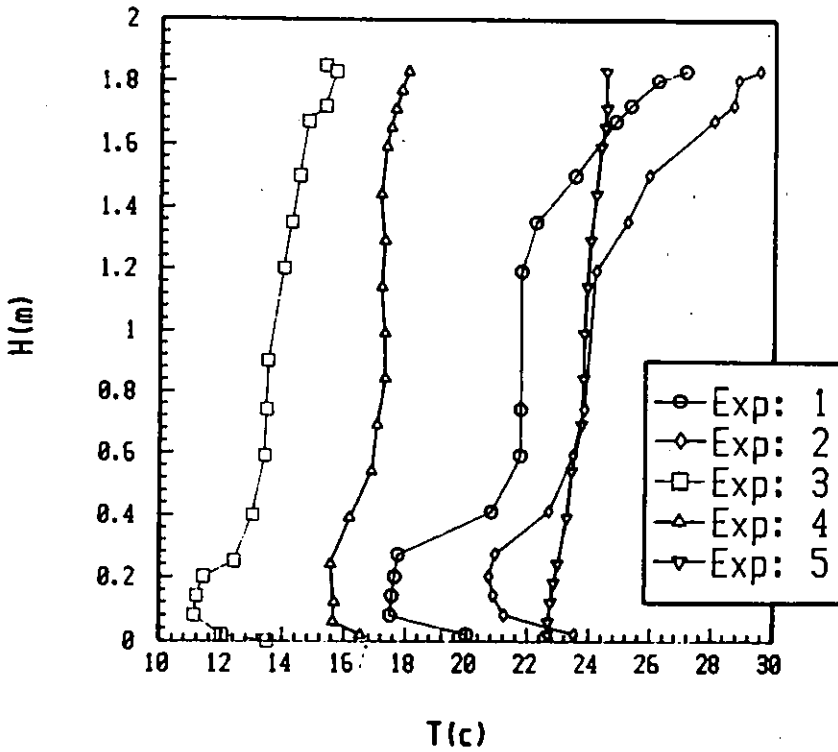
Figure 3.15 : T°C.Median axis aperture
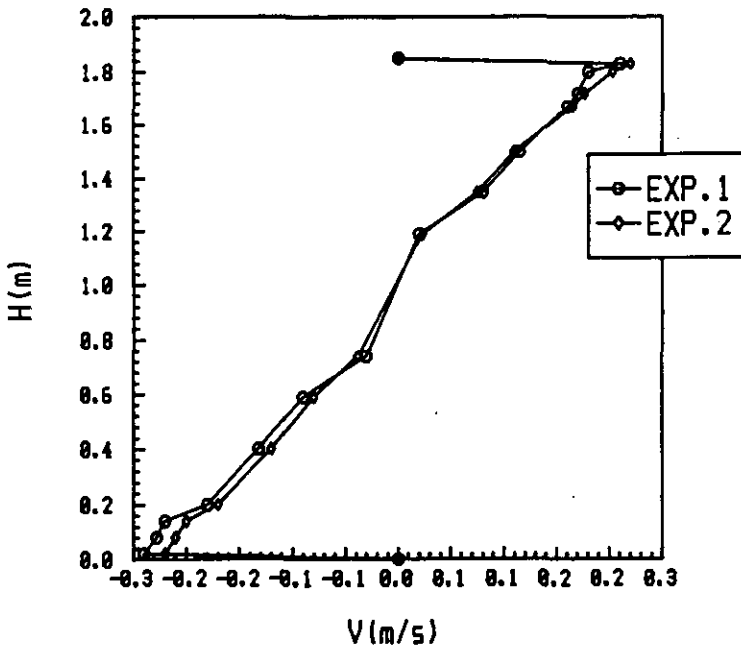
Figure 3.16 : Velocity profiles

For the other tests, the vertical profiles given in Figure 3.18 present a lower neutral level (at ≈0.90 meter). These experiments correspond to a single active vertical surface (hot or cold). This boundary condition leads to a different flow pattern within the cell, and the displacement of the neutral plane is only the result of this fact. Furthermore, the temperature profiles presented in Figure 3.18 show a different behavior for experiment 5. In this case the active surface is hot which leads to a quite perfect thermal stratification of air in both rooms (Figure 3.13 and Figure 3.16) and through the opening. An other important result is a very good symmetry with respect to the central vertical axis of the opening. Figure 3.17 shows the horizontal velocity profile measured 2 cm from the top of the opening.
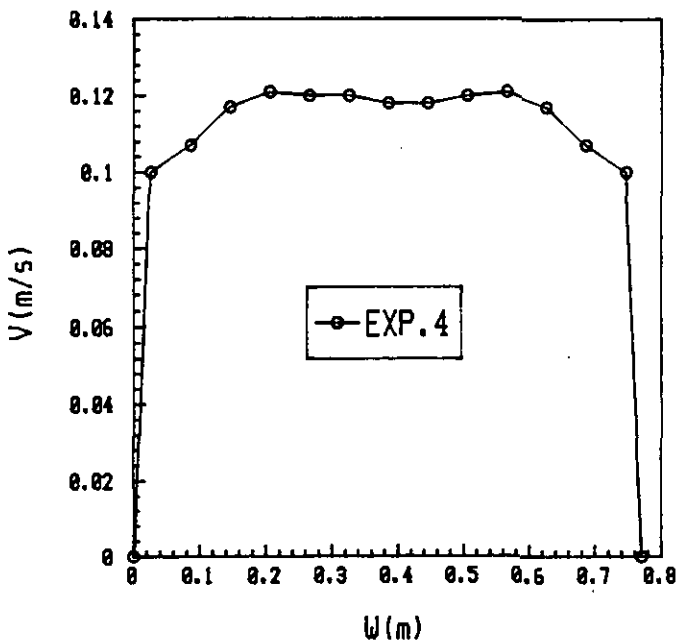
Figure 3.17: Horizontal velocity profiles
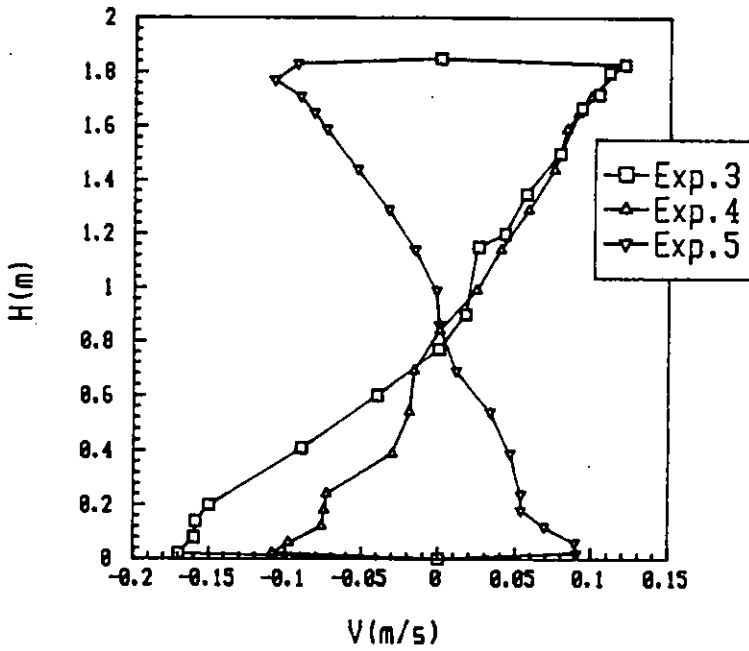
Figure 3.18: Velocity profiles(m/s)

3.3.4. Discharge coefficient evaluation.

At first, we calculate the experimental mass flow rate by integration of the experimental velocity and density profiles provided by the temperature field. Table 3.9 presents the direct results of this calculation. Due to the precision of velocity measurements for low velocities, the mass balance is checked within 10 % for most of our experiments. Test 4 presents the maximum gap between the air flowing at the upper part of the opening and the mass flow below the neutral plane. Nevertheless, in order to simplify our approach of discharge coefficients, we use in the following parts of our report the average value $(m'_h + m'_b)/2$.

a) - Constant air density. In order to check the validity, or the limits, of the rough Bernoulli's approach with constant air density on both sides of the opening, we define at first the discharge coefficient as the ratio between the mass flow calculated from the experimental data, and a theoretical value calculated assuming constant zone temperature on both sides (see section 2.1.3.1). The values obtained (Table 3.10 and Table 3.11) are quite similar to those presented by *Fissore and Liebecq* (Section 3.2) and close to those described by *Mahajan & Hill [1987]*.

Exp:	m'_h	m'_b
1	.081	.088
2	.079	.090
3	.058	.064
4	.055	.034
5	.040	.032

Table 3.9:Experimental mass flow rates(kg/s)

Exp:	m'_{exp}	m'_{th1}	Cd_1
1	.084	.220	.38
2	.084	.225	.37
3	.061	.142	.43
4	.0448	.0978	.46
5	.036	.102	.35

Table 3.10: Mass flow rates(kg/s) and Cd_1 values

b) - Constant density gradients. Using the measured vertical temperature profiles, we are able to fit the density profiles on both sides of the opening by a straight line defining a constant density gradient in each room. Then, by Bernoulli's approach, we calculate the theoretical mass transfer through the opening taking into account these linear gradients of density on both sides (see section 2.1.3.2). The ratio between the experimental mass flow rate and the theoretical one delivers a new evaluation of a Cd coefficients, Cd_2 (Table 3.11). It is seen that the theoretical mass flow rate m'_{th} is not significantly modified by the new calculation prodedure.

Exp:	m'_{exp}	m'_{th2}	Cd_2
1	.084	.223	.37
2	.084	.210	.40
3	.061	.113	.54
4	.044	.095	.47
5	.036	.130	.27

Table 3.11: Mass transfer (kg/s) and Cd2 value

c) - Local Cd determination. The experiments give us the vertical temperature profiles in both rooms, and the temperature and velocity profiles in the vertical plane of the opening. At each height, we are able to calculate both the density of the flowing air and the local theoretical velocity (Eq. 2.27). Then, the ratio between the experimental value measured in the vertical mid-axis of the opening and the former theoretical value delivers a local value of the discharge coefficient Cd(z).
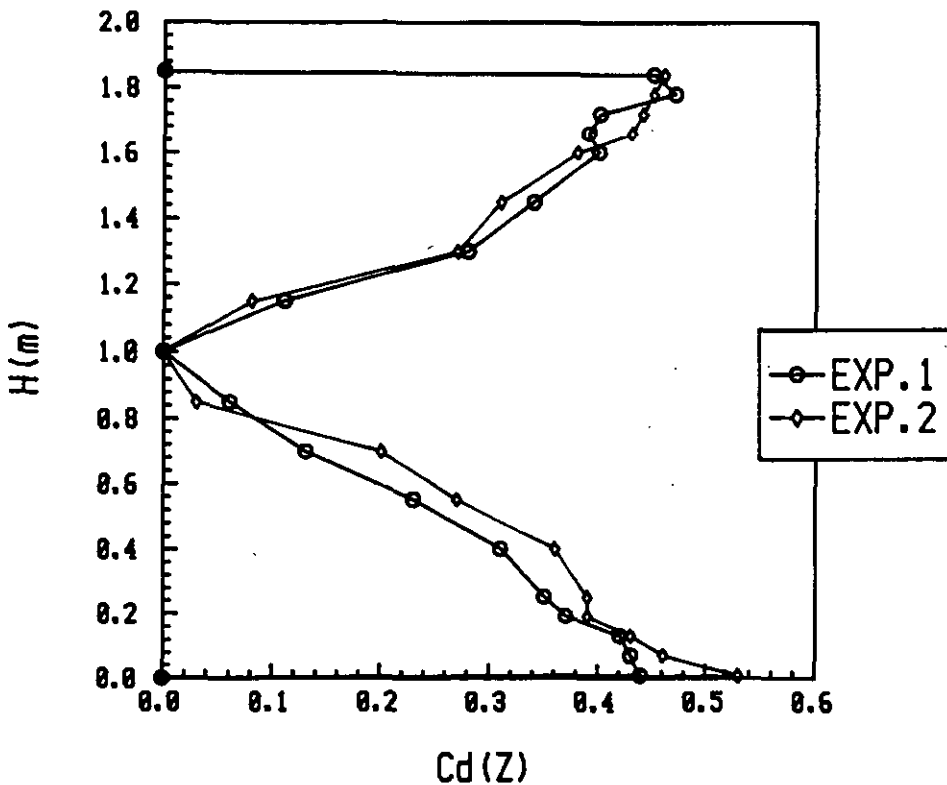

Figure 3.19: Local Cd profiles, experiments 1 and 2.

Figure 3.19 shows that in tests 1 and 2, when symmetrical boundary conditions are applied, the Cd(z) distribution presents a good symmetry. In opposition, Figure 3.20 shows a clear asymmetry in case of tests 3, 4 and 5 performed with only one active vertical surface. The results are not sufficient to come to general conclusions, but it is clear that we can expect different kinds of Cd distribution corresponding to different kinds of boundary conditions. This point can be very helpful in order to model more accurately the effect of heating systems or air conditioning on heat and mass transfers through large openings.
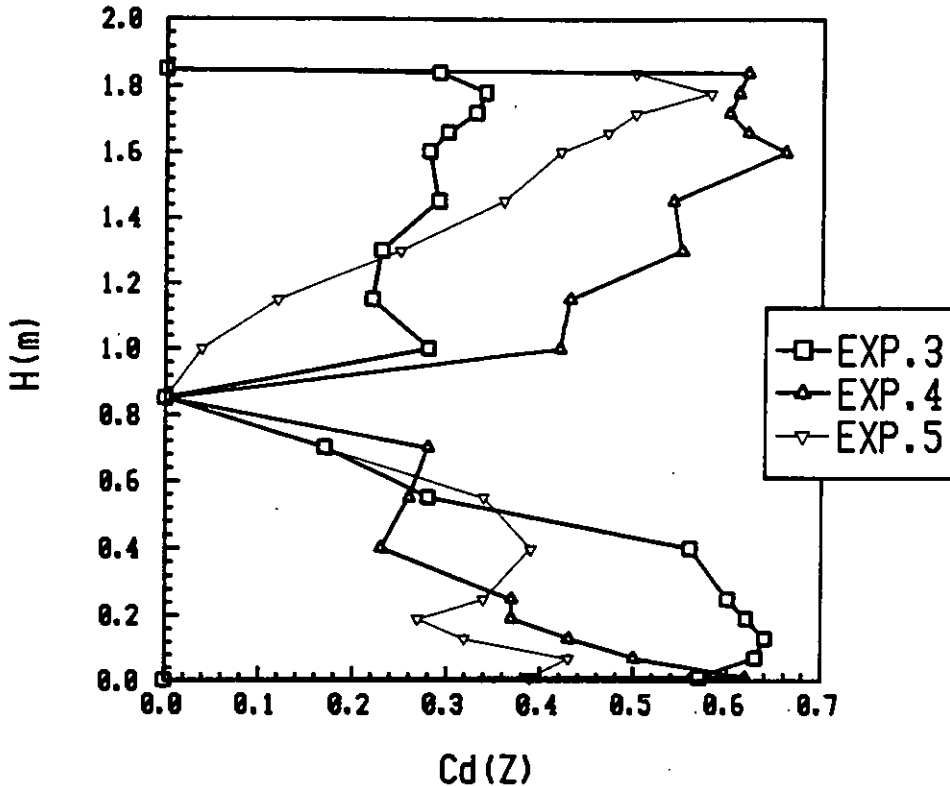
Figure 3.20: Local Cd profiles experiments 3, 4 and 5.

3.3.5 Conclusion

Taking into account the whole complexity of the problem, we proposed a general solution to include large openings in the pressure network of a multizone model (section 2.1.3). The models we proposed are applicable in most of the large opening configurations. It is a combination of the theoretical solutions developed using Bernoulli's assumptions, and of empirical knowledge acquired from experiments in a real configuration. The global values of the Cd coefficients found assuming isothermal cells on both sides of the opening agree with those found by Liebeck and Fissore in their Liege experiment (section 3.2). To take into account a linear thermal stratification does not change significantly the values of Cd coefficients. The vertical Cd distribution seems to be related strongly with the boundary conditions. If the behavior of the Cd distribution found in the first set of experiments carried out in Lyon are confirmed, further studies are then necessary to define average profiles of Cd distribution corresponding to typical boundary conditions or flow patterns found in buildings in case of heating or air conditioning. More experiments are obviously necessary, nevertheless these experiments are very difficult to carry out and very expensive, furthermore, in most cases it is very hard to change significantly the design parameters of such experiments. Another possibility at the INSA, is to use a C.F.D model for parametric studies.

3.4   The Desys Test Cell at CSTB, Sophia Antipolis, France

3.4.1   Experimental setup.

To study in real conditions the thermal behaviour of buildings and of their heating or cooling equipments and to study the air flow patterns within buildings, CSTB has built a real-scale test cell, located in Sophia Antipolis and called DESYS. The test cell area is 86 m², partitioned in three main zones, thermally decoupled one from the other. In the southern zone (divided into two rooms), an experiment, designed to measure heat and mass transfer through a large vertical opening, is in progress.

The walls of the test cell are quite airtight; experiments have been done with a blower door to measure the airtightness of each component of the test cell envelope.

Different heights and positions of the large opening can be tested with various boundary conditions. The boundary conditions are obtained with heating or cooling systems ; in this paper, we mainly report about the experiments made with a "standard" large opening (height = 2.08 m and width = 0.89 m) and with electric emitters as the heating system. About 30 experiments of that kind have been made and we have obtained a considerable range of temperature profiles in each room.

The experiments are made near steady state. The temperature of the walls are measured with surface sensors ; the air temperatures are measured with 13 sensors (type : PT 100, accuracy : ± 0.1 K) in each room (see Figure 3.21).
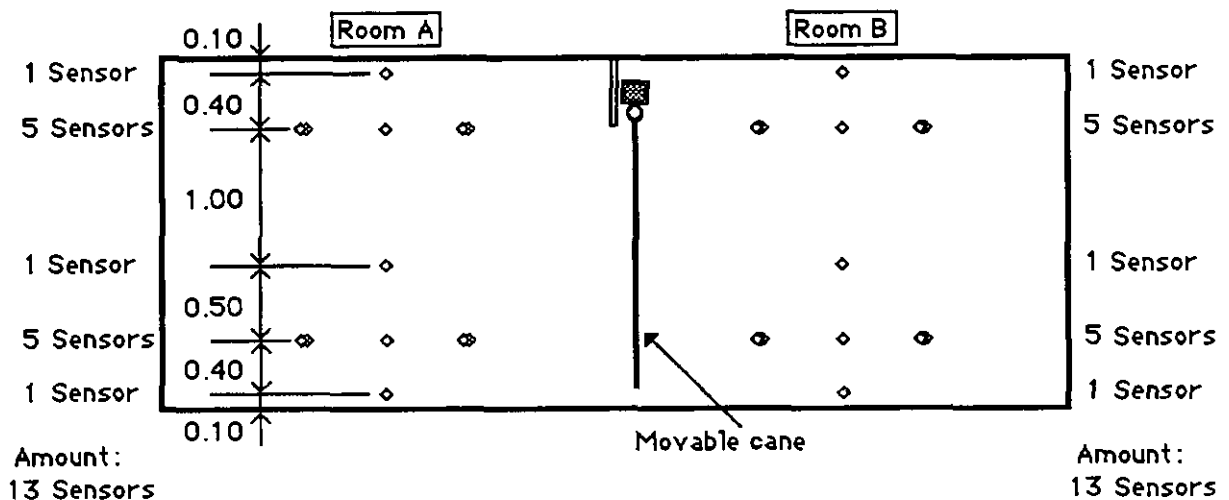
Figure 3.21 : Distribution of the air temperature probes in each room.

The air velocities in the large opening are measured with 9 omni-directional anemometers (DANTEC 54R10, with an accuracy: above 5 cm/s, of about 5 %) fixed on a movable support (see Figure 3.22). Thus, an image of the whole velocity field in the large opening can be obtained. Moreover, the air temperatures in the opening are also measured, almost at the same points, with the DANTEC 54R10 sensors. The data acquisition is made with a DANTEC multiflow analyzer.

The measurement system has been adjusted to make 8 measures (equally distributed) along the width of the large opening. Thus, for each run, air temperatures and velocities are measured in 72 points in the doorway. For each experiment, ten to twenty measurements of the air temperatures and velocities in the large opening are made, then averages are computed and we

have as a goal to find a relationship between the average mass flow rate and the average pressure difference.
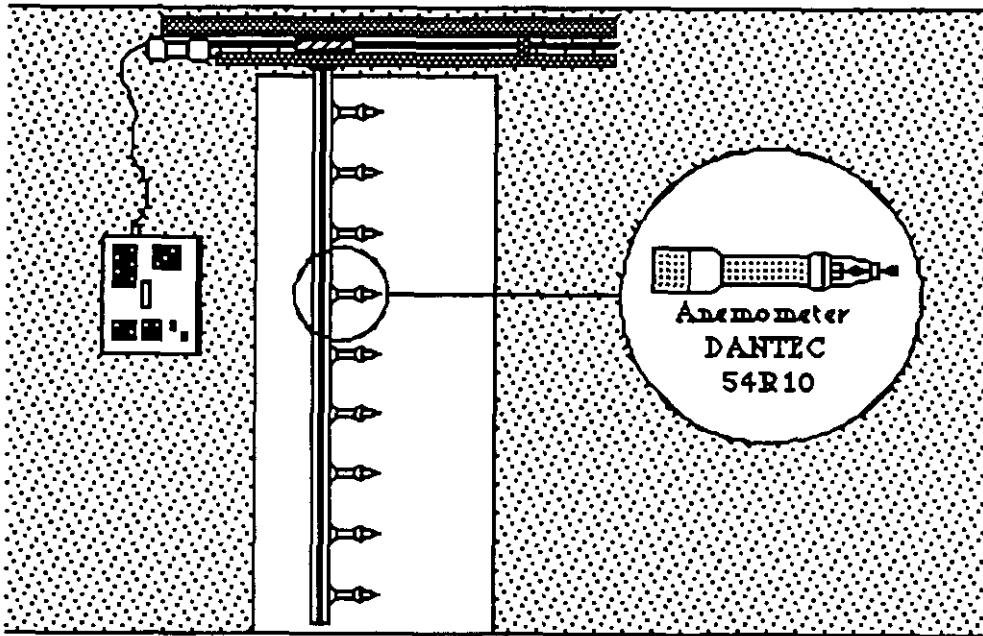
Figure 3.22 : Movable support with its nine anemometers in the large opening.

Velocity. Assuming that the average values of each variable (as a function of time) have been computed, the mean velocity profile is computed as follows :

$$V(z) = \sum_{i=1}^{8} V_i(z) / 8$$

(3.6)

where, $V_i(z)$ is the air velocity in the doorway at height z and for the i position of the movable support, and $V(z)$ is the mean air velocity in the doorway at height z, velocities in (m/s).

Temperature. For the air temperature profile the computations are similar :

$$T(z) = \sum_{i=1}^{8} T_i(z) / 8$$

(3.7)

where, $T_i(z)$ is the air temperature in the doorway at height z and for the i position of the movable support , and $T(z)$ is the mean air temperature in the doorway at height z, temperatures in degree K.

It was found that both air temperature and velocity are essentially constant on a horizontal plane.

Mass flows and heat flux are computed from experimental data with :

$$\dot{m}_t = \sum_{j=np+1}^{9} \left[\rho\,(z_j)\ V\,(z_j)\ S_j \right]$$

(3.8)

$$\dot{m}_b = \sum_{j=1}^{np} \left[\rho\,(z_j)\ V\,(z_j)\ S_j \right]$$

(3.9)

$\dot{m}_t$ Mass flow through the upper part of the opening (kg/s)

$\dot{m}_b$ Mass flow through the lower part of the opening (kg/s)

np Number of probes located below the neutral plan

$\rho(z_j)$ Air density at height z_j (kg/m^3)

$V(z_j)$ Mean air velocity in the doorway at height z_j (m/s)

S_j Area of the doorway attributed to the measurements made at height z_j (m^2)

The neutral plane is computed with the mass balance equation : $\dot{m}_t = \dot{m}_b$

The heat flux, Φ, exchanged by natural convection between the two rooms through the large opening, is computed as :

$$\Phi = C_p \left\{ \sum_{j=np}^{9} \left[\rho\,(z_j)\ V\,(z_j)\ T\,(z_j)\ S_j \right] - \sum_{j=1}^{np} \left[\rho\,(z_j)\ V\,(z_j)\ T\,(z_j)\ S_j \right] \right\}$$

(3.10)

where C_p is the air thermal capacity (J/kg.K)

3.4.2 Aim of the study and results.

Our goal is to develop and to validate two models based on the Bernoulli's equation. The first model corresponds to an assumption of isothermal air volume in each room, the second one assumes that the temperature profiles in each room are linear.

To compute the mass flows we use Eq. 2.18, assuming :

- either that ρ_h and ρ_c are equal to constants in both rooms ;

- or that T_h and T_c are linear functions of z and then ρ_h and ρ_c are defined as :

$\rho_h = \rho_0\ T_0/T_h(z)$ and $\rho_c = \rho_0\ T_0/T_c(z)$

3.4.2.1. Assumption of isothermal air volumes. We search for a model in which only the average temperatures in each room are known. Trying to fit Eq. 2.10 with our experimental results leads us to assert that the physical phenomena can't be described with only one discharge coefficient (Cd) ; this is due to the fact that, to obtain Eq. 2.10, we assumed that the local pressure drop coefficient did not depend on height ; in fact it does ; moreover, our experimental velocity profiles are not symmetric. Therefore, integrating Equation 2.18 with a discharge coefficient, C_t, for the upper part of the opening and with a discharge coefficient, C_b, for the lower part of the opening leads to :

$$\dot{m}_t = C_t\ (2/3)\ W\ \sqrt{(2\,\rho_h)}\ \ \Delta P(z_l)^{3/2}\ /\ [g\,(\rho_c - \rho_h)]$$

(3.11)

$$\dot{m}_b = C_b \ (2/3) \ W \ \sqrt{(2 \ \rho_b)} \ \Delta P(z_b)^{3/2} \ / \ [g \ (\rho_c - \rho_h)] \tag{3.12}$$

Using a recursive least square method, we find that :

$$C_t = 1.07$$
$$C_b = 0.28$$

Equations 3.11 and 3.12, with the identified values for C_t and C_b, give quite good results to compute the mass flows and the neutral plane if the simulated system is in the validity range of these equations ; this means that $Gr_{H,\Delta T} \in [\ 5.10^8 \ ; \ 3.6.10^9\ ]$ and that the heating system is an electrical or a hot water radiator. Moreover, the computation of $\dot{m}_t$ and $\dot{m}_b$ needs an iterative method because both mass flows and neutral plane are unknown. Note that these relationships are not very accurate to compute the air velocities in the opening (see Figure 3.23) :
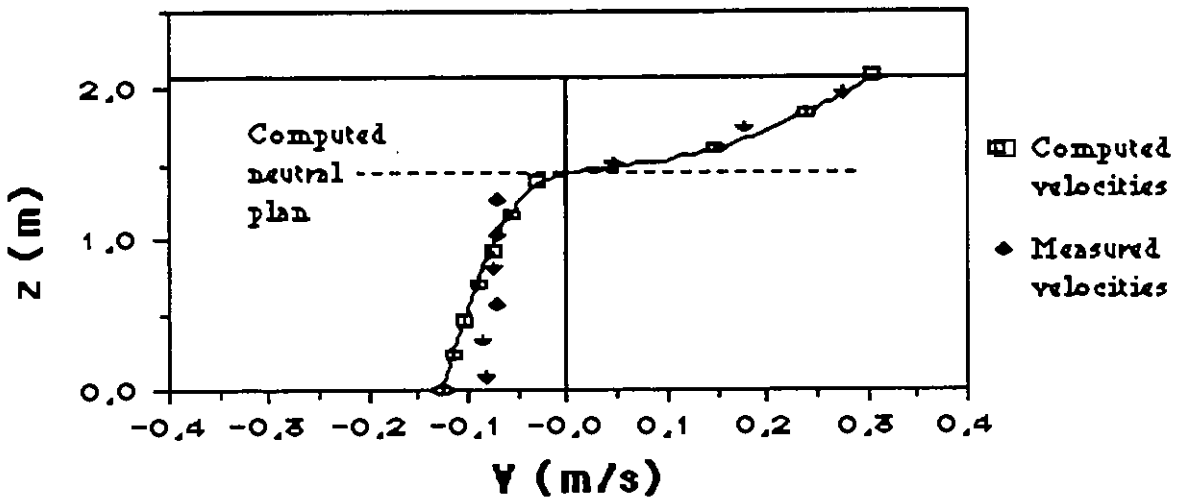
Figure 3.23 : Example of comparing the measured air velocities with the computed air velocities assuming that the temperatures in both rooms are isothermal.

In addition, we tried to find a simplified relationship to directly compute the mass flows knowing only the temperature difference. The demonstration of this relationship[Melouk, 1990, p.19-20] leads to :

$$\dot{m} = C \ Gr^{0.5} \ Pr \ (W \ \lambda \ / \ C_p) \tag{3.13}$$

Gr   Grasshof number related to the height of the opening and the difference between the room average temperatures

Pr   Prandtl number (Pr $\approx$ 0.71)

W   Width of the opening (m)

λ Air thermal conductivity (W/m.K)

C_p Air thermal capacity (J/kg.K)

C   Empirical coefficient

For a large opening as described in § 3.4.1 : $C \approx 0.14$

Eq. 3.13 can be used to compute air flows in a large opening between two rooms: either both

heated; or one heated, the other not; or none of them heated (note that the correlation can't be used if a cooling system or a pulsed air heating system is used). The validity domain is:

$$5 \; 10^8 < Gr < 3.6 \; 10^9$$

The Grasshof's number is computed as previously mentioned.

From experimental data, a correlation to compute the C coefficient as a *function of the opening dimensions* has been validated :

$$C = 0.138 \; (H_r/z_t) + 0.16 \; (z_b/H_r) \tag{3.14}$$

where H_r is the height of the rooms in (m).

The interest of using Eq. 3.13 is that it computes (only) the mass flow (not the neutral plan) directly from the rooms isothermal temperatures (an iterative process is not required).

3.4.2.2. Assumption of linear temperature profiles. The real air temperature profiles in both rooms are approximated by linear air temperature profiles. Then, we try to find a relationship to compute as accurately as possible the air flows and the air velocities in the opening.

The air velocities are given by :

$$V(z) = C(z) \; V_{th}(z) \tag{3.15}$$

$V(z)$ Real air velocity (m/s)

$C(z)$ Local discharge coefficient

$V_{th}(z)$ "Theoretical" air velocity (m/s)
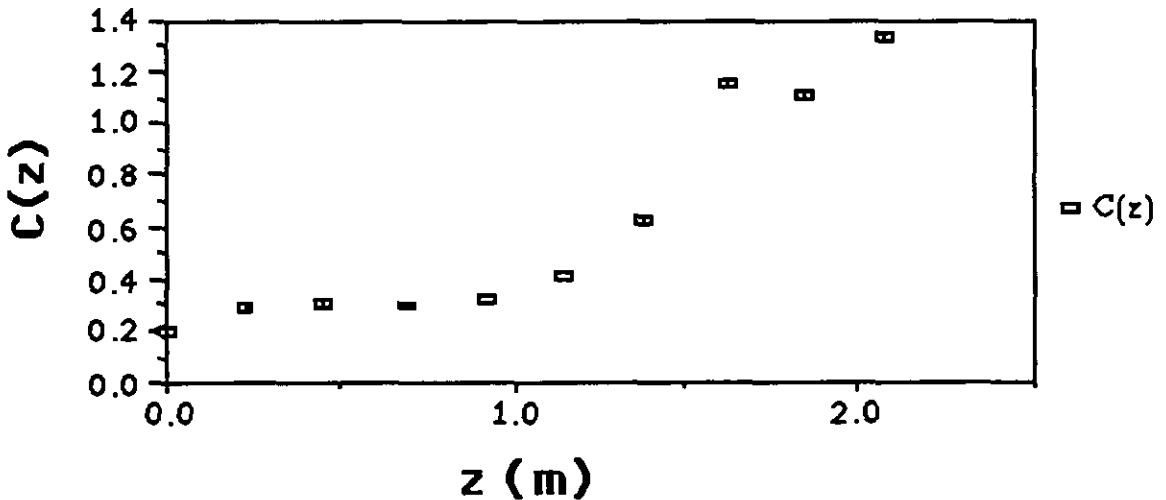
Figure 3.24 : Values of C(z) assuming linear air temperature profiles in each room.

$V_{th}(z)$ is computed from Bernoulli's equation assuming that the local pressure drop coefficients through the opening are equal to 1 and that the air temperature profiles in each room are linear.

Then, the C(z) coefficients are computed, for each experiment, as follows :

$$C(z) = V(z)/V_{th}(z) \tag{3.16}$$

We find average values for C(z) that are given in Figure 3.24 :
We correlated them as follows :

$$C_t(z) = 2.65 \, z^2 - 9.56 \, z + 9.38 \qquad\qquad z_n < z \le z_t \qquad (3.17)$$

$$C_b(z) = 0.71 \, z^3 - 1.24 \, z^2 + 0.67 \, z + 0.19 \qquad\qquad z_b \le z \le z_n \qquad (3.18)$$

The mass flows are computed by integrating the computed air velocities. But, this kind of computation requires the use of an iterative method (because both mass flows and neutral plane are unknown) ; this iterative method converges less easily than the one applied with equations 3.11 and 3.12 (because with equations 3.15, 3.17 and 3.18, there are two different formulae to compute the velocities around the assumed neutral plane level). The validity range of equations 3.17 and 3.18 is the same as for equations 3.11 and 3.12 and the same remarks about the possibility of computing the neutral plane also applies here.

With this model the computed and measured mass flows and air velocities are very similar (see Figure 3.25) :
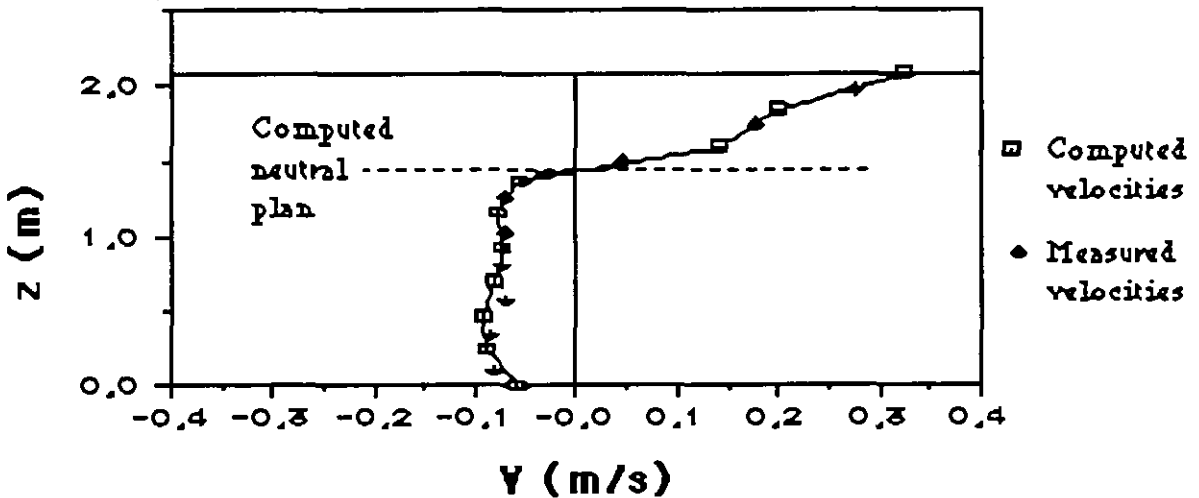
Figure 3.25 : Example of comparing the measured air velocities with the computed air velocities assuming that the temperature profiles in both rooms are linear.

3.4.3 Discussion.

Because of our experimental conditions (rooms heated with electrical emitters), the vertical stratification in each room is quite important ; the air velocity profile in the opening is not symmetrical, the neutral plan is not at the middle height of the opening. The correlations that have been developed take into account these phenomena. Furthermore, the main hypothesis on which all the theoretical developments are based (i.e. the Bernoulli's equation) is not strictly valid in this frame (mainly because, in reality, the air velocities in the rooms are not negligible by comparison with the air velocities in the doorway). That is why we find empirical "discharge" coefficients which can be greater than 1 (as C_t or $C(z)$ in the upper part of the opening).

Nevertheless, the developed relationships can be applied in current cases where rooms are heated or not (but not if the rooms are cooled or heated with a pulsed air heating system). The relationships are valid in a range of Grasshof's numbers [5 10^8, 3.6 10^9] which involves most of the current cases in building simulation (Grasshof's numbers are computed with the difference of the rooms average temperatures -ΔT- and the opening height -$H = z_t - z_b$- as characteristic dimensions).

If the configuration of the simulated system is similar to our current experimental configurations (i.e., one room heated, the other one not), then, with an assumption of isothermal air temperatures in both rooms, the mass flows *and the neutral plane height* can be computed with accuracy but not the air velocities in the opening. Such a model, based on Bernoulli's equation, needs the identification of two discharge coefficients, one for the upper part of the opening, the other for the lower part. A simplified model (see Eq. 3.13), to compute directly the mass flow from the rooms temperatures difference, has been developed and validated within the above mentioned Grasshof range.

With the assumption of linear air temperature profiles in each room, *the air velocities in the opening* (and then the mass flows) can be computed with accuracy. This model needs the definition of "local" discharge coefficient, $C(z)$, which in fact can be directly linked to the inverses of the square root of the pressure drop coefficients. But the $C(z)$ coefficients also take into account implicitly all the (more or less valid) physical assumptions which have been made.

Finally, we have to emphasize that *the computation of heat transfers* due to the mass transfers is not directly possible with the $\dot{m}=f(\Delta P)$ relationships (because of the stratified temperature profiles); specific relationships such as $Nu=f(Gr,Pr)$ have been developed for that purpose. Furthermore, a more comprehensive analysis has been done, as stated in the introduction of this chapter, to take into account the height and the position of the opening in the partition wall. Simplified relationships, to compute heat transfers, have been validated.

3.5   Numerical Comparison with the Concordia CFD-code

In the frame work of subtask 2.1, some of the experimental natural convection data described in sections 3.2 to 3.4, have been compared with the Concordia numerical CFD code.

There are two sets of data from the Liège University but for lack of time the comparison was only made with the first set of data *[Baranowski et al. 1989]*, where the heating and cooling radiators were placed parallel to the opening and radiation heat transfer through the doorway played an important role. The second set of high quality data that became later available *[Fissore et al., 1990]* differed by the position of the radiators (Figure 3.4a).   Further comparison was made with data obtained by *Lieman [1990]* on the Lyon test-cell (Figure 3.11 and section 3.3), and allowed partial validation of the numerical model.

The validation also included a comparison of the predicted results in natural convection with experimental data obtained by *Nansteel and Greif [1984]*, while for forced convection a comparison with the PHOENICS code was carried out. A more detailed account of the validation procedure is described in *[Haghighat et al. 1991a]* .

3.5.1   Description of the code and the numerical procedure

The Concordia code employs finite-difference method and the k-ε two-equation model of turbulence to obtain the approximate solution of governing equations for the three-dimensional turbulent flow in rectangular enclosures.

The governing equations can be written in a common form as follows:

$$\frac{\partial \rho \phi}{\partial t} + \frac{\partial}{\partial x_i}\left(\rho u_i \phi\right) = \frac{\partial}{\partial x_i}\left(\Gamma_{\phi,eff}\frac{\partial \phi}{\partial x_i}\right) + S_\phi$$

(3.19)

where ϕ denotes the variables u_i, h, c, k, or ε. S_ϕ represents the source term for each of the variables. Eq. 3.19, is a more general form of Eq.2.3 and not limited to incompressible flows.

At the region near a solid surface, where the viscosity effects become important, the wall function method is adopted to modify the k-ε two-equation model. The principle of the wall function method is using the momentum flux due to shear stress and the heat flux at solid surfaces to modify the source terms in the conservation equations for the grid nodes near the solid surfaces. The numerical procedure is as follows :

(1) The boundaries of the control volume for h, c, k and ε are identical with the physical boundaries. For the velocity components u, v and w, the staggered control volumes are employed.

(2) The hybrid scheme developed by *Spalding [1972]* is adopted, which is a combination of the central-difference scheme and the upwind scheme. The upwind scheme is also included in the numerical model as an option.

(3) In order to ensure the mass continuity at the door opening where the flow properties may change rapidly, an overall correction on the velocity component in the direction perpendicular to the partition (the x direction) is added. The overall correction term is derived from the mass continuity over the sections parallel to the partition, and can be expressed as

$$\Delta u = \frac{Q_{up}-Q}{\sum A_{x,j}}$$

(3.20)

where Q represents the air volume flow rate across the section before velocity is overall-

corrected; Qup denotes the upstream flow rate; and A is the surface area of control volume perpendicular to the x direction.

(4) The SIMPLE algorithm *[Patankar and Spalding, 1972]* is employed to solve the finite-difference equations.

(5) the false-time step and the Alternative Direction Implicit (ADI) interactive procedure with under-relaxation are employed.

(6) Convergence of the iteration process is pronounced when the total absolute value of residual sources in the continuity equation is small enough (less than 1% relative error) and when the variation in value of variables between two iterations is small enough (less than 0.1% relative error). The reason for choosing the residual source in the continuity equation as an indicator is that the convergence of the continuity equation in this study is lower than other variables.

3.5.2 Comparison with Experimental Data Obtained by Nansteel and Greif

The Nusselt number is plotted as a function of Rayleigh number to compare computational and experimental results. The lowest curve in Figure 3.26 corresponds to the data correlation proposed by *Nansteel and Greif [1984]* and describing heat transfer measurements in a water cell. The correlation refers to the wall temperatures and is typical for boundary layer flow (Figure 2.10; section 2.2.2). For comparison, the extrapolated correlation for bulk flow (Eq. 2.33) is also plotted (upper curve, the Nusselt numbers are divided by 100).
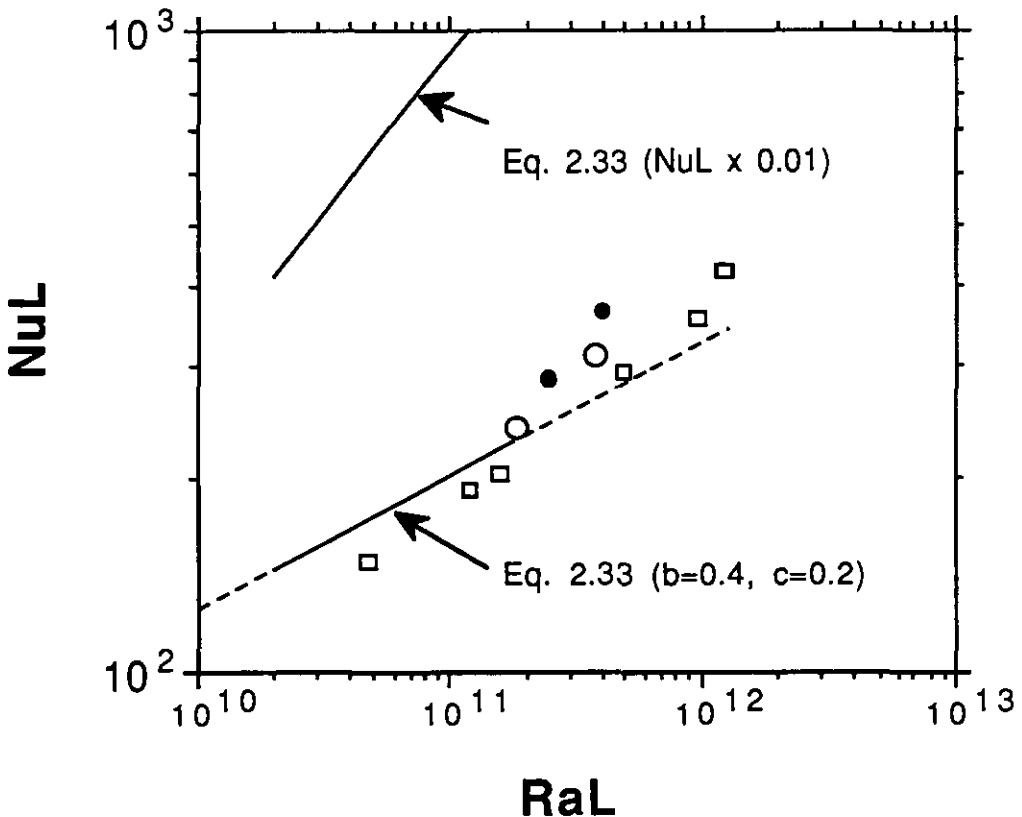
Figure 3.26 A plot of Nusselt numbers for the heat flow through a partition as a function of Rayleigh number.   Comparison of the results computed with the Concordia code *(open squares)* with experimental data. Lower curve (Eq.2.33) :   correlation of *Nansteel and Greif (1984)* with H/Hr=3/4, data obtained on a water test cell. The circles are data from *Weber (1980)* in air. The upper curve (Eq.2.33) is to compare with the slope of the correlation for bulk flow *(Brown and Solvason, 1962)*   (note that the Nusselt numbers are divided by 100).

The thermal boundary conditions used in the computation are the same as those in the experiment. Since the cell size is restricted by the number of grids, the parameter w_D/W, which is 0.25 in numerical calculation, does not match the value 0.093 adopted in the experiment performed by *Nansteel and Greif [1984]*. However, it was found in their experiment that the door width has little influence on the inter-zone heat convection rate. For example, the inter-zone convective heat transfer rate for the case with w_D/W was only 5% higher than that with $w_D/W = 0.093$ when the door height is 3/4 of room height.

Figure 3.26 shows that in the relatively high Rayleigh number region ($Ra_L > 3.10^{11}$), the computed Nusselt number is slightly higher than the (dashed) projection of the correlation line obtained by Nansteel and Greif, and slightly lower than the experimental data obtained by *Weber [1980]*. In the region of $Ra_L < 3.10^{11}$, the predicted Nusselt number is slightly lower than experimental data obtained by Nansteel and Greif. The k-ε model combined with the wall function method, although applicable in the region that the experiment covers, may not give good predictions of heat flux from walls when the Rayleigh number is relatively low. The low-Reynolds-number k-ε model of turbulence would be more suitable to predict the natural convection phenomena in buildings.

In general however, the agreement is satisfactory between computed values of Nu and these experimental data.
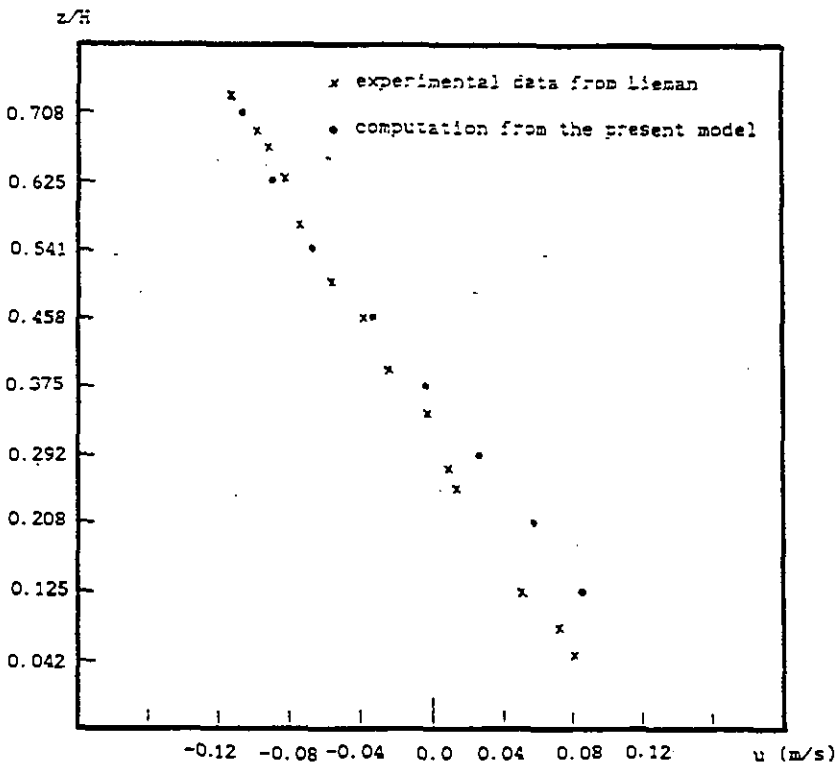
Figure 3.27 Lyon test cell : The velocity distribution at the centre of the door opening as measured *(Lieman et al 1991)* and from numerical computation.

3.5.3 Comparison with experimental data obtained in the Lyon test cell

The two-zone enclosure used in the experimental study *[Lieman 1990]* was described in section 3.3 (Figure 3.11). A partition was placed at the middle of the room length with a centrally located door opening (1.85 m height and 0.77 m width). There was a step of 0.08 m height at the door opening. The thickness of the partition was 0.07 m.

The isothermal boundary conditions for walls, ceiling and floor were:

TW = 11.70 °C   TE = 17.93 °C

TN = 17.32 °C   TS = 17.20 °C

TT = 17.10 °C   TB = 16.71 °C

Figure 3.27 shows the velocity distribution at the centre of the door opening obtained by experimental measurement and numerical computation. Discrepancy is observed in the low region of the door opening. It is because that the 0.08 m step on the floor of the door opening is neglected in our computation since it is too small to be considered in a uniform mesh system adopted. In the east part of the door opening, the predicted velocity distribution is in very good agreement with the experimental data.

The temperature distribution at the centre of the door opening plane is presented in Figure 3.28. The computed temperatures at the middle region of the door height are lower than the measurements by more than one degree. At higher and lower regions the agreement between computation and measurements is satisfactory.
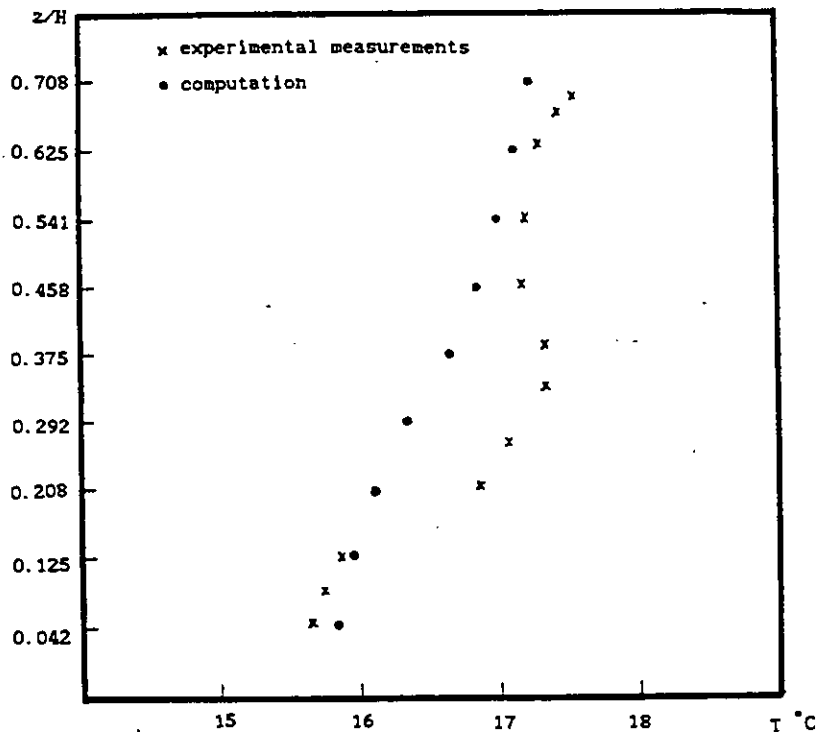
Figure 3.28 Lyon test cell : The vertical temperature distribution at the centre of the door opening

3.5.4   Comparison with experimental data obtained in the Liège test cell

The Liège test cell is described in section 3.2 (Figure 3.4). A partition with a centrally located door opening was placed at 2.46 m from the western wall. The door opening height and width were 2.185 m (including a 0.13 m step on the floor) and 0.685 m respectively. The western wall was kept a higher temperature (distribution) by a 1215 W constant and uniform power supply, while the heat loss from the eastern cold wall was measured to be 1227 W. The other

four walls were maintained at constant temperature. The convective part of the heat flow was about 80% and 20% was transferred by radiation.

Figure 3.29 shows the temperature distribution at the vertical axis of the door opening obtained from the measurement and the prediction by the numerical model. The computed temperature gradient is higher than that from measurements. It may be because the boundary conditions used in the computation are not exactly the same as those under which the experiment was performed. In the computation, the temperature at the hot and cold walls are all assumed uniform in temperature, while actually there are temperature distributions on both hot and cold walls. Furthermore, the radiation heat transfer and the net heat gain on the walls through conduction are neglected.
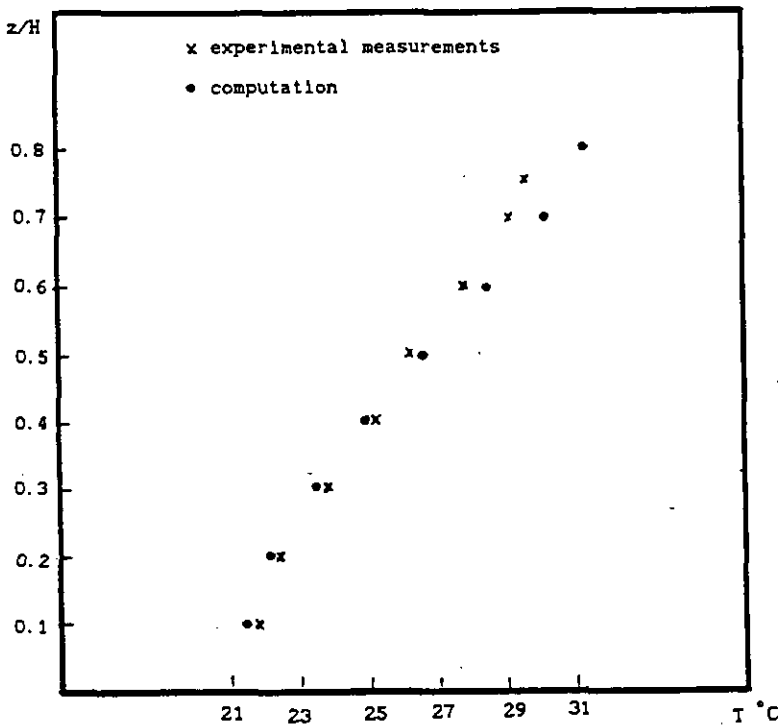
Figure 3.29   First Liège test series: Temperature profile at the center of the door opening

3.5.5   Comparison with results predicted by PHOENICS code

The configuration used in computation for comparison is presented in Figure 3.30. A partition is fixed at the middle of the enclosure dividing it into two equal-sized zones. A ventilation supply opening is located on the western wall in zone A, and an exhaust opening is mounted on the ceiling in zone B. The air velocity at the supply opening is 0.1 m/s which provides a ventilation rate of 2.5 ACH.

The ceiling, floor and walls are considered to be well insulated, therefore an isothermal airflow could be assumed. The thickness of the partition is negligibly small in comparison with the lenth of the enclosure. Besides, it sis assumed that the contaminant source is a point source, and its emission rate is negligibly small in comparison with the ventilation flow rate.

In Figure 3.31, the velocity distribution at the door opening calculated with the Concordia code is compared with the prediction of the Phoenics code. The agreement of both the velocity distribution and the average contaminate concentration in each zone computed by Concordia code and PHOENICS code is very good.
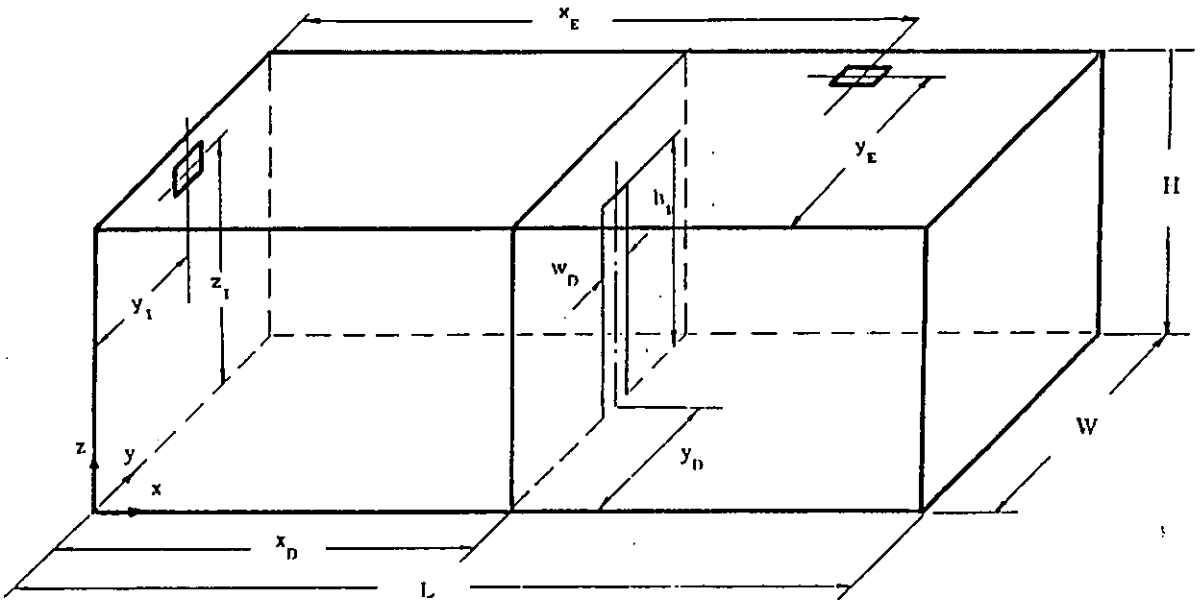
Figure 3.30 The configuration of a partitioned enclosure used in comparing the Concordia and the Phoenics-code.
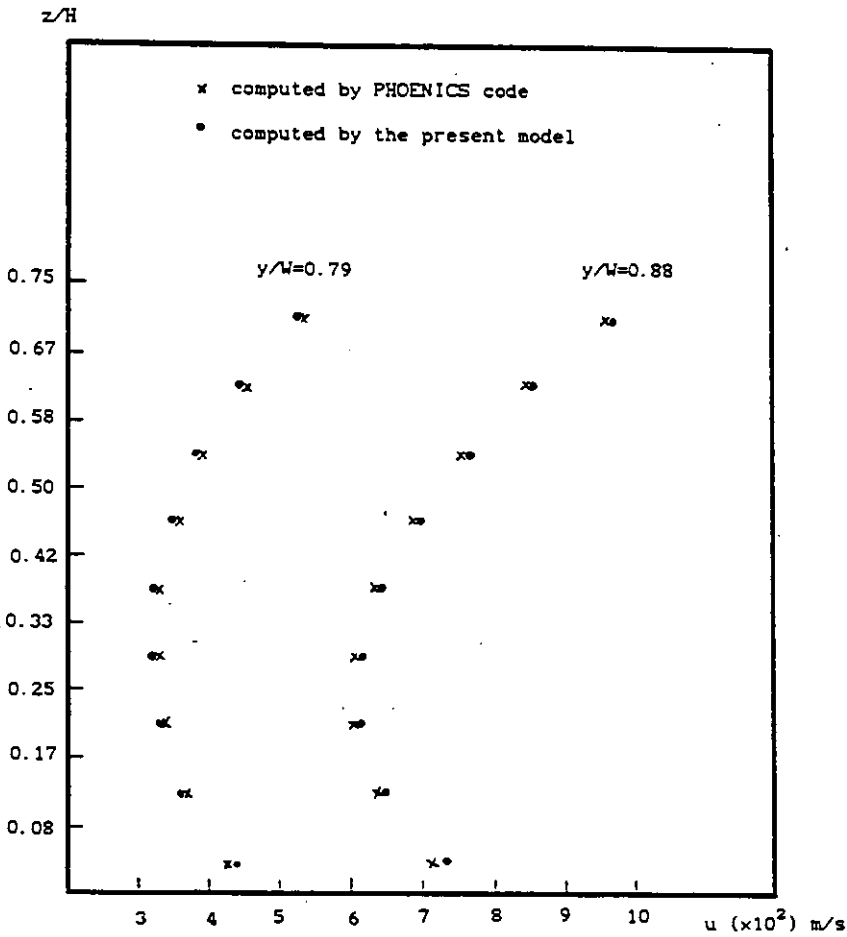
Figure 3.31 The velocity distribution at the door opening calculated with the Concordia code compared with the Phoenics code (x/L=0.5).

3.6 Synthesis of the Test-Cell Results

The three set-ups described in sections 3.2, 3.3 and 3.4 have as a common characteristic that they are real scale experiments (Figure 3.32). The test rooms at University of Liège and at INSA Lyon are climatic test rooms ; the CSTB's set-up is in natural environment.
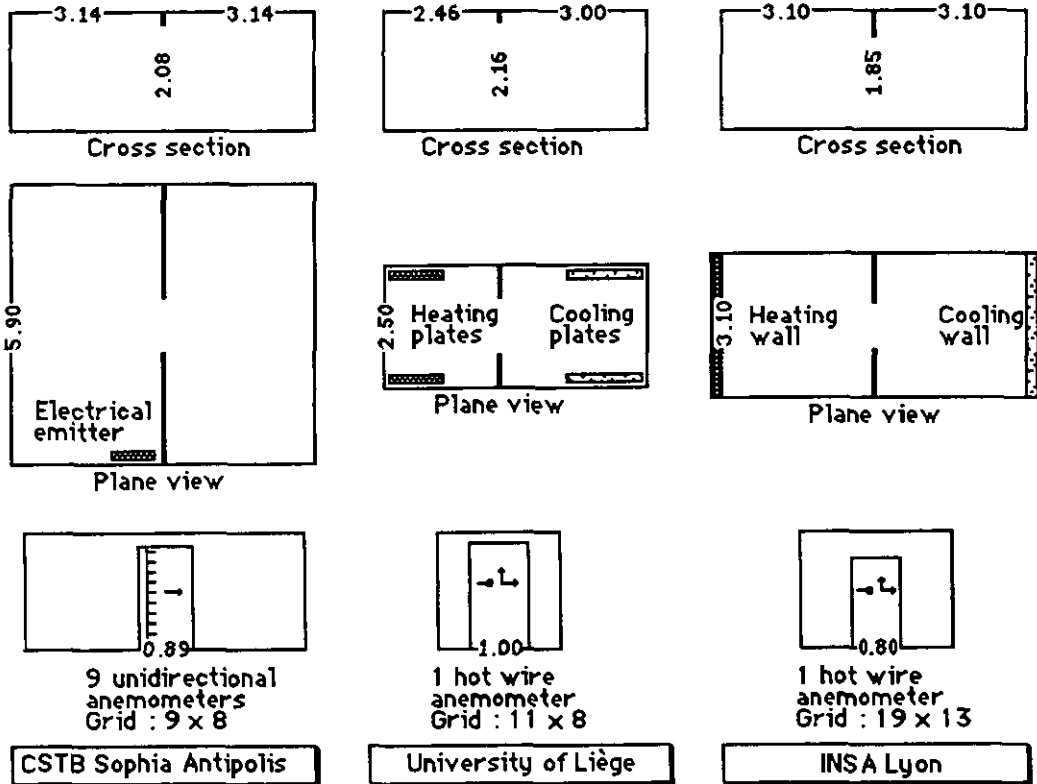

Figure 3.32 : The three laboratory set-ups compared.

To facilitate the comparison of the typical velocity profiles, they are plotted as a function of the ratio z/H where H is the opening height ; then, for all the experiments, the ration z/H varies between 0 and 1 (see Figure 3.33). The velocity profiles are specific for each experimental set-up; the various heating or cooling devices explain why the shapes are different :

- in the CSTB experiments, the neutral plane is approximately located at two thirds of the opening height ; this is because the electrical emitter creates a specific air movement in the heated room (a hot plume), resulting in a typical vertical temperature profile with a 2 K/m gradient.

- in the Liège experiments, the neutral plane is slightly above the mid height of the opening; this result fits well with the INSA experiments when both the opposite walls are active.

- in the INSA experiments with only the cooling wall active, the velocity profile is asymmetric and the neutral plane is below the midheight of the opening; this asymmetry results from the typical air movement (a cold plume), is opposite to the CSTB experiment, and is in agreement with previous experiments performed in the Liège test cell with an asymmetrical heating and cooling configuration : the cooling plates were close to the opening and faced it, then the neutral plane was well below the mid height of the opening.
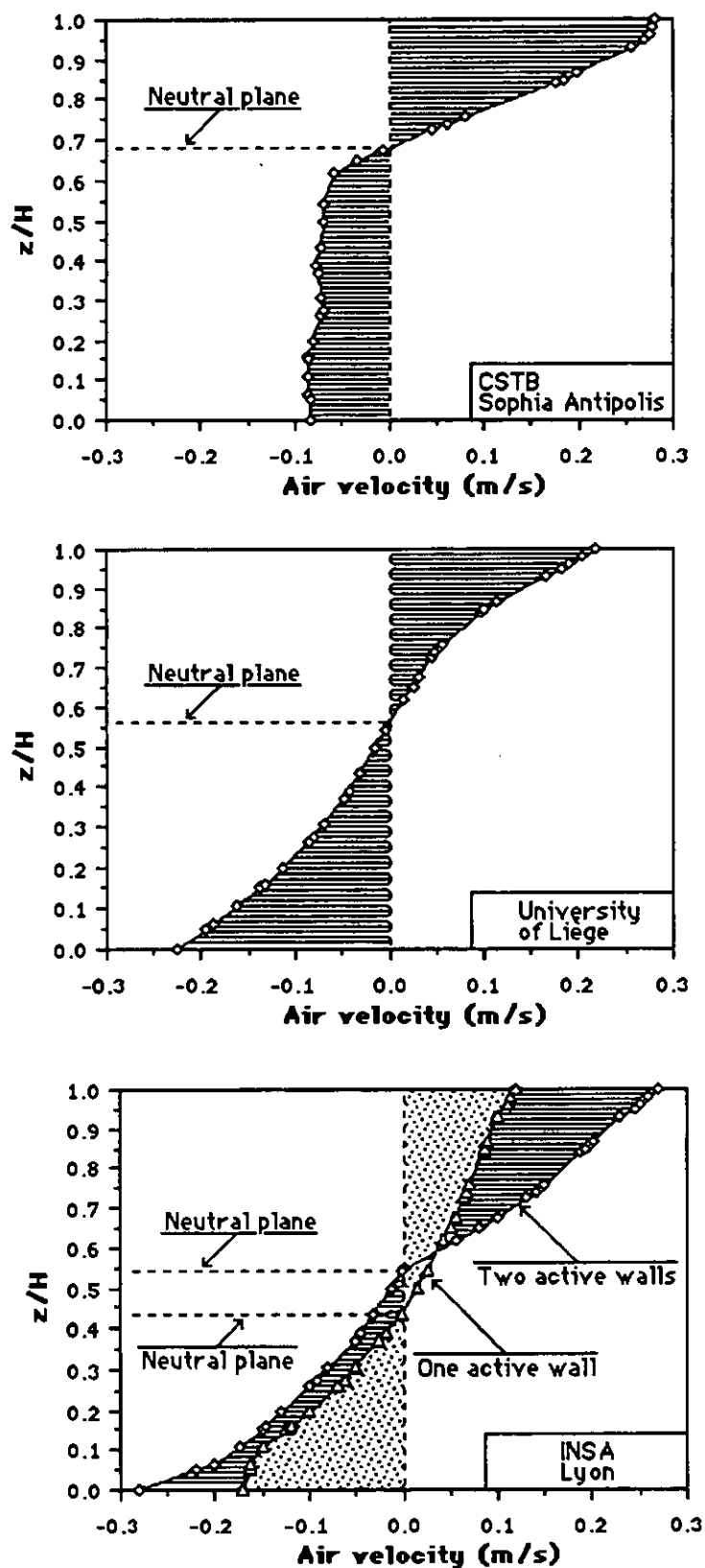
Figure 3.33 : Typical velocity profiles (the plot symbols do not indicate the points where the velocities were measured but only the points were the experimental results have been interpolated in order to plot them in the same way) *(Pelletret et al. 1991).*

Both CSTB and INSA calculated the experimental mass flows by integration of the measured velocity profiles. University of Liège calculated the experimental mass flows both by integrating the measured velocity profiles and computing it from the heat balance of the test rooms; computing them with a heat balance appeared to be more accurate in their case.

To compare the three test cell results, the Cd coefficients, are plotted versus the difference between the rooms average temperatures. For the INSA experiments this difference is taken as the difference between the central air temperatures measured in each room (see Figure 3.34).
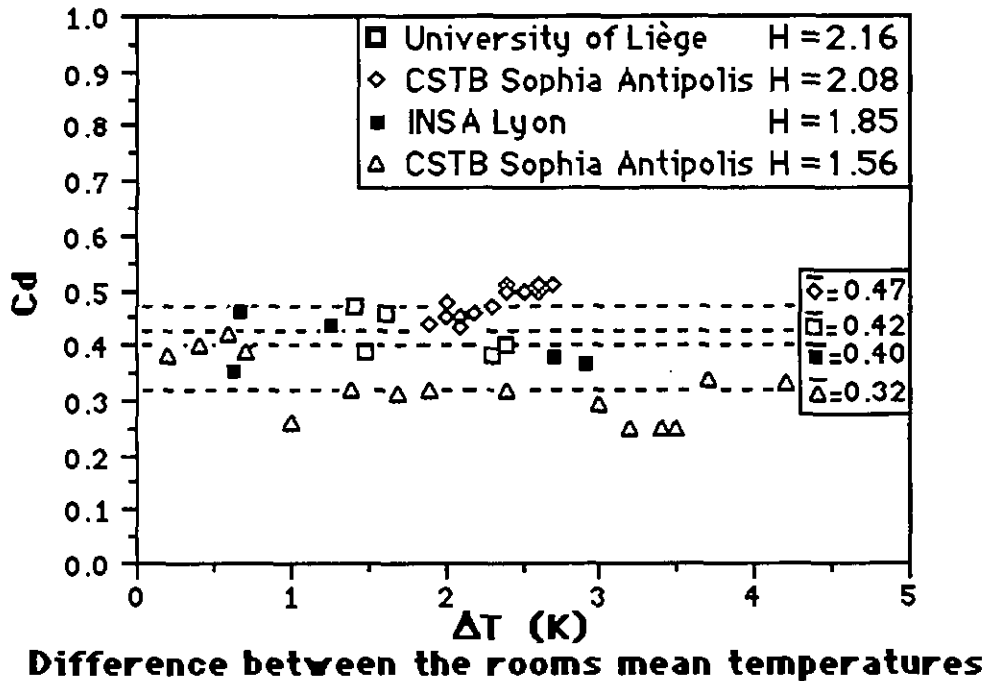
Figure 3.34 : Discharge coefficients with an assumption of isothermal air volumes.

The results obtained from the three test cell experiments are close one to each other and the following observations can be made :

- the Cd mean value computed from the CSTB's experiments is slightly higher than the Cd mean value computed from the Liège's experiments while the heights are similar (2.08 m and 2.16 m) ; this is possibly due to the hot plume caused by the electrical emitter in the heated zone of the CSTB set-up, influencing the air movement in the opening. And this assertion is strengthened by the INSA's results : for the asymmetric experiments (with only a cooled wall), the Cd coefficient is about 0.45 (close to the mean value of the CSTB's experiments), which is 20% higher than the Cd mean value computed with symmetric boundary conditions.

- the discharge coefficient in the CSTB experiment appears to depend systematically on opening height and position. Indeed, according to Eq.3.14, the mass flow decreases with the level of the top of the opening, z_t , and increases with the bottom level, z_b.

  This systematic effect is partly due to the use of the *mean* room temperature for calculating the flow. Indeed, the highest air temperatures in the hot zone, are found above the top of the door level where the air is nearly stagnant and has little influence on the flow. This means that the mean temperature of the hot zone is higher than the average temperature of the circulating air in the hot zone (below the top of the door level), and the discharge

coefficient appears to change systematically with the door height or position.

The use of the mean room temperature as the known input parameter is common in building simulation programmes, and a correlation like Eq. 3.14 is a useful result when the temperature of the circulating air is unknown. However from the physical modeling point of view, the mean room temperature is not the right parameter determining the flow (For a more detailed discussion of the influence of the definition of the room mean temperature, see section 3.7).

Comparing the discharge coefficients of Figure 3.34 with the orifice coefficients measured by Wilson and Kiel (Eq. 2.28a; Figure 2.8), the agreement is surprisingly good, their correlation predicting (below 5K) values for Cd between 0.40 and 0.42. This would suggest that the modeling of a steady-state mass flow in a test cell is similar to that of a gravity current entering a hallway. The orifice coefficient was interpreted as the combined effect of flow contraction and interfacial mixing, the latter having an important effect on the temperature and velocity profile near the neutral level (Figure 2.9b). Wilson and Kiel postulated that a high level of wind turbulence explained the fact that their data were about 10% lower than those reported by Lilienblum. This postulate needs probably revision now that it has been shown that test-cell experiments (where the turbulence level is very low) also provide these lower Cd values.
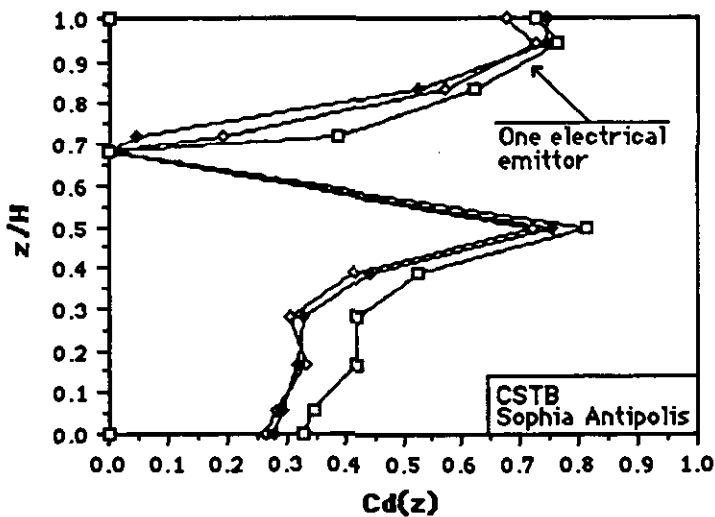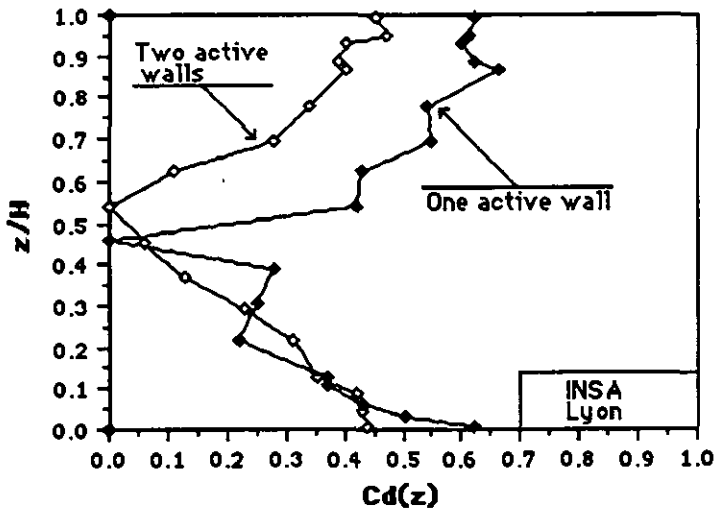

Figure 3.35 : The ratio between experimental velocities and the calculated velocities (local discharge coefficients) with an assumption of linear air temperature profiles.

Using the measured temperature profiles in each room and applying the Bernoulli equation (Eq. 2.27), one can define for each value of z a local discharge coefficient Cd(z), being the ratio between the measured and calculated velocity.

In Figure 3.35 are plotted as a function of z/H, the typical Cd(z) profiles for the INSA and the CSTB experiments. For the INSA experiments, one profile corresponds to a symmetric case (two active walls), showing a symmetric Cd(z) profile. The other plotted Cd(z) profile is for a single cold active wall and is asymmetric. The asymmetry of the profile varied for the three experiments (Figure 3.20). On the other hand the twenty CSTB experiments yielded very similar profiles.

Comparing again with the observations of Wilson and Kiel (Figure 2.9b), only the INSA case with two active walls gives the same picture. Apparently the case of a cold gravity wave penetrating a warmer fluid should be treated as a 'symmetric' case.

The error in the local discharge coefficients is largest near the neutral level, where the experimental velocities are very low. Also a too low estimate of the height of the neutral level can cause a peak in the discharge coefficient because at the neutral level, a non-zero experimental velocity will be divided by zero.

The uncertainty in the neutral level can be quite large, of the order of 5cm, due to the use of omnidirectional velocity probes.and velocity values close to the turbulence level (a few cm/s). This may have influenced the Cd(z) peak at z/H=0.5 in Figure 3.35, that resulted after automatic analysis of the measurement data.

The combination of very small discharge coefficients near the neutral level, with velocities that are low, means that the flow near the neutral level is of little relative importance. Therefore the mean mass discharge coefficient of about 0.4 for the INSA data (Figure 3.34) is quite close to the maximum of the local discharge coefficient in Figure 3.35, and the horizontal velocity profile (Figure 3.17) is nearly constant.

Local discharge coefficients are peaking near 0.75 for the asymmetric case (Figure 3.35), this is interesting because this was exactly what was reported by authors interpreting velocities taking explicitly temperature profiles into account (section 2.1.4; Hill et al 1986).

Conclusion. In conclusion, the joint research effort led to validate models based on the Bernoulli equation assuming either isothermal air volumes or linear temperature profiles. The discharge coefficients in both case are quite similar; Cd varies from 0.37 in case of pure natural convection to 0.51 if a (cold or hot) plume exists. An average value of 0.45 seems adequate to correctly model a large variety of configurations such as non heated rooms, or one room heated not the other one or both heated and for an opening's height higher than 2 m. The discharge coefficient decreases with the opening's height ; a very simple relation as Cd = 0.21 H fits well the experimental results in the range H $\in$ [1.5 m ; 2 m].

The vertical Cd distribution seems to be strongly related with the boundary conditions. Further studies are necessary to define average Cd distribution corresponding to typical boundary conditions or real flow patterns observed in buildings in case of heating or air conditioning.

3.7 Model Developments at LESO, EPFL, Switzerland.

3.7.1 Analytical versus numerical Bernoulli models

The use of analytical models in a multizone air flow model has the advantage of speed and simplicity. More detailed and accurate models are available but they require in general a numerical solution of their algorithm, and therefore considerably more computer time. Indeed, for the calculation of the mass and heat flow while taking detailed zone temperature stratification into account, the density has to be integrated numerically (Eqs. 2.18 and 2.30). Therefore, it is useful to discuss the criteria for switching to a faster analytical isothermal zone expression.

First of all, to use a more detailed model more input data are needed. But even when all possible data are available, one would like to have insight in the gain in precision by using the detailed model or, the loss in precision by using analytical expressions for the mass and heat flow through large openings.

In this section, various cases of zone temperature stratification are discussed. For each case the mass and heat flow is calculated with the Bernoulli model using both (i) the isothermal zone approximation and (ii) the detailed temperature stratification, after which the results are compared.
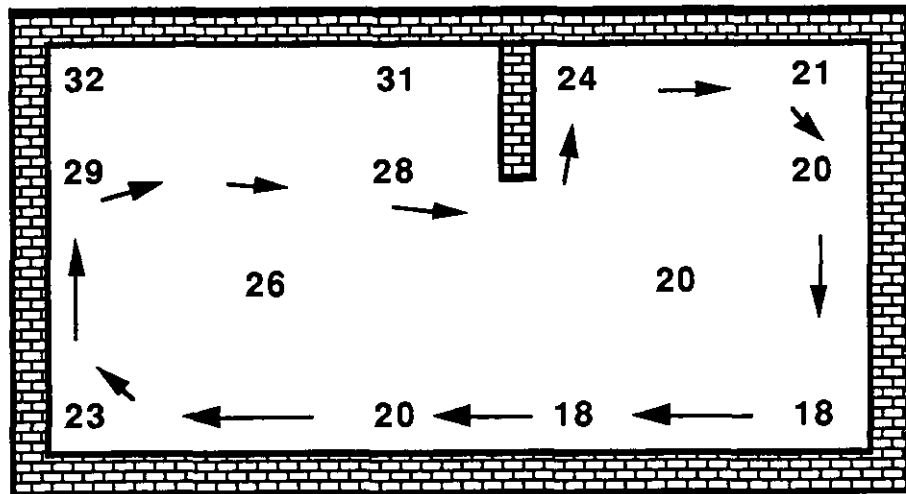
Figure 3.36 A typical flow pattern and temperature distribution in a two-zone configuration :

(1) starting in the hot zone, warm air is trapped above the top of the door level, and below, warm air flows horizontally in the direction of the opening;

(2) after entering the cold zone, the air cools gradually when in contact with the ceiling of the colder room where a horizontal temperature gradient is formed;

(3) the warm ceiling air is further cooled by flowing down along the cold zone walls forming a vertical temperature gradient ;

(4) floor air in the cold zone flows in the direction of the opening;

(5) after entering the warm zone, the cold air warms gradually by the hot room floor where a horizontal temperature gradient is formed.

(6) the relatively cool floor air is further warmed by rising up along the hot zone walls forming a vertical temperature gradient.

3.7.1.1 Characteristic zone temperatures.

In the isothermal zone approximation, discussed in section 2.1.3.1, the difficulty is how to determine the temperature characterizing a given zone. This would be no problem when the zone temperature could indeed be considered a constant, but in most cases where large openings are connecting zones at different temperature, the air temperature is varying in both the vertical and horizontal direction. A typical temperature distribution is shown in Figure 3.36.

Various choices for the single zone air temperature are possible. For the hot and cold zone temperatures of the case presented in Figure 3.36, a few choices are given in Table 3.12.

Choice	T_h (°C)	T_c (°C)	ΔT (K)
-1-at the center of the zone	26	20	6
-2- at the center of where air is circulating	25	20	5
-3- averaged over the total zone volume	27	21	6
-4- averaged over where air is circulating	25	20	5

Table 3.12 Possible hot and cold zone reference temperatures in Figure 3.36.

With the assumption of a linear temperature stratification (section 2.1.3.2), the temperature gradient is not uniquely defined either. Indeed, in the example of Figure 3.36, the floor temperature in the hot zone varies by three degrees, which causes the gradient to increase continuously from the back wall to the opening. The zone temperatures below the neutral level are influenced by the inflowing cold air, and it is unknown how to use Eq. 2.17 correctly, i.e. *which temperature difference drives the gravity current flowing from the cold to the hot zone?*

However until now, no attention has been paid in the literature to the specific condition for the derivation of Eq. 2.17, which is that the relevant temperatures (densities) should be determined in *non-moving air.* This implies that temperatures measured on the central axis of zones with open doors can be irrelevant for the calculation of airflow through large openings (air temperatures below the neutral level are lowered by inflowing gravity currents e.g. hot zone in Figure 3.36; air temperatures near the ceiling are increased by hot plume flow e.g. cold zone in Figure 3.36). Insights on this point could be gained for example with the help of CFD, analyzing numerically calculated flow and temperature fields with the Bernoulli model.

In the following, the relevant temperatures are considered to be known, and only the models used for the experimental data analysis will be intercompared.

3.7.1.2 Algorithms

Zone temperature difference. Given the detailed temperature profiles $T_h(z)$ and $T_c(z)$ in the hot and cold zones, the isothermal zone (IZ) approximation requires the definition of an interzonal temperature difference ΔT. The choice here is the temperature at the middle of opening height

$$\Delta T = \Delta T(H/2) = T_h(H/2) - T_c(H/2) \tag{3.21}$$

A different choice for ΔT, for example by averaging over height, has not been studied yet; it would alter the quantitative results but not the method of analysis.

Massflow. The mass flow in the IZ approximation is calculated with Eqs.2.21 and 2.20, neglecting the second order term in the interzonal temperature difference ΔT. This IZ massflow is called m_{IZ}.

The mass flow is also calculated exactly, using the detailed Bernoulli model and the requirement of mass conservation (Eq.2.18), the result is m_{EX}. The ratio between the massflows calculated with these two models, is the mass flow factor

$$C_m = m_{EX} / m_{IZ}. \tag{3.22}$$
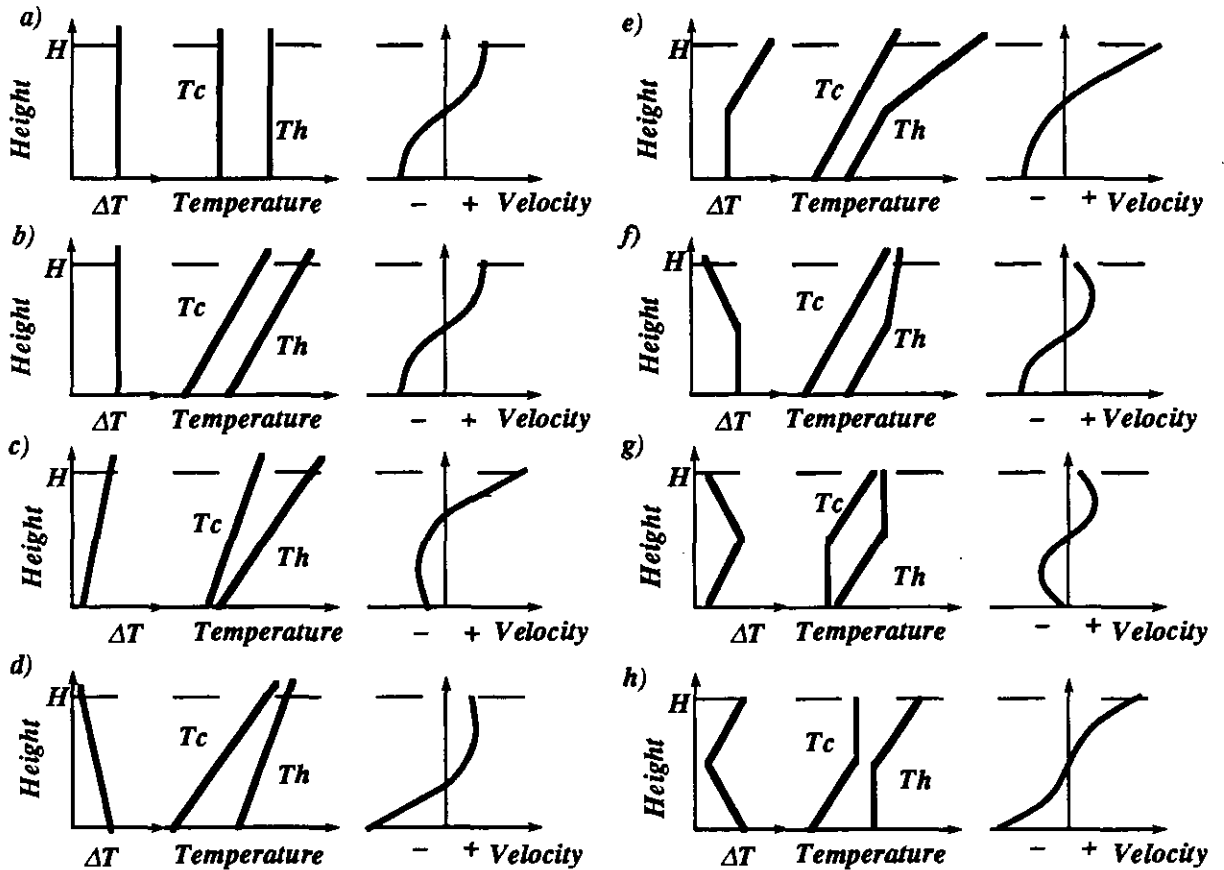
Figure 3.37 a-h. Typical vertical zone temperature profiles and corresponding velocity profiles. Are given schematically and as a function of height in the aperture: zone temperatures, the inter-zone temperature difference and the velocity. The used temperature profiles are defined by four parameters per zone : the temperature at zero height, two temperature gradients and the height at which the gradients cross.

Heatflow. Similarly, the heat flow is first calculated in the IZ approximation (Eq. 2.29)

$$\Phi_{IZ} = C_p \, m_{IZ} \, \Delta T \tag{3.23}$$

and then in detail (Eq. 2.30) to obtain the exact heat flow Φ_{EX} . The ratio between the heatflows calculated with the two models gives the heat flow factor

$$C_t = \Phi_{EX} / \Phi_{IZ}. \tag{3.24}$$

97

Stratification coefficient. Wether temperature stratification is significant depends on the relative importance of the vertical temperature variations $T_1(z)$ and $T_2(z)$ in zones 1 and 2. A stratification factor is therefore defined, Strf, which compares the vertical zone temperature differences, T(H)-T(0), with the inter-zone temperature difference, ΔT

$$Strf = (T_h(H)\text{-}T_h(0) + T_c(H)\text{-}T_c(0) \ ) \ / \ \Delta T \qquad (3.25)$$

where the temperatures are determined at the top (z=H) and bottom (z=0) of the opening. For linear profiles b_h and b_c it follows that $Strf=H(b_h+b_c)/\Delta T$ (compare Eq. 2.31).

Simulations. For a number of typical temperature profiles the factors C_m and C_t have been calculated as a function of Strf. This stratification coefficient was varied by varying ΔT, leaving the profiles, $T_h(z) - T_h(0)$ and $T_c(z) - T_c(0)$, unchanged.
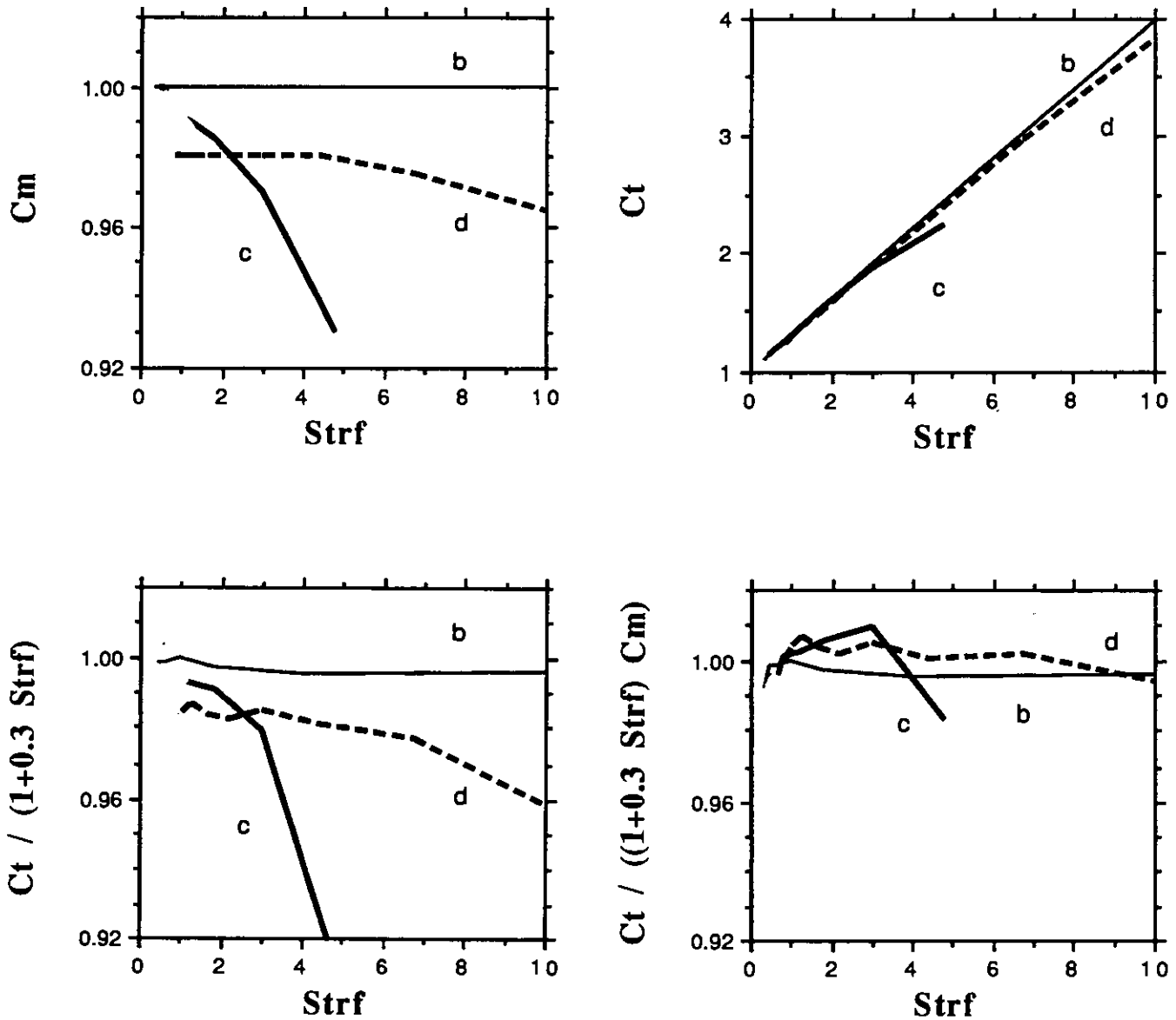
Figure 3.38. The mass and heat flow factors C_m and C_t for zone temperature profiles b, c and d of Figure 3.37; the aperture dimensions used are H=2m and W=1m.

### 3.7.1.3   Typical temperature stratification situations

In Figure 3.37 are shown typical vertical zone temperature profiles for which the parameters C_m and C_t have been calculated.

Linear temperature profiles. The results for linear temperature profiles (cases a-d) are presented in Figure 3.38 and the others (cases e-h) in Figure 3.39   A caracteristic for linear temperature profiles is that $\Delta T(H/2)$, the temperature difference at half opening height (Eq.3.21), coincides with the zone temperature difference averaged over opening height.

Figure 3.37 a : Both zones have the same temperature throughout the volume, the zone temperature difference, $\Delta T(z)$, is constant, the velocity profile is parabolic; the isothermal zone approximation is exact for both mass and heat flow, and the factors C_m and C_t are equal to unity.

Figure 3.37 b : Both zones have the same linear temperature profile, $\Delta T(z)$ has a constant value and the velocity profile is parabolic as for isothermal zones: $C_m=1$. The heat flow factor C_t is found to vary linearly with the coefficient Strf (Figure 3.38b) :

$$C_t = 1 + 0.3 \; \text{Strf} \tag{3.26}$$

This suggests that we could improve an analytical model by dividing C_t by the right hand side of Eq. 3.26 (see Figure 3.38 c), This approach is well known from the literature (Eq. 2.31).

Figure 3.37 c : Both zones have a linear temperature profile, but the hot zone is more strongly stratified. The inter-zone temperature difference, $\Delta T(z)$, *increases* linearly with height, the neutral level is above midheight, and the velocities are higher near the top of the opening. C_m decreases a few percent with increasing stratification (Figure 3.38 a). The increase in heat flow is less than predicted by Eq.3.26 (Figure 3.38 b and c), however dividng by C_m shows that this is largely due to the relative decrease in massflow (Figure 3.38 d).

Figure 3.37 d : Linear temperature profiles as previously, but the inter-zone temperature difference, $\Delta T(z)$, *decreases* with height, the neutral level is below midheight, and the velocities are higher near the bottom of the opening. Again, C_m decreases with increasing stratification (Figure 3.38 a) and the heat flow factor is within one percent given by

$$C_t = (1 + 0.3 \; \text{Strf}) \; C_m \tag{3.27}$$

Non-linear temperature profiles. A two-piece linear temperature profile as given in Figures 3.37 e, f, g and h is defined by two parameters for each linear part : one gradient and one temperature at a given height. The height at which the two gradients cross is quite arbitrarily chosen at H/2. The stratification factor is changed by variation of $\Delta T(H/2)$ while the gradients are kept constant.

It is caracteristic for non-linear temperature profiles that $\Delta T(H/2)$, the temperature difference at half opening height (Eq.3.21), is generally larger or smaller than the zone temperature difference averaged over opening height. Using average temperatures instead of temperatures at half opening height would probably lead to the most coherent interpretation. However, the present choice is expected to give more information on the possible error in calculated mass and heat transfer values when few zone temperature data are available.

Figure 3.37 e : Both zones have the same same linear temperature profile below H/2. Higher, the temperature difference, $\Delta T(z)$, increases linearly with height, the neutral level is above midheight, and the velocities are higher near the top of the opening. This case is typical for a convective heat source in the hot zone.

$\Delta T(H/2)$, the temperature difference at half opening height is smaller than the average temperature difference, and the massflow factor C_m increases considerably with stratification (Figure 3.39 a). The value of C_t (Figure 3.39 b) is large and the normalization with Eq. 3.27 is not complete (Figure 3.39 c and d).
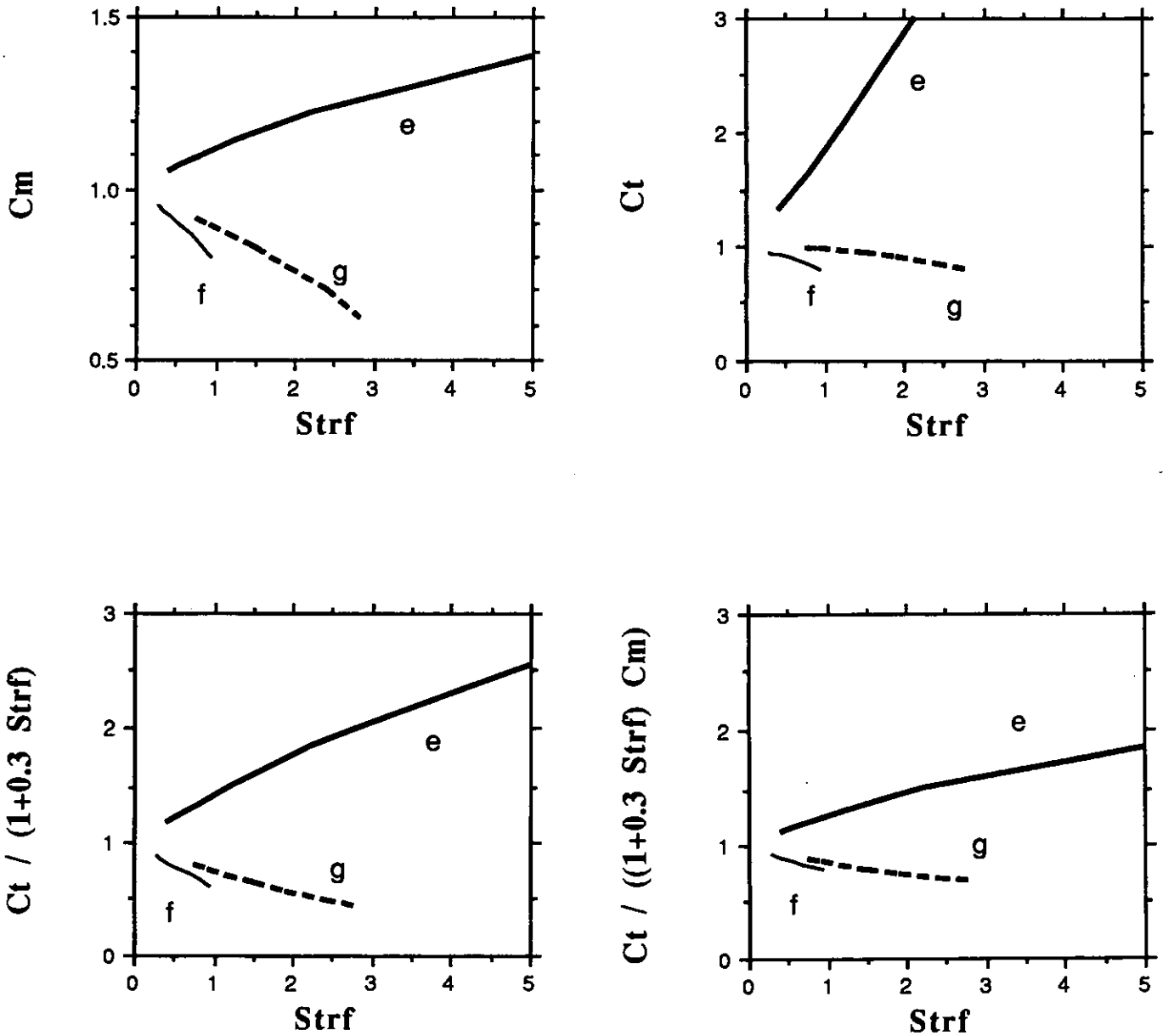

Figure 3.39 The mass and heat flow factors C_m and C_t for zone temperature profiles e, f and g of Figure 3.37; the aperture dimensions used are H=2m and W=1m.

Figure 3.37 f : The same linear temperature profile until midheight, then the inter-zone temperature difference, $\Delta T(z)$, decreases linearly with height, the neutral level is below midheight. $\Delta T(H/2)$ is larger than the average temperature difference and C_m is smaller than unity (Figure 3.39 a). The heat flow factor C_t is of the order of C_m but Eq.3.27 is not valid (Figure 3.39 c and d).

Figure 3.37 g : In the cold zone, the temperature is constant below H/2 and increases above midheight. In the warm zone, the temperature is constant above and decreases below midheight. The inter-zone temperature difference, $\Delta T(z)$, shows a maximum near midheight, and this is expected to be typical for a convectively heated coldzone connected to a cooled warm zone. $\Delta T(H/2)$ is much larger than the average temperature difference and the result is similar to case f.

Figure 3.37 h : The temperature profiles are inversed with respect to case g (heated hot zone and cooled cold zone). The inter-zone temperature difference, $\Delta T(z)$, shows a minimum near midheight. $\Delta T(H/2)$ is much smaller than the average temperature difference and both Cm and Ct are larger than unity. This case is not shown.

Conclusion In the modeling of interzone heat and mass flow, it is still uncertain how to define the caracteristic zone temperatures that drive Bernoulli flow, and presumably this uncertainty is the dominating cause for the spread of values for discharge coefficients found in the literature. The solution of this problem would be helped by a systematic comparison between CFD simulations and simplified modeling.

For the multizone air flow modelling practice of using linear zone temperature profiles, it is important to know that different 'choices' of the interzone temperature difference ΔT can lead to large differences in the computed mass and heat flow. However the error produced by the replacement of numerical calculations with an analytical expression, can be made small by using correction factors which are a function of stratification coefficient (Figures 3.38a and d; Eq. 3.27).

For non-linear temperature profiles, the assumption of linear profiles can cause relatively large errors (Figure 3.39). However it is possible to continue this analysis in more detail, and to propose analytical (non-dimensional) models for a large number of standard cases. It is expected that the approximation error can be made smaller than the error made by fitting a linear profile to a measured temperature profile.

3.7.2   Modeling flow through horizontal openings

Air flow through large openings in horizontal partitions were briefly reviewed in section 2.1.6. It turned out that very few experimental data are available in the literature. No systematic horizontal opening experiments could be performed in the framework of Annex 20, but the following notes should help future work, both in developing algorithms for pressure networks and in defining new horizontal opening experiments to validate these algorithms.

In Figure 2.11 the parameters for natural convection through an opening in a horizontal partition of thickness H were defined. The air flows are to be given as a function of the pressure at the top, p_1, and bottom, p_2, of the opening.

When the air density above a partition of thickness H, is the same as the density below the opening, $\rho_1=\rho_2$, the hydrostatic pressure is $p_1-p_2= \rho_1 gH$.

$\rho_1<\rho_2$, one-way flow

When there is a density difference, and the low density is on top of the higher density, $\rho_1<\rho_2$, the hydrostatic pressure difference is $\rho_1 gH-\rho_2 gH<0$, and we have the following (stable) flow conditions :

- $p_2 < p_1+\rho_1 gH$:   downward air flow

- $p_2 > p_1+\rho_2 gH$:   upward air flow

- $\rho_1 gH < p_2-p_1 < \rho_2 gH$:   no flow (threshold effect)

This is illustrated in Figure 3.40, where the air velocity is plotted as a function of pressure difference, using the latter flow conditions and the Bernoulli relation Eq. 2.17.
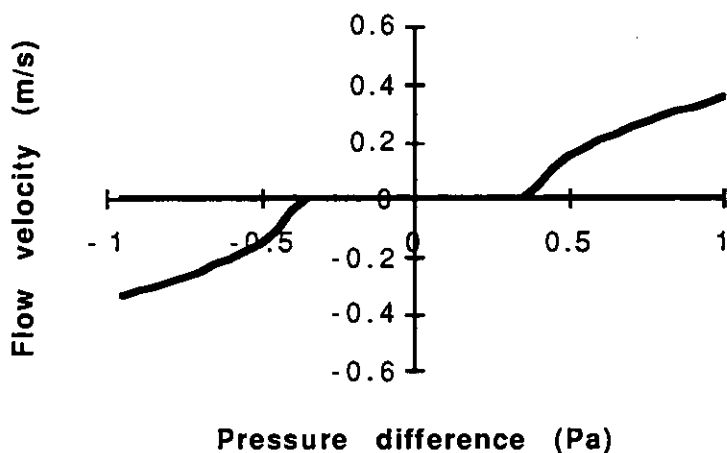
Figure 3.40 The air velocity as a function of pressure difference, over a horizontal partition with $\rho_1<\rho_2$. The velocity is positive when the flow is directed downward, and zero pressure in the plot corresponds to $p_1-p_2=(\rho_1+\rho_2)gH/2$. The calculation refers to a 20K temperature difference at roomtemperature and a partition thickness of 0.3m.

$\rho_1 > \rho_2$, two-way flow :

When the higher density fluid is on top of the lower density, $\rho_1 > \rho_2$, the hydrostatic pressure difference is $\rho_1 gH - \rho_2 gH > 0$, and we can have stable one-way or unstable two-way flow under the following conditions :

- $p_2 < p_1 + \rho_2 gH$:   one-way downward air flow

- $p_2 > p_1 + \rho_1 gH$:   one-way upward air flow

- $\rho_2 gH < p_2 - p_1 < \rho_1 gH$:   two-way flow

This is illustrated in Figure 3.41, where the velocities are plotted as a function of pressure difference as in Figure 3.40, using the two-way flow conditions and Eq. 2.17.

Pressure difference (Pa)
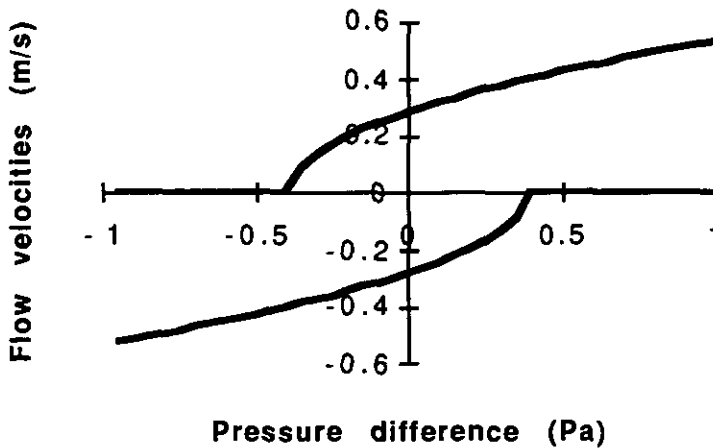
Figure 3.41. The air velocity as a function of pressure difference, over a horizontal partition with $\rho_1 > \rho_2$. The velocity is positive when the flow is directed downward, and zero pressure in the plot corresponds to $p_1 - p_2 = (\rho_1 + \rho_2)gH/2$. The calculation uses the same parameters as in Figure 3.40.

For the modeling of the *spreading of contaminants*, it is important to know the relation between the countercurrent flows. The investigations of *Epstein [1988]* are almost exclusively limited to the case of zero net flow, a very particular case for openings that are part of a pressure network.

The problem to be solved is in the question "How to calculate the volume flow rates through an opening of total area A, using velocities as given in Figure 3.41?" A model is needed for the opening area through which there is upward (area A_2) or downward (area A_1) flow, with the condition $A_1 + A_2 = A$. Does the ratio A_1/A_2 depend on Reynolds number? on velocity?

Indeed with regard to the effective value of the discharge coefficient, it will be composed of a contraction coefficient and a factor representing the mixing of counterflows as was the case for vertical openings (Figure 2.9), and these could also depend on the ratio between the counterflow velocities.

The required properties of a model are (i) $A_1 + A_2 = A$, (ii) $A_1 = A/2$ for zero netflow (iii) and the equivalent area A_1 goes to zero when the velocity tends to zero. Further it is known that with zero net flow and equal upward velocity, u_2, and downward velocity, u_1, the (equivalent opening) areas are equal ($A = 2A_1 = 2A_2$).

A trial formulation satisfying these properties is postulated as follows :

- downward volume flow

$$Q_{12} = Cd\; u_{12}A_1 = Cd\; u_{12}\; A\; \frac{u_{12}{}^n}{u_{12}{}^n + u_{21}{}^n}$$

(3.28a)

- upward volume flow

$$Q_{21} = Cd\; u_{21}A_2 = Cd\; u_{21}\; A\; \frac{u_{21}{}^n}{u_{12}{}^n + u_{21}{}^n}$$

(3.28b)

In Figure 3.42, the flow rate is calculated from Figure 3.41 and Eq.3.28 using n=2 (smoothest curves were obtained with n=4). This shows the first order representation of the counterflows through a horizontal opening. Clearly, this model and the correct value of the power n should be determined by comparing predictions (Figure 3.42) with experimental data.
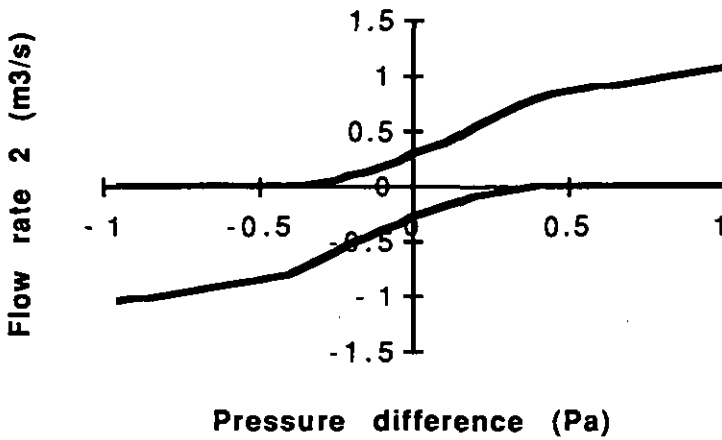
Figure 3.42. Prediction of first order model for the two-way volume flow rate through a horizontal opening, as a function of pressure difference. Positive flow is directed downward, and the flow rate is calculated from the velocities of Figure 3.41 and Eq. 3.28 (with n=2). The opening area in this example is $A=2m^2$.

Finally, with reference to Figure 2.12, the present considerations are only referring to the second (Bernoulli) regime. Without new experimental data on unequal counterflows, it can only be guessed what the flow in the other regimes will be.

3.7.3 Bulk-density versus boundary-layer driven flow

The two different flow regimes encountered in interzone heat transfer studies i.e. bulk-density and boundary-layer driven flow, have been discussed in chapter 2 (Figures 2.15 and 2.16; sections 2.1.5, 2.2 and 2.3). In particular *Scott et al. [1988]* , showed that the two flow regimes can be linked by a simple dimensional resistance model (Figure 2.17). The features of correlations as discussed in section 2.2.2, are all included.

The elements making up the model are discussed here (Figure 3.43 and Figure 3.44) to help pointing out new research needs .
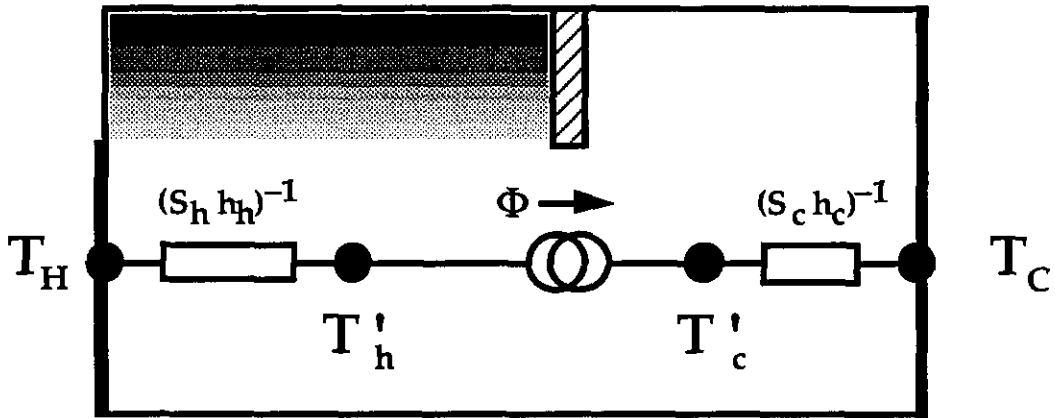
Figure 3.43 Elements of a thermal resistance model describing the convective heat transfer between two zones. The heat flux Φ flows from the hot wall (heat transfer coefficient h_h, surface area S_h, temperature T_H), to the hot zone air (temperature T'_h). Similarly from the cold zone air (temperature T'_c) to the cold wall (heat transfer coefficient h_c, surface area S_c, temperature T_C). The hot and cold zone air temperatures (T'_h and T'_c) are linked by an air flow model (Eq. 2.29 or 2.31), which is represented by a heat source rather than by a non-linear conductance (Davies M G ,1988).
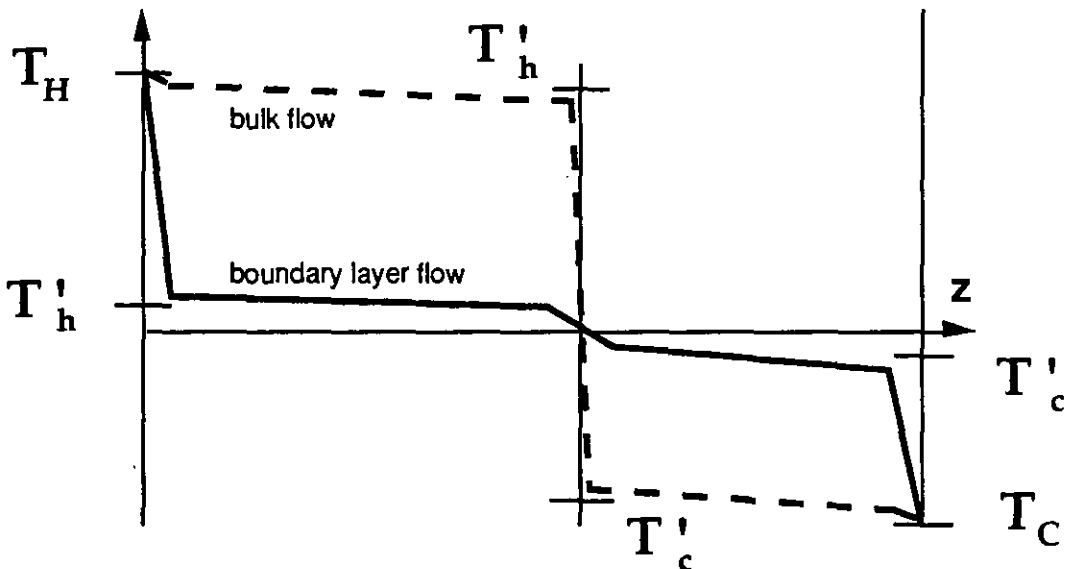
Figure 3.44 Typical horizontal temperature gradients on a central axis in a two-zone configuration for two flow regimes : density driven flow and boundary layer driven flow.

The elements of the model (Figure 3.43) comprise a ventilation model for the heat transfer between zones and resistances for the air-to-surface heat transfer. As discussed in section 2.3, in the density driven flow regime the fluid temperature in each zone is close to the wall temperature, while in the boundary layer driven flow regime there is a large temperature drop at the wall. This is illustrated in Figure 3.44 where the temperature variation over the hot and cold zone is schematically given.

With regard to the ventilation model, it is worth noting that ventilative heat transfer (Eq. 2.29 or 2.31) should not be treated as a conductance but rather as a source *[Davies M G ,1988]*. Further it was concluded in sections 3.6 and 3.7.1, that the prediction of interzone heat and mass transfer is subject to uncertainty even when the zone temperature fields are completely known. Future research should therefore be directed to the identification of the temperatures that primarily drive convective flow.

An important parameter is the stratification in each zone. *Neymark et al. [1989]* postulated that stratification scales linearly with typical height and temperature difference (Eq. 2.37a). However, this result can not simply be translated to real situations where it is difficult to attribute a single value to the stratification. Indeed, it is a well known day-to-day experience that temperature stratification decreases with the distance from a door (due to the heat transfer with the floor and walls, also illustrated in Figure 3.36).

Another important parameter is the relevant heat exchanging surface area in each zone. For a well insulated warm zone *this surface does not extend above the top of the opening level where* the air is stably stratified. But when the heat flow is upward or when the partition is not well insulating, there is convection all over the hot zone and the whole hot wall surface is more or less participating in the heat transfer.

Finally, it is interesting to note that test cell experiments are in general performed under boundary layer flow conditions. The heated surface areas are relatively small and the thermal boundary layer resistances are much larger than the opening resistance, as a consequence the air-air temperature drop over the opening is much less than the temperature difference between the heated end walls (e.g. Table 3.8 and Fig. 3.44).

3.7.4 Dynamical or steady state modeling?

It is important to know when the air flow modeling should be treated explicitly time dependent and when it is sufficient to describe the air flow as a succession of quasi-steady-state situations with a time variation of the boundary conditions. *[Moser 1989]* discussed this problem by *considering the physical time scales in building air flow.*

However in the description of a time-dependent situation as a succession of quasi-steady-state situations, it is often not well defined what the significant boundary conditions for the problem are. For example, from the modeling point of view the question could be : "Is the flow determined by the wall surface temperatures or by air temperatures?" and from a more practical point of view : "Are the wall temperatures known or are the air temperatures known?"

The significance of the simple model shown in Figure 3.43, is not only that it gives insight in the first order effects of wall temperatures and wall surface area on the inter-zone heat transfer. This dimensional model gives also an estimate of the temperature changes (and therefore the mass and heat flows) following the opening of a door between zones 1 and 2. Indeed, depending on the computer model used, it is predicted that the air temperature of zone 1 remains constant, becomes equal to the temperature of zone 2, or is situated in between these two extremes due to heat transfer with the walls (Figure 3.45).

Fixed wall temperatures are used as a first approximation to predict the heat transfer rate after the *opening of a door to, for example, a warm sunspace or a cold storage.* Taking the wall temperature equal to its zone temperature before the door was opened, the air temperature (and therefore the heat flow) can be estimated with the model of Figure 3.43. Both a sunspace and a cold room have in general relatively small wall surface areas. Therefore the temperature drop between the wall and the air will be large in these examples, and the heat transfer will be significantly lower than when estimated from the zone temperatures before the doors were

opened. For longer opening times, the wall temperatures will change and a thermal model for the surface temperature (Eq. 2.41) becomes necessary.
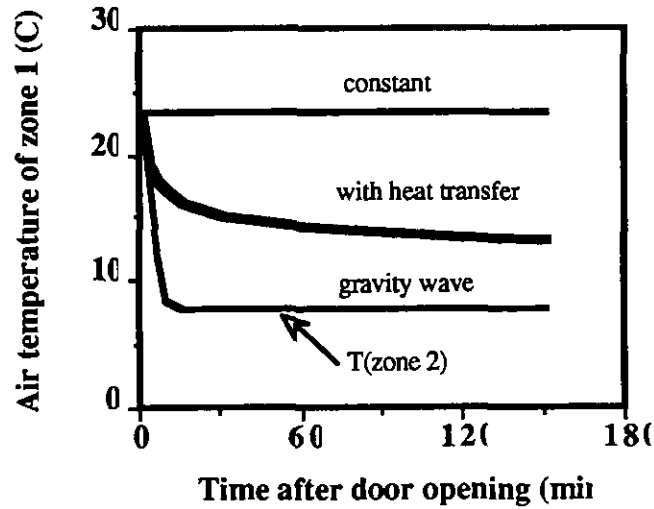
Figure 3.45: The predicted air temperature in zone 1 (after the opening of a door to zone 2) for three different models.

Interestingly, discharge coefficients for air flow through a door have been measured for a variety of boundary conditions. In section 3.6, discharge coefficients measured in test-cells (steady state conditions) were compared with those measured in a hall-way just after a door is opened (Figure 3.46a). Surprisingly the results appear to be equivalent. This illustrates that a further study of the role of dynamic boundary conditions would help understanding their relevance for the flow.

Figure 3.46

(a) : After opening a door between zones at different temperature a gravity wave penetrates at constant velocity (compare Figures 2.4 and 2.9b); the flow velocity depends only on the initial density difference between the fluids

(b) reflection of the wave at the back wall , the ventilation rate decreases

(c) ventilation stops after displacement of the inside air (adiabatic walls) .
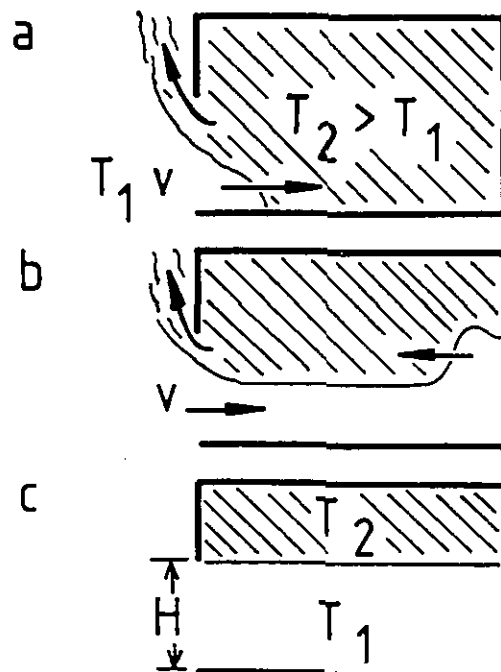
3.8 Conclusions on Internal Openings

The prediction of air flow and contaminant dispersal inside multizone buildings depends considerably on the way large internal openings like doors are modeled. Instead of developing non-dimensional correlations, the work on mass transfer in the test cells aimed in the first place at a better understanding of the basic physical phenomena and the attention was concentrated on the relation between velocity profiles and zone temperature profiles (Figure 3.1 : Model 2).

The joint research effort led to validate models based on the Bernoulli equation assuming either isothermal air volumes or linear temperature profiles. The discharge coefficient in both cases are quite similar and an average value of (0.45±0.1) seems adequate to model a large variety of configurations such as non heated rooms, or one room heated but not the other or both heated. This value is consistent with the value recommended by *ASHRAE [1989]*.

The local discharge coefficients derived from a comparison of measured and calculated velocity profiles appear to be strongly related with the boundary conditions, and are certainly related with interfacial mixing (Figure 2.9).

Comparison of analytical and numerical bernoulli models shows, that as long as the vertical zone temperature profiles are close to linear and similar, the interzone heat transfer can be well approximated by an analytical expression.(Eq. 3.27). Further, when the temperature profile is best approximated by a double linear profile, important deviations may result from a single linear profile approximation.(Figure 3.39).

Topics for further theoretical and experimental study include

- the relation between the zone temperaure stratification and the heating equiment,

- the search for the 'driving temperature difference' for Bernoulli flow

- flow through horizontal openings

- the transition between density driven and boundary layer driven flow

More experiments are obviously necessary although experiments are expensive, heavy to carry out , time consuming and , furthermore, in most cases, it is hard to change significantly the design parameters of the experimental set-ups ; that is why air flow modelling using computational fluid dynamics could be useful as long as the code is validated ; we have began to make progress in that direction trying to validate the "Concordia" code ; this task is not yet achieved but this is a promising way for general parametric studies.

Contents of chapter 4

4. NEW STUDIES OF SINGLE-SIDED VENTILATION

4.1 The Analysis of Single Sided Ventilation Measurements

What distinguishes external from internal openings? This distinction is made partly for historical reasons, and is based on the often dominant influence of the wind. Further we distinguish between cross-ventilation and single sided ventilation. The influence of wind on cross-ventilation is large (dominates stack flow in many cases) and is relatively well-known *[CIBSE 1986]* . Because the flow depends directly on the differences in pressure at the (multiple) openings the difficulty of predicting the flow is mainly due to the uncertainty in the pressure coefficients at the openings.

On the other hand when there is a single opening in one wall only (single sided ventilation), the effect of the wind is much reduced. Indeed, a steady wind blowing towards the opening is expected to increase only the inside pressure but not ventilation. Ventilation through a single opening implies both in and out flowing air, the mechanisms for which have been briefly discussed in section 2.4.2.

The difficulty in producing reproducible data on wind induced ventilation derives from the fact that the parameters that can reproducibly be measured (wind speed and direction, temperature) do not uniquely determine ventilation. The variability of the effect of wind on single sided ventilation is well illustrated by the large scatter of the data reported by *De Gids and Phaff [1982]* (Figure 2.26). The aim of the authors was to estimate the energy loss through windows that stay open for long periods of time. In order to fit data from different locations with a single correlation (Eq. 2.43), they have chosen to use the meteo data instead of locally measured data.

Before analysing new single sided ventilation measurements with the empirical model of Eq. 2.43, it is important to understand as much as possible the origin of the data scatter in Figure 2.26. For new data it would be expected that a locally measured air temperature and wind speed is more accurate than meteo data, and this is the reason to discuss briefly the influence of meteo data transfer, illustrated with the data set of *Phaff et al. [1980]*.

Warren [1986] recommended a procedure for the analysis of single sided ventilation data which is also illustrated with the latter data set.

4.1.1 Meteo data transfer

The original data of Figure 2.26 have only been published in *Phaff et al. [1980]*, and in spite of the fact that it contains many tables with valuable information, the authors considered the quality of the locally measured wind data not sufficiently high. This gives us the possibility though to discuss and illustrate the problem of 'meteo data transfer'.

Temperature. Comparing Eq. 2.25a and 2.43 we have for the stack effect

$$Q = \frac{1}{3} C_d WH \sqrt{\frac{g}{T} H\, \Delta T} = \frac{A}{2} u_{eff} = \frac{A}{2} \sqrt{C_2 H\, \Delta T} \; ; C_2 \approx 0.0052 \qquad (4.1)$$

where C_d=0.6 was used and ΔT is the locally measured interzone temperature difference. The fit to the data in Figure 2.26 was based on data from the meteo-station and resulted in a fitted stack effect factor C_2=0.0035.

In Figure 4.1 is plotted the local temperature difference, dTL=Tin-T(local), as a function of the meteo temperature difference, dTM=Tin-T(meteo). It is seen that the meteo outside temperatures are systematically lower than the local temperatures. Using local temperatures would result in C_2 values in close agreement with 4.1, but retracing the plot of Figure 2.26

using locally measured temperatures does not result in an obviously improved correlation.

We note that for the analysis of new data, a plot as given in Figure 4.1 could be very helpful to check the consistency of locally measured data.
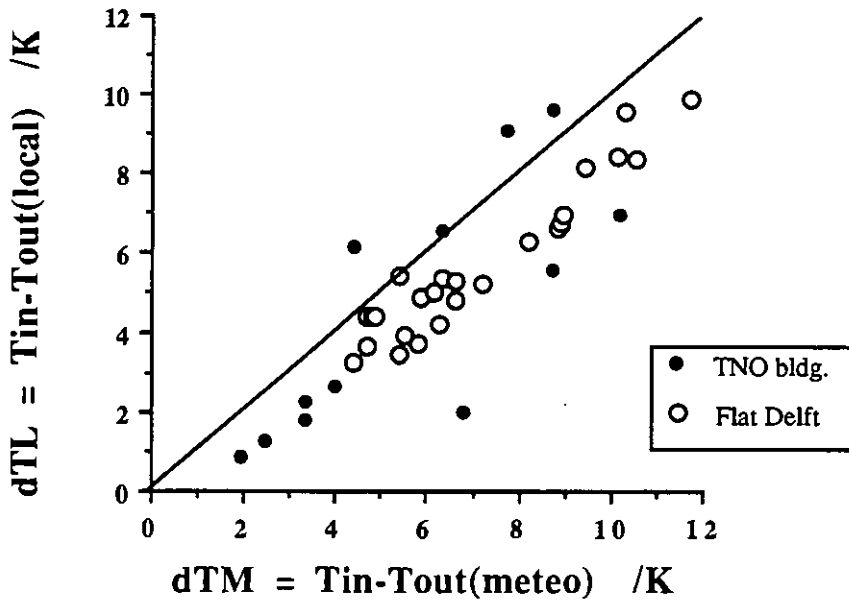
Figure 4.1. Comparison of the inside-ouside temperature differences based on 'local' and 'meteo' outside temperatures. The straight line gives the identity dTM=dTL. Data from Table 12 in *Phaff et al. (1980)*.
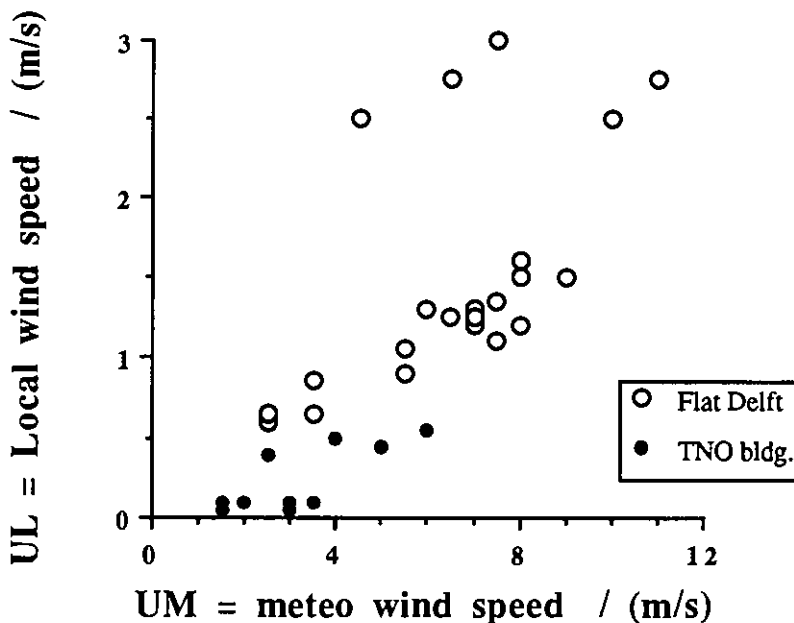
Figure 4.2. Local wind speed as a function of meteo windspeed. Data from Table 12 in*Phaff et al. (1980)*.

Wind. The transfer of meteo wind data depends strongly on the terrain and the surroundings of a building. The 'local' wind speed, UL was measured at 2m from the façade near the

112

opening. The local velocities measured at the TNO building (Figure 4.2) were systematically too low in value due to the use there of a cup anemometer, insensitive for wind speeds below 1m/s. The Flat Delft data in Figure 4.2 show quite good correlation between UL and the meteo wind speed UM, UL being about 20% of UM with the exception of three data where the locally measured speed is up to 55% of UM.

In Figure 4.3, the wind speed ratio UL/UM is plotted as a function of wind direction with respect to normal incidence. It turns out that the highest local velocities correspond to nearly normal incidence, ±45°.

As for Figure 4.1, it should be noted that meteo wind data can be used to make a plot similar to Figure 4.3, which is very helpful in checking the consistency and quality of local wind data.
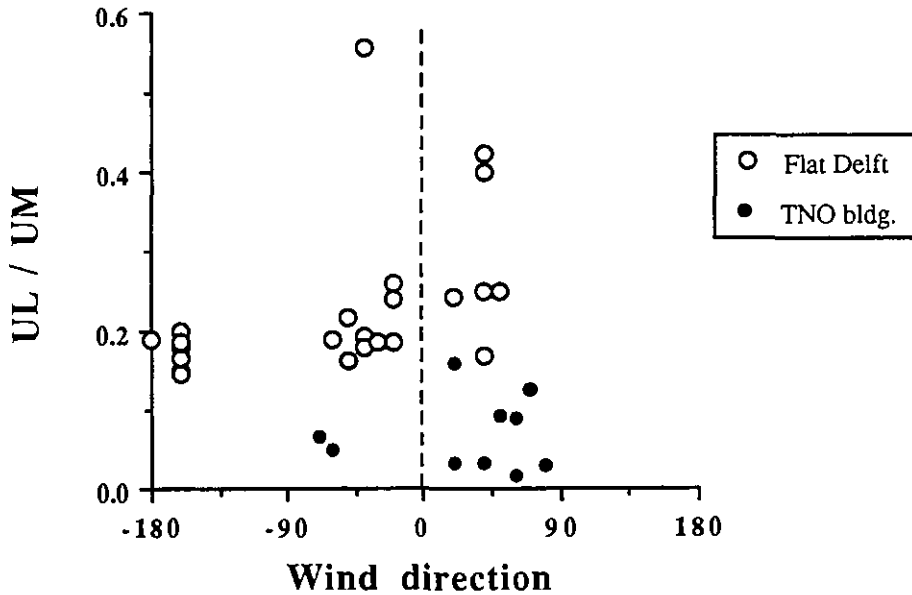
Figure 4.3. Wind speed ratio (data from Figure 4.2) as a function of wind direction. Zero degrees correspond to normal wind incidence.

4.1.2 Warren plot

For the analysis of the measured ventilation rates we will follow as a first step in the analysis, the recommendation of Warren [1986] to separate out those data which are dominated by stack effect .

This may be done by plotting a 'Warren-plot', where the ventilation parameter F (Eq. 2.46) is given as a function of the square root of Ar, the Archimedes number ($Ar^{0.5}=1/Fr$, the inverse Froude number, Eq. 2.15). Both F and Ar are defined with respect to reference data, in this case meteo and local data, labeled M and L respectively. Comparing Eqs. 2.43 and 2.46, the ventilation parameter F, equals half the equivalent air velocity derived from tracer gas decay (Figure 2.26), divided by the reference velocity :

$$F_M = \frac{Ueq}{2\,U_M} \quad ; \quad F_L = \frac{Ueq}{2\,U_L}$$

(4.2)

The Archimedes numbers for meteo and local data are defined as :

$$\sqrt{Ar_M} = \frac{\sqrt{\frac{g}{T}\,H\,dT_M}}{U_M} \quad ; \quad \sqrt{Ar_L} = \frac{\sqrt{\frac{g}{T}\,H\,dT_L}}{U_L}$$

(4.3)

For large Archimedes number the stack effect will dominate and, using Eq. 4.1, the measured

values of the ventilation parameter F should approach an asymptote represented by :

$$F = 0.2 \sqrt{Ar}$$

(4.4)

This asymptote representing stack ventilation, is given in the Warren plot of Figure 4.4.
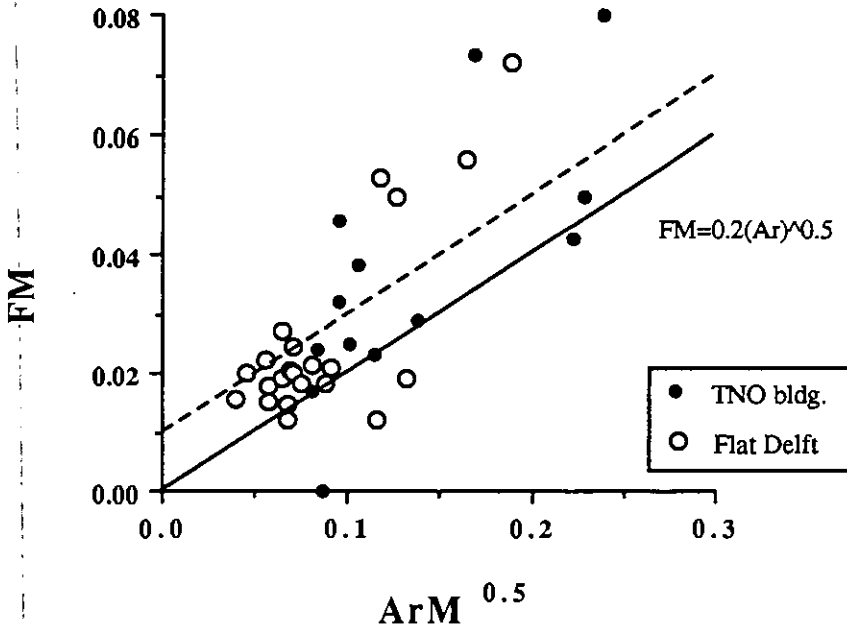
Figure 4.4. A Warren-plot based on meteo data. The straight line gives the calculated contribution from the stack effect
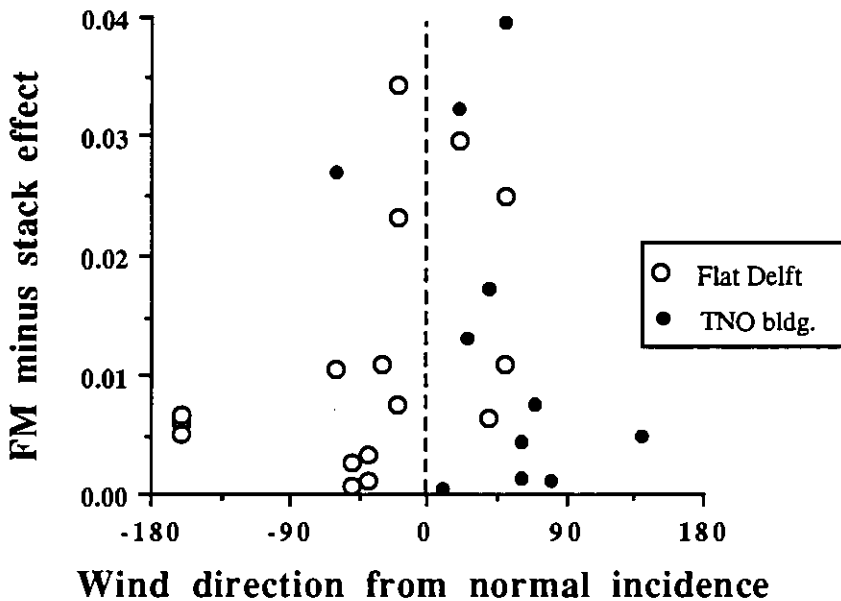
Fig 4.5 The 'meteodata' ventilation parameter corrected for stack effect (Eq. 4.4) as a function of wind direction.

To isolate results attributable largely to wind effect, one can discard points lying along to or close to this line, for example all data points below the (quite arbitrary drawn) dashed line.

In Figure 4.5, we have plotted the difference between the ventilation parameter, FM, and the stack effect (Eq.4.4) as a function of the angle between the wind velocity and the normal to the façade. A striking feature is that for both data series, many data refer to near normal wind incidence where a variability of more than an order of magnitude in the ventilation can be found, and this for both data series.

In Figure 4.6, the result of a Warren plot analysis is given for locally measured temperature and velocity. Only the results for the 'Flat Delft' data are given because both F_L and Ar_L were unphysically large (i.e. >>1) for the 'TNO building data; this is another indication that the locally measured velocities at the TNO building (Figure 4.4) were systematically too small.

An interesting feature of Figure 4.6 is the high value of the wind induced ventilation rate, with a value as high as 0.3 for normal incident wind (60% of the theoretical maximum Eq. 2.46). This possible importance of high ventilation at normal incident wind was not reported earlier.
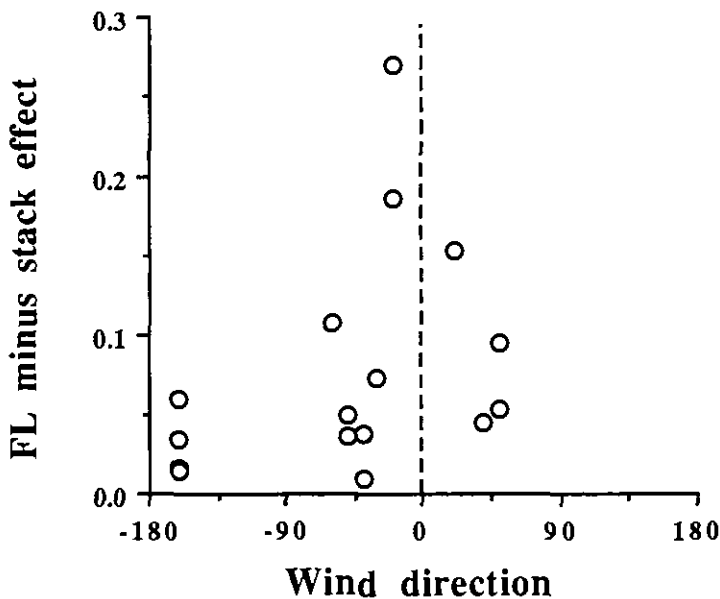
Figure 4.6 The 'local' ventilation parameter corrected for stack effect as a function of wind direction (Flat Delft data only).

The data shown in Figure 2.26 use meteo data and do not distinguish between the influence of wind direction and the influence of more or less turbulence. The origin of the scatter is mainly due to the mixing of these effects and the use of meteo data is not the main cause

The mean values of the ventilation parameter given by *Warren [1986]* , are for reference wind FM=0.025 and for local wind FL=0.1. Comparing these values with Figures 4.5 and 4.6 there is rough agreement for these mean values.

Conclusion. The empirical model of Eq. 2.43 and the 'Warren plot' can both be used for the analysis of *new data sets, using meteo data or locally measured temperature and velocity data.* Particular attention should be given to data corresponding to nearly normal incident wind. Meteo data can be used to check the quality and consistency of locally measured temperature and wind data by making plots like Figures 4.1 and 4.3.

4.1.3 Fluctuating wind pressures and pulsation flows

In a 'Warren-plot' analysis there is no possibility to distinguish between the influence of steady wind effects and turbulent wind effects. On the other hand in the empirical model proposed by *De Gids and Phaff* (Eq. 2.43), a fixed turbulent term $C_3=0.01$ is proposed, a value corresponding to an equivalent velocity component of 0.1m/s. *Phaff et al [1980]* also provide estimates for the fluctuating velocity component derived from velocity measurements in the window opening. We have plotted this estimate in Figure 4.7 as a function of meteo wind speed, showing that the fluctuating component is not constant, but rather is an increasing function of the wind speed. Clearly, there is need for new measurements and better ventilation models to take these fluctuating air flows into account.
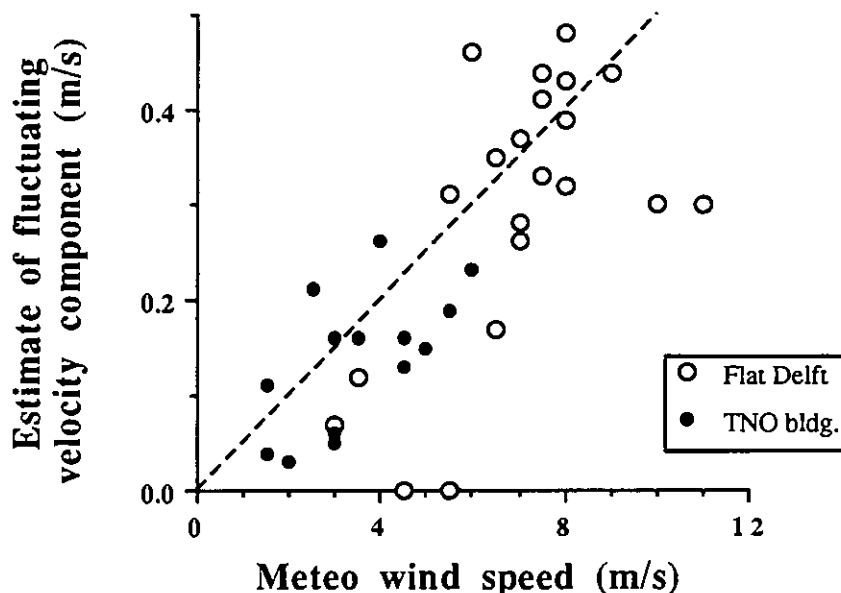
Figure 4.7 The fluctuating velocity component is not constant but increases with wind speed. The dashed line is to guide the eye.
Data from Table 12 in *Phaff et al. (1980)*.

Cockroft and Robertson [1976], studied ventilation with normal wind incidence, and proposed a theory to take pressure fluctuations into account and more recently, *Haghighat et al.[1991]* proposed a new model approach. To understand the interpretation of the measurements of pulsating flows (see section 4.2) the models will be qualitatively discussed.

A quick estimate can be made of the air change rate resulting from a fluctuating pressure at a single large opening of a volume V. It is then assumed that the pressure variations are instantaneous, this means that the size of the opening does not limit the flow. For a change in pressure of δp (Pa), the air density changes by $\delta \rho = \rho \, \delta p / p$ and this causes an air flow of $\delta V \cong V \, \delta p / p$. Therefore pressure fluctuations of frequency f(Hz) and amplitude δp would induce an average air change rate of:

$$Q(fluctuating) = u_{ac}\frac{A}{2} = f\,V\frac{dp}{p}$$

(4.5)

This is the maximum value one can expect for a single frequency component of the external wind. As an example, taking a room of 100m^3 and wind pressure fluctuations at 1Hz and 20Pa amplitude, then 0.02m^3/s of air flows in and out. Assuming complete mixing this fluctuating wind pressure would cause a total influx of fresh air of 0.7ACH.

The model Eq. 4.5 predicts a fluctuating velocity component that increases linearly with the

pressure variation, and therefore with the square of the wind velocity. In Figure 4.7, the plotted fluctuating velocity component is a measure of the root mean square value and can not be compared directly with Eq. 4.5.

In general there is a pressure drop over the opening, and for rapid fluctuations the inertial mass of the air will limit the acceleration of the air. In Figure 4.8, we show the analogous electrical elements included in the air flow model proposed by *Haghighat [1991]*. The effect of the non-zero air-mass is represented by an impedance L, whose impedance value increases with frequency. R is the nonlinear air flow resistance of the opening which increases with the air flow rate, and the amount of air stored in the volume is represented by a capacitance.
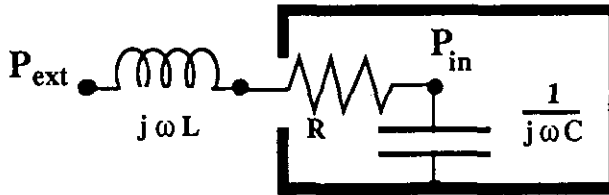
Figure 4.8 The equivalent circuit for the modelling of ventilation induced by pressure fluctuations

For particular forms of the external pressure, the 2nd order nonlinear differential equation corresponding to this model has to be solved numerically to find the internal pressure and the air flow, which both can be compared with experiments.

For a given situation the problem can be simplified by estimating the relative magnitude of the three circuit elements in Figure 4.8. The nonlinear flow resistance and the capacity are forming a low pass filter, and an estimate of the cut-off frequency f_c, will show whether the flow impedance $2\pi f_c L$ can be neglected. When this is the case, the calculation of the internal pressure is reduced to the solution of a first order nonlinear differential equation. This is the approximation used for the interpretation of the measurements in section 4.2.

4.1.4 Ventilation effectiveness of pulsation flows.

It must be kept in mind that the model presented schematically in Figure 4.8 allows the prediction of internal pressure fluctuations as a function of external pressure changes, but is not a complete ventilation model. Moreover it does not include two-way flow, neither does it take onto account effects related to the finite velocity of pressure (sound) waves.

To convert the pressure variations to air change rates one has to make assumptions about the ventilation effectiveness. Under particular circumstances, air can just fluctuate in the opening without mixing with the inside air. Indeed, for example *Cockroft and Robertson [1976]* found that the ventilation rate was only 30% of the value which would correspond to complete mixing.

To evaluate the ventilation effectiveness, some of the basic questions that remain to be answered are: 'Under which condition the air would just fluctuate in the opening and when would fluctuating air flows penetrate deeply into the ventilated space and mix with the air?'.

4.2 Natural Ventilation and Wind Turbulence

(CSTB, Marne-la-Vallée, France)

4.2.1 Introduction

This paragraph presents in particular the experimental work on single-sided ventilation of the research group at the CSTB, Marne-la-Vallée (France). The air flow rate through a horizontal narrow opening in a test house is measured with a tracer gas, and comparison is made with a ventilation model that takes the compressibility of the air into account.

The purpose of their study was to improve the understanding of the behaviour of ventilation openings in real situations. There was concern about the validity of the assumptions made in most models of ventilation in dwellings. In particular the following effects are often neglected:

a) Variations in wind velocity

b) The compressibility of air

c) Two-way flow through an opening

d) The effects of convection within a room

These are not satisfactory under some conditions.

As discussed in section 2.4.2, experimental and theoretical studies of single-sided ventilation *[Cockroft and Robertson 1976; Warren and Parkins 1985; Haghighat et al. 1991]* have shown that the ventilation rate of a building is affected by the effect of air compressibility and fluctuations in wind pressure. Improvements to these approximations have been considered, and incorporated into the model discussed in this section.

In order to validate this improved model of ventilation a series of experiments were performed at Bouin, France. Essentially they involved measuring the ventilation rate in a well-sealed house with a single ventilation opening in it. The house is specially set up to be able to rotate, so that the opening is always at the same angle to the wind.

Not all of the above assumptions have been taken into account, two-way flow and flow caused by convection will have to be investigated further. However, it is found that the improved model gives better agreement with the experimental data.

4.2.2 Modelling of ventilation

4.2.2.1 Description of the model

$$Q_i = \sum_{j=0}^{n} q_{ij} - q_{ji} = \frac{d (\rho_i V_i)}{dt}$$

(4.6)

where Q_i is the net flow into the zone labelled i (kg/s)

           q_{ji} is the flow from zone j to zone i (kg/s)

           ρ_i is the density of gas in zone i (kg/m^3)

           V_i is the volume of zone i (m^3)

           t   is time (s)

           the summation is taken over all the zones of the model

If air is assumed incompressible, then Q_i is equal to 0. However this can lead to errors, as is

shown by the extreme case of a one room house with a single ventilation opening. Assuming the density constant leads to the conclusion that there is no flow at all, which is clearly incorrect. So assuming that air is a perfect gas, and that any changes in pressure occur adiabatically, Eq. 4.6 leads to:

$$Q_i = \frac{V_i}{\gamma R T_i} \frac{dP_i}{dt} = C_d A \sqrt{\frac{2(P_{ext} - P_i)}{\rho}}$$

(4.7)

where P_i is the pressure in zone i (Pa)

          γ is the ratio of specific heats, C_p/C_v, 1.4 for air.

          R   is the gas constant (for air, R= 287 J/kgK)

          T_i is the temperature in zone i (K)

The set of differential equations defined by Eq. 4.7 is solved to find the values of the pressures in each zone and the ventilation flows. The method used to solve the system is the Levenberg-Marquardt algorithm, which minimises the sum of the squares of functions.

To run the model, the wind-induced pressures on the outside surfaces of the building are needed. These data can be taken from wind tunnel tests, or as in this study, measured on the building itself.

For a single-zone building ventilated through one external opening, Eq. 4.7 yields:

$$\frac{dP_{in}}{dt} = \pm \frac{A}{V} \gamma R T_{in} C_d \sqrt{2 \rho |P_{ext} - P_{in}|}$$

(4.8)

where P_{in} is the internal pressure (Pa)

          P_{ext} is the external pressure (Pa)

          A   is the area of the opening (m^2)

          C_d is the discharge coefficient ≈ 0.6

          ρ is the density of air flowing through the opening, i.e. ρ_i for outflow, the external density for inflow

4.2.2.2   Improvements to the model

(a) Variations in wind velocity

It is necessary to include time dependence in the model because of fluctuations in the wind velocity. These lead to a continuous variation in the pressure at the outside of the building. Hence, even if the pressure inside balanced the average wind pressure on the outside, flow would occur [Riberon et al. 1989]. In the model it is accounted for by re-running the model many times with the experimentally measured variations in surface pressure. From the sum of all of the calculated flows through the opening for different times, the ventilation rate and the expected tracer gas concentration can be calculated.

(b) The compressibility of air

Most ventilation models assume that air is incompressible. This simplifies the work, but can lead to errors in some circumstances. In particular this will happen if the flow is dominated by a single opening [Riberon et al., 1990].

Figure 4.10 shows the effect of including the compressibility of air into the model, in a simple one zone case, using pressure data from wind tunnel tests. Lines 1-3 were calculated with different wind approximations, only line 4 includes compressibility. In this example it is clear that the compressibility of air is an important factor. This is because of the large difference in the opening areas, $200 \ cm^2$ and $10 \ cm^2$. Note that in other situations there is little difference between results with and without compressibility. Hence it is important to recognize when it needs to be included.
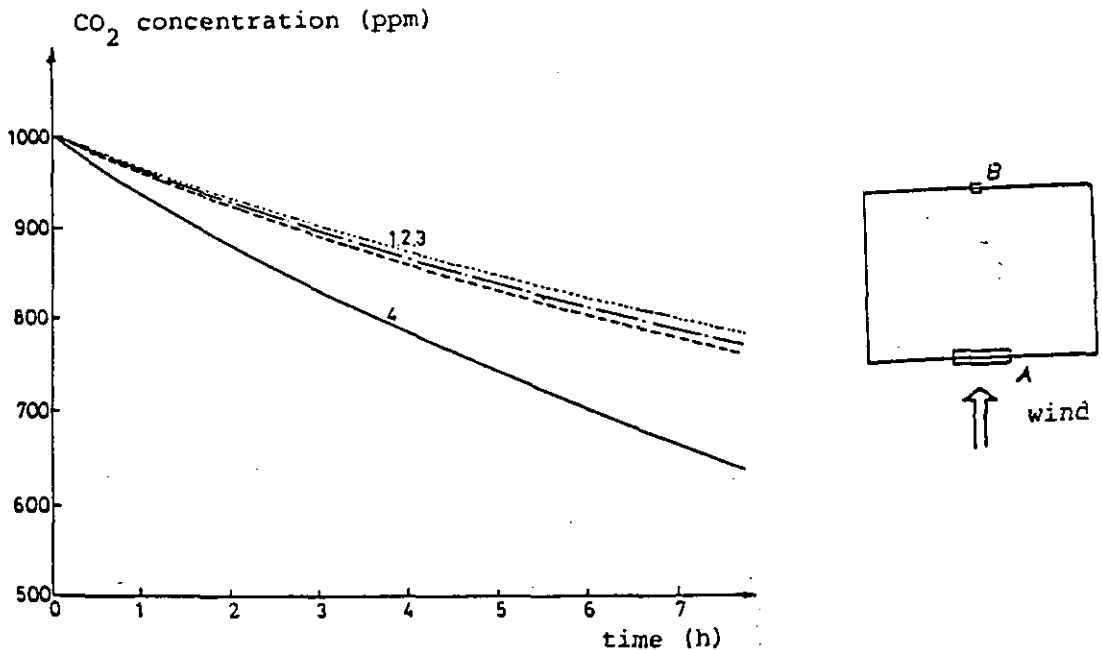
Figure 4.10 Simulated tracer gas decay for a single zone and normal wind incidence
1 : incompressible air, constant wind pressure
2 : incompressible air, temporal wind fluctuations
3 : incompressible air, spatial and temporal wind fluctuations
4 : compressible air, spatial and temporal wind fluctuations

(c) Two-way flow through an opening

In some cases it can be assumed that at any time the flow in a small opening will be in the same direction for the whole opening. However for a system where there is only one significant ventilation opening this will not be valid.

For a tall opening the variation in stack effect pressure with height causes two-way flow. However, for heights of a few cms this effect is small. From Eq. 4.1, for a temperature difference between inside and outside of 10 degrees, there would be a pressure difference of the order of 0.02 Pa between two points 5 cms apart. The effect of a temperature gradient inside the room is even smaller, less than 10^{-4} Pa per cm for a 5 degree per metre gradient. These may be neglected compared to wind pressure variations of the order of 1 Pa.

The variation of wind pressure across a surface is more important. This pressure distribution has not been modelled but measured, see section 4.2.2.3. The model can represent a single opening by a number of smaller openings, but with the same total area. The flow through each can then be found, in order to predict the effect on the ventilation rate of two-way flow.

(d) The effects of convection within a room

The flow of air through an opening as a result of convection currents in the room is not considered here. It could have an effect, particularly for a room with large heat inputs.

121

Similarly, rapid changes in indoor temperature with time can also cause air flow. For example, if a heating control system in a room causes a twice hourly fluctuation of temperature of 1K, this will cause an increase in the air change rate of about 0.01.

Note that the inclusion of each of (a), (b), (c) and (d), leads to an increase in the predicted ventilation flow.

4.2.3 Experimental method and results

4.2.3.1 Description of experimental facilities

In order to study the behaviour of a single opening under real conditions, a test house at Bouin was used, see Figure 4.11. It is a single zone building on an exposed site near the Atlantic coast. The volume of the test house is 93.6 m³. The equivalent air leakage area of the house was measured as less than 5 cm², which is small enough to be neglected in this study.
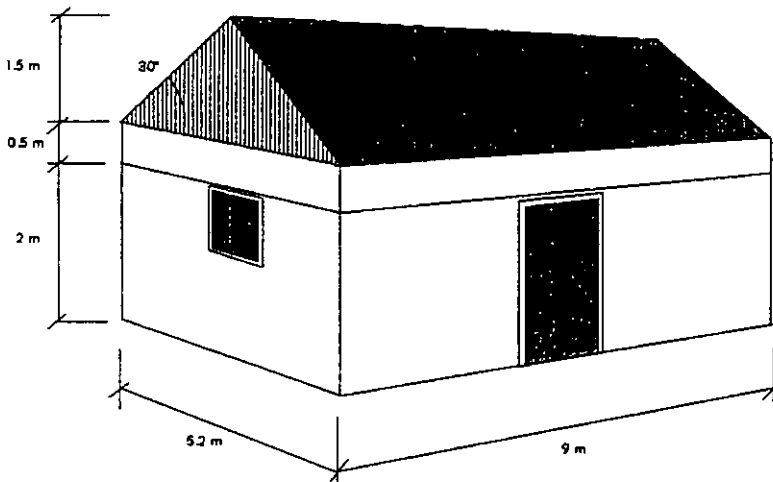
Figure 4.11 Bouin test house

A key feature of this site is the mounting of the building on a turntable. This means that it can be rotated during an experiment, keeping the same side to the wind throughout a test. This avoids the problems caused by the effect of changing wind direction on pressure.

The ventilation rate is calculated from tracer gas concentrations measured in the room. The wind-induced external pressures, internal pressures, wind speed and direction and tracer gas concentration are all measured simultaneously, at a rate of 5 Hz. Each test consists of a 10 minute mixing period, with the opening sealed, and then a 20 minute decay period.

The wind pressure is measured close to the opening. This pressure is equal to the difference between the total pressure and the external static pressure. The internal pressure is also measured with respect to this same external static pressure.

The tracer gas concentration is measured from five different sampling points in the room, to ensure the result is representative of the whole room. These points are 1.5 m above the floor, and linked through a manifold to the gas analyser. During the mixing period, small fans are used to provide complete mixing of the tracer gas. Full details of the site and the measuring equipment used can be found in *[Riberon and Villain, 1989]*.

4.2.3.2   Experimental results

A single opening was introduced into the building envelope and maintained either windward or leeward. Two sharp-edged slots were investigated, and the ventilation rates found from the tracer gas concentrations, are given in Table 4.1.

Opening	100 cm^2	200cm^2
Length	40 cm	40 cm
Height	2.5 cm	5 cm
Thickness	1 cm	1 cm

Test	opening area (cm2)	wind velocity (m/s)	wind incidence angle ϕ	tracer measured (ACH)	compressibility calculated (ACH)	F (Eq. 2.46)
1	100	7.7 (1.2)	18 (7)	0.21	0.20	0.07
2	100	5.1 (0.9)	0 (?)	0.20	0.09	0.10
3	100	10.2 (1.5)	229 (8)	0.58	-	0.15
4	200	5.8 (1.15)	10 (10)	0.35	0.24	0.07
5	200	5.8 (1.1)	191 (10)	0.20	-	0.045
**.	230	5	0	0.02	0.06	<10^{-3}

Table 4.1   ** [Cockroft and Robertson 1976]
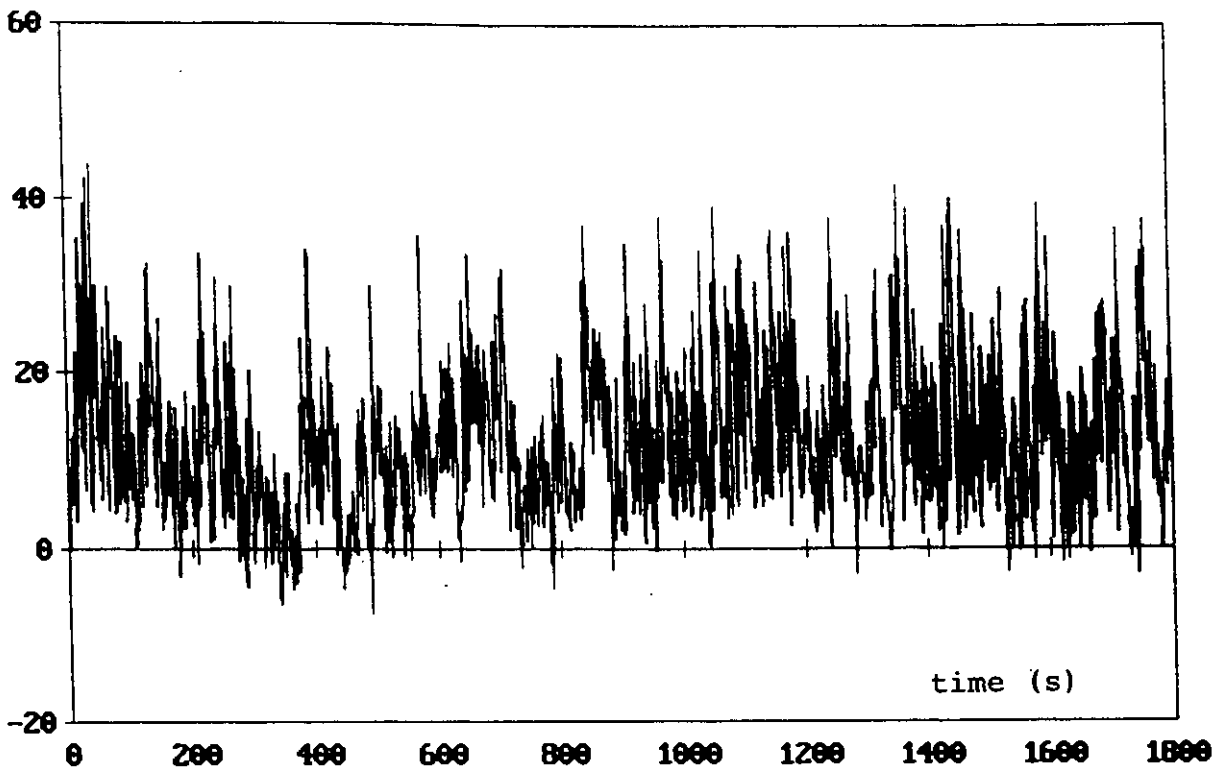
Figure 4.12 : Dynamic pressure (Pa) at the opening as a function of time (windward 100 cm^2 opening)

4.2.3.3 Comparison between predictions and measurements

a) Test 1

Figure 4.12 shows the wind pressure measured on the outside of the opening. Taking into account this input and the air compressibility assumption, the computer model has been used to predict indoor air pressure and air flows.

Figure 4.13 gives the measured and predicted pressure of the indoor air and Figure 4.14 gives the predicted and measured variations of the tracer gas concentration. Both Figures 4.13 and 4.14 show that the measured and predicted values are in close agreement.

b) Tests 2 to 5

The modelling results for these tests are not given here. They do not always show good agreement between predicted and measured results. More research is needed to find satisfactory explanations for these discrepancies.
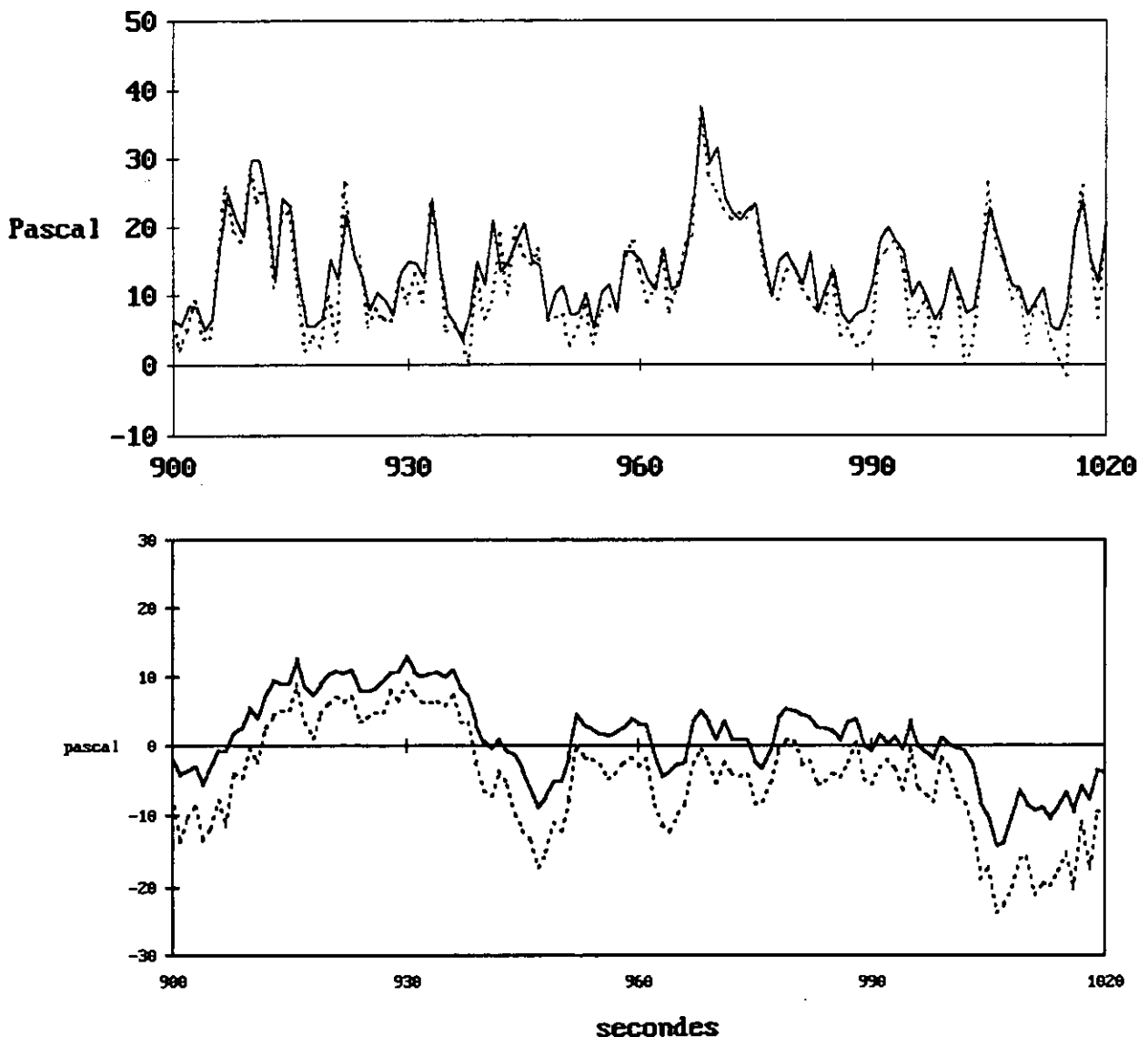
Figure 4.13. The measured and calculated (dashed curve) internal pressure of the BOUIN house for 100 cm2 : top: windward test 1; below: leeward test 3 . Input for the calculation is the measured outside pressure.

124
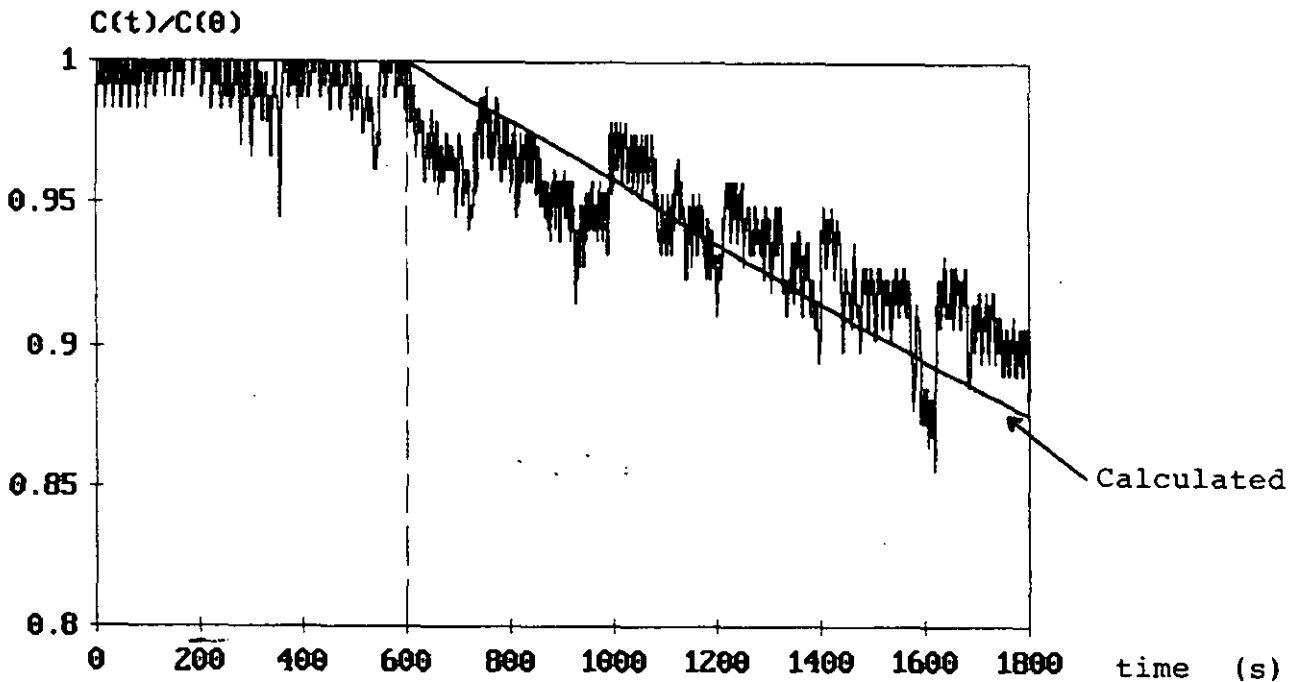
Figure 4.14 :Tracer gas concentration ratio versus time. This Figure depicts measured and predicted data for a 100 cm^2. windward opening ; fluctuations of measured data are due to the measurement device employed

4.2.3.4 - Investigation of two-way flow within the opening

During test 2 extra measurements were taken to measure the extent to which two-way flow was occurring. Instead of just taking a not an spatial average value of the pressure for the whole opening, the pressure was measured at eight points within the opening (see Figure 4.15). These points were at the centres of eight equally sized parts of it. The pressure was measured both inside and outside the building, allowing the direction of flow through each part to be measured.

For test 2, the measured ventilation rate is 0.20 ach. Assuming one way flow through the opening the model predicts 0.09 ach. By modelling the opening with eight smaller openings, it is possible to predict that flow will be into the building for some parts of the opening, and out for others. When this occurs the rate of renewal of air is increased, but the net flow through the opening is the same. With this improvement the model predicts 0.15 ach. This result is closer to the measured data, but they are still different, suggesting there is more work to be done.

4.2.4   Discussion

Table 1 summarizes the ventilation configurations studied with the test house in BOUIN. Are given the average wind velocity, the wind direction (from normal incidence to the opening) and the ventilation rates calculated from the measured decay of tracer gas concentrations. The standard deviation of the wind velocities and the wind direction is given between parentheses. Test cases 1, 2 and 4 are therefore with the opening to windward and cases 3 and 5 with the opening on the lee side. We note that the stack effect is calculated to be less than 0.01ACH and can therefore be neglected.

125

The external wind pressure is measured at the orifice and can then be used directly as input for a simulation programme to calculate the internal pressure and the air change rate.
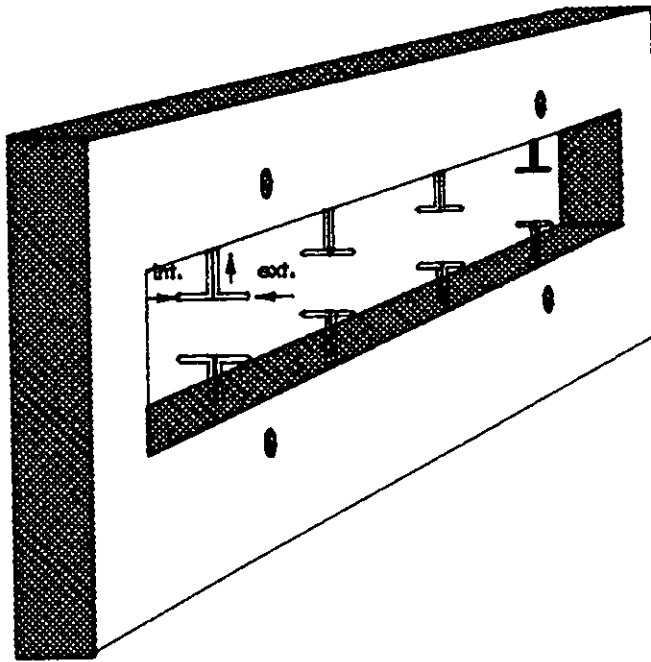
Figure 4.15 :The four tapping points located in the frame are used for the determination of average wind pressure The eight tapping points in the aperture are used for the investigation of two-way flow

For the simulations with the air infiltration program SIREN of the CSTB, it was assumed that the only mechanism for air exchange is the compressibility of the air. Therefore the external pressures measured at the opening are averaged, and the internal pressure is calculated by solving the first order differential equation (Eq. 4.8) numerically. In Figure 4.13a are plotted the measured and calculated internal pressure for the windward test 1. It is seen that the algorithm reproduces the main features of the internal pressure variations. Figure 4.13b concerns the same plot for leeward test 3, but this time there is a systematic difference between the observed and calculated pressure. This could be due to the simplifying assumption that there is no two-way flow. In particular in test 3, the incidence of the wind is not normal but almost at an angle of 45° so that eddy flow can be expected.

4.2.4.1 Data analysis by other research groups

The French group has made measured data available for analysis by other groups in Subtask 2. Different sets of wind pressure and velocity data have been received at the University of Concordia, Canada and at the EPFL, Lausanne.

The solution of Eq. 4.8, with experimental data points every 0.2sec as input, can become unstable when the relevant frequencies are approaching the sample rate of 5Hz. Indeed there appeared to be a numerical problem with the solution for the larger 200cm^2 opening. This data set was reanalysed with a computer code specially written to solve Eq. 4.8 (code TURBUL developed by J.-M. Furbringer), and the numerical instability and aliasing problems were immediately apparent. Using a NAG FORTRAN library routine, the internal pressure could be correctly calculated from the external pressure data as shown in Figure 4.16.

126
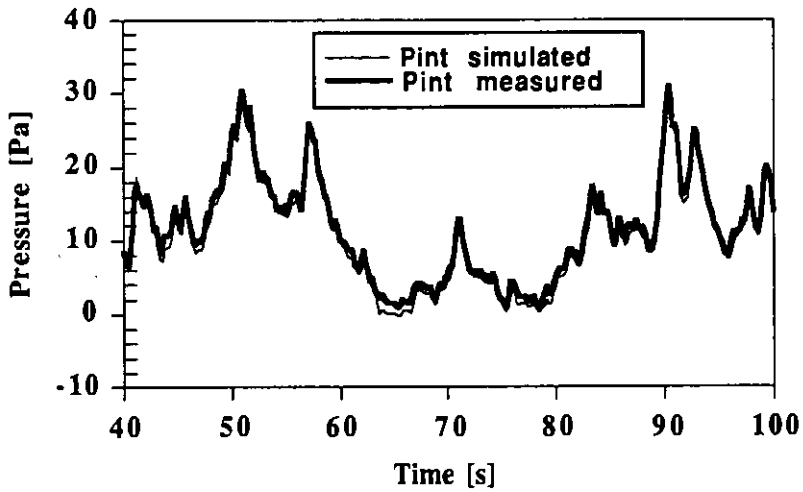
Figure 4.16. The measured internal pressure of the BOUIN house for 200cm2 windward test 4, compared with the prediction calculated with the code TURBUL (Furbringer 1992). In spite of the low sampling frequency oscillations in the calculated pressure could be avoided.
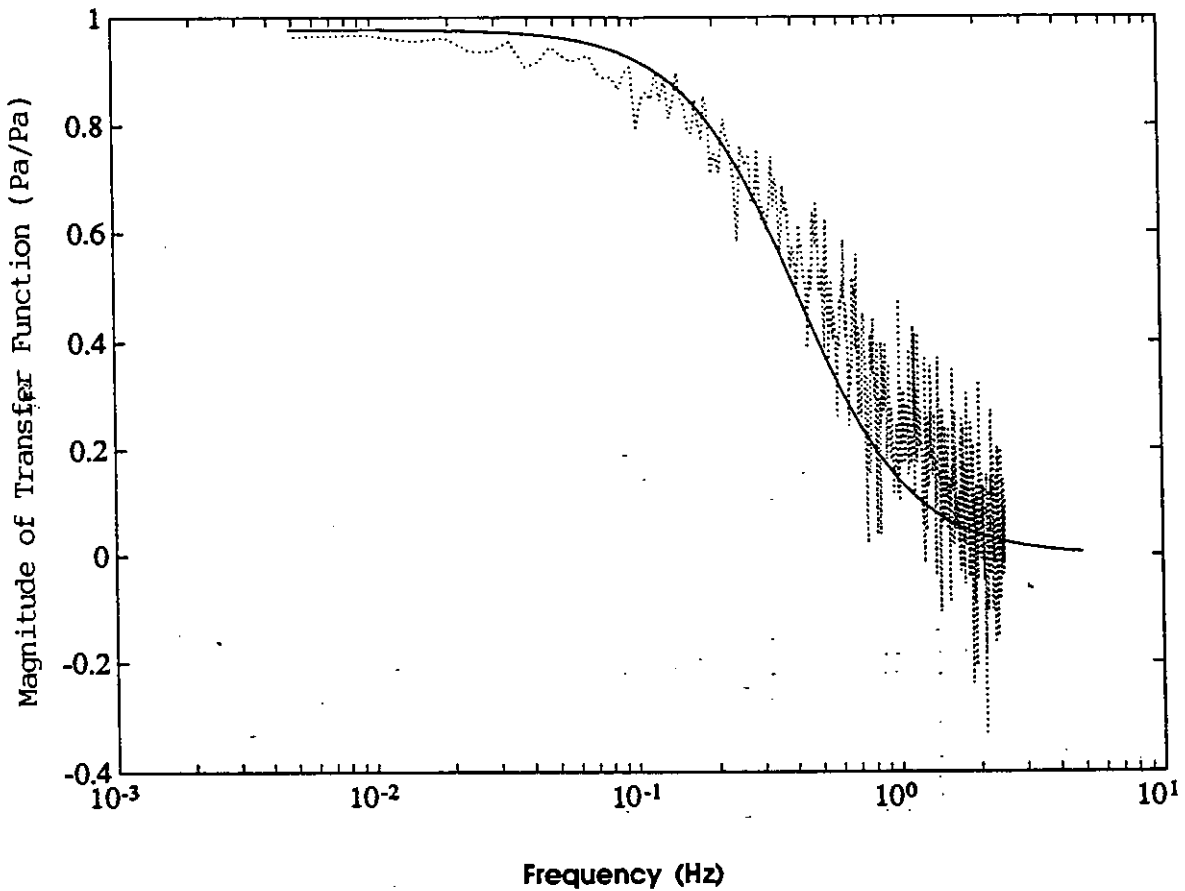
Figure 4.17. Test 1. Comparison between theoretical and experimental (dotted) transfer functions of internal pressure with respect to external pressure (C_d=0.3)

127

The data set of test 1, was re-analysed at the University of Concordia with the model described in *[Rao and Haghighat, 1991]*. Full agreement could be obtained by reducing the discharge coefficient to 0.3 (Figure 4.17). For C_d=0.6, the theoretical curve is shifted to higher frequencies by a factor of nearly three. At the writing of this report the low value of this fitting parameter was not yet understood.

**4.2.4.2 Ventilation.** As was briefly mentioned in section 4.1.4, to calculate the air change rate resulting from fluctuating pressures one has to know which part of the inflowing fresh air flows out without mixing with the inside air.

Assuming that the inflowing air mixes completely, the air change rate calculated from the measured outside pressure variations corresponds therefore to an upper limit for this mechanism. With the code SIREN, 0.09 ACH was obtained for test 2, which is about half the measured air change rate. Using the same procedure, the code TURBUL gave 0.24 ACH for test 4, which is also less than the measured air change rate (see Table 4.1).

These results contrast with the findings of *Cockroft and Robertson [1976]* who found that only one-third of the fluctuating air flow into the enclosure was finally mixed with the bulk of air in the enclosure. Their setup was very different though, using a 225 cm^2 opening in a 3.5m^3 isothermal model, and wind simulated with a variable speed fan. The result is included for comparison in Table 4.1.

With a comparable opening size but with a 30 times larger volume, the BOUIN data do not show evidence for incomplete mixing. A factor that may be important is the 5-10K inside-outside temperature difference in the BOUIN experiments. Indeed the colder air entering the enclosure is likely to fall immediately being automatically replaced by inside air during the backflow. Systematic experiments are necessary to study this mechanism.

Finally the fact that the measured internal pressure can be simulated in detail means that Eq. 4.8 applies to these particular cases. On the other hand the limits of this model with respect to opening sizes is not known in particular with regard to ventilation.

Indeed, with increasing opening-to-volume ratio, the time constant (equivalent to R times C in Figure 4.8) decreases and a much higher measurement frequency than used in the present experiments is required.

Finally, in the last column of Table 4.1 are given the ventilation coefficients F (see Eq. 2.46). They appear to be high compared with the scale model measurements showing that for a correct prediction of ventilation rates a detailed knowledge of the ventilation mechanisms is necessary.

Conclusion. The data sets obtained on the BOUIN rotatable test house have proved to be of high quality allowing its use by different research groups for the testing of different models on pulsating flows.

This study has shown that fluctuating windpressures induce air flows through a single opening in a room. These pulsating flows which are related to air compressibility and wind turbulence, are not predicted by conventional ventilation models.

In addition to pulsation flow, two-way flow caused by differences in pressure existing over the opening area were observed, and will be further studied. The effect of convective flow in a room on the ventilation rate should also be examined.

Future work planned in the Bouin house will include investigating the ventilation rate with two openings, one above the other to account for the stack effect, and the influence of an extract fan in the system.

4.3. Single-sided Ventilation Experiments
(BBRI, Limelette, Belgium)

4.3.1. Experimental setup

A single-sided ventilation experiment was set up in an attic space of a 4-storey row house in the city of Gent (volume ca 28 m3). The highly insulated roof contains 'Velux' roof windows in both North and South roof slopes (width 1.25 m, height 0.80 m) (See Figure 4.18).
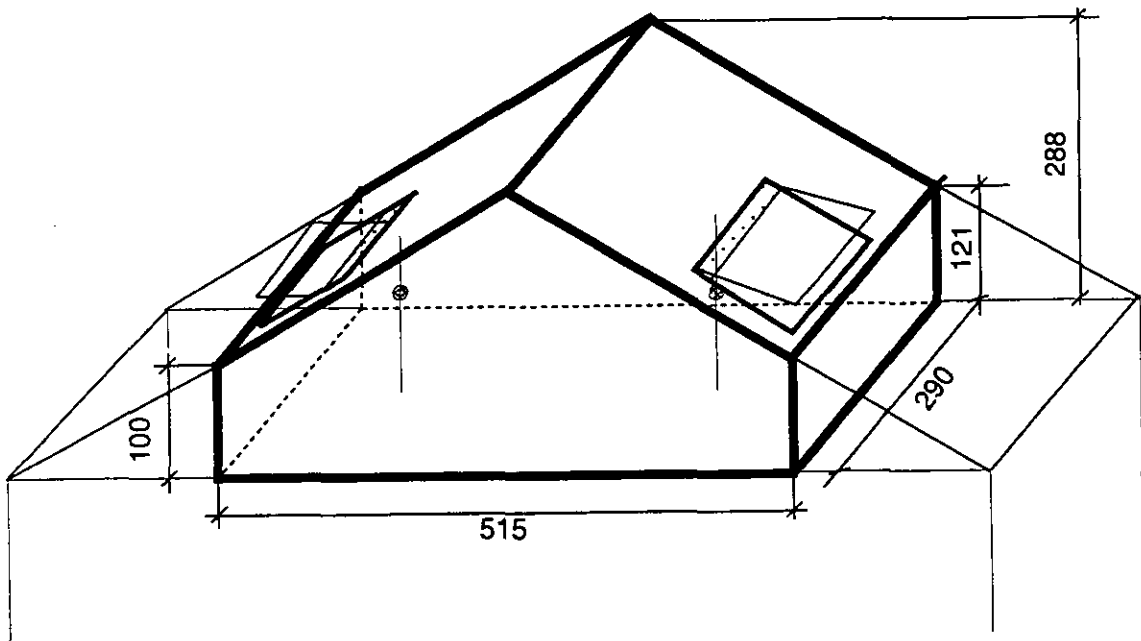
Figure 4.18. The attic in Gent with 2 roof windows

The North window is mid-hinged, while the South window is top-hinged. Both windows have a ventilation slit with closing flap over the whole width on top of the window (net opening section 123 cm2).

Air change rates and climatic parameters were monitored during a three week measuring period. A pressurisation test gave an airtightness level of 20 vol/h at 50 Pa. By means of the BBRI-MATE (Multipurpose Automated Tracergas Equipment), N$_2$O tracer gas was injected at a constant rate of 1 ml/s. Air samples were taken at 28 points. The gas concentration was determined with a Servomex Infra-Red analyser. The room air temperatures are measured at 12 points by means of thermocouples. The outdoor climate is measured through :

- the outdoor temperature;
- the wind velocity and direction at ca. 2 m above the roof top.

Pressure differences are measured between both façades (N - S), between inside and outside of both windows and between left and right ends of the ventilation slit at the outside of both windows by means of electronic micro-manometers (see Figure 4.19). The pressures, the wind velocity and the wind direction are measured about every 4 minutes, while the tracer gas concentrations and the temperatures are measured every 40 minutes.

Air change rate measurements were carried out for various configurations of openings of the windows and ventilation slits. Reported are the results of two experiments on single-sided ventilation: one with the south window (top-hinged) opened over 7.5 cm height while the north window, the ventilation slits of both windows and the entrance door were kept closed; the other with the north window (mid-hinged) open over 5.5 cm (both on top and bottom) and other openings closed (see section 4.3.2). In order to test the validity of the assumption of a single pressure coefficient, a separate analysis was made of the pressure measurements at the outside of the ventilation slit of the north window (see section 4.3.4).
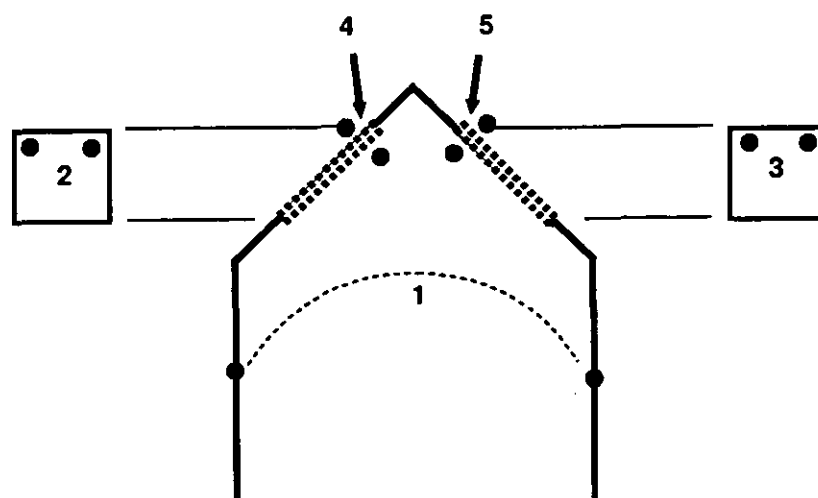
Figure 4.19. Location of the electronic micro-manometers in the attic in Gent for the measurement of the pressure difference (1) between both façades (N - S); (2) (3) between left and right at the outside of the ventilation slits; (4) (5) between inside and ouside at both windows.

4.3.2. Results of single-sided ventilation experiments

The results of ten days monitoring of the attic with the south window slightly opened (1 500 cm^2) are given in Figures 4.20 to 4.24.

The outside temperature (Figure 4.20) swinged between about 15 °C in the afternoon and ca. 8 °C at night. The same figure shows the distribution of the indoor air temperatures (12 measuring points). The average indoor temperature in the unheated attic exceeds the outdoor temperature by 6 to 11 K. For the calculation of the stack effect, the measuring point close to the opening has been used (as indicated on Figure 4.19). The wind velocity was varying between 1 and 4 m/s with a few peaks above 5 m/s (Figure 4.21). The wind direction was mainly between south (180°) and south-east (135°), (Figure 4.22) .

The pressure differences over the building (N - S façades) as shown in Figure 4.23, are clearly correlated to the wind speed.

In Figure 4.24 are shown the pressure differences between left and right sides of the ventilation slit at the outside of the south window. During two days very important pressure differences (up to 20 Pa) were found. This phenomenon is further discussed in section 4.3.4.

The air change rates given in Figure 4.25 are calculated from the N_2O concentrations measured close to the window opening.
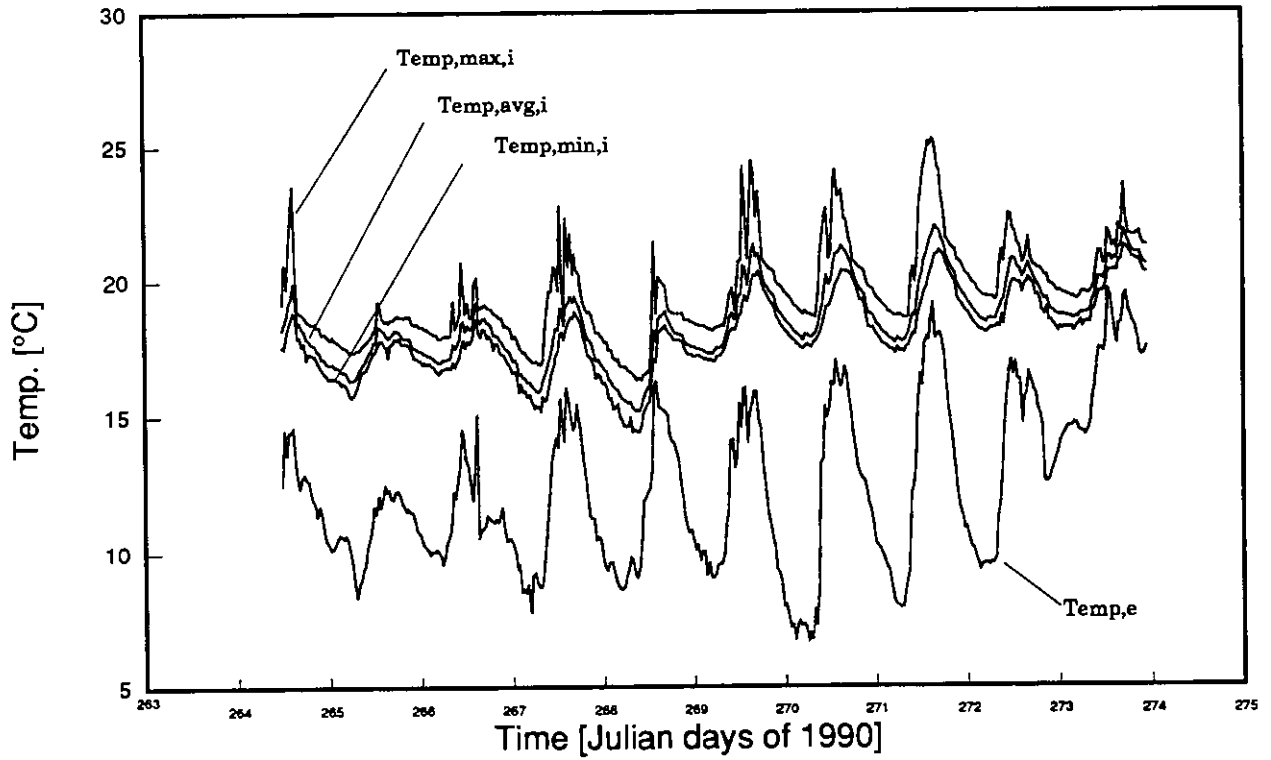
Figure 4.20.   Measured outdoor (Temp, e) and inside air temperatures :
maximum, minimum and average values of 12 measurements.
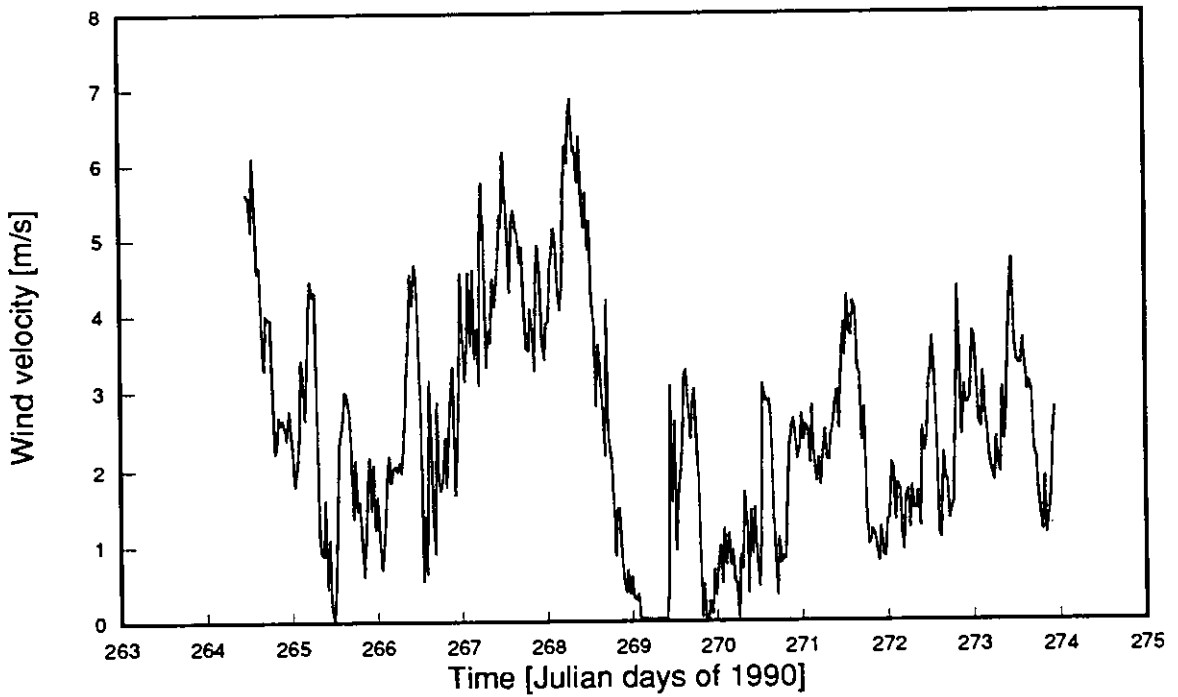
Figure 4.21.   Measured wind velocities

131
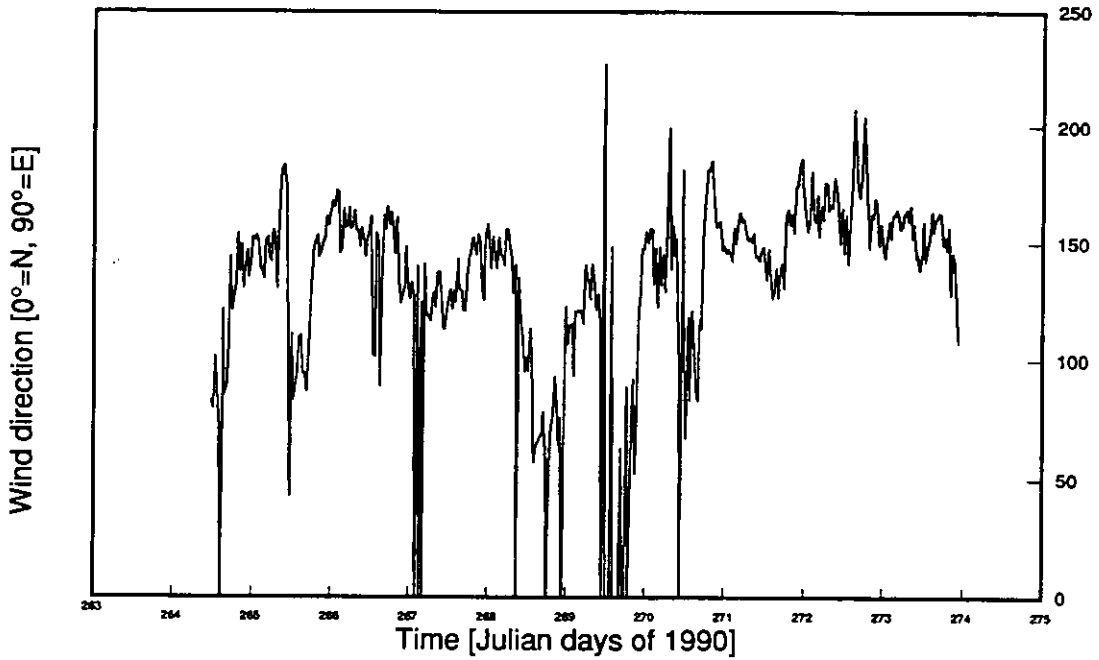
Figure 4.22.   Measured wind directions
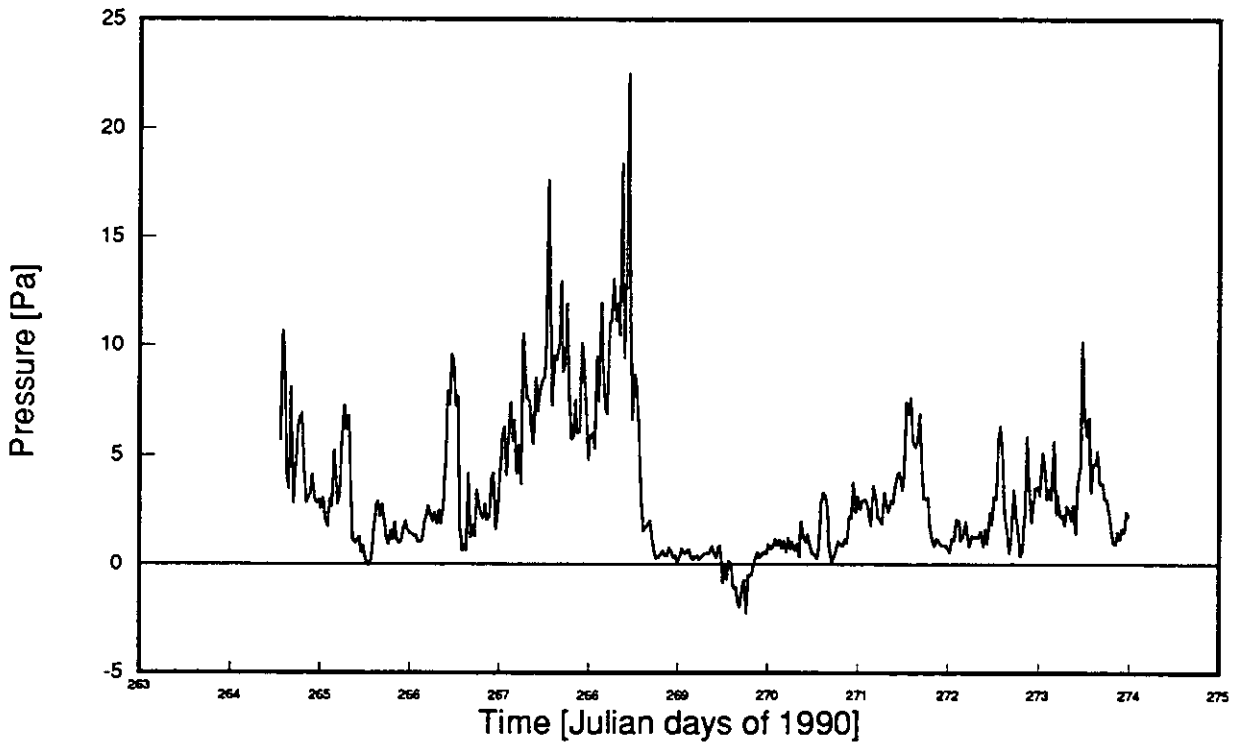
Figure 4.23.   Measured pressure differences over both façades (N - S)
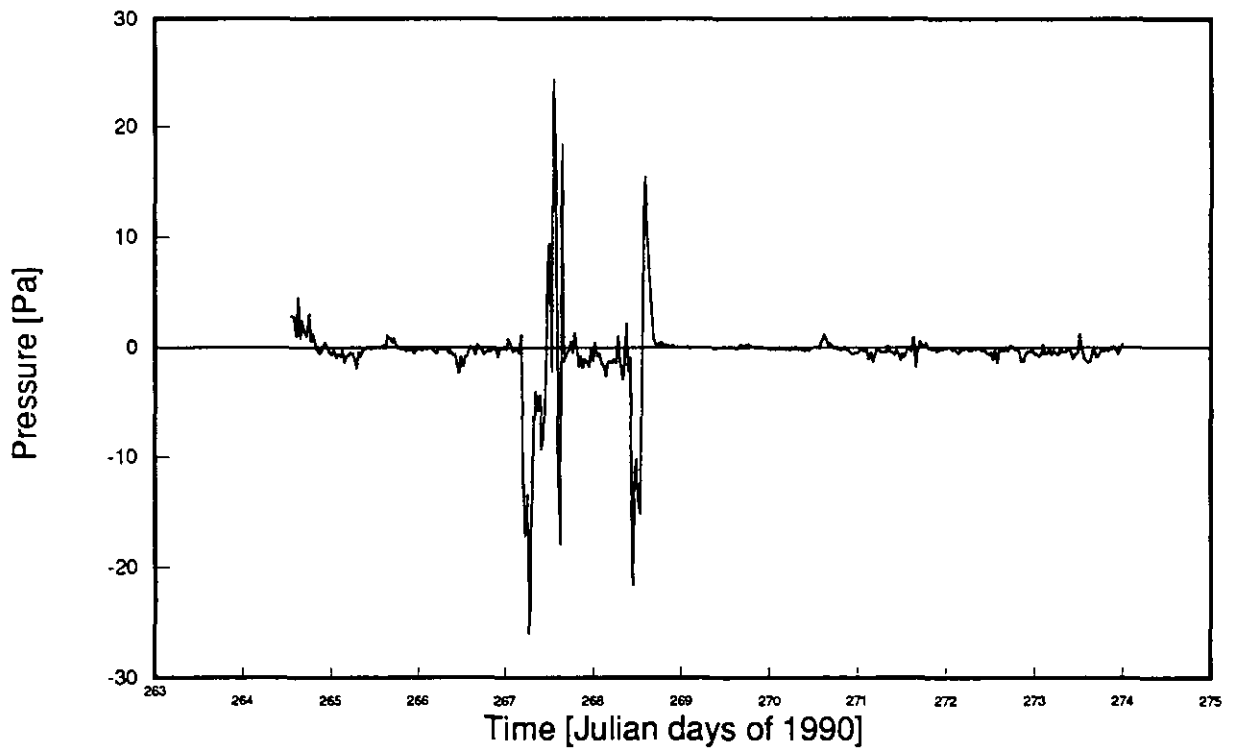
Figure 4.24.   Pressure differences between left and right ends of the
ventilation slit at the outside of the south window.
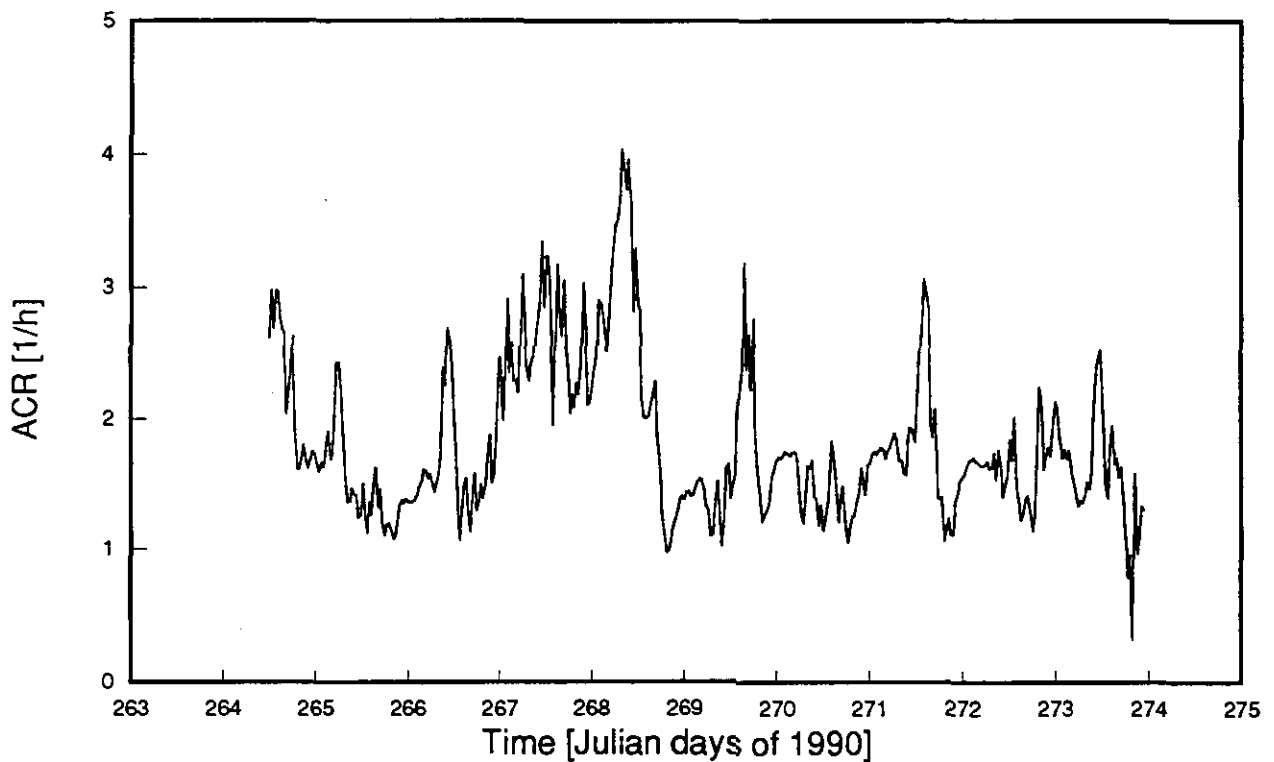
Figure 4.25. Air change rates calculated from the measured N₂O concentrations.

133

4.3.3. Modelling the air flow rates

The empirical model of Eq. 2.43 has been applied to the measured values using a multiple linear regression. The thermal height of the attic window opening (H = 0.47 m) is obtained by projection on the vertical plane. The discharge coefficient is taken $C_d = 1$ as a first approximation. The effective opening area was $A = 0.15$ m^2 for the south window and $A = 0.18$ m^2 for the north window.

The best fit to Eq.2.43 for the case with the south window opened is found for :

$C_1 = 0.0029$ (SDT = 2 %)

$C_2 = 0.0046$ (SDT = 5 %)

$C_3 = 0$

Where a correlation coefficient r = 0.92 is obtained. No good correlations were found for other models which include a fixed turbulent term (C_3). The C_2 value is in good agreement with the stack model of Eq.4.1. The wind coefficient C_1 is three times higher than the value found by Phaff et al. [1980]. This may not be surprising because the wind data were measured at 2m above the roof level, providing values much closer to the local wind (near the roof window) than the meteo wind would give.

The interesting point of this fit is that ventilation was described with a single parameter C_1 and that a good correlation could be obtained. The proposed model is then :

$$Q = \frac{1}{2} A \sqrt{0.003 \, u_w^2 + 0.005 \, \Delta T \, H}$$

(4.9)

The results are plotted in Figure 4.26 with the relative differences compared to the measured values in Figure 4.27.

A similar measurement campaign was carried out for the case with the north window open and all other openings closed. The same regression analysis led to a negative correlation between the wind velocity and the stack effect. For a given wind, an increased temperature difference inside - outside corresponded to a reduced air flow rate :

$$Q = \frac{1}{2} A \sqrt{0.038 \, u_w^2 - 0.041 \, \Delta T \, H}$$

(4.10)

The coefficients are one order of magnitude higher than in Eq. 4.9. However the wind and stack contributions in Eq.4.10 are subtracted one from the other and similar ventilation rates were measured.

A probable explanation for this strange result is the presence of a leakage (~0.02m^2) in the opposite south wall-roof junction (about 1.5m below the window) which was revealed during checking with a pressurisation test after the experiment. This means that with the north window open, and for certain wind directions, cross-ventilation contributed to the ventilation rate. The wind induced air flow from the north to the south opening, was then opposed to the stack ventilation from the lower south opening to the north window, making a correlation like Eq. 4.10 plausible.

The influence of this south leakage opening on the stack ventilation with the south window open can be estimated from the following reasoning. The neutral level for a single opening A_2 is near the center of A_2, but for two openings A_1 and A_2, with a height difference between the opening centers of H_{12}, the neutral height would be H'=H_{12}/(1+(A_2/A_1)^2) [ASHRAE, 1985], that is a few centimeter below the center of the window opening. Therefore the stack flow is expected to increase by at most a few percent.
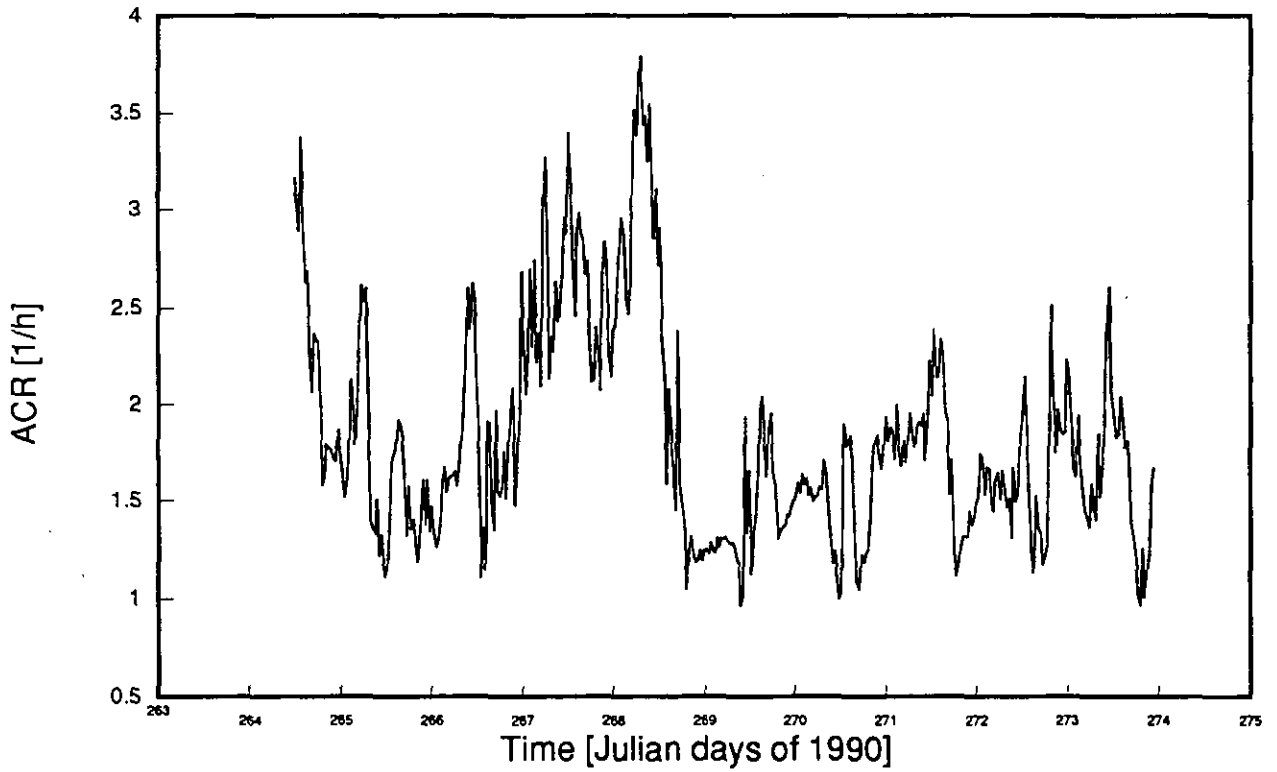
Figure 4.26.   Calculated air change rates following the model (Eq. 4.9).
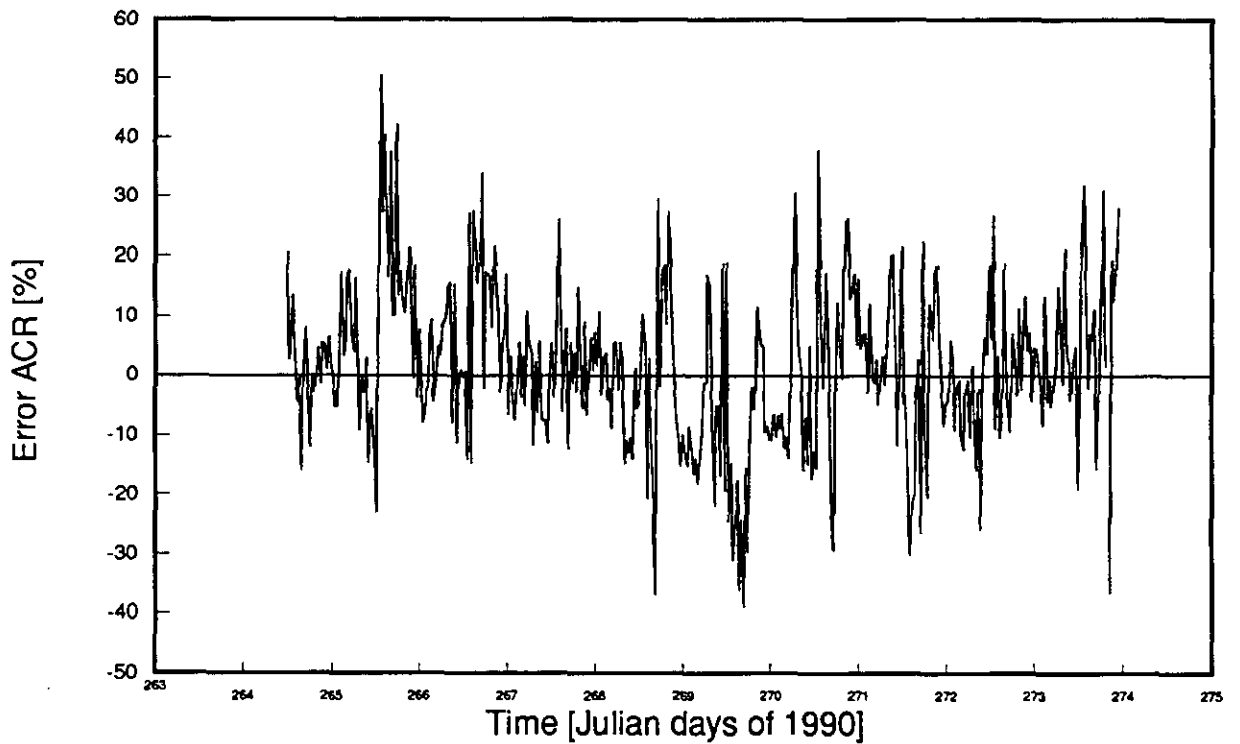
Figure 4.27.   Relative difference between measured (Figure 4.25) and
                    simulated air change rates (Figure 4.26).

4.3.4. Pressure coefficients for ventilation slit

In general for the modelling of ventilation through openings of small height the air flow is calculated from the pressure difference between the inside and the outside and one single pressure coefficient is assumed for the outside.

In order to test the validity of the assumption of a single pressure coefficient, a series of measurements has been carried out on the ventilation slit at the upper side of the Velux roof windows of the attic. This slit is a wide horizontal but narrow vertical opening (118 by 3 cm). Pressure tubes were mounted at both ends of the slit at the outside, and directly connected to an electronic pressure reading device with automatic zero correction.

Measurements of the pressure difference, the wind speed and the wind direction are available every 4 minutes for a period of 5 weeks.

The analysis is done for the ventilation slit of the north window. The measured pressure differences at the outside were converted into a 'pressure coefficient difference DC_p' :

$$DC_p = 2 \cdot \frac{DP}{\varrho \cdot u^2}$$

(4.10)

where : DP = pressure difference left-right (Pa)

u = wind speed measured 2 meter above roof level (m/s)

These results have been sorted for the wind direction, i.e. per sector of 45 °.

Figure 4.28 presents the difference of pressure coefficients found with the wind velocities coming from the south direction (wind sector 157.5 ° to 202.5 °).

WIND DIRECTION	Nr. observ. (u>2 m/s)	AVERAGE DCp (u > 2m/s)	95 %-value DCp	COMMENTS
0°	12	- 0.11	- 0.35	Average significantly different from zero
45°	111	- 0.06	- 0.21	Less pronounced negative trend
90°	576	- 0.01	- 0.13	No clear trend
135°	1713	- 0.02	- 0.16	No clear trend
180°	815	- 0.03	- 0.21	Slightly negative trend
225°	26	- 0.04	- 0.19	Small number of observations
270°	136	- 0.13	- 0.46	Clear negative trend
315°	380	- 0.16	- 0.46	Clear negative trend

Table 4.2   Differences in pressure coefficients at the outside of a long ventilation slit. (the 95 %-value means that 5 % of the measured pressure differences were lower)
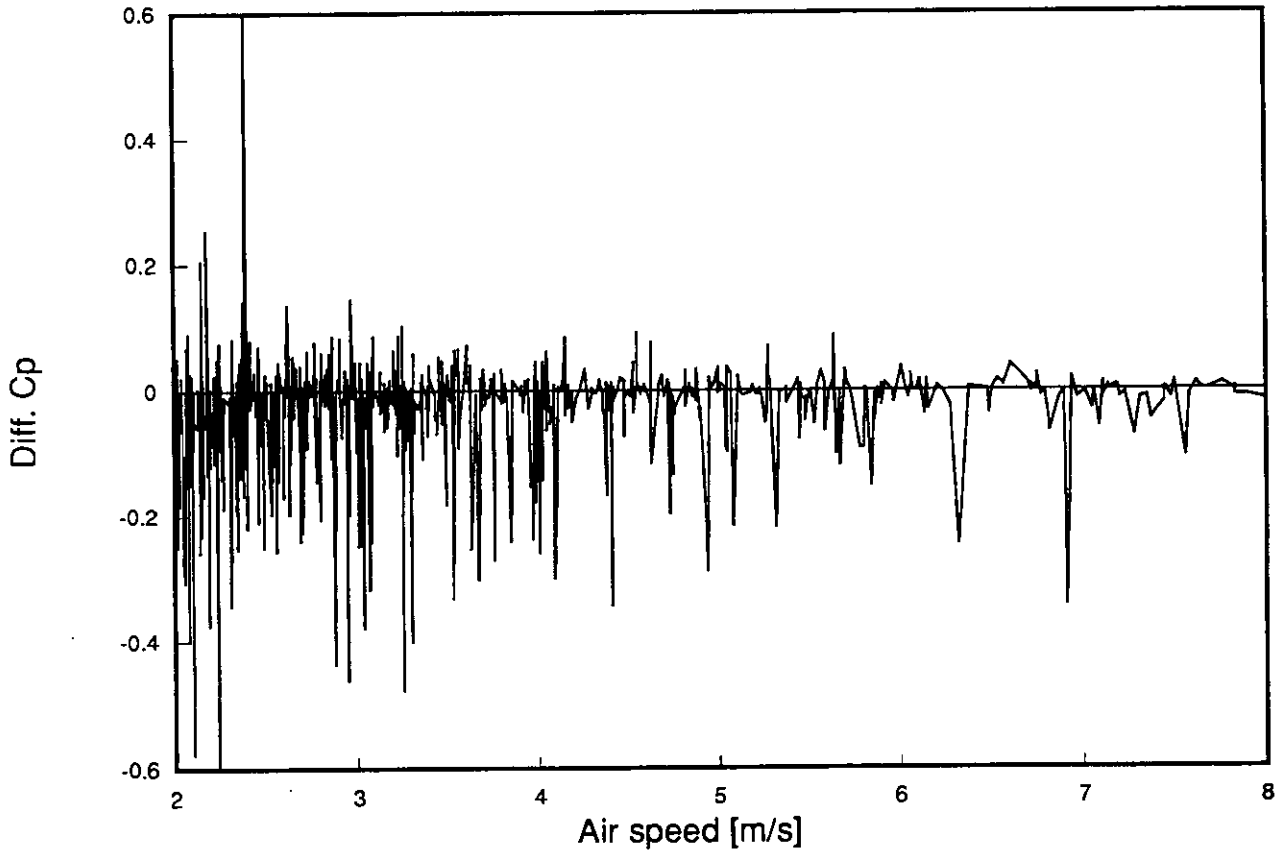
Figure 4.28   Difference in pressure coefficients at left and right sides of the ventilation slit at the outside of the north window for the winds, higher than 2 m/s, coming from the south direction (157.5° to 202.5°)
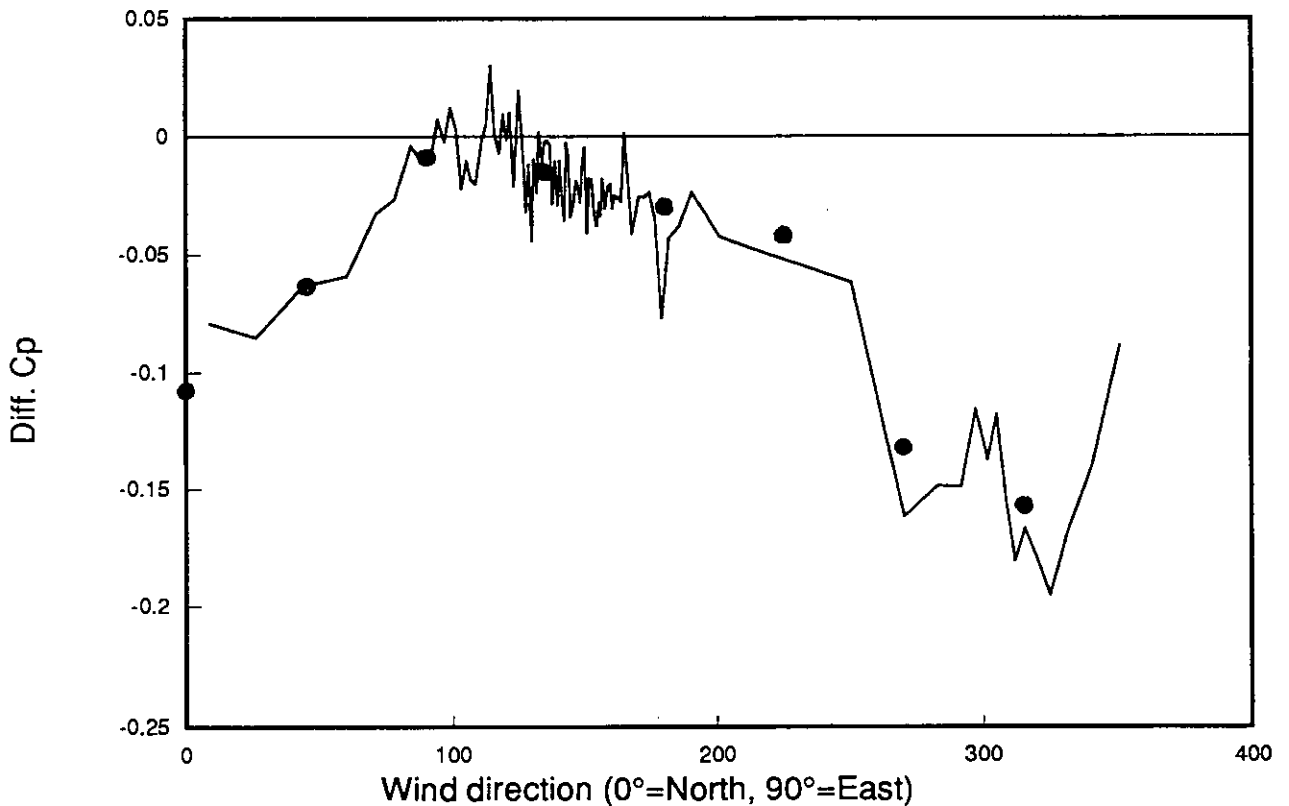
Figure 4.29. Variation of DCp-values with wind direction. The dots are average values.

Only wind velocities exceeding 2 m/s are taken into account.

The general trend curve of Figure 4.29 gives the average values per 20 readings of the difference in left-right pressure coefficient as a function of the wind direction. The dots indicate the averages over 45 ° wind sectors. The results clearly show that on the average for certain wind orientations there is a considerable difference in the pressure coefficients at both ends of the slit . The average DC_p-value varies quite consistently with the wind direction. This is indicated in Table 4.2 and in Figure 4.29.

Average differences of 0.15 between the left and right Cp values are found for certain wind directions. The effect appears to be not symmetric with respect to normal wind incidence as might be expected. The pressure coefficients at the right side are almost always higher than those at the left side. This may be explained by the asymmetric shape of the adjacent roof constructions.

The results indicate that the assumption of a homogeneous pressure coefficient for the whole width of the ventilation device in a Velux window (or any similar type of opening) does not correspond to the reality of the local environment. Such an assumption is acceptable if the air flow through the ventilation device is of a single direction : inwards or outwards. In cases where the air flow is more complex (e.g. in a rather airtight room with only one ventilation opening), a more detailed behaviour might be envisaged. A possible solution can be to divide the ventilation slit into 2 parts, each part representing 50 % of the original opening and to give each of them a different range of pressure coefficients so that the difference in pressure coefficients between the two parts is related to the average difference as given in Table 4.2.

Such an approach will allow a more precise description of single-sided ventilation for such devices.

Conclusion. A single-sided ventilation experiment was set up in an attic space with window ajar, to measure *long term ventilation rates* with varying wind and temperatures. A fit of the data to the empirical model proposed by *De Gids and Phaff [1982]*, Eq. 2.43, is found to give a good description of the ventilation rates. With a stack effect parameter close to the theoretical value, and a zero turbulence parameter, the ventilation rate is finally described with a single parameter for the wind velocity.

The assumption of a single pressure coefficient for a large opening is found to be not correct, and future investigations will have to pay more attention to pressure differences causing two-way flow.

4.4   Heat Loss and Buoyancy and Wind Driven Flow through an Open Window in One Wall only   (BRE, Garston, Watford, UK)

4.4.1.   Introduction

In collaboration with EPFL, Switzerland, a series of tests were carried out at BRE, to measure the time dependence of ventilation rates following the opening of a window, due to the combined effect of the wind and the thermal properties of the room. The objective was to validate a prediction model *[Van der Maas et al. 1989, 1990]* for single-sided ventilation which includes the effect of heat transfer and which can be combined with knowledge of occupants behaviour.

4.4.2.   Test Room

The tests were carried out in a large corner office room located on the top storey of a four-storey, naturally-ventilated building. The room (Figure 4.30) comprised three external walls glazed to their full height, one internal wall, and a false ceiling. The east and north-facing walls, and the ceiling, were made airtight with polythene sheet. This ensured that ventilation would be single-sided through an open window in the south face. The lower edge of the open window was 12.3 m above the ground. The volume of the room was 242 m^3, and the internal wall surface area was 262 m^2; other dimensions are shown in Figure 4.30.

4.4.3.   Measurements

Ventilation rates (Q m^3/s) were measured continuously by monitoring the concentration (C parts by volume) of a tracer gas (SF_6) released at a metered constant rate (S m^3/s), and dispersed through a single 'desktop' mixing fan. The ventilation rate was calculated using the relationship Q=S/C.

Air samples were taken at eight locations (Figure 4.30) within the room. Air temperature was recorded with thermistor probes at two locations at 1.1m height, and surface temperatures were measured using similar probes on the walls, floor and ceiling. Air velocity through the open window was measured using two ultrasonic anemometers (Gill Instruments) fixed in the aperture of the central window, as indicated in Figure 4.30. Orthogonal vector components of the flow were measured, one perpendicular to the plane of the opening, and two within the plane. Measurements were taken at intervals of 12 ms, which were averaged over intervals of 0.25 s. Reference wind speed and directin, and air temperature, averaged over 15 minute intervals, were recorded at 10m height at a location approximately 100m to the southwest of the building.

4.4.4.   Measurement procedure

Several preliminary tests were carried out to determine the approximate thermal properties of the room *[Van der Maas et al. 1989, 1990]* . Surface and air temperatures were continuously monitored as three electric fan heaters were switched on for several hours and then off again. These measurements were used to determine an approximate value for the thermal effusivity and thermal time constant, as discussed in more detail later.

For the subsequent series of measurements, two electric fan heaters (total 5.4 kW) were used to preheat the room for approximately 24 hours before each test. Initially the windows were firmly closed, and the tracer gas measurements began. The heaters were then switched off and the window was fully opened (to 180°). Measurements proceeded for approxiamtely two hours. Tests were repeated over a period of several summer months, and consequently over a range of external conditions.

N

glazing

wood panel

8.18

C5
x

tracer
release

C4, T3
x

x T2 floor

internal (block) wall

x T5

C6
x

C3 (C8 above)
x

C7
x

10.0

wood panel

glazing

C2
x

T4
x

key:
C1 - C8 tracer samples
T1 & T3 air temperature
T2, T4 & T5 surface
temperatures

C1, T1
x

'window wall' - south face

plan view

position of anemometers
in open window (no.3)

0.33

0.64

0.28

1.4

2.78

1   2   3   4   5

section

outside elevation of south face
(openable panes numbered)

Figure 4.30 BRE testroom and measurement locations (dimensions in metres).

4.4.5 BRE office room

4.4.5.1 Room thermal model

Figure 4.31 shows an example of the results of the preliminary tests to determine the thermal characteristics of the room. The heat transfer through the combined room surfaces was analysed using a simplified dynamic model based on the solution for heat transfer through a semi-infinite and homogeneous solid (Eq. 2.40). Using this model, the measured data were used to determine a thermal time constant and an experimental value for the wall thermal effusivity, b, where $b=\sqrt{(\lambda \rho c)}$, and λ is the thermal conductivity, ρ the density and c the specific heat .

The solid lines in Figure 4.31 represent predicted results using a thermal effusivity of b= 850 [J/ (m^2 $K.s^{0.5}$)] and a time constant of 20 minutes. The uncertainty in the average value of b was estimated to be about 20%, due mainly to the uncertainty in the background drift of room temperature. The agreement is surprisingly good considering the significant differences in construction of the floor, ceiling and wall, which may be expected to have complex thermal properties.
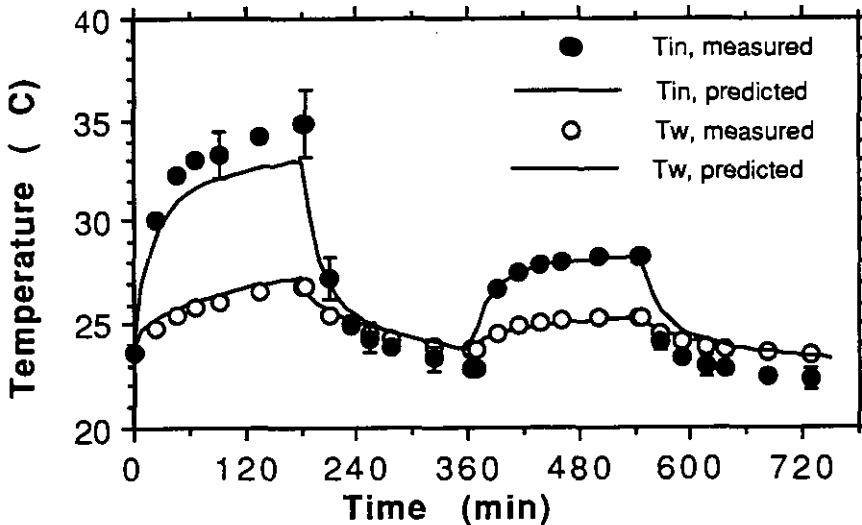
Figure 4.31 Example results of preliminary tests to determine average thermal characteristics of BRE test room. Electric fan heating was applied (9kW) between t=0 and t=180 min, and (5kW) between 360 min and 540 min. The reference surface temperature, Tw, is that of the floor. The measured thermal effusivity of 890 was used to compute the solid curves, for comparison.

4.4.5.2 Ventilation studies

For each of eleven tests, the effective velocity through the opening was determined from the measured ventilation rate using $u_{eff}=2Q/A$ (compare Eq. 2.44). The theoretical average velocities were also calculated assuming stack flow (Eq. 4.1), using the difference in air temperature between inside and outside measured after about one hour in each test. These were similar in each case, giving a common stack velocity of approximately 30cm/s. Figure 4.32 shows both theoretical stack velocity and measured effective velocity varying with the reference wind speed. The former is nearly constant which is indicated with a dashed line. The straight line corresponds to a linear variation where the velocity in the window would be 11% of the wind speed.

No correlation with wind direction was observed. Point Q corresponds to the window in the

lee of the wind, and represents a ventilation rate 50% lower than expected by stack effect alone. These results are in contradiction with Eq. 2.43, because the combined effect of wind and stack flow is not larger than each separate contribution.

The measured ventilation rate was greater than predicted for stack effect in cases F and P only. For P the wind blew normally toward the open window, and the measured effective velocity was twice that predicted for stack alone. The measured ventilation flow number, F (Eq. 2.46), was 0.06 in this case, which may be small considering the significant wind speed of 6m/s, but which result is comparable with the data plotted in Figure 4.4.
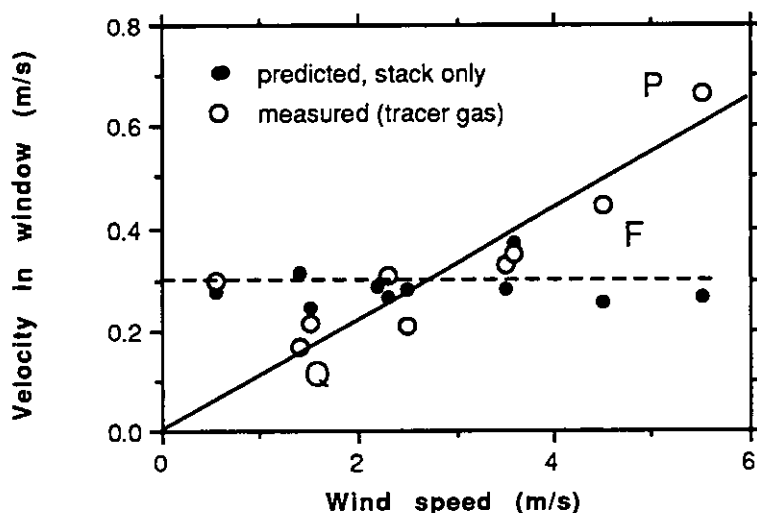
Figure 4.32. All results from BRE test room; measured effective air velocity and theoretical stack velocity of airflow through window plotted against observed wind speed. The two lines are to guide the eye and indicate a constant stack effect (dashed) and a linear increase with wind speed.
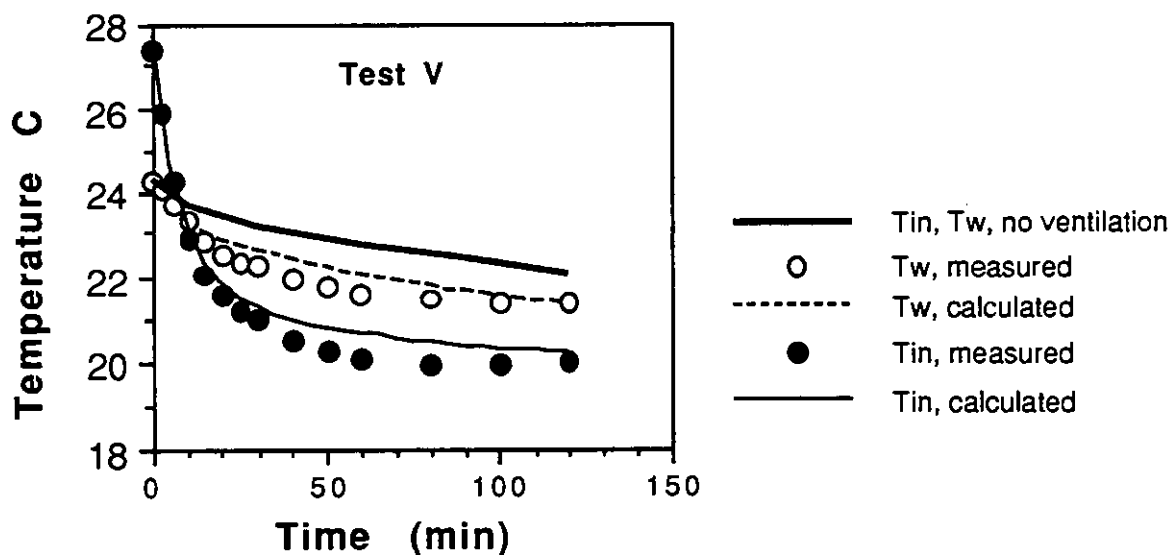
Figure 4.33. An example (test V) of results of ventilation tests in BRE test room. Background heating is switched off at t=0 and the window is opened. The thin lines are predictions for the assumption of stack ventilation, the thick curve is the predicted cooling when the heater is switched off and the window stays closed.

4.4.5.3   Assessment of combined thermal and ventilation model

The air and floor temperatures were predicted using the combined thermal and ventilation model described earlier (Eq. 2.41). The ventilation rate was calculated using Eq. 4.1 descrbing buoyancy-driven (stack) flow. The measured and predicted air and floor temperatures are shown in Figure 4.33 for one example (test V). The air temperature was initially much higher than the floor temperature, and fell with a time constant of approximately 10 minutes. The predicted results are only slightly higher than the measured data, and show an acceptable agreement. After about one hour, the difference in temperature between the floor and the air was approximately constant and equal to about 1.5 K for both predictions and measurements. It should be noted that there are no free parameters in the model which might otherwise 'tune' the predicted results.
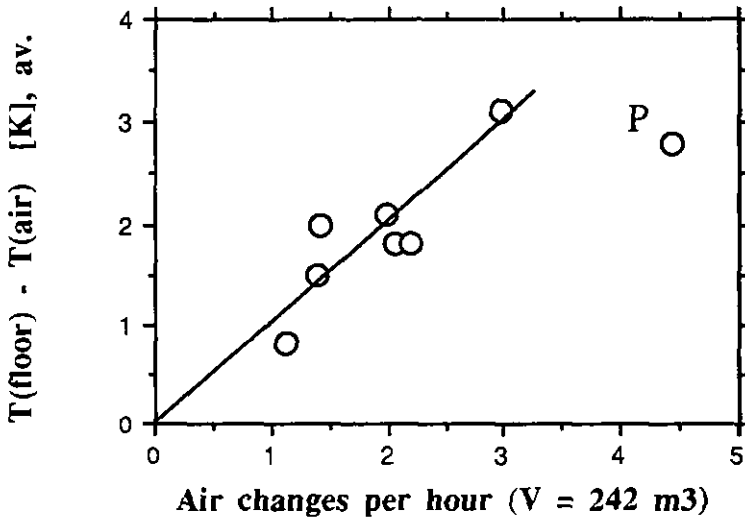
Figure 4.34. BRE test results; relationship between average floor-air temperature difference and air change rate in ACH. Point P represents an enhanced air change rate and corresponds to a high wind speed.

Since the inside-outside temperature difference, $T_{in} - T_{out}$, is similar for each test (around 10K), then Eq. 2.41 predicts a linear relationship between ventilation rate, Q, and $T_w - T_{in}$, the temperature difference between the room surfaces and the air. The room surface temperature may be adequately represented by the floor temperature, and Figure 4.34 shows how $T_w - T_{in}$ (after one hour) vary with air change rate, for each test. A correlation is apparent, with the exception of point P. Using Eq. 2.41, the straight line in Figure 4.34 would correspond to a value for the product $hC_2 \approx 3$ [W/Km^2]. The effective heat exchanging surface area factor C_2 however is difficult to estimate in the present case, because of the very low heat storing capacity of the ceiling and part of the walls.

Conclusion. The ventilation rate is increasing with the wind speed but combines not with the stack effect as predicted by Eq. 2.43. The measured time dependence of ventilation rates following the opening of a window is consistent with a prediction model for single-sided ventilation which includes the effect of heat transfer (section 2.4.1.2).

It is proposed to carry out further analysis of the data to systematically compare measurements of surface temperature with predictions obtained from the combined thermal and ventilation model, Eq. 2.41, using measured ventilation rates.

4.5 Ventilative Heat Flow Rates after Opening a Window

(LESO-PB, Lausanne, Switzerland)

4.5.1 Time dependence through inhabitant behavior

In a real building, the air and heat flow rates are primarily affected by the presence of large openings and consequently by the inhabitant behavior with respect to the opening of doors and windows. The simulation of inhabitant behavior by the generation of time series of window and door openings or window opening angles is discussed in *[Fritsch et al 1990; Roulet et al. 1991]* , the last reference being a Technical Report of Subtask-2 .

For the determination of the energy consequences of inhabitant behavior, an algorithm is required to calculate the ventilative energy loss as a function of opening duration. This energy can be estimated by integrating Eq. 2.29 (or Eq.2.39) over the opening time interval. The assumrtion that the inside temperature stays constant during window opening was tested by *Phaff et al [1980]*, and they found the average inside air temperature to drop by about 30% of the inside-otside temperature difference (van der Maas et al., 1990). Moreover an important stratification built up, the temperature drop at floor level being strongest. In particular for small rooms and large windows the energy losses are then largely overestimated. The prediction of the time dependence of the decrease in temperature requires the coupling of the ventilation model with a thermal model.

To avoid the use of a complete building thermal model with its many additional input parameters, a simplified model to take heat transfer into account was proposed (Figure 2.20). This model shows the first order effects of how energy flows through large openings are influenced by opening duration (determined by user behavior) and constructional details of the ventilated zone (volume, position of the opening, wall material and wall surface area).

4.5.2 Heat transfer analogy between opening a window and switching on a baseboard heater.

The detailed modeling of the air flows and heat transfer after opening a window is complex because of the many parameters involved. By recognizing that the description of both air flow pattern and heat transfer with an open window, has similarities with the case of a room heated by a convective heater*[van der Maas, 1990c]*, one can take advantage of existing research results. *Inard [1988]*, for example was interested in predicting thermal gradients and comfort conditions in a heated room, as a function of the heater characteristics. He found that the dimensions and heating power of baseboard heaters determine the size and temperature of the rising hot plume, which is the driving force for warm air circulation in the room.

Figure 4.35a, shows the typical air flow pattern and temperature stratification in a room with an initial air temperature of 20 °C some time after turning on a baseboard heater. The temperatures and velocities are highest at the ceiling, while below the level of the heating equipment the air velocities are low and the temperatures remain virtually unchanged until the floor warms up by the heat radiated from the ceiling. Indeed at floor level the heat flux is downward, there is stable stratification and no natural convection.

An analogous (although 'upside-down') flow pattern and temperature distribution is found in a room with initial air temperature of 20 °C (Figure 4.35b), but after the window is opened on a winter day. The lowest temperatures and highest air velocities are on the floor, while the temperature of the trapped warm air above the window remains unchanged until cooled by the heat radiated to the floor. At the ceiling, the heat flux is upward and no natural convection because of the stable stratification.

In both cases the vertical temperature gradient depends on the characteristics of the hot and cold plume's dimensions and temperature. For an open window the latter are determined by the temperature of the outside air, the opening width and height and the position of the window.

Further for both cases, the time development of the temperature field are expected to depend in a similar way on the room geometry and the wall materials.
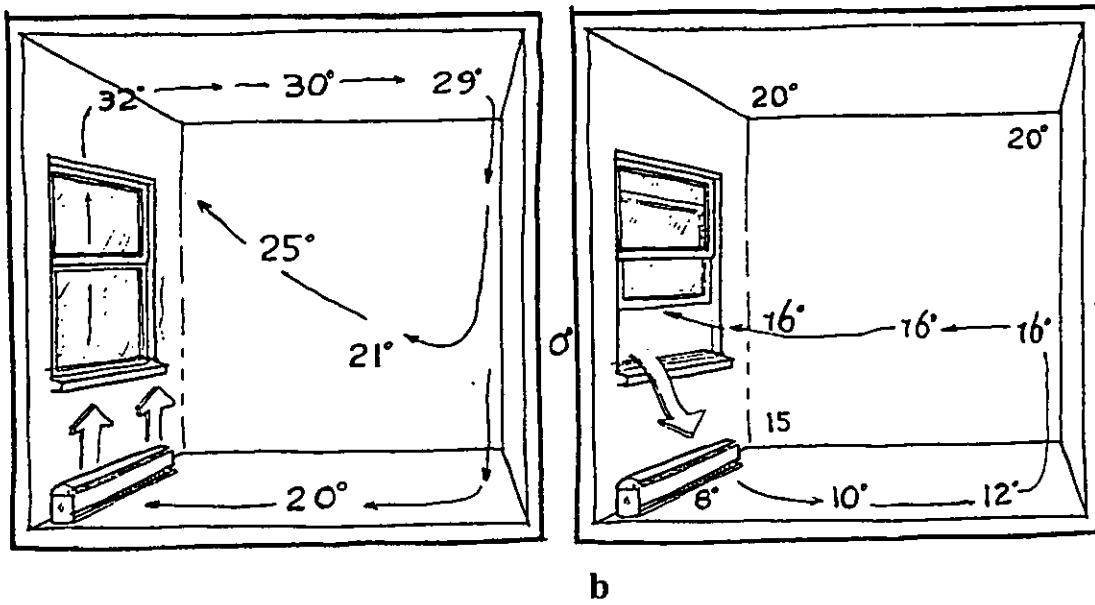
Figure 4.35.Analogy between the air flow pattern and temperature stratification in a room initially at 20°C with (a) heater turned on, (b) window opened (winter condition).

Air temperature stratification
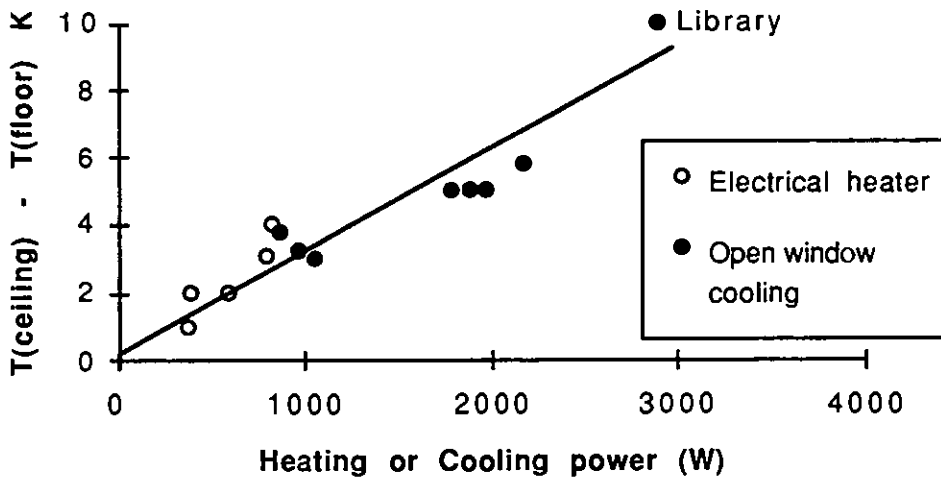
Figure 4.36. The ceiling to floor air temperature difference plotted versus the heating or cooling power. Heater data *(Figure 47 in Inard 1988)*. Open window cooling data *(Figure 10 in Van der Maas et al. 1989)*. Library: new data point. The straight line is drawn to guide the eye and corresponds to $\Delta T=0.3\%\Phi$.

Inard [1988] observed in a 2.8 by 4 by 4m size climatic test room, that the temperature gradient was correlated with the convective heating power but almost independent on the type of emitter. However, the temperature gradient is found to depend strongly on the way the heated room is cooled, e.g. a cold ceiling (floor) will tend to reduce (increase) the gradient.

Figure 4.36 shows as a function of heating (cooling) power that ceiling to floor temperature differences can be similar when due to an electrical heater or due to an open window. This similarity is in favor of the analogy between an open window and a heater. One could therefore use as an order of magnitude for the floor to ceiling temperature difference with open windows, 0.3% of the cooling power. This value can easily vary by a factor of two, but it is a starting point, which is much better than having no estimate at all. Contributing to the uncertainty is the decrease of the temperature gradient with distance from the large opening (e.g. Figure 3.36).

This analogy is expected to be helpful for the understanding of comfort conditions with open windows. It is clear that at present this open window model is incomplete and needs further development.

4.5.3 Measurement setup for ventilative cooling

In a series of experiments performed at the LESO-PB, the algorithm coupling heat and mass transfer during single-sided ventilation (Figure 2.20) is tested on different rooms. The thermal characteristics of each room are determined in a separate test with the window closed: constant heating power is applied, and from a plot of the air temperature as a function of the square root of time, one obtains an experimental value of the thermal effusivity b (Eqs. 2.40 and 2.41).

The air velocity is measured with an omni-directional DISA anemometer, with a time constant <0.1s. Wall temperatures variations were detected by scanning the walls with a radiation infrared thermometer and the temperatures were measured with thermocouples. Velocity and temperature profiles were analogue recorded by mounting the probes on a motor-driven trolley moving in the opening. The inflowing cold air temperature was measured at the bottom of the window opening. In addition air temperatures, wind velocity and direction are measured on a mast on top of the roof. The heat loss tests were performed at night.

Three rooms with vastly different thermal characteristics have been studied. We will consider here only one room of the LESO building $40m^3$ volume and $70m^2$ wall surface (see the floor plan in Figure 4.37. This room is characterized by an average thermal effusivity of the walls of b=1000 [J/ (m^2 K.$s^{0.5}$)] with a 20% uncertainty.
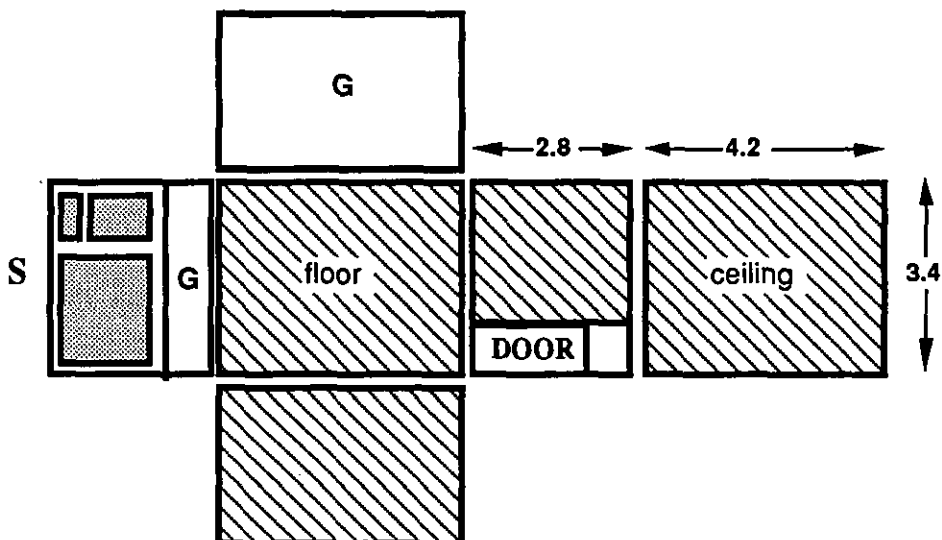
Figure 4.37. Floorplan of the LESO test room. The walls, floor and ceiling have 10cm glasswool insulation as a second layer. The first layer is 10cm concrete (dashed) and 1cm gypsum (G). The door is of wood. The windows have an U-value of 1.5W/m2-K. The maximum window opening is 0.85 by 1.05m² and the distance between the top of the opening and the ceiling is 0.7m. The width of the window could be reduced to 27cm by placing a wood board in the opening.

4.5.4 Observed wind effects

A single-sided ventilation algorithm predicting the ventilation energy loss caused by an inhabitant who leaves a window open for a certain period of time (section 2.4.1 2), has been tested for various cases where the wind velocity was low and the stack effect was dominating [van der Maas et al 1989, 1990]. We present here an experimental result for the ventilation and heat loss rate in the presence of wind. The case without wind is used as a reference.

In van der Maas et al. [1989] was reported a test in this room without wind (<1m/s). The 0.85m wide window was left open for 10 hours during a windless night, with the outside temperature nearly constant at 5.5°C, drifting 0.5°C during the test. The unfurnished office room was initially at 21.5°C for 24 hrs, and the time dependent decrease in air and wall temperature was reasonably well explained by the model illustrated in Figure 2.20, using only stack flow (Eq. 4.1).

A number of short duration tests with a strong southern wind were conducted, recording the velocity profile in the window opening for shorter and longer periods. The wind at the LESO façade is strongly attenuated by surrounding buildings and difficult to characterize from meteo values.

Two interesting features were observed in the presence of wind. Firstly, the velocity showed strong fluctuations and local flow direction reversals lasting tens of seconds were observed. Secondly the ouflowing air stream above the neutral level, was considerably less perturbed than the inflowing cold airstream below the middle of the opening.
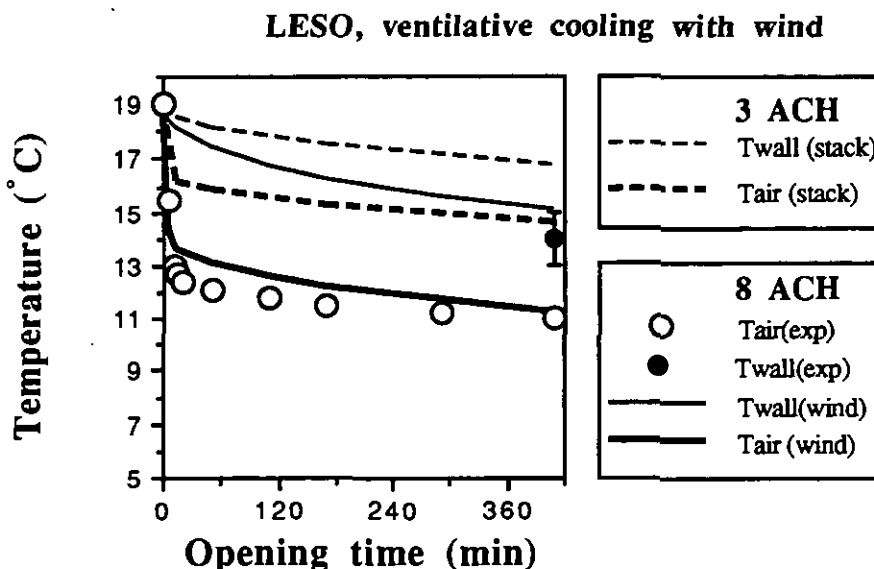
Figure 4.38 The window width is 0.27cm and the wind increases the ventilation rate and therefore the cooling. The windy case is calculated with an effective velocity of 0.65m/s in the window instead of the stack velocity of 0.21m/s.

A test with a strong southern wind was conducted for 7 hours at night and with the window opening reduced to one third of the width (W=0.26m; outside temperature near 4.5°C). The room was initially at 19°C for 24 hrs in thermal equilibrium with the building, and the effect of the wind was to increase the average air velocity in the window to 0.6m/s, about two times the expected stack velocity.

In Figure 4.38, we compare the cooling rate from stack flow with the observed cooling.

The picture is consistent.

(i) There is strongly increased cooling of the walls.

(ii) The temperature drop T_w–T_{in} is more than two times larger than expected from the stack effect. This is consistent with Eq. 2.41, predicting that an increase in the air change rate would result in a decrease of the inside air temperature.

(iii) The velocity in the window is more than two times higher than the stack velocity.

Comparison with the model shows that taking not the stack velocity but a window air velocity of 0.65 m/s, the observed cooling can virtually be explained.

We have no useful wind data to correlate the air flow in the window with the external wind velocity. The wind at the LESO building is strongly attenuated by surrounding buildings and difficult to characterize.

14	16	16.5
11		13
9	11	12

S	W	9		9	12	13		13	17		17	16	15
		10		10	12.5	13		13.5	17		17	16	15
		10		10.5	12.5	13		DOOR	17		17	16	15

12	13	13.5
13	14	14
15	16	16
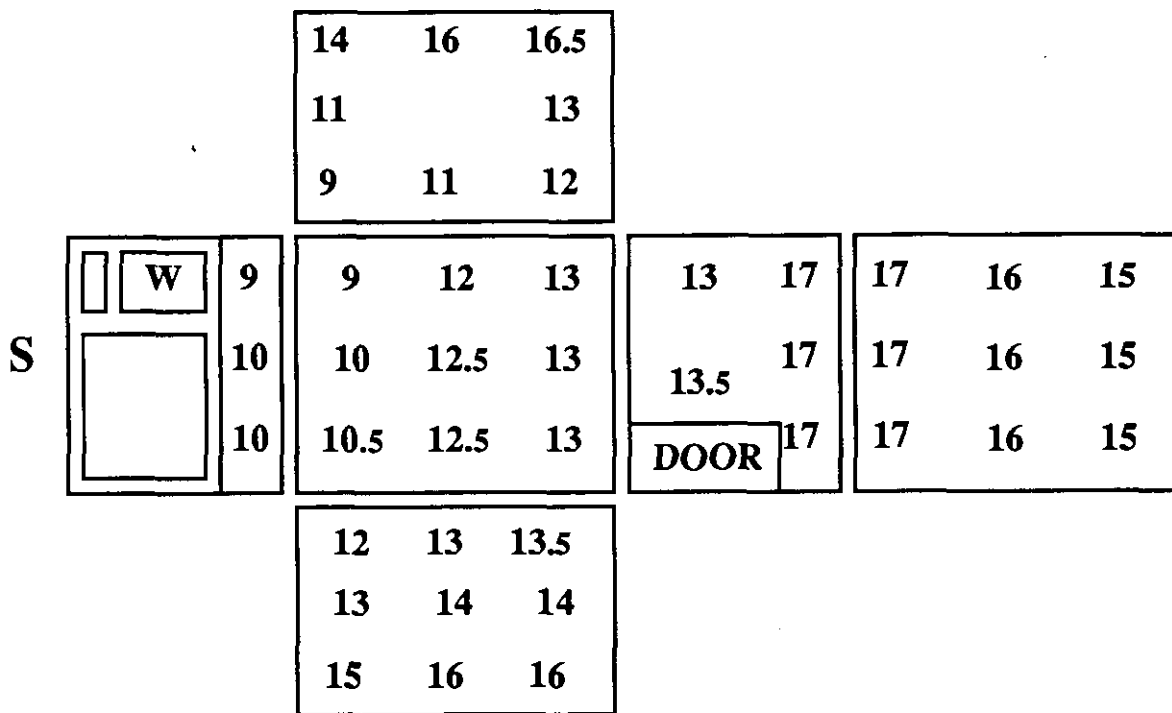
Figure 4.39 The temperature distribution after one night cooling with the window open on a map similar to Figure 4.37. A single-zone model can not take such a thermal distribution into account.

The cooling of the floor was strongest near the window. The room was quite isothermal at 19°C, before the cooling started. On the map in Figure 4.39 are given the wall temperatures after one night with the window open. The details of the floor temperature distribution can not be predicted by a single zone model.

4.6   Conclusions on External Openings

This chapter described new studies at four European laboratories, on the effects of wind on the ventilation and/or heat loss rates through openings in one external wall only.

Methods to analyse single-sided ventilation measurements have been briefly discussed. The analysis when made in terms of wind speed and inside-outside temperature difference leaves considerable scatter in the data points, suggesting that other uncontrolled parameters play a role. Simple plots are recommended to check the consistency of locally measured data and to reduce the uncertainty caused by meteo data tranfer. It was found that for nearly normal wind incidence the variability in the ventilation rate is considerable.

Theoretical models of single-sided ventilation were used to analyse the experimental results of full scale measurements, and resulted from international collaboration as follows:

> • CSTB test house at Bouin, France, with horizontal slit, which demonstrate the constribution of air compressibility to flow through relatively small openings to large volumes; data have also been analysed by research groups in other countries, showing that the compressibility effect is quite well understood for a single opening and at normal wind incidence;

> • BBRI attic test room at Gent, Belgium, with open window, which show that long term correlations of ventilation with measured parameters including wind and temperature are well described by a simple model with a single parameter for the wind speed. Moreover a significant influence of the distribution of pressure coefficient on the induced two-way flow has been identified;

> • BRE office at Garston, England, in collaboration with measurements at

> • EPFL offices at Lausanne, Switzerland, both with single windows, which demonstrate the use of a simplified combined thermal and ventilation model to describe the time dependence of ventilation rates following opening of a window, and show the effect of steady wind. The model allows a better prediction of the energy consequences of inhabitant behaviour to be made in multi-zone air flow models. The ventilation produced by combining wind and stack effect is not found to be systematically larger than the stack effect seperately, which is in disagreement with the empirical model.

These research contributions give valuable new insights into the mechanisms of single-sided ventilation and the related energy losses.

5   SUMMARY AND GENERAL CONCLUSIONS.

5.1 Summary

The general objective of the IEA/ECB Annex 20 "Air FlowPatterns within Buildings", was to evaluate the performance of single- and multi-zone air and contaminant flow simulation techniques and to establish their viability as design tools. To reach this goal, the work was divided into two parallel subtasks: one on single-room air and contaminant flow, the other on multi-zone air and contaminant flow and measurement techniques. An overview of the work realized in Annex 20 can be found in *[Moser 1991]*.

Energy aspect of the ventilation of buildings.

The trend to air-tight buildings with improved thermal insulation causes ventilation to make up a considerable and increasing part of the building energy use. There are two opposed aspects when considering a reduction of the energy used for the ventilation of buildings, because while lower ventilation rates do result in lower energy consumption, inhabitants ask for high indoor air quality and this requires in general increased ventilation rates.

The issue then becomes how to realize good indoor air quality using a minimum amount of energy. In addition to rules for minimum ventilation rates, it is required to have a high ventilation efficiency and therefore the control over the flow and concentration of contaminants. Moreover other comfort parameters need to be kept under tight control (surface and air temperatures, local air velocities and turbulence causing the sensation of draught).

The detailed understanding and mastering of air flows in buildings is therefore a condition for the design and construction of energy efficient buildings.

Multi-zone air and contaminant flow and measurement techniques.

While subtask 1 studied the details of temperature and velocity fields in single building zones, the scope of subtask 2 was the simulatation of the incoming and outgoing air flows for a multizone building with known leakage and under given weather conditions *[Moser, 1991]* .

The latter objectives included the development of new algorithms for specific problems as flow through large openings (the present report), inhabitant behavior *[Roulet et al 1991]* , air flow driven contaminants *[Phaff and de Gids, 1992]* and multi-zone ventilation efficiency *[Bienfait Haghighat and Phaff, 1992]*. These algorithms are contributions to the development of better multi-zone computer models, a goal pursued in parallel with the Annex 20, by the COMIS workshop and since 1991 as Annex 23 *[Feustel 1992]*.

Further, to allow an experimental basis to be given to such a computer model and to validate it, a vital product of subtask 2 is the publishing of a handbook describing state-of-the-art measurement techniques *[Roulet and Vandaele, 1991]*.

Subtask 2.1: Large openings.

Large openings are important flow elements because they have a major influence on both the air flow pattern and contaminant distribution inside a multi-zone building, and on the heat and air exchange with the ouside. In particular the occurrence of two-way flow complicates the prediction of contaminant flow and energy flow rates in and out of a multizone building.

The research project on 'Air flow through large openings in buildings' involved experts from six different countries (see acknowledgements), and its goal was to test available and newly

developed algorithms for the calculation of heat and mass flow through doors and windows.

A literature review (chapter 2) showed the existence of gaps in knowledge and allowed to define the needed new experimental and theoretical work. Early reports on the studies presented in chapters 3 and 4 have been presented at the 1991 AIVC meeting *[Pelletret et al.1991; Bienfait et al 1991]*.

As described in chapter 3, the *steady state* mass flow rates through doors have been measured in test-cells, and compared with a Bernoulli model resulting in values for the average mass discharge coefficient which are in fair agreement with values recommended by *ASHRAE [1989]*.

Comparison of analytical and numerical bernoulli models showed, that for linear vertical zone temperature profiles (similar in both zones) the interzone *heat transfer* can be well approximated by an analytical expression. However, approximating a non-linear temperature profile by a linear profile can result in considerable errors in the heat flow.

Other topics that have been briefly discussed were the use of a resistance model to describe the transition between bulk density driven and boundary layer driven flow and also the modeling of flow through horizontal openings. The dynamical modeling of mass and heat flows following the opening of doors (for example to a warm sunspace or a cold storage) was briefly considered.

In chapter 4, the analysis of single sided ventilation measurements was discussed. It was then shown that fluctuating wind pressures can induce ventilation through relatively small large-openings and further, how the long term ventilation of an attic can be described taking only the stack effect and the windvelocity (non-fluctuating) into account. Finally, in order to test a model for a better evaluation of the energy consequences of user behaviour, the time dependent ventilation and energy loss rate after opening a window has been studied in different offices and under various wind conditions.

5.2 General Conclusions

The joint research effort in subtask 2 on 'Airflow through large openings in buildings' allowed to cover a large number of situations where existing and new algorithms have been tested on their validity range, and we can draw the following conclusions :

Mass discharge coefficients.

Detailed measurements of the temperatures and air velocities in a doorway have been performed in three different test-cell environments. Models based on the Bernoulli equation have been used to fit the data assuming either isothermal air volumes or linear temperature profiles. The *mass-discharge* coefficients in all cases are quite similar and an average value of (0.4 ± 0.1) is found to describe a large variety of configurations with heated and non-heated rooms. This value is consistent with the value recommended by *ASHRAE [1989]* for interzone temperatures smaller than 5K.

Local discharge coefficients (the ratio between locally measured and calculated velocity) appear to be strongly related with the boundary conditions. Values as high as 0.7 near the top of the opening which confirms the existence of high values reported in the literature. On the other hand values well below 0.5 immediately above and below the neutral plane are consistent with the observations of counterflow mixing made by *Wilson and Kiel [1990]*.

More experiments are obviously necessary although experiments are expensive, difficult to carry out, time consuming and, in most cases it is hard to change significantly the design parameters of the experimental setups; that is why air flow modelling using computational fluid dynamics could be useful as long as the code is validated; a start has been made in that direction trying to validate the 'Concordia' code; this task is not yet completed but it is a promising direction for general parametric studies.

Energy flow calculation

The assumptions of isothermal air volumes or linear zone-temperature profiles are the most practical and easiest to use in multi-zone air flow- and building- simulation programmes. For heat flow calculations the influence of linear temperature profiles is important as illustrated by expression Eq.2.31. Moreover, for *non-linear temperature profiles*, the application of Bernoulli and a linear approximation can lead to large errors in the calculated inter-zone heat transfer.

Boundary layer driven flow

A simple thermal resistance model can be used to describe the transition between bulk density and boundary layer driven flow. Boundary layer flow dominates when the temperature difference between the air and the heating or cooling surface is much larger than the inter-zone air temperature difference. Several of the test cell experiments corresponded to the latter situation but although these cases showed typical flow patterns (due to warm or cold plumes) the mass discharge coefficients were not substantially changed. However because of the important zone temperature stratification, the *heat flow is considerably higher* than when it would be estimated from the mean zone temperature difference alone.

Single sided ventilation

It has been shown in separate single-sided ventilation experiments that

(i) the contribution of air compressibility to the single sided ventilation rate can be considerable in particular for relatively small openings to large volumes.

(ii) a systematic variation of the pressure coefficient over the opening has been observed and appears to vary with wind direction; the resulting two-way flow significantly contributes to the

airchange rate under conditions of single sided ventilation

(iii) the ventilation rate of the attic in Gent (long term observation under varying conditions of wind speed and direction) is well described by a simple model with a single free parameter.

(iv) ventilation heat loss rates after opening a window are described by a simple model allowing a better estimate of the energy consequences of inhabitant behaviour; this model predicts a temperature reduction which is of increased importance for smaller rooms and larger openings

(v) with respect to the (calculated) stack ventilation rate, the effect of the wind can be an increase (at high wind speeds) or a decrease of the air exchanged through a single large opening; the latter decrease is not explained by currently used ventilation models.

The validation process of more detailed single sided ventilation models has only started. One difficulty in future research will be the simultaneous presence of pressure fluctuations, two way flow and stack effect.

Practical conclusions with regard to ventilation and energy losses

From the correct understanding of the role of the parameters describing heat and mass flows during the opening time of a door or window the following practical conclusions can be drawn.

- *Short duration window ventilation* works well in the heating season, and is usually adequate to renew the air and reduce the concentration of odors, CO_2 and humidity in the air. However it should be realized that the ventilation efficiency is only high below the upper level of the window opening although a turbulent wind will lead to increased mixing. To prevent the pollutant to be absorbed by the walls, ventilation should take place when the pollutant is produced (ventilation during cooking), or immediately after. In the summer, when the outside air is warmest, only the air above the bottom of the window is refreshed by single sided ventilation; therefore it is ineffective to ventilate e.g. a cool cellar by natural means..

- *Long term ventilation* is best suited to remove heat and pollutants that are absorbed by or diffused in walls and furniture. Drying of walls and cooling can only be accomplished by long term ventilation.

- *Energy loss*. The energy loss rate is proportional to the product of ventilation rate and temperature difference, but in particular for lasting ventilation the energy loss is overestimated when the effect of decreasing air temperature is not taken into account. This effect is largest in small rooms or more generally, where openings cover a considerable fraction of the wall (e.g. door to sunspace or cold storage).

- *Discomfort*. Opening doors and windows cause a cold draught at floor level. After closing, the air temperature returns rapidly to the wall temperature in an unfurnished room, slower in the presence of furniture. As a guide line one can state that the overall time it takes to return to the initial temperature is about equal to the opening time.

- *Temperature gradients* in the presence of open windows can be understood by analogy with a heater in a room (a problem which is well-known from the literature). As an attempt for a design guide-line one can relate the floor-ceiling temperature difference to a percentage of the heating or cooling power.

5.3 Recommendations for Future Research

Additional research is needed before reliable models and design guidelines can be made available to the building designer or energy analyst. This work should cover :

1. The interzone coupling and in particular, the interaction between a wide variety of thermal boundary conditions (heating and cooling equipment; wall temperatures; large opening between zones); the prediction of the zone air temperature stratification from knowledge of these thermal boundary conditions. Vertical temperature profiles are essential for the calculation of the interzone heat transfer with a Bernoulli model. Future test-cell work aiming at the validation of these Bernoulli models should then make fully use of the possibility to analyse detailed temperature and velocity fields created with a CFD model.

2. Study of heating and cooling resulting from inter-zone convection under combined natural and forced convection situations. This includes the interaction between natural ventilation and an air distribution system in the building.

3. Further development and validation of dynamic simplified models for the heat transfer through multiple openings, including horizontal openings.

4. Further development and validation of detailed single sided ventilation models, including the effect of pressure fluctuations, two way flow (i.e. Cp distribution over the opening), interaction between wind and stack effect in particular at nearly normal incident wind, and the influence of the position of the window pane.

5. The study of the relationship between reference meteorological wind and local wind values for a number of typical cases and the relation to single sided ventilation. This is because a major uncertainty in predicting single sided ventilation is a lack of knowledge of the relevant wind and air temperature local to the opening.

6. The implementation of the algorithms in multi-zone air flow and energy analysis programmes and assessing the ability of the improved models to predict energy consumption and indoor temperatures in multi-zone buildings

REFERENCES

Allard F, Brau J, Inard C and Pallier J M, 1987 "Thermal experiments of full-scale dwelling cells in artificial climatic conditions", Energy and Buildings, Vol 10, 49-58.

Allard F, Bonnotte D and Liman K, 1990. "Air flow through large openings: experimental study of the discharge coefficient", Annex 20 working report, RID 2.01.

Allard F, Inard C and Simoneau J P, 1990. "Experimental study and numerical simulation of natural convection in a room with heated ceiling or floor", Roomvent'90,Oslo,session A2.

Allard F and Utsumi Y, 1992 "Air flow through large openings", Energy and Buildings Vol 18, pp133-146

Anderson R A, 1986. "Natural convection research and solar building applications", Passive Solar Journal, 3(1), pp33-76.

ASHRAE, 1985, 1989. "ASHRAE handbook - 1985 Fundamentals" and "ASHRAE handbook - 1989 Fundamentals", Atlanta, American Society of heating, Refrigeration and Airconditioning Engineers, Inc.

Bajorek S M and Llyod J R, 1982. "Experimental investigation of natural convection in partitioned enclosures", Journal of Heat Transfer, Vol 104, pp 527-532

Balcomb J D and Yamaguchi K, 1983. "Heat distribution by natural convection", Proc. 8th National Passive Solar Conf, Santa Fe, NM. pp 289-294.

Balcomb J D, Jones G F and Yamaguchi J, 1984. "Natural convection airflow measurement and theory." Proc. 9th National Passive Solar Conf, Columbus, OH.

Balcomb J D, Jones G F and Yamaguchi J, 1984. "Natural air motion and stratification in passive buildings", Proc. Passive and Hybrid Solar Energy Update, Washington DC.

Barakat S A,1985. "Inter-zone convective heat transfer in buildings: A review". Heat transfer in buildings and structures-HTD-Vol 41, pp 45-52; ASME-AIChE National Heat transfer Conference Denver, CO. (also in Journal of Solar Energy Engineering, Vol 109, pp 71-78, May 1987).

Baranowski A, Eppe J P, Liebecq G, Sebbar Y, Wasacz M, 1989. "Experimental Study of Convective Heat Exchange Between Zones". Université de Liège, Lab de Thermodynamique, Research Report for CSTC-WTCB, November 1989.

Bauman F, Gadgil A, Kammerud R, Altmayer E and Nansteel M, 1983. "Convective Heat Transfer in Buildings : Recent Research Results". ASHRAE Trans. Vol. 89, Part 1A.

Bejan A, 1984. Convection heat transfer , Wiley, NY.

Bejan A and Rossie A N, 1981. "Natural convection in horizontal duct connecting two reservoirs", ASME J Heat Transfer Vol. 103, pp 108-113.

Benjamin T B, 1968. "Gravity currents and related phenomena", J Fluid Mech, Vol 31, pp 209-248.

Bienfait D, Riberon J, Barnaud G, Villain J, 1990. "Effect of wind pressure fluctuations on air movements inside buildings", 11th AIVC conference, Belgirate.

Bienfait D, Vandaele L, Van der Maas J and Walker R, 1991. "Single sided ventilation" Proc. of the 12th AIVC Conference in Ottawa, Air movement and ventilation control within buildings, Vol 1, pp 73-98

Boardman C R, Kirkpatrick A and Anderson R, 1989. "Influence of aperture height and width on interzonal natural convection in a full scale, air-filled enclosure", submitted to ASME J Solar Energy Eng (Proc. Ntl Heat Transfer Conf Philadelphia Aug 1989).

Brown W G and Solvason K R, 1962. "Natural convection through rectangular openings in partitions 1- Vertical Partitions", Int J Heat and Mass Transfer, Vol 5, pp 859-868.

Brown W G, 1962. "Natural convection through rectangular openings in partitions-2: Horizontal Partitions", Int J Heat and Mass Transfer, Vol 5, pp 869-881.

Chang L C, Lloyd J R, and Yang K T, 1982. "A finite difference study of natural convection in complex enclosures", Proc. of 7th Int Heat Transfer Conf. Vol 2

CIBSE 1986. "CIBSE Guide Volume A - Design Data", London SW12 9BS, UK.

Clarke J A, 1985. Energy simulation in building design, Adam Hilger Ltd, Bristol, UK.

Cockroft J P and Robertson R, 1976. "Ventilation of an enclosure through a single opening", Building and Environment, Vol 11, pp 29-35.

Cockroft J P 1979. "Heat transfer and air flow in buildings", PhD Thesis, University of

Glasgow.

Crommelin R D and Vrins E M H, 1988. "Ventilation through a single opening in a scale model", Air Infiltration Review, Vol 9(3), pp 11-15; Publication P 87/048, TNO Delft.

Davies M G, 1988. "Thermal sources and fluid flow", Bldg & Env Vol 23, pp25-28; "Modelling ventilation - Source, not conductance" Bldg Serv Eng Res Tech Vol 9, pp39-40.

De Gids, W, and Phaff, H, 1982. "Ventilation Rates and Energy Consumption due to Open Windows", Air Infiltration Review Vol 4 (1), pp 4 - 5.

Emswiler J E, 1926. "The neutral zone in ventilation", Trans American Soc Heat Vent Eng 32, pp 59-74

Epstein M, 1988. "Buoyancy-Driven Exchange flow through small openings in horizontal partitions". Trans. of the ASME, Journal of Heat Transfer Vol.110, pp885- 892.

Etheridge D W, 1984 "Air leakage characteristics of houses A new approach", BSER & T, Vol 5, pp 32-36,

Feustel H, Allard F, Dorer V B, Rodriguez Garcia E, Herrlin M K, Mingsheng L, Phaff H C, Utsumi Y, Yoshino H, 1990. "Fundamentals of the multizone air flow model COMIS", Tech. Note AIVC 29, Berkshire RG12 4AH, GB, 1992

Feustel H E and Dieris J, 1992. "A survey of airflow models for multizone structures", Energy and Buildings Vol 18, pp79-100.

Fissore A, Liébecq G and Sebbar Y, 1990. "Experimental analysis of convective heat transfer through large openings", Université de Liège (B), Report to the CSTC for IEA Annex 20 subtask 2.1 , Order #042829, December 1990.

Fritzsche C and Lilienblum W, 1968. "Neue messungen zur bestimmung der Kälteverluste an Kühlraumtüren", Kältetechnik - Klimatisierung, 20(9),pp279-286.

Fritsch R, Kohler A, Nygård Ferguson M and Scartezzini J -L, 1990. "Stochastic model of users behavior in regard to ventilation", Building and Environment 25, pp173-181.

Fürbringer J -M, 1992. "Renouvellement d'air par une grande ouverture unique", internal report, LESO-PB, EPFL, Lausanne.

Goux F, 1987. "Etude numérique de la convection naturelle en régime laminaire dans une cavité 2D ou 3D munie d'obstacles", Rapport de DEA , INSA de Lyon .

Graf A, 1964. "Theoretische Betrachtung uber den Luftausauch zwischen zwei Raumen", Schweiz Blatt fèr Heizung und Luftung, Vol. 31, pp 22-25.

Grosso M, 1992. "Wind pressure distribution around buildings: a parametric model", Energy and Buildings Vol 18, pp101-132.

Gusten J, 1989. "Windpressures on low rise buildings, an air infiltration analysis based on full scale measurements", PhD Thésis, Chalmers University of Techn., Gothenburg, Sweden.

Haghighat F, Jiang Z, Wang J C Y, 1989. "Natural Convection and air flow pattern in a partitioned room with turbulent flow", ASHRAE Trans. Vol 95, Part 2, pp 600-610.

Haghighat F, Wang J C Y, Jiang Z, 1990a. "Three dimensional analysis of airflow pattern and contaminant dispersion in a ventilated two-zone enclosure", ASHRAE Transactions Vol 96, Part 1, pp 831-939.

Haghighat F, Wang J C Y, Jiang Z, 1990b. "Development of a three dimensional numerical model to investigate the air flow and age distribution in a multi-zone enclosure". Proc. of 5th Int. Conf. on Indoor air quality and climate: Indoor Air'90, Toronto, Canada.

Haghighat F, Jiang Z, Wang J C Y and Allard F, 1991a. "Air movement in buildings using computational fluid dynamics", submitted to The ASME J of -Solar Energy Eng.

Haghighat F, Rao J, and Fazio P, 1991b. "The influence of turbulent wind on air change rates–a modelling approach", Building and Environment Vol 26, 95-109

Hendrix W A, D R Henderson and H Z Jackson, 1989. "Infiltration heat gains through cold storage room doorways", ASHRAE Trans. 95(2), pp 1155-1168.

Hill D D, 1985. "Analysis and measurements of interzonal convection in a passive solar building", Master Thesis, Colorado State University, Fort Collins (CO).

Hill D D, and Mahajan B M, 1986. "Convection between zones with non-linear temperature distributions", Air movement and distribution conference, Purdue University, May 1986.

Hill D D, Kirkpatrick A, and Burns P, 1986. "Analysis and measurements of interzonal natural convection heat transfer in buildings", Trans. of the ASME J. of Solar Energy Engineering,Vol 108, pp 178-184.

Inard C, 1988. "Contribution a l'étude du couplage thermique entre un emetteur de chauffage et un local", Ph D Thesis, INSA, Lyon, France

Inard C and Buty D, 1991. "Simulation of thermal coupling between a radiator and a room with zonal models", Proc. of the 12th AIVC Conference in Ottawa, Air movement and ventilation control within buildings, Vol 2, pp 125-132.

ISO Standard 7345, 1987. "Thermal insulation-physical quantities and definitions", International Organisation for Standards, Geneva, 1987.

Janikowski H E, Ward J and Probert S D, 1978. "Free convection in vertical, air filled rectangular cavities fitted with baffles", 6th Int Heat Transfer Conf, Toronto.

Jiang Z, Haghighat F, and Wang J C Y, 1991. "Thermal comfort and indoor air quality in a partitioned enclosure under mixed convection", Building and environment 1992.

Jones G F, Balcomb J D and Otis D R, 1985. "A model for thermally driven heat and air transport in passive solar buildings." ASME, 85-Winter annual meeting, HTD. Miami Beach.

Jones G F and Otis D R, 1986. "On the correlation of natural convection heat transfer in divided enclosures", Int Comm Heat and Mass Transfer, Vol 13, pp 109-113.

Jones W P, 1985. Air conditioning engineering, 3rd edition, E Arnold, London.

Kahwaji G, Burns P J and Winn C B, 1989. "Convective Heat Transfer Coefficients From a Full-Scale Test in the REPEAT Facility", Trans. of the ASME 132, Vol. 111, 1989.

Kelkar K M and Patankar S V, 1987. "Numerical prediction of natural convection in partitioned enclosures", ASME Winter Annual Meeting, pp 63-71.

Khodr Mneimne H, 1990. "Transferts thermo-aérauliques entre pièces à travers les grandes ouvertures", PhD Thesis, Nice University.

Kiel D E, 1985. "Measuring and modeling airflow through doorways", Master Thesis, University of Alberta, Edmonton (Canada).

Kiel D E and D J Wilson, 1986. "Gravity driven flows through open doors", Proc. of the 7th Annual Air Infiltration Centre Conference on Occupant Interaction with Ventilation Systems, paper 15, 16 p, Statford upon Avon (U K).

Kiel D E and D J Wilson, 1989. "Combining door swing pumping with density driven flow", ASHRAE Trans. 95(2), pp 590-599.

Lamrani M A, 1987. "Transferts thermiques et aerauliques à l'intérieur des bâtiments", PhD Thesis, Université de Nice, France.

Lane Serff G F, Linden P F and Simpson J E, 1987. "Transient flow through doorways produced by temperature differences", Proceedings of ROOMVENT'87 Air Distribution in Ventilated Spaces, Stockholm.

Lebrun J and Ngendakumana P, 1987. "Air Circulation Induced by Heating Emitters and Corresponding Heat Exchanges Along the Walls : Test-room Results and Modelling", Roomvent 87, session 2a, Stockholm, June 1987.

Lebrun J and Liébecq G, 1987. "Prediction and on site measurements of convective couplings between thermal zones.", Roomvent '87, Stockholm.

Liddament M W, 1986. "Air infiltration calculation techniques. An applications guide", AIVC report AIC-AG-1-86, Berkshire RG12 4AH, GB.

Lidwell O M, 1977. "Air exchange through doorways. The effect of temperature difference, turbulence and ventilation flow", J Hyg Cambridge, Vol 79, pp 141-154.

Lieman K, 1990. Rapport de Dea, Centre de Thermique - INSA, Lyon (F).

Lin N M and Bejan A, Natural convection in a partially divided enclosure, Int J Heat and Mass Transfer, Vol 26, N 12, pp 1867-1878, 1983

Lloyd J R, Yang K T and Liu V K, 1979. "A numerical study of one-dimensional surface, gas and soot radiation for turbulent buoyant flows in enclosures", Proc. 1st Natl Conf Num Math in Heat transfer pp 142-161 Univ of Maryland

Mahajan B M, 1987. "Measurements of interzonal heat and mass transfer by natural convection", Solar Energy 38(6), pp437-446.

Mahajan B M and Hill D D, 1986. "Interzonal natural convection for various aperture configurations", ASME Winter Annual Meeting, Anaheim (CA), 86-WA/Sol-1

Mahajan B M and Hill D D, 1987. "Flow coefficients for interzonal natural convection for various apertures", Solar Eng.-1987, Vol 1, pp300-306, Edited by Yogi Goswami et al.

Melouk, 1990. "Contribution à l'étude des transferts aérauliques et thermiques à travers une grande ouverture dans un logement bizone," CSTB, France, report DPE/90-918

Mokhtarzadeh-Dehghan M R, El Telbany M M M, Reynolds A J, 1989. "Transfer Rates in Single-sided Ventilation", Brunel University, UK.

Moser A, 1989. "Trends in airflow design and management, contributions by IEA Annex 20"

Proc. of the 10th AIVC Conference, Progress and trends in air infiltration and ventilation research, Vol 1, pp45-62

Moser A, 1991. "The message of Annex 20: air flow patterns within buildings" Proc. of the 12th AIVC Conference in Ottawa, Air movement and ventilation control within buildings, Vol 1, pp 1-26

Mounajed R, 1989. "La modelisation des transferts d'air dans les batiments. Application à l'étude de la ventilation", PhD Thesis, C S T B, Marne la Vallée, France

Münch W, Rüden H, Schkalle Y-D and Thiele F, 1986. "Flow of micro-organisms in a hospital stair shaft - Full-scale measurements and mathematical model", Energy and Buildings Vol 9, pp253-262.

Nansteel N W and Greif R, 1981. "Natural convection in undivided and partially divided rectangular enclosures", Journal of Heat Transfer, Vol 103, pp 623-629.

Nansteel N W and Greif R, 1984. "An investigation of natural convection in enclosures, with two and three dimensional partitions", Int J Heat and Mass Transfer, Vol 27, N 4, pp 561-571

Neymark J, Boardman C R, Kirkpatrick A and Anderson R, 1989. "High Rayleigh number natural convection in partially divided air and water filled enclosures", Int J Heat Mass Transfer Vol 32, pp 1671-1679.

Otis D R and Jones G F, 1988. "Neutral planes in stratified, thermally driven multiple room enclosures", Solar Energy, Vol 40, N 2, pp 135-137.

Patankar S V and Spalding D B, 1972. "A calculation procedure for heat mass and momentum transfer in 3D parabolic flows", Int J Heat Mass Transfer Vol 15, p1787.

Pelletret R, 1988. "Interzone air movement and heat transfer modeling", Proc. of User 1 Work conference SCS Int KIH, Ostende, Belgium, Sept 1988.

Pelletret R and Khodr Mneimne H, 1988. "Les transferts internes en thermique du bâtiment", Report DPE 88-630, CSTB, Sophia Antipolis, France.

Pelletret R and Khodr Mneimne H, 1990. "Les transferts internes en thermique du bâtiment", Report CSTB/TTA/90-931, Sophia Antipolis, France.

Pelletret R, Liébecq G, Allard F and van der Maas J, 1991. "Modelling of large openings", Proc. of the 12th AIVC Conference in Ottawa, Air movement and ventilation control within buildings, Vol 1, pp 99-110.

Phaff J C, de Gids W F, Ton J A, v d Ree D, and van Schijndel L L M, 1980. "Ventilatie van gebouwen. Onderzoek naar de gevolgen van het openen van een raam op het binnenklimaat van een kamer" (Investigation of the consequences of opening one window on the internal climate of a room; data tables and Figures in Dutch version). Delft IMG-TNO rapport C448, March 1980 Airbase #2201.

Phaff H, 1991. "Airflow driven contaminants. Transport through buildings Annex 20 Subtask 2.5", Proc. of the 12th AIVC Conference in Ottawa, Air movement and ventilation control within buildings, Vol 1, pp 123-140.

Rao J and Haghighat F, 1991. "Wind induced fluctuating air infiltration in buildings" Proc. of the 12th AIVC Conference in Ottawa, Air movement and ventilation control within buildings, Vol 1, pp 111-122

Riberon J, Moujaned R, Barnaud G, Villain J, 1989. "Turbulence du vent et ventilation", Séminaire AFME, Sophia Antipolis 19 sept 1989.

Riberon J, Villain J, 1990. "Etude en vraie grandeur des débits effectifs de renouvellement d'air", CSTB GEC/DAC-90 101R, Champs-Sur-Marne, France, July 1990.

Riberon J, Barnaud G, Villain J, 1990. "Wind turbulence and ventilation", Annex 20 working report. RID 2.01.

Riffat S B, 1989. "A study of heat and mass transfer through a doorway in a traditionally built house", ASHRAE Trans. Vol 95, part 2, pp 584-589.

Rodriguez E A and Allard F, 1992. "Coupling COMIS airflow model with other transfer phenomena", Energy and Buildings Vol 18, pp147-158.

Roldan A, 1985. "Etude thermique et aréaulique des enveloppes de bâtiment. Influence des couplages intérieurs et du multizonage", PhD Thesis, INSA de Lyon (France).

Roulet C -A and Vandaele L, 1991. "Airflow patterns within buildings - measurement techniques", Tech. Note AIVC 34, Berkshire RG12 4AH, GB, 1992 (Technical Report of Annex 20).

Roulet C -A and Scartezzini J, 1991. "Stochastic model of inhabitant behaviour in regard to ventilation", 12th AIVC Conference 24-27, Ottawa .

Roulet C -A, Cretton P, Fritsch R and Scartezzini J -L, 1991. "Stochastic model of inhabitant behavior in regard to ventilation", IEA/ECB-Annex 20, Airflow Patterns within buildings, Subtask-2 Technical Report

Rouse H, 1946. Elementary mechanics of fluids, H Wiley-NY, Chapman & Hall-London (also 1953. Basic mechanics of fluids).

Sandberg M, 1989. "Flow through large internal openings", Draft report Third Expert Meeting in Aalborg, Denmark, May 30-June 2, 1989

Schaelin A, van der Maas J and Moser A, 1992. "Simulation of air flow through large openings in buildings" ASHRAE Symposium, on "Airflow in realistic rooms- CFD and Physical data", June, Baltimore ASHRAE Trans. Vol 98, BA-92-2-4.

Scott D, Anderson R, and Figliola R, 1988. "Blockage of Natural Convection Boundary Layer Flow in a Multizone Enclosure", Int J Heat and Fluid Flow, Vol 9, pp 208 - 214.

Shaw B H and Whyte W, 1974. "Air movement through doorways. The influence of temperature and its control by forced airflow", Bldg. Services Eng. Vol 42(12), pp 210-218.

Shaw B H, 1976. "Heat and mass transfer by convection through large rectangular openings in vertical partitions", Ph D Thesis, University of Glasgow, UK.

Simoneau J P, Inard C, and Allard F, 1988. "Numerical Approach of Interaction Between an Injection and Laminar Natural Convection in a Thermally Driven Cavity", ASME Winter Ann Meeting, Chicago, Vol 99, pp 45 - 51

Sirén K E, 1988. "A procedure for calculating concentration histories in dwellings", Building and Environment, Vol. 23(2), pp103-114.

Spalding D B, 1972. "A novel finite-difference formulation for differential expression involving both first and second derivatives", Int J Num Methods Eng, Vol 4, p551.

Tang D, Robberechts B, 1989. "Inter-zone convective heat transfer and air flow patterns", Annex 20, Third Expert Meeting in Aalborg, DK. Annex 20 Working report 2.01.

Turner J S, 1973. Buoyancy effects in fluids, Cambridge University Press.

Van der Maas J, Roulet C -A and Hertig J -A, 1989. "Some aspects of gravity driven air flow through large apertures in building", ASHRAE Trans.Vol 95, part 2, pp 573-583.

Van der Maas, J, 1989. "Airflow through large internal and external openings", Status Report subtask 2.1, Fourth Annex 20 Expert Meeting in Lommel, B. Working report. RID 2.01.

Van der Maas J, Roulet C -A and Hertig J -A, 1990. "Transient single sided ventilation through large openings in buildings", ROOMVENT '90, Oslo, C48.

Van der Maas J, Roulet C -A, 1990. "Ventilation and energy loss rates after opening a window", Air Infiltration Review, Vol 11, No 4, pp 12–15.

Van der Maas J, 1990. "Is the window open or closed?" Newsletter of the IEA-Annex 20: Flowflash 3, April (also : in SOLPLAN REVIEW No 33, June, p13).

Van der Maas J, Roulet C-A, 1991. "Nighttime ventilation by stack effect", ASHRAE Transactions, V.97, Pt. 1, 9pp.

Vandaele L and Wouters P, 1989. "Air flows through large openings. An overview of existing approaches", IEA Annex 20 Subtask 2 report, Third Expert Meeting, Aalborg, DK. Working report RID 2.01.

Walton G N, 1984. "A computer algorithm for predicting infiltration and inter-room airflows", ASHRAE Trans. Vol 90, part 1.

Walton G N, 1989. "Airflow network models for element based building airflow modeling", ASHRAE Trans. Vol 95 part 2, pp 611-620.

Wang J C Y, Jiang Z and Haghighat F, 1991. "Influence of air infiltration on airflow in a ventilated isothermal two-zone enclosure", Energy and Buildings Vol 17, pp43-54.

Warren P R, 1977. "Ventilation through openings on one wall only", Proc. of the ICHMT conference 'Energy conservation in heating cooling and ventilating buildings', Dubrovnik, 1977. Vol 1, pp 189-206, Hemisphere Publishing Corp Washington, 1978.

Warren, P R, 1986. "The analysis of Single-Sided Ventilation Measurements", Air Infiltration Review, Vol 7 No 2, pp 3-5

Warren P R,1988. "Flow through external openings, Draft Report", Annex 20: Second Expert Meeting in Warwick, UK, Nov 7-10.

Warren P R and Parkins L M, 1985. "Single-sided ventilation through open windows", 3rd ASHRAE Conf. on the thermal performance of the exterior envelopes of bldgs., Clearwater Beach, FA, December 1985.

Weber D D, 1980. "Similitude modeling of natural convection heat transfer through an aperture

in passive solar heated building", Ph D Thesis, Los Alamos Scientific Lab. LA8385-T.

White M D, Winn C B, Jones G F and Balcomb J D, 1985. "The influence of geometry on natural convection in buildings." Proc. 10th National Passive Solar Conf, Columbus, OH.

Wilson D J and Kiel D E, 1990. "Gravity driven counterflow through an open door in a sealed room", Building and Environment, Vol 25(4), pp 379-388.

Wouters P, 1987. "De ventilatie problematiek in gebouwen (The problematics of ventilation in buildings)", DPWB, National Belgian R&D programme on energy.

Zohrabian A S, Mokhtarzadeh-Dehghan M R, Reynolds A J, 1989. "Buoyancy-driven air flow in a stairwell model with through-flow", Brunel University, UK.

Addresses of participants in Annex 20 - subtask 2.1

Dr. Francis Allard
CETHIL - URA CNRS 1372
INSA de Lyon, Bâtiment 307
F-69621 Villeurbanne Cédex, France
Phone   : +33 72 43 84 62
Fax   : +33 72 43 85 22

Dr. Jacques Riberon
Centre Scientifique et Technique du Bâtiment (CSTB)
Centre de Recherche de Marne-la-Vallée
84, Avenue Jean Jaurès - Champs-sur-Marne
B.P. 02, F-77421 Marne-la-Vallée-Cédex 2, France
Phone   : +33 1 64 68 83 23
Fax   : +33 1 64 68 83 50

Dr. Fariborz Haghighat
Centre for Building Studies
Concordia University
1455 de Maisonneuve Blvd. W.
Montreal, Que., Canada H3G 1M8
Phone   : +1 514 848 3192
Fax   : +1 514 848 7965

Dr. Georges Liébecq
Université de Liège, Laboratoire de Thermodynamique
Campus du Sart Tilman, Bât. B-49 , B-4000 Liège, Belgium
Phone   : +32 41 56 48 00
Fax   : +32 41 56 48 12
(present address: ECONOTEC, quai de la Boverie 24, B-4020 Liège, Belgium)
Phone   : +32 41 42 80 82
Fax   : +32 41 41 47 80

Dr. Jacobus van der Maas
Laboratoire d'Energie Solaire et de Physique du Bâtiment (LESO-PB)
Ecole Polytechnique Fédérale de Lausanne (EPFL)
CH-1015 Lausanne, Switzerland
Phone   : +41 21 693 -3363 (-1111)
Fax   : +41 21 693 -2722

Dr. Roger Pelletret
Centre Scientifique et Technique du Bâtiment (CSTB)
Centre de Recherche de Sophia Antipolis
B.P. 209, F-06904 Sophia Antipolis Cedex, France
Phone   : +33 93 65 34 00
Fax   : +33 93 65 29 37

ir. Luk Vandaele
Belgian Building Research Institute (BBRI)
(Wetenschappelijk en Technisch Centrum voor het Bouwbedrijf / Centre Scientifique et Technique de la Construction)
Aarlenstraat 53 / 10
B-1040 Brussels, Belgium
Phone   : +32 2 653 88 01
Fax   : +32 2 653 07 29

Mr. Richard Walker
Building Research Establishment (BRE)
Garston, Watford WD2 7JR, United Kingdom
Phone   : +44 923 66 44 69
Fax   : +44 923 66 40 95